Alma Mater Studiorum – Università di Bologna

DOTTORATO DI RICERCA IN
SCIENZE BIOTECNOLOGICHE, BIOCOMPUTAZIONALI,
FARMACEUTICHE E FARMACOLOGICHE

Ciclo XXXIII

Settore Concorsuale: 03/D1

Settore Scientifico Disciplinare: CHIM/11

The human gut microbiome in disease: Role in chemotherapy treatments and relationship with clinical outcomes

Presentata da: Federica D'Amico

Coordinatore Dottorato	**Supervisore**
Prof.ssa Maria Laura Bolognesi	Prof.ssa Patrizia Brigidi

Esame finale anno 2021

TABLE OF CONTENTS

ABSTRACT

The human gut microbiome (GM) is an extremely plastic entity, capable of adapting in response to various intrinsic and extrinsic factors (e.g., diet, lifestyle, age, geography). However, several circumstances can disrupt this homeostatic balance, forcing the GM to shift from a health-associated mutualistic configuration to a disease-associated profile. Beyond the direct involvement of some GM members in cancer development and progression, a new frontier of microbiome research is understanding the relationship between GM and drugs, with a main focus on chemo-immunotherapies and patient clinical outcomes. In this work, the role of the enteric pathogen *Salmonella enterica* in colorectal carcinogenesis was characterized by 2D and 3D *in-vitro* models. A synergistic effect of the CRC-associated mutation (*i.e.*, APC gene) and infection with genotoxin-producing *Salmonella* promoted a tumorigenic microenvironment by increasing cellular genomic instability. Subsequently, the involvement of the GM in anti-cancer therapeutic responses was investigated by using next-generation sequencing approaches in different patient cohorts. The trajectory of GM before and during treatments was characterized for women affected by epithelial ovarian cancer and pediatric patients undergoing hematopoietic stem cell transplantation (HSCT). The common results of these studies were the loss of gut microbial homeostasis during the course of therapies, including the reduction of microbial diversity accounted for by the decrease in health-associated microorganisms and the bloom of pathobionts. Interestingly, a distinctive GM profile was identified in ovarian cancer patients with a poor response to chemotherapy compared to patients in remission. On the other hand, maintenance of GM homeostasis through enteral feeding in pediatric patients undergoing HSCT was associated with a better prognosis, reducing the risk of clinical

complications (*i.e.*, graft-versus-host and veno-occlusive diseases, systemic infections). In this context, the gut resistome – the pattern of antibiotic-resistance genes encoded by the GM – was evaluated longitudinally in pediatric patients from pre to post HSCT. The results highlighted new acquisitions and consolidation of antibiotic-resistance genes already present in patients developing clinical complications. The antibiotic exposure impact was also evaluated in infant patients under continuous low-dose antibiotic prophylaxis for vesico-ureteral reflux highlighting an impairment of the GM eubiotic configuration even in the absence of other concomitant treatments, with possible long-term health implications. Dramatic GM dysbiosis was finally observed in another category of patients undergoing multiple drug therapies, *i.e.*, critically ill patients with COVID-19, and correlated with an increased risk of bloodstream infections. All these findings pointed out the importance of maintaining GM homeostasis during chemotherapy treatments, in order to improve patients' clinical outcomes. Further studies are needed to fully understand the GM character on cancer development and chemotherapy treatments scenes, with the ultimate goal of developing novel microbiome-based therapeutic approaches to prevent clinical complications and ensure long-term positive responses.

Chapter 1 – INTRODUCTION

1.1 Exploring the human gut microbiome: historical hints and variations across lifespan

Microorganisms that normally inhabit the gastrointestinal tract are key contributors maintaining the physiological homeostasis of the colonizing host[1]. Although this sentence may seem obvious in 2020, several studies have been performed in these past few years focusing on understanding the close and complex relationship between the gut microbial community (*i.e.*, gut microbiota, GM) and the human host. Taking a step back, the first signs of the presence of microbes inside the human intestinal tract took place in the late 1800s in Europe, when the German pediatrician Theodor Escherich consolidated the study of the "human gut flora"[2]. It is properly due to Prof. Escherich the discovery of what he called "*Bacterium coli commune*" (*i.e.*, the famed *Escherichia coli*) in human feces and afterwards the "*Bacillus bifidus communis*" (*i.e.*, *Bifidobacterium animalis*) in the intestinal niche of neonates and breast-fed infants. So, at a time when the only known microorganisms were involved in the development of several pathologies (e.g., cholera, anthrax and tuberculosis), Escherich and colleagues gave a new insight into microbiology by speaking for the first time of "good bacteria"[2]. Afterwards, for the GM research the road was downhill and until recently, a frequent repeated slogan in the microbiome field was that human body contained 10 times more microorganisms than human cells. However, this was a rough calculation

[1] Turnbaugh PJ et al. The human microbiome project: exploring the microbial part of ourselves in a changing world. *Nature*. **2007**;449:804-810.

[2] Farré-Maduella E, Casals-Pascual C. The origins of gut microbiome research in Europe: From Escherich to Nissle. *Human Microbiome research*. **2019**;14:100065.

performed around 40 years ago[1,3,4], and the novel technological approaches currently developed, allowed us to determine that the ratio between human and microbial cells is likely closer to 1:1, with the balance slightly in favor of microbes[5]. The GM is deeply complex and includes not only bacteria, which are the most represented, but also archaea, micro-eukaryotes (e.g., fungi), along with viruses[6]. So far, its collective genome, known as microbiome, is estimated to harbor 150- to 500-fold more genes compared to the host and implicated in providing functional traits that complement the human repertoire and relevant to our metabolic, immunological and neurological homeostasis[7,8,9].

The first microbial stimuli derive from the early moments of the infant's life and are strictly connected to the birth mode, the maternal microbiota, antibiotic exposure and early-life feeding practices[10,11]. In this moment, when the infant-GM symbiosis is going to be established, the GM is featured by lower bacterial diversity and functional complexity, as well as higher degree of interpersonal variation compared to the healthy adult GM profile[12,13]. The first colonizers of the infant GM are typically facultative anaerobes, followed by the accumulation of obligate anaerobes, including *Bifidobacterium*, *Bacteroides* and *Clostridium*

---

[3] Costello EK, et al. Bacterial community variation in human body habitats across space and time. *Science*. **2009**;326:1694-1697.

[4] Savage DC. Microbial ecology of the gastrointestinal tract. *Annu Rev Microbiol*.**1977**;31:107-133.

[5] Sender R, Fuchs S, Milo R. Revised estimates for the number of human and bacteria cells in the body. *PLoS Biol*. **2016**;14:e1002533.

[6] Rajilić-Stojanović M, de Vos VM. The first 1000 cultured species of the human gastrointestinal microbiota. *FEMS Microbiol Rev*. **2014**;38:996-1047.

[7] Neish AS. Microbes in gastrointestinal health and disease. *Gastroenterology*. **2009**;136:65-80.

[8] Gill SR, et al. Metagenomic analysis of the human distal gut microbiome. *Science*. **2006**;312:1355-1359.

[9] Candela M, et al. Intestinal microbiota is a plastic factor responding to environmental changes. *Trends Microbiol*. **2012**;20:385-391.

[10] Robertson RC, et al. The human microbiome and child growth - first 1000 days and beyond. *Trends Microbiol*. **2019**;27:131-147.

[11] Derrien M, Alvarez AS, de Vos WM. The gut microbiota in the first decade of life. *Trends Microbiol*. **2019**;27:997-1010.

[12] Bäckhed F, et al. Dynamics and stabilization of the human gut microbiome during the first year of life. *Cell Host Microbe*. **2015**;17:690-703.

[13] Yatsunenko T, et al. Human gut microbiome viewed across age and geography. *Nature*. **2012**;486:222-227.

during the following 6 months[12]. These microorganisms are involved in human milk oligosaccharide metabolism as the only source of nutrition and most of the gut microbial community colonization is strictly dependent on the mother's breast milk[14]. Furthermore, both structural components of microbes and products of microbial metabolism (e.g., vitamins, amino acids) have been found to be involved in the child's immune system development, maturation and education[15,16], as well as in growth and maturation of the endocrine and central nervous system[17]. From the moment of birth, gastrointestinal epithelial cells are continually exposed to a vast number of microbial antigens and metabolites. In spite of this close proximity, microorganisms and host are living in perfect symbiosis due to the maturation and development of the immune system helped by the GM contribution[18]. Microbiome disruption during the early life window can be associated to several problems, such as specific immune-associated alterations[19,20]. In fact, germ-free mice are characterized by poor growth, decreased weight and mucosal surface area of the small intestine, decreased intestinal motility, increased mucus production, increased size of the cecum and mild diarrhea[21]. These animal models not only develop intestinal symptoms but also show altered neurodevelopment, deficiencies in stress responsivity, anxiety-like behaviors, and impaired sociability and cognition[22]. A link between intestinal dysbiosis and disease has been

[14] Pannaraj PS, et al. Association between breast milk bacterial communities and establishment and development of the infant gut microbiome. *JAMA Pediatr*. **2017**;171:647-654.

[15] Vangay P, et al. Antibiotics, pediatric dysbiosis, and disease. *Cell Host Microbe*. **2015**;17:553-564.

[16] Rooks MG, Garrett WS. Gut microbiota, metabolites and host immunity. *Nat Rev Immunol*. **2016**;16:341-352.

[17] Macpherson AJ, et al. How nutrition and the maternal microbiota shape the neonatal immune system. *Nat Rev Immunol*. **2017**;17:508-517.

[18] Cani PD. Human gut microbiome: hopes, threats and promises. *Gut*. **2018**;67:1716-1725.

[19] Olszak T, et al. Microbial exposure during early life has persistent effects on natural killer T cell function. *Science*. **2012**;336:489-493.

[20] Cox LM, et al. Altering the intestinal microbiota during a critical developmental window has lasting metabolic consequences. *Cell*. **2014**;158:705-721.

[21] Underwood MA, et al. Neonatal intestinal dysbiosis. *J Perinatol*. **2020**;1-12 [Epub ahead of print]

[22] Luczynski P, et al. Growing up in a bubble: using germ-free animals to assess the influence of the gut microbiota on brain and behavior. *Int J Neuropsychopharmacol*. **2016**;19:pyw020.

suggested for type 1 diabetes[23], atopic disease and asthma, as well as childhood obesity[24,25]. Hence, the gut microbial development in early-life period represents an important element of host's life for several reasons related to the maturation and development of the lifespan GM-host relationship. (**Figure 1**).

[23] Vatanen T, et al. The human gut microbiome in early-onset type 1 diabetes from the TEDDY study. *Nature*. **2018**;562:589-594.

[24] Chua HH, et al. Intestinal dysbiosis featuring abundance of *Ruminococcus gnavus* associates with allergic diseases in infants. *Gastroenterology*. **2018**;154:154–167.

[25] Maruvada P, et al. The human microbiome and obesity: moving beyond associations. *Cell Host Microbe*. **2017**;22:589-599.

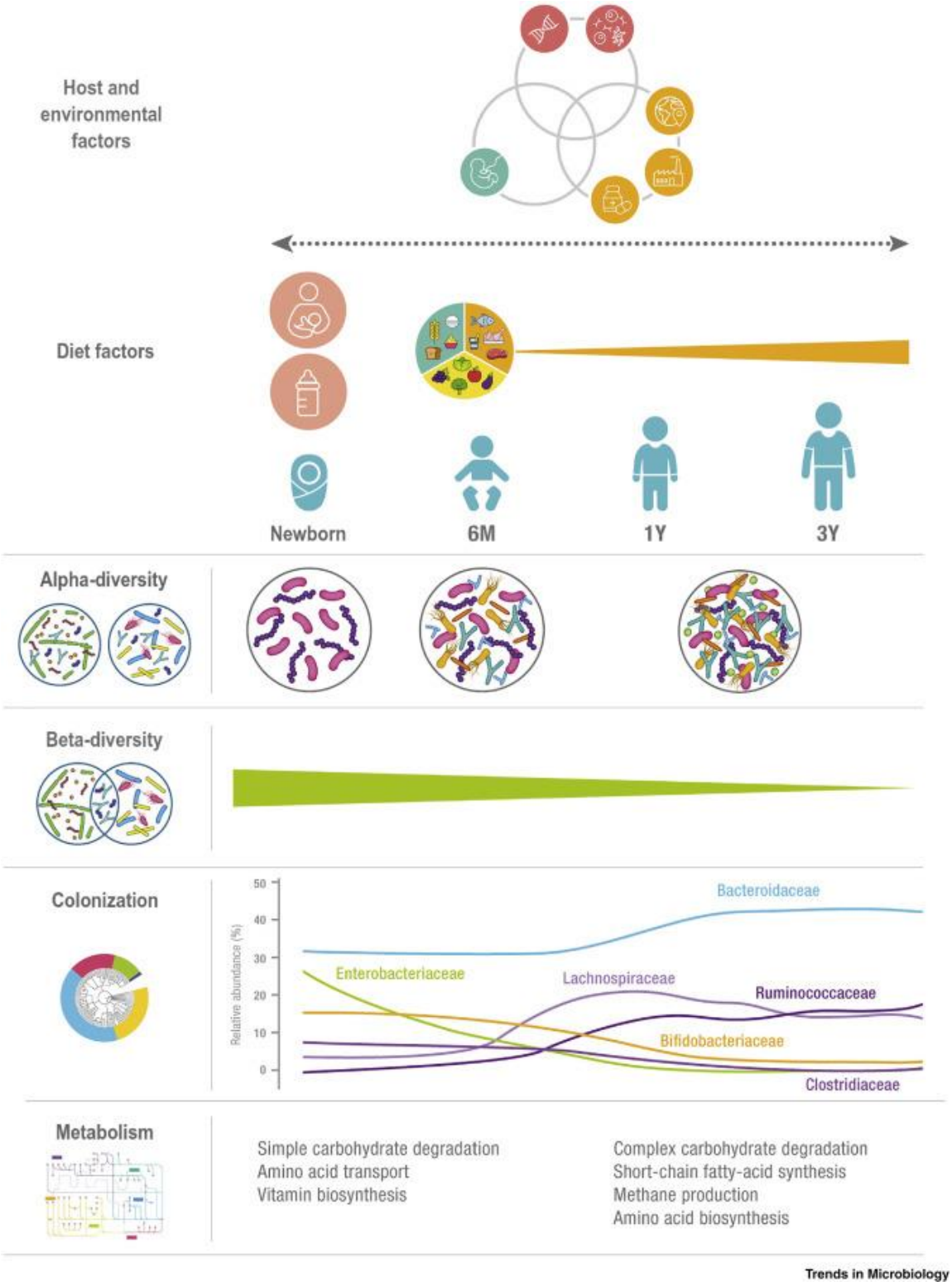

Figure 1. **Development of the early-life gut microbial community.** Bacterial alpha-diversity and functional complexity increase with age, while interindividual variations (beta-diversity) decrease[26].

[26] Derrien M, Alvarez AS, de Vos WM. The gut microbiota in the first decade of life. *Trends Microbiol.* **2019**;27:997-1010.

With the introduction of solid foods, a rapid increase in the structural and functional diversity of the infant microbiota occurs, progressively creating a mature adult-like state. The development of the complete adult GM is regulated by a complex interplay between the host and several environmental factors, such as diet, lifestyle, geography and environmental bacteria exposure[27,28]. All the factors mentioned above, from the first days of life up to the adult's development, contribute to select a GM eubiotic configuration (*i.e.*, a healthy and balanced ecosystem that coexists with its host) that provides functional traits necessary for the host's survival[29]. The mature microbiome is usually dominated by species capable of degrading complex carbohydrates, such as glycans, and mucins, as well as producing short-chain fatty acids (SCFAs), just to name some of the few roles of the GM in favor of host homeostasis[30]. In this second phase of life, carbohydrates are one of the most important sources of energy for the host. However, human enzymes cannot degrade most complex carbohydrates and plant polysaccharides. Instead, several microorganisms inhabiting the gut microbial niche are able to digest carbohydrates, such as cellulose, xylans, resistant starch and inulin, yielding energy for microbial growth. The end products of this microbial fermentation, such as SCFAs, mainly acetate, propionate and butyrate, can be beneficial for gut health as local (*i.e.*, butyrate) and peripheral (*i.e.*, acetate and propionate) energy sources, inflammation modulators, vasodilators and regulators of gut motility and wound healing[12,31]. SCFAs also affect proliferation and differentiation of the colonic epithelial cells,

---

[27] Tremaroli V, Bäckhed F. Functional interactions between the gut microbiota and host metabolism. *Nature*. **2012**;489:242-249.

[28] Rothschild D, et al. Environment dominates over host genetics in shaping human gut microbiota. *Nature*. **2018**;555:210-215.

[29] Gill SR, et al. Metagenomic analysis of the human distal gut microbiome. *Science*. **2006**;312:1355-1359.

[30] Robertson RC, et al. The human microbiome and child growth - first 1000 days and beyond. *Trends Microbiol*. **2019**;27:131-147.

[31] Bergman EN. Energy contributions of volatile fatty acids from the gastrointestinal tract in various species. *Physiol Rev*. **1990**;70:567-590.

as well as the modulation of gene expression[32]. Furthermore, SCFAs, by acting as signaling molecules, can have a systemic role influencing the expansion and function of hematopoietic and non-hematopoietic cell lineages[33]. For example, the inhibition of histone deacetylases SCFAs-mediated promotes a tolerogenic, anti-inflammatory cell phenotype that is crucial for maintaining immune homeostasis[34]. Many other immunoregulatory properties of SCFAs are associated with the activation of the G protein-coupled receptors expressed by numerous cell types, including immune cells and intestinal epithelial cells. In this context, SCFAs promote the colitis attenuation in *in-vivo* models and possess epigenetic potential by protecting the host from disease development[35,36,37].

[32] Davie JR. Inhibition of histone deacetylase activity by butyrate. *J Nutr*. **2003**;133:2485S-2493S.

[33] Koh A, et al. From dietary fiber to host physiology: Short-chain fatty acids as key bacterial metabolites. *Cell*. **2016**;165:1332-1345.

[34] Rooks MG, Garrett WS. Gut microbiota, metabolites and host immunity. *Nat Rev Immunol*. **2016**;16:341-352.

[35] Vinolo MAR, et al. Suppressive effect of short-chain fatty acids on production of proinflammatory mediators by neutrophils. *J Nutr Biochem*. **2011**;22:849-855.

[36] Thorburn AN, et al. Evidence that asthma is a developmental origin disease influenced by maternal diet and bacterial metabolites. *Nat Commun*. **2015**;6:7320.

[37] Maslowski KM, et al. Regulation of inflammatory responses by gut microbiota and chemoattractant receptor GPR43. *Nature*. **2009**;461:1282-1286.

1.2 Plasticity of the gut microbial community

Despite the large number of species (more than 1,000[38]) colonizing the gastrointestinal tract, the healthy-like gut microbial community is mostly dominated by two phyla, Firmicutes and Bacteroidetes, that together share about 90% (approximately 65% and 25%, respectively) of the intestinal microbial niche[39]. However, in the past few years some of the key functional traits of the GM have also been acknowledged to the subdominant fraction of this complex ecosystem: Actinobacteria (5%), Proteobacteria (8%), Fusobacteria (1%) and Verrucomicrobia (1%). These last phyla have recently received attention in regards to the GM-host symbiotic relationship, as well as disease etiology (e.g., colorectal cancer development[40] and immune-chemotherapy response impairment[41,42]). Indeed, it's currently known, despite some disputes, that there is a conserved set of gut colonizers, called the core microbiome, that is fundamental in supporting the mutualistic symbiotic relationship with the host and thus the correct functioning of the gut[43]. However, longitudinal studies highlighted that the intestinal microbiota of each individual is an extremely dynamic entity[44,45], raising questions about how significant is this degree of plasticity for human health and homeostasis. This issue has a more intrinsic complexity; what is the definition of a healthy

---

[38] Qin J, et al. A human gut microbial gene catalogue established by metagenomic sequencing. *Nature*. **2010**;464:59-65.

[39] Ley RE, Peterson DA, Gordon JI. Ecological and evolutionary forces shaping microbial diversity in the human intestine. *Cell*. **2006**;124:837-48.

[40] Fukugaiti MH, et al. High occurrence of *Fusobacterium nucleatum* and *Clostridium difficile* in the intestinal microbiota of colorectal carcinoma patients. *Braz J Microbiol*. **2015**;46:1135-1140.

[41] Gopalakrishnan V, et al. Gut microbiome modulates response to anti–PD-1 immunotherapy in melanoma patients. *Science*. **2018**;359: 97-103.

[42] Yu T, Guo F, Yu Y. *Fusobacterium nucleatum* promotes chemoresistance to colorectal cancer by modulating autophagy. *Cell*. **2017**;170:548-563.

[43] Turnbaugh PJ, Gordon JI. The core gut microbiome, energy balance and obesity. *J Physiol*. **2009**;587:4153-4158.

[44] Kau AL, et al. Human nutrition, the gut microbiome and the immune system. *Nature*. **2011**;474:327-336.

[45] Maslowski KM, Mackay CR. Diet, gut microbiota and immune responses. *Nat Immunol*. **2011**;12: 5-9.

microbiome? Usually, the stability of a community is associated with its ability to stand after a stress-related perturbation (resistance) or to change and return to an equilibrium state[46]. However, based on studies performed in the last few years defining strong interindividual differences of the GM profile, this statement about the stability is considered a bit too simplistic. An alternative conceptualization is an idealized collection of genes and pathways rather than specific populations that have a key role to promote host intestinal homeostasis carrying out a set of healthy metabolic functions[47]. Indeed, in 2012, a survey on 4,788 fecal samples collected from 242 healthy adults highlighted a marked variation in gut microbial population among subjects, but key metabolic pathways were conserved[48]. The definition of a healthy microbiome was then amended as: the ecological stability (*i.e.*, ability to resist community structure change under stress or to rapidly return to baseline following a stress-related change) given by an idealized health-associated composition and/or a desirable functional profile (including metabolic and trophic provisions to the host)[46]. Since then, in order to investigate the GM equilibrium in response to different environmental variables, several molecular studies have been specifically designed, demonstrating an unexpected degree of plasticity in response to diet[49], geographic origin[50] and antibiotic exposure[51], just to name a few (**Figure 2**). Until now, diet is considered one of the most important drivers for the gut microbial community health and functionality. Indeed, diet-GM relationship is the most widely studied in microbiome-related literature with 508,000 hits by using the "diet &

---

[46] Bäckhed F, et al. Defining a healthy human gut microbiome: current concepts, future directions, and clinical applications. *Cell Host Microbe*. **2012**;12:611-22.

[47] Nicholson JK. Host-gut microbiota metabolic Interactions. *Science*. **2012**;336:1262-1267.

[48] Human Microbiome Project Consortium. A framework for human microbiome research. *Nature*. **2012**;486:215-221.

[49] Muegge BD, et al. Diet drives convergence in gut microbiome functions across mammalian phylogeny and within humans. *Science*. **2011**;332:970-974.

[50] De Filippo C, et al. Impact of diet in shaping gut microbiota revealed by a comparative study in children from Europe and rural Africa. *Proc Natl Acad Sci USA*. **2010**;107:14691-14696.

[51] Palleja A, et al. Recovery of gut microbiota of healthy adults following antibiotic exposure. *Nat Microbiol*. **2018**;3:1255-1265.

gut microbiota" key-words on NCBI (National Center for Biotechnology Information) (research performed on 24/12/2020). Indeed, the GM is able to rapidly respond to large changes in diet, people who switch between plant- and meat-based diets, by adding every day specific dietary fibers to their diet or who follow either a high-fiber–low-fat diet or a low-fiber–high-fat diet for 10 days, achieved a compositional and functional GM shift after just 1-2 days of diet intervention, although their GM identity remained stable during the 10-day study[52]. This responsiveness of the GM profile is crucial for maintaining a balanced and health GM-host relationship. However, these findings also highlighted how the GM fluctuations are strictly influenced by the individual's microbial species configuration, showing subject-specific changes of the microbiota profile in response to short- or even long-term dietary intervention[53,54,55]. Interestingly, the comparison between long- and short-term dietary changes revealed that the GM consists of bacterial groups affected by short-term dietary changes and others that are exclusively modulated by long-term dietary habits[56]. Through selection of microbial populations that optimally degrade the available substrates, these continuous microbiota fluctuations provide the host with the capability to readily adapt to dietary changes. In a recent study from De Filippis et al.[57], it has been estimated that vegan and vegetarian diets in Western populations, which are mostly based on fiber intake through fruit and vegetables, were associated with higher production levels of SCFAs, whereas the most common animal-based diet supported much lower levels. In

[52] Wu GD, et al. Linking long-term dietary patterns with gut microbial enterotypes. *Science.* **2011**;334:105-108.

[53] Walker AW, et al. Dominant and diet-responsive groups of bacteria within the human colonic microbiota. *ISME J.* **2011**;5:220-230.

[54] Wu GD, et al. Comparative metabolomics in vegans and omnivores reveal constraints on diet-dependent gut microbiota metabolite production. *Gut.* **2016**;65:63–72.

[55] David LA, et al. Diet rapidly and reproducibly alters the human gut microbiome. *Nature*. **2014**;505:559-563.

[56] Arumugam M, et al. Enterotypes of the human gut microbiome. *Nature*. **2011**;473:174-180.

[57] De Filippis F, et al. High-level adherence to a Mediterranean diet beneficially impacts the gut microbiota and associated metabolome. *Gut*. **2016**;65:1812-1821.

parallel, the plant-based diet intake is also enriched in well-known SCFA-producing microorganisms[58], such as *Prevotella*, *Faecalibacterium*, *Roseburia*, *Lachnospira*. These results have corroborated the hypothesis of a major shift in the GM composition and functionality from our ancient ancestors, indicating that several aspects of modern lifestyle are changing our resident microbial community. For example, measure meant to kill or limit the exposure to pathogenic microorganisms (*i.e.*, antibiotics and sanitization), combined with other factors, such as industrialization and processed food introduction, have had unintended consequences to modify the human microbial ecosystem[59]. This concept of gut microbial community adaptation to diet and lifestyle fluctuations was confirmed by studying African populations, few of them are still hunter-gatherers, or traditional rural communities, who eat large quantities of plants and consuming up to sevenfold more fiber than people the industrialized world[60]. The gut microbial ecosystem of several of these populations studied to date, e.g., Hadza from Tanzania[60], rural Bassa from Nigeria[61], Cameroon's BaAka[62], as well as Inuit from the Canadian Arctic[63] and people from non-industrialized regions of Papua New Guinea[64], share some similarities; an increased abundance of taxa able to ferment polysaccharides (*i.e.*, *Prevotella*, *Treponema* and *Succinivibrio*), as well as an increased production of fecal SCFAs, useful for the maintenance of the GM-host homeostasis. These studies provided valuable information on the specific adaptations of the GM over time, as

---

[58] Louis P, et al. The gut microbiota, bacterial metabolites and colorectal cancer. *Nat Rev Microbiol*. **2014**;12:661-672.

[59] Sonnenburg ED, Sonnenburg JL. The ancestral and industrialized gut microbiota and implications for human health. *Nat Rev Microbiol*. **2019**;17:383-390.

[60] Schnorr SL, et al. Gut microbiome of the Hadza hunter-gatherers. *Nat Commun*. **2014**;5:3654.

[61] Ayeni FA, et al. Infant and Adult Gut microbiome and metabolome in rural Bassa and urban settlers from Nigeria. *Cell Rep*. **2018**;23:3056-3067.

[62] Gomez A, et al. Gut Microbiome of coexisting BaAka Pygmies and Bantu reflects gradients of traditional subsistence patterns. *Cell Rep*. **2016**;14:2142-2153.

[63] Girard C, et al. Gut microbiome of the Canadian Arctic Inuit. *mSphere*. **2017**;2:e00297-16.

[64] Martínez I, et al. The gut microbiota of rural papua new guineans: composition, diversity patterns, and ecological processes. *Cell Rep*. **2015**;11:527-538.

they recall ways of life that accompanied our history, from the hunting and gathering of our Paleolithic ancestors, to small-scale agriculture and permanent settlements of the Neolithic, to the post-industrial Westernized lifestyle. Over years of research, all these findings pointed out the importance of evolution for the GM profile and the role of long-term dietary habits in the course of urbanization in shaping the GM profile. Indeed, ancestral microorganisms, such as fiber-degrading bacteria, are at risk of being eliminated by the fast-paced globalization of foods, excessive sanitation and by the advent of Westernized lifestyle[65].

Apart from diet, several studies highlighted endogenous and environmental factors that influence the composition and activity of the GM by keeping a health-promoting microbial arrangement along the course of our life[66,67]. Different longitudinal studies on healthy subjects highlighted a personalized microbial community that is generally stable for months but quickly and profound disturbed, of course in a very personalized way, according to specific human experiences[68,69]. Recently, an elegant study from Turroni et al.[70] tried to overcome the uncontrolled environmental bias that was characteristic of the previous studies, by analyzing the GM profile of six volunteer astronauts isolated in sealed compartments, in conditions of a regulated environment with the supply of mostly tinned foods similar to those used in the International Space Station, over 520 days of a virtual, but realistic, mission to Mars. The individual GM compositional layout was not compromised also after this period of close shared life, confirming the resilience of the individuality of the GM.

---

[65] Yatsunenko, T. et al. Human gut microbiome viewed across age and geography. *Nature*. **2012**;486:222-227.

[66] Candela M, et al. Intestinal microbiota is a plastic factor responding to environmental changes. *Trends Microbiol*. **2012**;20:385-391.

[67] Candela M, et al. Dynamic efficiency of the human intestinal microbiota. *Crit Rev Microbiol*. **2015**;41:165-171.

[68] David LA, et al. Host lifestyle affects human microbiota on daily timescales. *Genome Biol*. **2014**;15:R89.

[69] Flores GE, et al. Temporal variability is a personalized feature of the human microbiome. *Genome Biol*. **2014**;15:531.

[70] Turroni S, et al. Temporal dynamics of the gut microbiota in people sharing a confined environment, a 520-day ground-based space simulation, MARS500. *Microbiome*. **2017**;5:39.

However, during this confined period the gut microbial community maintained a certain level of dynamism, by shifting between different steady states typically associated with rearrangements of autochthonous members of the subject's GM[70].

The individual configuration of the gut microbial community is also strictly dependent on the geographical origin of the host[71] . Several comparative analyses among people from Korea, China, Japan and the USA[72,73], as well as from different European areas[74], revealed in fact that the GM profile clustered according to geographic origin. In particular, Firmicutes was the most characteristic phylum of Western Americans, the Japanese were enriched in Actinobacteria, as well as Koreans and Chinese showed a Bacteroidetes-rich GM profile[72,73]. As for Italians, subjects from Northern Italy were characterized by Cyanobacteria taxa, whereas the Southern inhabitants shared a Nitrospirae-rich intestinal microbial profile[74]. According to the authors of these studies, these country-related, or even region specific, differences in intestinal microbiota profiles can partially result from host genetics, that as usually a limited impact on GM, while being largely dependent on environmental variables, such as climate and particularly dietary habits and lifestyle.

Most of the GM-focused researches characterized the adult-like gut microbial configuration, highlighting its stability over time and plasticity towards different types of perturbations. On the other hand, few studies characterized the GM profile across the entire human lifespan starting from the first days of life and the adult-like ecosystem (until 65 years), going through

---

[71] He Y, et al. Regional variation limits applications of healthy gut microbiome reference ranges and disease models. *Nat Med*. **2018**;24:1532-1535.

[72] Nam, Y.D. et al. Comparative analysis of Korean human gut microbiota by barcoded pyrosequencing. *PLoS ONE*. **2011**;6:e22109

[73] Shin JH, et al. Lifestyle and geographic insights into the distinct gut microbiota in elderly women from two different geographic locations. *J Physiol Anthropol*. **2016**;35:31.

[74] Fontana A, Panebianco C, Picchianti-Diamanti A, et al. Gut microbiota profiles differ among individuals depending on their region of origin: An Italian pilot study. *Int J Environ Res Public Health*. **2019**;16:4065.

elderly profile (66-75 years), until centenarians (99-104 years) and semi-supercentenarians (105-109 years)[75,76,77,78]. It is currently known that aging leads to physiological and functional changes in several aspects of human life, including intestinal motility[79], lifestyle, nutritional behavior, immune-system activity[80], and, of course, can affect the GM[81,82]. In this context, the gut microbial community has been proposed as a possible mediator of healthy aging that preserves host-environment homeostasis by counteracting inflammaging, intestinal permeability, and deterioration of cognitive and bone health. According to these studies, the core microbiota is characterized by *Bifidobacteriaceae*, *Bacteroidaceae*, *Lachnospiraceae*, and *Ruminococcaceae* families and remains approximately stable during aging but varies in the cumulative relative abundance of its members. In particular, in elderly subjects an age-related reduction of diversity in gut ecosystem has been observed, as well as an increased colonization by subdominant opportunistic species and pathobionts, such as members of *Streptococcaceae*, *Enterobacteriaceae* and *Staphylococcaceae* families, accompanied with a reduction of health-associated microorganisms known for producing SCFAs, in particular butyrate[83]. This gut microbial configuration may contribute in the establishment of a pro-inflammatory loop that is detrimental for the GM-host relationship, as well as contributing to

---

[75] Biagi E, et al. Through ageing, and beyond: gut microbiota and inflammatory status in seniors and centenarians. *PloS one*. **2010**;5:e10667.

[76] Cheng J, et al. Contribution of the intestinal microbiota to human health: from birth to 100 years of age. *Curr Top Microbiol Immunol*. **2013**;358:323-346.

[77] Claesson MJ, et al. Composition, variability, and temporal stability of the intestinal microbiota of the elderly. *Proc Natl Acad Sci USA*. **2011**;108:4586-4591.

[78] Biagi E, et al. Gut microbiota and extreme longevity. *Curr Biol*. **2016**;26:1480-1485.

[79] Guigoz Y, Doré J, Schiffrin EJ. The inflammatory status of old age can be nurtured from the intestinal environment. *Curr Opin Clin Nutr Metab Care*. **2008**;11:13–20.

[80] Shanley DP, et al. An evolutionary perspective on the mechanisms of immunosenescence. *Trends Immunol*. **2009**;30:374-81.

[81] Biagi E, et al. Ageing of the human metaorganism: the microbial counterpart. *Age*. **2012**;34:247-267.

[82] Biagi E, et al. Ageing and gut microbes: perspectives for health maintenance and longevity. *Pharmacol Res*. **2013**;69:11-20.

[83] Santoro A, et al. Microbiomes other than the gut: inflammaging and age-related diseases. *Semin Immunopathol*. **2020**;42:589-605.

host inflammatory disorders development[75,84]. However, some peculiarities emerged in semi-supercentenarians GM profile, characterized by changes that, even accommodating opportunistic and allochthonous bacteria, might possibly support health maintenance during aging, such as an enrichment and/or higher prevalence of health-associated groups (e.g., *Akkermansia*, *Bifidobacterium*, and *Christensenellaceae*). The differences in the GM profile detected between semi-supercentenarians and other adult groups could support the possibility that, to attain longevity, a complex and pervasive remodeling, including the gut microbial ecosystem, should occur, favoring the balance between inflammatory and anti-inflammatory processes that usually happen with oldness. Furthermore, shotgun metagenomic approaches characterized the GM profile through age, centenarians and semi-supercentenarians also show a functional rearrangement characterized by an increased capability of xenobiotic degradation (*i.e.*, chemical substances that are foreign to life), probably as a functional response to life-long exposure to these compounds. On the other hand, from the adult-like profile through semi-supercentenarians, the reduced contribution of pathways related to carbohydrate and amino acid metabolism, as well as lipid degradation emerged, suggesting an association with age-related changes in dietary habits[84]. According to these findings, the hypothesis advanced to date is that all these functional and compositional bacterial features might be involved in the establishment of a new oldness homeostasis, thus contributing to reach the extreme limits of human life[78,84].

In conclusion, the key role of the intestinal microbial community emerged as a plastic and adaptable factor to different lifestyle habits, as well as diet and aging, meeting the

[84] Rampelli et al. Shotgun metagenomics of gut microbiota in humans with up to extreme longevity and the increasing role of xenobiotic degradation. *mSystems*. **2020**;5:e00124-20.

physiological needs of the human super-organism, thus maintaining the GM-host homeostasis throughout the lifespan (**Figure 2**).

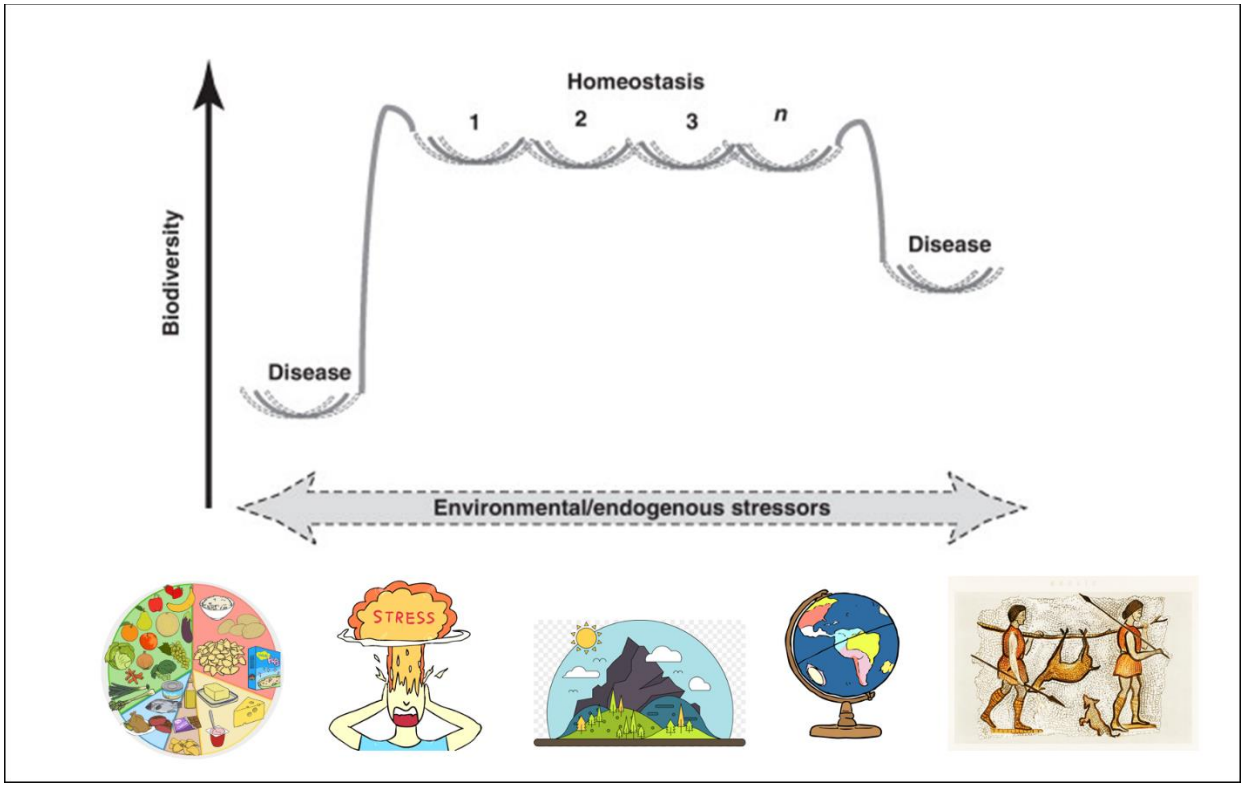

Figure 2. **Plasticity of the gut microbial community.** The gut microbial community is a plastic factor characterized by a subject-specific eubiotic structure that can change under limited stress perturbations but rapidly return to its equilibrium state (resilience). However, under certain conditions, strong environmental stressors (diet and/or other environmental factors, such as infection, hygiene, and sanitization) and factors of endogenous origin (such as stress, inflammation) can force the GM to shift from the mutualistic configuration that supports homeostasis (from 1 to n) to a disease-associated profile, generally characterized by a lower level of phylogenetic and functional biodiversity. Different healthy configurations are represented, showing the variability within and between individuals. Figure adapted from Candela et al.[85].

[85] Candela et al. Intestinal microbiota is a plastic factor responding to environmental changes. *Trends Microbiol.* **2012**;20:385-391.

1.3 Disturbance of the microbiome-host mutualistic relationship

Despite all the novel findings about the plasticity and resilience of the gut microbial community, under some circumstances, diet and other environmental factors, can promote the GM to shift from a mutualistic configuration supporting health and homeostasis to a disease-associated profile, usually characterized by a lower level of phylogenetic and functional biodiversity (**Figure 2)**. Indeed, the unbalanced GM observed in obese people[86,87] and the progressive loss of key intestinal microbial species as a result of a Westernized lifestyle[88] provide two remarkable examples of disturbance of the microbiota–host mutualism triggered by environmental stressors.

In eubiotic conditions, there are different host systems that are able to recognize and monitor the presence of microorganisms in the body. For example, in the gastrointestinal tract, the epithelial cells play a major role as guardians that are able to translate key information to the organ-specific immune cells. The innate immune system of the gastrointestinal tract is able to recognize pathogen-associated molecular patterns (PAMPs) from different types of microorganisms (e.g., lipopolysaccharides, peptidoglycans, lipoteichoic acids and so on) by using pattern recognition receptors (PRRs). The gastrointestinal tract is also one of the most important reservoirs of microorganisms in a relatively limited space. Thus, intestinal epithelial cells and the local immune system are constantly exposed to a variety of microbial antigens and metabolites that sometimes can improperly activate the immune system. However, an enduring mutualistic relationship GM-host is established from the first days of life, the host

[86] Turnbaugh PJ, et al. A core gut microbiome in obese and lean twins. *Nature*. **2009**;457:480-484.

[87] Gentile CL, Weir TL. The gut microbiota at the intersection of diet and human health. *Science*. **2018**;362:776-780.

[88] Kau AL, et al. Human nutrition, the gut microbiome and the immune system. *Nature*. **2011**;474,327-336.

has evolved to coordinate and integrate conserved metabolic signaling, microbial sensing and immune response pathways to ensure its survival in a microbially dominated world[89,90]. If, or when, due to a persistent perturbation of the gut microbial homeostasis, this intricate GM-host partnership goes awry, an intestinal dysbiosis is established. There are internal (*i.e.*, immune-response dysregulation and inflammation)[91] and external factors (*i.e.*, antibiotic exposure, dietary components, pathogen infections)[92] that can induce a gut microbial imbalance and several studies have been proposed to explain these occurrences. Dysbiosis, a common characteristic of both local and systemic GM-related diseases, is likely to impair the normal functioning of GM in maintaining host homeostasis, and potentially induce a selective suppression of certain health-associated members, leading to dysregulated production of microbial-derived products and/or metabolites. This loss of symbiont microorganisms is generally associated with a burst of subdominant taxa, which may be harmful for the host contributing to local and systemic diseases[93] (**Figure 3**). In order to characterize the role of the gut microbial community several host diseases, Rothschild et al.[94] analyzed the GM of over 1,000 healthy subjects defining a microbiome-association index that quantifies the overall association between the microbiome and a host phenotype. According to their results, a significant association between GM and host phenotypes has been observed, particularly for body-max index (BMI) (25%), waist-to-hip ratio (24%), fasting glucose levels (22%), glycemic status (25%), high density lipoprotein (HDL) cholesterol

[89] Rooks MG, Garrett WS. Gut microbiota, metabolites and host immunity. *Nat Rev Immunol*. **2016**;16:341-52.

[90] Cani PD. Human gut microbiome: hopes, threats and promises. *Gut*. **2018**;67:1716-1725.

[91] Zuo T, Ng SC. The gut microbiota in the pathogenesis and thrapeutics of inflammatory bowel disease. *Front Microbiol*. **2018**;9:2247.

[92] Palleja A, et al. Recovery of gut microbiota of healthy adults following antibiotic exposure. *Nat Microbiol*. **2018**;3:1255-1265.

[93] Kho ZY, Lal SK. The human gut microbiome - a potential controller of wellness and disease. *Front Microbiol*. **2018**;9:1835.

[94] Rothschild D, et al. Environment dominates over host genetics in shaping human gut microbiota. *Nature*. **2018**:555;210-215.

levels (36%), as well as monthly lactose consumption (36%)[94]. As a matter of fact, BMI and waist-to-hip ratio, as well as cholesterol/HDL and triglycerides, are blood and anthropometric indexes strongly associated with central obesity[95]. Thus, the increased percentage of worldwide obesity reflects environmental and lifestyle changes, including the spread of a high-fat Western diet, that together play a major role in obesity development in industrialized countries[96,97]. In this scenario, diet-dependent changes in GM composition can be involved in the etiology and severity of obesity[97]. Subjects exhibiting overall adiposity, insulin resistance and dyslipidemia are characterized by low bacterial richness[98], as well as a reduction in Bacteroidetes and a proportional increase of Firmicutes members[99]. Hence, the GM offers an important window into the consequences of diet (*i.e.,* high-fat and sugar-rich diets) and lifestyle (*i.e.,* sedentary) changes associated with human migration. Recently, it has been estimated that USA immigrants from different countries are more likely to develop metabolic disease post-immigration, with a fourfold increase in obesity risk within 15 years of USA emigration compared to subjects remaining in their birth country[100]. A recent longitudinal study of a multi-generational Asian-American cohort emigrating to the USA highlighted a reduction in gut microbial diversity and function[101]. Within the gram-negative Bacteroidetes phylum, bacterial strains from the genus *Prevotella*, whose enzymes degrade plant fiber, became displaced by dominant strains from the genus *Bacteroides* according to an individual's time spent in the USA. The ratio of *Bacteroides* to *Prevotella* increased by a

---

95 Hamer M, et al. Normal-Weight central obesity and risk for mortality. *Ann Intern Med*. **2017**;166:917-918.

96 Swinburn BA, et al. The global obesity pandemic: shaped by global drivers and local environments. *Lancet*. **2011**;378:804-814.

97 Sun L, et al. Insights into the role of gut microbiota in obesity: pathogenesis, mechanisms, and therapeutic perspectives. *Protein Cell*. **2018**;9:397-403.

98 Le Chatelier E, et al. Richness of human gut microbiome correlates with metabolic markers. *Nature*. **2013**;500:54-546.

99 Ley RE, et a. Microbial ecology: human gut microbes associated with obesity. *Nature*. **2006**;444:1022-1023.

100 Lauderdale DS, Rathouz PJ. Body mass index in a US national sample of Asian Americans: Effects of nativity, years since immigration and socioeconomic status. *Int J Obes*. **2000**;24:1188-1194.

101 Vangay P, et al. US immigration westernizes the human gut microbiome. *Cell*. **2018**;175:962-972.

factor of 10, correlating with the time in decades spent in the USA. Prior to this study, three clusters of variation in the human gut microbiome were identified[102]. The GM cluster characterized by high relative abundance of *Bacteroides* and low of *Prevotella* dominated in subjects following a long-term Western diet, high in animal protein, choline and saturated fat[103]. A second GM profile, associated with a plant-based diet rich in fiber, simple sugars, and plant-derived compounds, showed an enrichment in *Prevotella*, while low percentage of *Bacteroides*. While less distinct, a third potential gut microbial composition was found with a slightly higher amount of the genus *[Ruminococcus]* within the *Lachnospiraceae* family. The enrichment of *[Ruminococcus]* taxon is usually associated with subjects affected by irritable bowel syndrome (IBS)[104], and transient blooms of pro-inflammatory *[Ruminococcus]* have been associated with active flare-ups in inflammatory bowel disease (IBD)[105]. Indeed, *[Ruminococcus] gnavus* is a prevalent gut-colonizing microorganism that over-proliferates in IBD patients and is associated with a high concentration of tumor necrosis factor alpha (TNFα), a major pro-inflammatory cytokine[106]. Moreover, GM dysbiosis associated with the overgrowth of pathobiont microorganisms can promote the development and maintenance of different intestinal diseases, such as the IBD conditions known as Crohn's disease and ulcerative colitis[107]. IBD are chronic gastrointestinal disorders characterized by an overreactive immune response with still unknown etiology leading to bloody diarrhea, mucus

[102] Arumugam M, et al. Enterotypes of the human gut microbiome. *Nature*. **2011**;473:174-180.

[103] Wu GD, et al. Linking long-term dietary patterns with gut microbial enterotypes. *Science*. **2011**;334:105-108.

[104] Rajilic-Stojanovic M, et al. Intestinal microbiota and diet in IBS: Causes, consequences, or epiphenomena?. *Am J Gastroenterol*. **2015**;110:278-287.

[105] Hall AB, et al. A novel *Ruminococcus gnavus* clade enriched in inflammatory bowel disease patients. *Genome Med*. **2017**;9:103.

[106] Henke MT, et al. *Ruminococcus gnavus*, a member of the human gut microbiome associated with Crohn's disease, produces an inflammatory polysaccharide. *Proc Natl Acad Sci USA*. **2019**;116:12672-12677.

[107] Kim ER, Chang DK. Colorectal cancer in inflammatory bowel disease: The risk, pathogenesis, prevention and diagnosis. *World J Gastroenterol*. **2014**;20:9872-9881.

in the stools, abdominal pain, and weight loss, as well as by GM dysbiosis[108]. The occurrence of IBD is raising worldwide by counting more than 2 million Europeans and 1.5 million North Americans affected by these pathologies at the end of 2019[109]. Although the mechanisms of pathogenesis are still unknown, the cross-talk between GM and host shows the potential to contribute to the disease development, in combination with different environmental factors[110]. Indeed, IBD patients are characterized by a high responsiveness of T-lymphocytes toward non-pathogenic antigens normally present within the gastrointestinal niche with the production of pro-inflammatory mediators that can compromise the homeostatic relationship GM-host. Thus, this group of disorders result in oxidative stress for both host tissues and the gut microbial community involving intestinal dysbiosis, decrease of community richness, as well as proliferation of facultative anaerobic taxa (e.g., *Enterobacteriaceae* family and *Bacteroides fragilis*), including adherent invasive strains, such as some *Escherichia coli* strains. Furthermore, an intestinal inflammatory state, both GM- and host-mediated, can lead to functional and structural gut epithelial barrier impairment, as well as mucus layer thinning[111,112,113]. There are several other common features observed in IBD patients, such as the reduction of health-associated *Faecalibacterium prausnitzii* and *Roseburia,* both belonging to Firmicutes phylum. These microorganisms play an important anti-inflammatory role by reducing pro-inflammatory cytokines (e.g., IL-12, INFγ), increasing anti-inflammatory

[108] Xia B, et al. Inflammatory bowel disease: definition, epidemiology, etiologic aspects, and immunogenetic studies. *World J Gastroenterol*. **1998**;4:446-458.

[109] Jairath V, Feagan BG. Global burden of inflammatory bowel disease. *Lancet Gastroenterol Hepatol*. **2020**;5:2-3.

[110] Kho ZY, Lal SK. The human gut microbiome – a potential controller of wellness and disease. *Front Microbiol*. **2018**;9:1835.

[111] Winter SE, Baumler AJ. Dysbiosis in the inflamed intestine: Chance favors the prepared microbe. *Gut Microbes*. **2014**;5:71-73.

[112] Martinez-Medina M, Garcia-Gil LJ. *Escherichia coli* in chronic inflammatory bowel diseases: An update on adherent invasive *Escherichia coli* pathogenicity. *World J Gastrointest Pathophysiol.* **2014**; 5:213-227.

[113] Ryan FJ, et al. Colonic microbiota is associated with inflammation and host epigenomic alterations in inflammatory bowel disease. *Nat Commun*. **2020**;11:1512.

mediators (e.g., IL-10) and promoting the intestinal barrier integrity through butyrate production[114,115]. On the other hand, as mentioned above, the IBD-associated pro-inflammatory loop with mucus barrier impairment supports the increase of mucolytic species, such as *[Ruminococcus]* spp., which further aggravate the barrier function by stimulating severe inflammatory responses[116,117]. The conclusion shared by the literature is that all these findings strongly indicate a bidirectional relationship between IBD and GM dysbiosis, in which dysbiosis potentially contributes to the disease onset and also represents a secondary consequence of gut inflammation. Although in the last decade the research about the role and functions of the GM in health and disease has rapidly evolved, it is still not so clear if dietary interventions, as well as probiotic and prebiotic intake, could prevent and/or alleviate GM-related pathologies, such as obesity and IBD. However, there are several examples of these GM-directed therapeutic approaches. The probiotic treatment with *Lactobacillus rhamnosus* and *Bifidobacterium* spp. has shown to significantly decrease plasma cholesterol, triglycerides and white adipose tissue in animal models[118], whereas prebiotic intake, such as inulin-type fructans, has demonstrated anti-adipogenic effects in animal models by increasing health-associated and/or SCFA-producing microorganisms, such as *Roseburia, Bacteroides* and *Bifidobacterium*[119,120]. Likewise, similar approaches have

---

[114] Sokol H, et al. *Faecalibacterium prausnitzii* is an anti-inflammatory commensal bacterium identified by gut microbiota analysis of Crohn disease patients. *Proc Natl Acad Sci USA*. **2008**;105:16731-16736.

[115] Machiels K, et al. A decrease of the butyrate-producing species Roseburia hominis and *Faecalibacterium prausnitzii* defines dysbiosis in patients with ulcerative colitis. *Gut*. **2014**;63:1275-1283.

[116] Salzman NH, et al. Enteric defensins are essential regulators of intestinal microbial ecology. *Nat Immunol*. **2010**;11:76-83.

[117] Png CW, et al. Mucolytic bacteria with increased prevalence in IBD mucosa augment in vitro utilization of mucin by other bacteria. *Am J Gastroenterol*. **2010**;105:2420-2428.

[118] Lee HY, et al. Human originated bacteria, *Lactobacillus rhamnosus* PL60, produce conjugated linoleic acid and show anti-obesity effects in diet-induced obese mice. *Biochim Biophys Acta*. **2006**;1761:736-744.

[119] Dewulf EM, et al. Inulin-type fructans with prebiotic properties counteract GPR43 overexpression and PPARg-related adipogenesis in the white adiposetissue of high-fat diet-fed mice. *J Nutr Biochem*. **2011**;22,:712-722.

[120] Neyrinck, AM, et al. Prebiotic effects of wheat arabinoxylan related to the increase in *Bifidobacteria*, *Roseburia* and *Bacteroides/Prevotella* in diet-induced obese mice. *PLoS One*. **2011**;6:e20944.

been used in IBD conditions. For example, enteral nutrition with a fiber-rich formula in children suffering from Crohn's disease has been found to reduce intestinal inflammation and markedly improve gut microbial composition, leading to the hypothesis of a fiber-rich diet intervention to improve the patient's quality of life[121,122]. However, despite a great amount of data, the use of probiotics and prebiotics in human host to prevent and treat obesity and IBD remains still debated[123,124]. Thus, the limitations that usually are addressed to probiotic treatments involved the possible inflammatory activity in patients with immune-associated diseases, such as IBD. For this reason, non-viable bacterial products or metabolic by-products derived from probiotic strains (*i.e.,* SCFAs) are considered as an alternative for to both stimulate a health-associated GM configuration and limit the viable microorganisms use[125]. Recently, a novel microbial intervention has been proposed, the fecal microbial transplantation (FMT), in which a healthy donor GM is transplanted into a patient in order to positively modify the individual's own disease-associate microbiome[126]. The GM modulation by FMT principally follows the probiotic principle, but the patient will not be treated with specific strains, but instead with a fecal suspension infusion from a healthy donor[127]. Currently, this treatment is approved for recurrent *Clostridioides difficile* infections (*i.e.*, the updated name for *Clostridium difficile* infections) in adulthood, and is now also tested in

[121] Llewellyn SR, et al. Interactions between diet and the intestinal microbiota alter intestinal permeability and colitis severity in mice. *Gastroenterology*. **2018**;154:1037-1046.

[122] Chiba M, et al. Lifestyle-related disease in Crohn's disease: Relapse prevention by a semi-vegetarian diet. *World J Gastroenterol*. **2010**;16:2484-2495.

[123] Brusaferro A, et al. Is it time to use probiotics to prevent or treat obesity?. *Nutrients*. **2018**;10:1613.

[124] Lewis JD, Abreu MT. Diet as a trigger or therapy for inflammatory bowel diseases. *Gastroenterology*. **2017**;152:398-414.

[125] Wegh CAM, et al. Postbiotics and their potential applications in early life nutrition and beyond. *Int J Mol Sci*. **2019**;20:4673.

[126] Vieira AT, Fukumori C, Ferreira CM. New insights into therapeutic strategies for gut microbiota modulation in inflammatory diseases. *Clin Transl Immunol*. **2016**;5:e87.

[127] Borody TJ, Khoruts, A. Fecal microbiota transplantation and emerging applications. *Nat Rev Gastroenterol Hepatol*. **2011**;9:88-96.

different clinical procedures for treating numerous pathological conditions, ranging from metabolic and neoplastic to autoimmune disorders[128]. However, transplanting an entire community of microbes involves risks, such as the pathogen/pathobiont transmission with high risk of infections[129], as well as the incomplete long-term stabilization of an extraneous microbial configuration in a new unknown environment characterized by different genetic, immune, metabolic, and nutritional features[130]. To date, few FMT attempts have been performed to treat IBD and the general conclusion is that results are not consistent and sometimes are quite difficult to interpret, due to the non-complete remission of treated patients[131]. Further studies are still necessary to optimize and improve this technique and to increase FMT usage as clinical treatment beyond the *C. difficile* infections.

Summarizing all these findings, diet is nowadays one of the most known important driving forces able to shape the GM. Dietary interventions and targeted nutritional therapies, such as medical foods, dietary supplements, living microorganisms, as well as microbial metabolites and FMT, could provide a great promise for the prevention and treatment of microbiota-related diseases. However, much experimental research is needed before these opportunities can be fully realized. So, the ultimate goal of microbiome research should be to comprehensively describe the full host-GM landscape to guide precision approaches in the field of personalized medicine, such as the development of next-generation probiotics or specific microbial communities, tailored to address each individual issue.

---

[128] Shapiro H, Suez J, Elinav E. Personalized microbiome-based approaches to metabolic syndrome management and prevention. *J Diabetes*. **2017**;9:226-236.

[129] Lee JC, et al. Obesogenic diet-induced gut barrier dysfunction and pathobiont expansion aggravate experimental colitis. *PLoS ONE*. **2017;**12:e0187515.

[130] Suez J, Elinav E. The path towards microbiome-based metabolite treatment. *Nat Microbiol*. **2017**;2:17075.

[131] Rossen NG, et al. Fecal microbiota transplantation as novel therapy in gastroenterology: A systematic review. *World J Gastroenterol*. **2015**;21:5359-71.

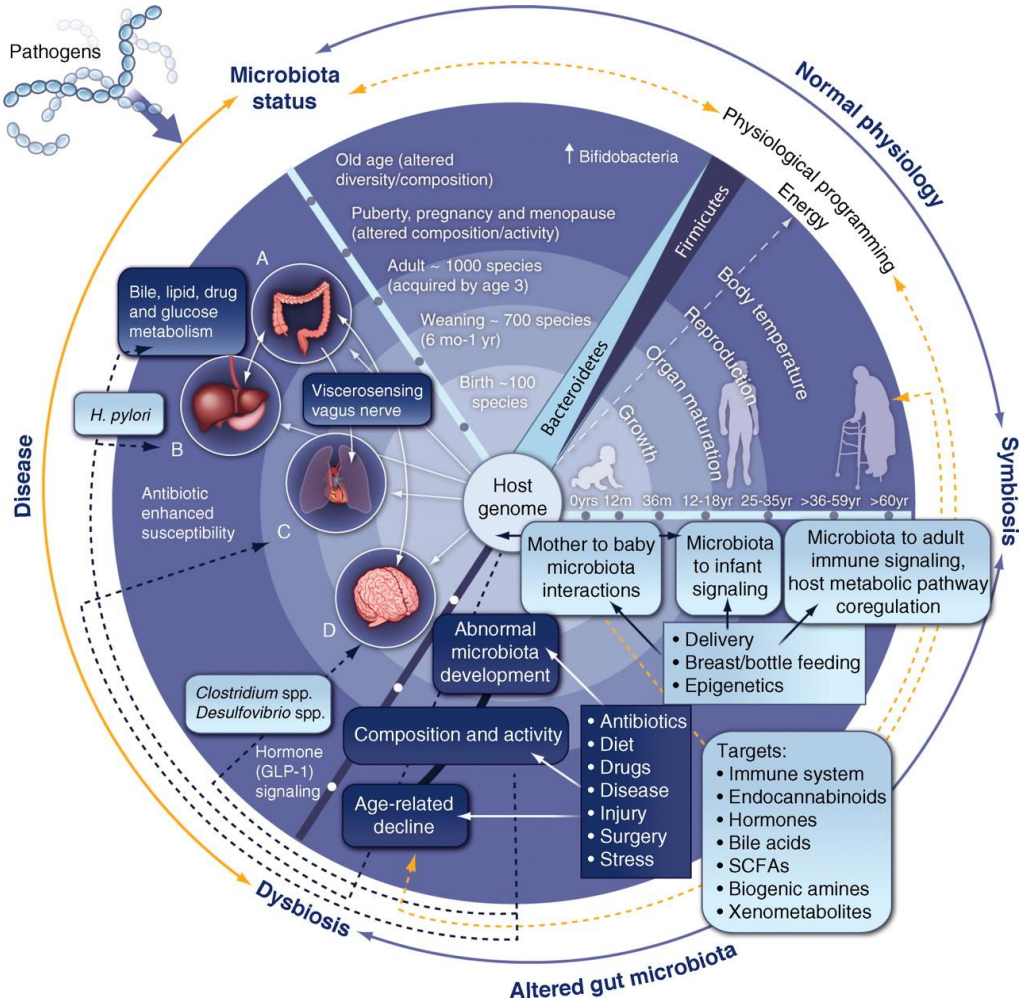

Figure 3. **The gut microbiota in development and disease.** The influence of the GM on human health is continuous from birth to old age. Early environmental factors (e.g., method of delivery), nutritional factors (e.g., breast or bottle-feeding), and epigenetic factors have been implicated in the development of a healthy gut and its microbial symbionts. Changes in gut microbial composition in early life can influence the risk for developing disease later in life. In adulthood, extrinsic factors (such as diet, stress, disease and injury) continuously influence the diversity and function of the GM with implications for human health. Disruption of the GM homeostasis can lead to a variety of different diseases, including (A) IBD, IBS and colorectal cancer; (B) gastric ulcers, nonalcoholic fatty liver disease, obesity and metabolic syndrome; (C) asthma, atopy, and hypertension; and (D) local and systemic hormone signaling[132].

[132] Nicholson JK. Host-gut microbiota metabolic interactions. *Science*. **2012**;336:1262-1267.

1.4 Analyzing the gut microbial ecosystem

The first preliminary studies aimed to characterize the human gut ecosystem were conducted by using well-known approaches of traditional microbiology that have recently evolved to culturomics (*i.e.*, a culturing technique that uses multiple culture conditions for the identification of microbial species)[133]. In parallel, novel culture methods and complex media with many supplements have been developed in order to mimic the natural environment of microorganisms in their ecological niche, including anaerobic conditions[134]. Nowadays, culturomics has been coupled with several methods to determine the taxonomic classification of microorganisms, from MALDI-TOF mass spectrometry to next-generation sequencing (NGS) approaches, a milestone in microbiome studies[135]. However, despite the large advantages in culturomic methods, what can be cultured is still biased, especially because any given culture condition will allow some bacteria to grow much faster than others[136]. For the past 15 years, the culture-independent amplicon analysis (*i.e.,* the amplification of a specific fragment of DNA by orders of magnitude) by using the polymerase chain reaction (PCR) coupled with NGS approaches has been the workhorse of the microbiome literature[137]. For this analysis, PCR primers match a specific gene, the bacterial 16S rRNA gene, in order to amplify all the variants that occur between the highly conserved regions used to design primers. The bacterial 16S rRNA gene contains 9 hypervariable regions (from V1 to V9), interspersed with highly conserved regions, that contain the

---

[133] Button DK, et al. Viability and isolation of marine bacteria by dilution culture: theory, procedures, and initial results. *Appl Environ Microbiol*. **1993**;59:881-891.

[134] Lagier JC, et al. Culturing the human microbiota and culturomics. *Nat Rev Microbiol*. **2018**;16:540-550.

[135] Allaband C, et al. Microbiome 101: Studying, analyzing, and interpreting gut microbiome data for clinicians. *Clin Gastroenterol Hepatol*. **2019**;17:218-230.

[136] Browne HP, et al. Culturing of 'unculturable' human microbiota reveals novel taxa and extensive sporulation. *Nature*. **2016**;533:543-546.

[137] Tringe SG, Hugenholtz P. A renaissance for the pioneering 16S rRNA gene. *Curr Opin Microbiol*. **2008**;11:442-446.

genomic information to discriminate among different taxa. To this point, several platforms are used to read the genomic information, with the choice usually falling on Illumina ones (San Diego, CA)[138]. In particular, in the Illumina sequencing approach, the DNA (e.g., the 16S rRNA amplicon) is bounded by two adapters to a flow cell and going to a bridge amplification process that generates a cluster of clonal populations. During this clonal amplification, a fluorescent labeled deoxyribonucleotide triphosphate is attached and detected by fluorophore excitation and read from the platform. In these molecular approaches, among the variables, it is very important to choose the right amplicon primers, because there are some differences between microbiome profiles according to the PCR primers used. The Human Microbiome Project consortium recommends V1 to V3 or V3 to V5 region-specific primers[139]. In general, the specific region amplified is much more important that the length of the fragment and a long sequence with biased primers can lead to incorrect results[140]. Another consideration should be done on the taxonomic assignment of 16S rRNA gene sequences. Several reference databases have been built over the years, resulting in a different bacterial nomenclature assigned to the same DNA sequence depending on the database used. In the past, this was a huge problem, but recent cooperation between rRNA-based taxonomy databases, such as SILVA[141], RDP[142] and Greengenes[143], has reduced this problem leading to greater consistency between results. Furthermore, what should be kept

[138] Caporaso JG, et al. Ultra-high throughput microbial community analysis on the Illumina HiSeq and MiSeq platforms. *ISME J.* **2012**;6:1621-1624.

[139] Human Microbiome Project Consortium. Structure, function and diversity of the healthy human microbiome. *Nature*. **2012**;486:207-214.

[140] Soergel DA, et al. Selection of primers for optimal taxonomic classification of environmental 16S rRNA gene sequences. *ISME J.* **2012**;6:1440-1444.

[141] Pruesse E, et al. SILVA: a comprehensive online resource for quality checked and aligned ribosomal RNA sequence data compatible with ARB. *Nucleic Acids Res.* **2007**;35:7188-7196.

[142] Cole JR, et al. Ribosomal Database Project: data and tools for high throughput rRNA analysis. *Nucleic Acids Res.* **2014**;42:D633-D642.

[143] McDonald D, et al. An improved Greengenes taxonomy with explicit ranks for ecological and evolutionary analyses of bacteria and archaea. *ISME J.* **2012**;6:610-618.

in mind is that many microbial species are very similar along the full length of the 16S rRNA gene and this makes it impossible to obtain reliable information down to species level by using this approach[144]. Although 16S rRNA gene sequencing has enabled a great part of scientific research on the microbiome, mere knowledge of bacterial genera and their relative abundance is not as useful for clinical analysis. The reason is that each genus can include a wide range of strains that are genetically distinct. An example is given even within the same species: the microorganism *E. coli* has a circular genome that can fluctuate from 4 to 6 million base pairs with several thousand distinct genes, some of which can be virulent. As a result, there are thousands of known strains of *E. coli* that have been sequenced and found to be genetically distinct, including at least one strain used as a probiotic (e.g., *E. coli* strain Nissle 1917) and another that can cause debilitating illness (e.g., *E. coli* strain O157)[145].

The contrast to the use of a single gene to perform the taxonomic classification of microorganisms, the metagenomic approach can be far more useful. This method involves a fragmentation of all the DNA, the sequencing of all these fragments and then puzzling them together to get a complete view of the microbial community, including its genomes[146]. The advantage of the shotgun metagenomic approach is that it allows the profiling of all the microorganisms present in a given sample, also including fungi and viruses, which cannot be characterized by 16S rRNA gene sequencing. Of course, producing this magnitude of data is more expensive than the amplicon-based approach, but with the progressive decrease in library preparation and sequencing costs, this technique is becoming much

[144] Wang Q, et al. Naive Bayesian classifier for rapid assignment of rRNA sequences into the new bacterial taxonomy. *Appl Environ Microbiol*. **2007**;73:5261-5267.

[145] Ogura Y, et al. Extensive genomic diversity and selective conservation of virulence-determinants in enterohemorrhagic *Escherichia coli* strains of O157 and nonO157 serotypes. *Genome Biol.* **2007**;8:R138.

[146] Riesenfeld CS, Schloss PD, Handelsman J. Metagenomics: genomic analysis of microbial communities. *Annu Rev Genet.* **2004**;38:525-552.

more accessible on a large scale. In addition, the amount of DNA required to perform the library preparation step can be less than one nanogram, allowing this approach to be used even for low-biomass samples, such as biopsies[147].

Leaving aside the genomic part of the microbiome landscape, another challenge is to determine the activity and functions of the whole microbiome-set. Metatranscriptomics and metaproteomics, *i.e.*, the sequencing of transcribed RNA and mass spectrometry-based approaches to sort out the proteins, respectively, are tremendously promising but still very difficult to be implemented. There are several limitations to these techniques, such as the reduced half-life time of bacterial transcripts, which usually last a few minutes[148]. Although these techniques are rapidly improving, they should be considered emerging approaches rather than ready for routine use. Furthermore, transcriptional studies necessarily require the association with metagenomic data from the same sample to normalize the expression of a particular gene on representation in the community[149].

The last, but not least, approach that can be bent to the whole microbiome world is metabolomics, *i.e.,* the study of small molecules, other than proteins, including products of bacterial metabolism, by using combined gas chromatography or liquid chromatography–mass spectrometry or nuclear magnetic resonance (NMR) methods. There are two main approaches for metabolomics analysis: targeted and untargeted metabolomics. In the targeted metabolomics there is a list of molecules leading to a most sensitive approach for detecting already known molecules of interest but for these reason does not allow for new

---

147 Allaband C, et al. Microbiome 101: Studying, analyzing, and interpreting gut microbiome data for clinicians. *Clin Gastroenterol Hepatol*. **2019**;17:218-230.

148 Har-El R, et al. Synthesis and degradation of lac mRNA in *E. coli* depleted of 30S ribosomal subunits. *Mol Gen Genet*. **1979**;173:135-144.

149 Segata N, et al. Computational metaomics for microbial community studies. *Mol Syst Biol*. **2013**;9:666.

discoveries[150,151]. However, most of the microbiome-derived molecules still remain to be discovered and therefore cannot be analyzed via targeted methods. On the other hand, untargeted metabolomics aims to detect as many metabolites as possible. The main challenge for untargeted metabolomics is the annotation of these metabolites. Moreover, this approach can fail to annotate molecules that are modified by the microbiome or host metabolism. For example, untargeted metabolomics is the preferable approach to determine the concentration of fecal SCFAs, such as butyrate, propionate and acetate, which are known to play an important physiological role in the GM-host relationship[152,153]. Once again, as the combination approach of culturomics and sequencing, the current preferred methods for microbiome analysis are associations of different approaches, such as shotgun metagenomics and metabolomics, that could provide a readout of the whole microbial composition and metabolism. Major considerations and summary of most of the common bioinformatics tools used to analyze each type of microbiome data explained so far are displayed in **Figure 4**.

Once the right microbiome approach or a combination of approaches has been chosen, it is important to understand how to analyze the microbiome data. For both 16S rRNA gene sequencing and metagenomics, everything is centered around microbiome diversity: alpha-diversity (*i.e.,* diversity within communities), which is often estimated as the number of species in a community (*i.e.,* species richness), and beta-diversity (*i.e.,* partitioning of diversity among communities), which is usually based on the number of shared species,

[150] Melnik AV, et al. Coupling targeted and untargeted mass spectrometry for metabolome-microbiome-wide association studies of human fecal samples. *Anal Chem*. **2017**;89:7549–7559.

[151] Aksenov AA, et al. Global chemical analysis of biology by mass spectrometry. *Nat Rev Chem*. **2017**;1:0054.

[152] Watrous J, et al. Mass spectral molecular networking of living microbial colonies. *Proc Natl Acad Sci USA*. **2012**;109:E1743-E152.

[153] Wang M, et al. Sharing and community curation of mass spectrometry data with Global Natural Products Social Molecular Networking. *Nat Biotechnol*. **2016**;34:828-837.

sometimes also considering the relative abundance of each microorganism in each group of samples. Particularly, alpha-diversity is usually characterized using the total number of species (richness), the relative abundance of species (evenness), or indexes that combine these two dimensions. For example, for species richness, observed_species, Chao1 and Faith's Phylogenetic Diversity (PD) are commonly used, whereas for both evenness and richness, Shannon and Simpson indexes play a major role. On the other hand, the partitioning of biological diversity among communities or along an environmental gradient (beta-diversity) is often characterized using the number of species shared between two or more communities. Beta-diversity metrics can be quantitative (using sequence abundance, e.g., Bray-Curtis or weighted UniFrac) or qualitative (considering only presence-absence of sequences, e.g., binary Jaccard or unweighted UniFrac). Moreover, microbiome data can also be clustered based on phylogeny (both UniFrac metrics) or not (Bray-Curtis, etc.). The most commonly used visualization method for alpha-diversity is a boxplot, as well as a violin plot and so on. For all beta-diversity metrics, a principal coordinates analysis (PCoA) is usually performed, in which points that are closer to each other represent microbial communities that are more similar in composition[154,155].

Although there is undoubtedly great interest in the microbiome, there is still a long way to go before we fully understand the complete host-GM landscape, with the final aim of improving each of these approaches in order to use the microbes for a better daily life, as well as in different aspects of the clinical field.

[154] Lozupone CA, Knight R. Species divergence and the measurement of microbial diversity*. FEMS Microbiol Rev*. **2008**;32:557-578.
[155] Goodrich JK, et al. Conducting a microbiome study. *Cell.* **2014**;158:250-262.

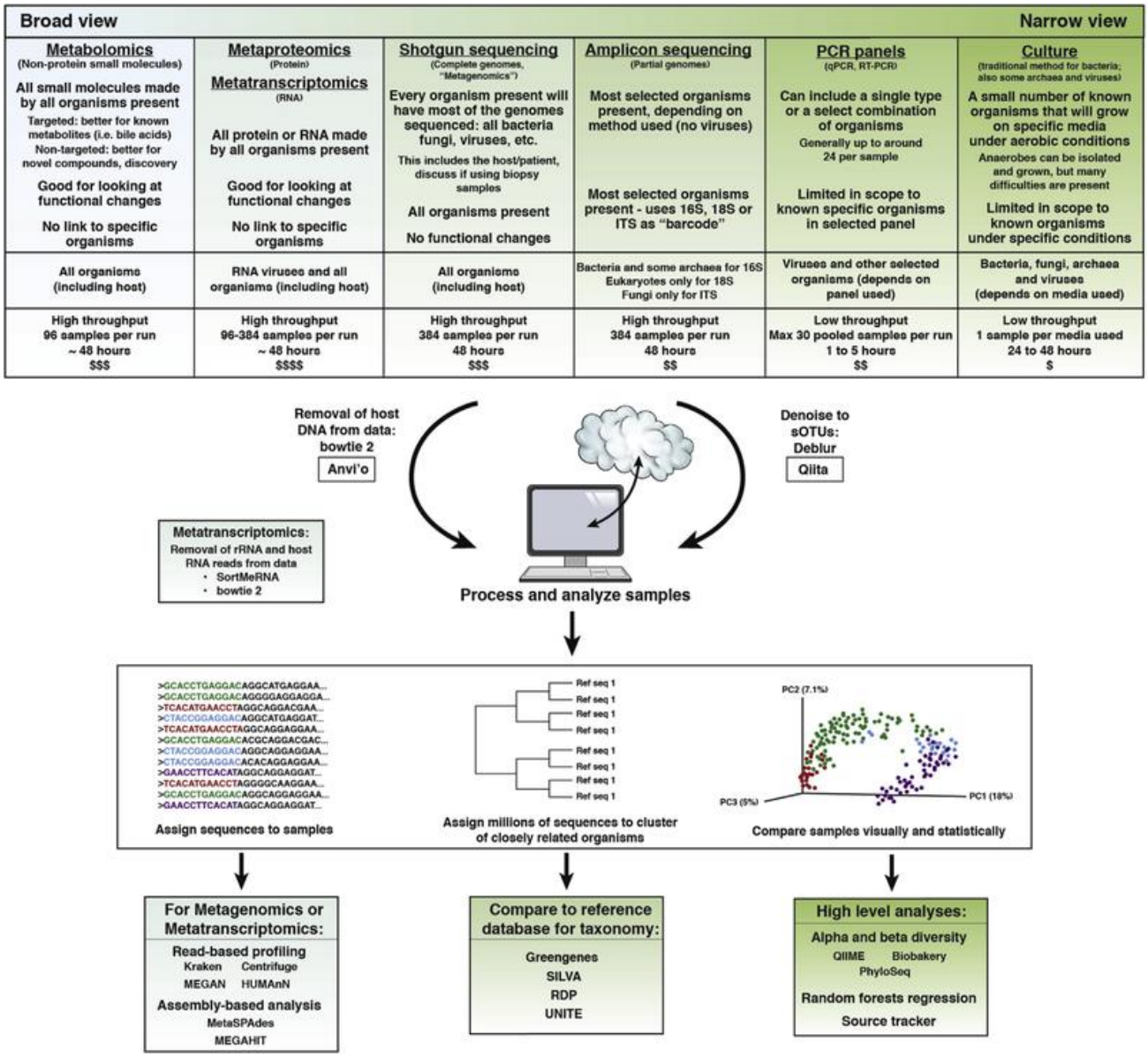

Figure 4. Summary of all the approaches useful in order to study the human microbiome, adapted from Allaband et al.[156]. Once samples are collected, they are processed and subjected to DNA sequencing to generate microbiome data. Two common types of protocols are amplicon sequencing and shotgun sequencing. In amplicon sequencing, PCR primers are used to target a specific region of a specific gene, focusing sequencing effort on just those fragments. One of the most widely used protocols targets the V3-V4 regions of the 16S rRNA gene[157]. In shotgun sequencing, the DNA in the sample is randomly sheared and sequenced, generating data from many different parts of the genomes. The specifics of the molecular protocol used before shotgun sequencing are important for what type of data is being examined, and this type of sequencing can be used,

[156] Allaband C, et al. Microbiome 101: Studying, analyzing, and interpreting gut microbiome data for clinicians. *Clin Gastroenterol Hepatol*. **2019**;17:218-230.

[157] Human Microbiome Project Consortium. Structure, function and diversity of the healthy human microbiome. *Nature*. **2012**;486:207-214.

for example, for metagenomics and metatranscriptomics. The initial processing performed on the data after sequencing depends on the type of sequencing performed. For amplicon studies, a common strategy is to upload the data into QIIME2[158] and use DADA2[159] to resolve sequence data into amplicon sequence variants (ASVs). Depending on the amplicon target, taxonomic assignments are generally performed against reference databases using naive Bayes classifiers, such as Greengenes[160], SILVA[161], RDP[162], or UNITE[163] (for fungal internal transcribed spacer [ITS]). Shotgun sequencing of host-associated samples first requires preprocessing to remove host DNA before analysis. Typically, the shotgun data are then summarized using tools such as Kraken[164], MEGAN[165], or HUMAnN2[166] to generate taxonomic or functional profiles, or are assembled with tools such as metaSPAdes[167] and MEGAHIT[168]. For both sequencing methods, higher-level analyses (e.g., alpha and beta diversity, taxonomic profiling, and machine learning) are subsequently implemented to assess patterns of microbiome variation in the context of the study design. Culture dependent methods refer to traditional microbiology, as well as culturomics, that are used to grow microorganisms in their optimal conditions (*i.e.,* anaerobic atmosphere, complex media).

---

[158] Bolyen E, et al. Reproducible, interactive, scalable and extensible microbiome data science using QIIME 2. *Nat Biotechnol*. **2019**;37:852-857.

[159] Callahan BJ, et al. DADA2: High-resolution sample inference from Illumina amplicon data. *Nat Methods*. **2016**;13: 581-583.

[160] DeSantis TZ, et al. Greengenes, a chimera-checked 16S rRNA gene database and workbench compatible with ARB. *Appl Environ Microbiol*. **2006**;72:5069-5072.

[161] Pruesse E, et al. SILVA: a comprehensive online resource for quality checked and aligned ribosomal RNA sequence data compatible with ARB. *Nucleic Acids Res.* **2007**;35:7188-7196.

[162] Cole JR, et al. Ribosomal Database Project: data and tools for high throughput rRNA analysis. *Nucleic Acids Res.* **2014**;42:D633-D642.

[163] Koljalg U, et al. UNITE: a database providing web-based methods for the molecular identification of ectomycorrhizal fungi. *New Phytol.* **2005**;166:1063-1068.

[164] Wood DE, Salzberg SL. Kraken: ultrafast metagenomic sequence classification using exact alignments. *Genome Biol.* **2014**;15:R46.

[165] Huson DH, et al. MEGAN Community Edition interactive exploration and analysis of large-scale microbiome sequencing data. *PLoS Comput Biol*. **2016**;12:e1004957

[166] Abubucker S, et al. Metabolic reconstruction for metagenomic data and its application to the human microbiome. *PLoS Comput Biol.* **2012**;8:e1002358.

[167] Bankevich A, et al. SPAdes: a new genome assembly algorithm and its applications to single-cell sequencing. *J Comput Biol*. **2012**;19:455-477.

[168] Li D, et al. MEGAHIT: an ultra-fast single-node solution for large and complex metagenomics assembly via succinct de Bruijn graph. *Bioinformatics*. **2015**;31:1674-1676.

Chapter 2 – ROLE OF THE GUT MICROBIOME IN CANCER DEVELOPMENT AND CHEMOTHERAPY

As interest in gut microbial community and its contribution to host homeostasis continued to grow and the NGS-derived progress made it easier, new outlets on GM-host relationship have been made. In recent years, numerous evidences pointed towards the central role of commensal bacteria colonizing the gastrointestinal tract as key determinants of health or pathologic conditions, including cancer[169]. Indeed, in case of intestinal dysbiosis, bacterial pathogens can negatively affect both the host metabolism and the GM-host immune system functionalities, thereby triggering tumor growth[170]. Importantly, this loss of intestinal homeostasis has been linked with both local (*i.e.*, colorectal cancer, gastric cancer) [171] and distant tumors, such as pancreatic[172], laryngeal[173] and gallbladder[174] carcinoma. To date, microbial pathogens are known to drive 20% of tumorigenesis and a large number of malignancies are associated with commensal microbial imbalance or dysbiosis[175]. One of the first connection that has been established between cancer and gut microbiome concerned the development and progression of colorectal cancer (CRC)[176]. It is well-known that cancer development is a multistep process whose progression is associated with gradual

[169] Zhang YJ, et al. Impacts of gut bacteria on human health and diseases. *Int J Mol Sci*. **2015**;16:7493-7519.

[170] Rea D, et al. Microbiota effects on cancer: From risks to therapies. *Oncotarget*. **2018**;9:17915-17927.

[171] Sheflin AM, Whitney AK, Weir TL. Cancer-promoting effects of microbial dysbiosis. *Curr Oncol Rep*. **2014**;16:406.

[172] Farrell JJ, et al. Variations of oral microbiota are associated with pancreatic diseases including pancreatic cancer. *Gut*. **2012**;61:582-588.

[173] Gong HL, et al. The composition of microbiome in larynx and the throat biodiversity between laryngeal squamous cell carcinoma patients and control population. *PloS one*. **2013**;8:e66476.

[174] Sharma V, et al. Role of bile bacteria in gallbladder carcinoma. *Hepato-gastroenterology*. **2007**;54:1622.

[175] Bhatt AP, Redinbo MR, Bultman SJ. The role of the microbiome in cancer development and therapy. *CA Cancer J Clin*. **2017**;67:326-344.

[176] Candela M, et al. Inflammation and colorectal cancer, when microbiota-host mutualism breaks. *World J Gastroenterol*. **2014**;20:908-922.

accumulation of genetic and epigenetic casual mutations that are usually slow and can take more than 10 years depending on the mutation frequency. CRC carcinogenesis is sporadic for approximately 90% of cases and develops gradually from normal epithelium to adenomatous polyps until the settlement of an invasive carcinoma[177,178]. However, several genetic predispositions that can increase the risk of developing CRC have been identified, first of all the mutation of APC gene (adenomatous polyposis coli) that leads to familial adenomatous polyposis (FAP). Patients suffering from FAP are characterized by the development of hundreds to thousands of adenomatous colonic polyps beginning, on average, at 16 years of age and by age of 35 years, 95% of individuals with FAP have polyps along the entire gastrointestinal tract[179]. *In-vitro* and *in-vivo* models carrying the APC gene point mutation are commonly used to simulate colorectal carcinogenesis[180]. Furthermore, environmental factors have been shown to be involved in CRC onset, including diet, chronic inflammation (e.g., IBD) and the gut microbial community. Several studies have recently connected the GM dysbiosis with the CRC development, as the gut microbial ecosystem of CRC patients is significantly enriched in pro-inflammatory opportunistic pathogens, such as *Fusobacterium*, several members of *Enterococcaceae* family and *Campylobacter*, as well as several microorganisms associated with metabolic disorders (*i.e.*, *Collinsella* and

[177] Vogelstein B, Kinzler KW. Colorectal tumors. The Genetic Basis of Human Cancer. New York: McGraw-Hill, **1998**: 565-587.
[178] Mármol I, et al. Colorectal carcinoma: A general overview and future perspectives in colorectal cancer. *Int J Mol Sci*. **2017**;18:197.
[179] Jasperson KW, Patel SG, Ahnen DJ. APC-Associated Polyposis Conditions. **1998** [Updated in **2017**]. Seattle (WA): University of Washington, Seattle.
[180] McCart AE, Vickaryous NK, Silver A. Apc mice: models, modifiers and mutants. *Pathol Res Pract*. **2008**;204:479-90.

Erysipelotrichaceae taxa)[181,182,183]. On the other hand, a depletion has been observed of microbial partners usually associated with the maintenance of intestinal homeostasis, among these *Faecalibacterium* and *Roseburia*[184]. However, all these studies, although milestones in GM-associated CRC carcinogenesis literature, were purely observational and did not provide any information regarding the mechanisms by which members of the gut microbial ecosystem can influence CRC or, more importantly, the triggers that shift the microbiota towards a carcinogenic configuration. Most of these questions were answered by coupling NGS-based approaches with animal models, as the example of APC gene mutated mice to simulate CRC development, that helped us to better delineate the role of gut microbial actors in this story. Basically, recent year researches on this topic confirmed the bacterial driver-passenger model that Tjalsma et al.[185] developed in 2012. In brief, due to several environmental (*i.e.*, diet, pathogen infections) and genetic triggers (*i.e.*, chronic inflammation, mutations), the gut microbial ecosystem can shift its homeostatic profile to a dysbiosis-associated configuration which settles in the gastrointestinal tract. According to this model, this pro-inflammatory state can initiate CRC development by indigenous bacteria with pro-carcinogenic features (*i.e.*, bacterial drivers) that drive colonic epithelial DNA damage leading to colorectal carcinogenesis. In a subsequent step, the local microenvironment is altered as a consequence of the ongoing tumorigenesis, as well as the intestinal inflammatory state, and bacterial drivers are replaced by bacterial passengers,

---

[181] McCoy AN, et al. *Fusobacterium* is associated with colorectal adenomas. *PLoS One*. **2013**;8:e53653.

[182] Castellarin M, et al. *Fusobacterium nucleatum* infection is prevalent in human colorectal carcinoma. *Genome Res*. **2012**;22:299-306.

[183] Zheng J, et al. *Campylobacter* induced interleukin-8 secretion in polarized human intestinal epithelial cells requires *Campylobacter*-secreted cytolethal distending toxin- and Toll-like receptor-mediated activation of NF-kB. *Infect Immun*. **2008**;76:4498-4508.

[184] Louis P, Flint HJ. Diversity, metabolism and microbial ecology of butyrate-producing bacteria from the human large intestine. *FEMS Microbiol Lett*. **2009**;294:1-8.

[185] Tjalsma H, et al. A bacterial driver-passenger model for colorectal cancer: beyond the usual suspects. *Nat Rev Microbiol*. **2012**;10:575-582.

microorganisms showing a competitive advantage in the tumor microenvironment allowing for tumor progression[185]. The bacterial drivers that have been identified so far are mostly GM subdominant commensals characterized by pro-carcinogenic features, such as the capability of inducing a chronic inflammatory state, synthesizing genotoxins that can directly damage DNA, producing toxic metabolites and activating dietary heterocyclic amines to pro-carcinogenic compounds[186]. Some examples of these functions have been found in autochthonous intestinal microorganisms, such as superoxide-producing *Enterococcus faecalis* strains[187,188] or toxigenic strains belonging to *Bacteroides fragilis* species[189,190]. Furthermore, the mechanism of action of *Salmonella enterica* and some strains belonging to *E. coli* is noteworthy. These two microorganisms are characterized by genotoxic features dependent on the production of cytolethal distending toxins (CDTs) able to induce G(2)/M cell cycle arrest and double-strand DNA breaks, with the final outcome to increase frequency and accumulation of mutations, chromosomal aberrations and anchorage-independent growth, all common traits of carcinogenesis[191,192,193]. When this pro-inflammatory state is established, bacterial passengers, usually subdominant gastrointestinal commensals, are able to proliferate, but unlike drivers, which are always pro-carcinogenic, they can be of

---

[186] Candela M, et al. Inflammation and colorectal cancer, when microbiota-host mutualism breaks. *World J Gastroenterol*. **2014**;20:908-922.

[187] Huycke MM, Abrams V, Moore DR. *Enterococcus faecalis* produces extracellular superoxide and hydrogen peroxide that damages colonic epithelial cell DNA. *Carcinogenesis*. **2002**;23:529-536.

[188] de Almeida CV, Taddei A, Amedei A. The controversial role of *Enterococcus faecalis* in colorectal cancer. *Therap Adv Gastroenterol*. **2018**;11:1756284818783606.

[189] Toprak NU, et al. A possible role of *Bacteroides fragilis* enterotoxin in the aetiology of colorectal cancer. *Clin Microbiol Infect*. **2006**;12:782-786.

[190] Haghi F, et al. The association between fecal enterotoxigenic *B. fragilis* with colorectal cancer. *BMC Cancer*. **2019**;19:879.

[191] Lara-Tejero M, Galán JE. Cytolethal distending toxin: limited damage as a strategy to modulate cellular functions. *Trends Microbiol*. **2002**;10:147-152.

[192] Ge Z, et al. Bacterial cytolethal distending toxin promotes the development of dysplasia in a model of microbially induced hepatocarcinogenesis. *Cell Microbiol*. **2007**;9:2070-2080.

[193] Guerra L, et al. Bacterial genotoxin triggers FEN1-dependent RhoA activation, cytoskeleton remodeling and cell survival. *Journal of Cell Science*. **2011**;124:2735-2742.

either pro-carcinogenic or protective nature, depending on the type of microorganism. In some cases, the carcinogenic tissue has been shown to be selectively colonized by opportunistic pathogens, such as *Clostridium septicum*[194], *Fusobacterium nucleatum*[195] and *Streptococcus gallolyticus*[196], as well as several members of *Enterobacteriaceae* family[197], which can be involved in CRC progression. In other cases, the tumor environment is enriched in passenger bacteria well-known to be associated with health, as *Roseburia* and *Faecalibacterium*, suggesting a possible protective role for these microorganisms as CRC quencher[198] (**Figure 5**). In conclusion, inflammation is a trigger factor to initiate the GM-dependent pro-inflammatory loop harmful for host health[199]. An abnormal inflammatory response can shift the balance between symbiont and pathobiont microorganisms, by favoring the latter. Pathobionts can then work as bacterial drivers, consolidating the inflammatory state and further compromising the GM-host mutualism, as well as supporting CRC development. To this point, disease progression causes changes in the microenvironment as a result of the growing tumor and bacterial drivers are gradually outcompeted by gut commensals with either tumor-promoting or tumor-suppressing properties (*i.e.*, bacterial passengers), that can restore or consolidate the CRC-associated microbial environment[200,201].

---

[194] Wentling GK, et al. Unusual bacterial infections and colorectal carcinoma—*Streptococcus bovis* and *Clostridium septicum*: report of three cases. *Dis Colon Rectum*. **2006**;49:1223-1227.

[195] Kostic A.D., Chun E., Robertson L. *Fusobacterium nucleatum* potentiates intestinal tumorigenesis and modulates the tumor-immune microenvironment. *Cell Host Microbe*. **2013**;14:207-215.

[196] Boleij A, Tjalsma H. The itinerary of *Streptococcus gallolyticus* infection in patients with colonic malignant disease. *Lancet Infect Dis*. **2013**;13:719-724.

[197] Tjalsma H, et al. A bacterial driver-passenger model for colorectal cancer: beyond the usual suspects. *Nat Rev Microbiol*. **2012**;10:575-582.

[198] Marchesi JR, et al. Towards the human colorectal cancer microbiome. *PLoS One*. **2011**;6:e20447.

[199] Candela M, et al. Human intestinal microbiota: cross-talk with the host and its potential role in colorectal cancer. *Crit Rev Microbiol*. **2011**;37:1-14.

[200] Mazmanian SK, Round JL, Kasper DL. A microbial symbiosis factor prevents intestinal inflammatory disease. *Nature*. **2008**;453:620-625.

[201] Sansonetti PJ, Di Santo JP. Debugging how bacteria manipulate the immune response. *Immunity*. **2007**;26:149-161.

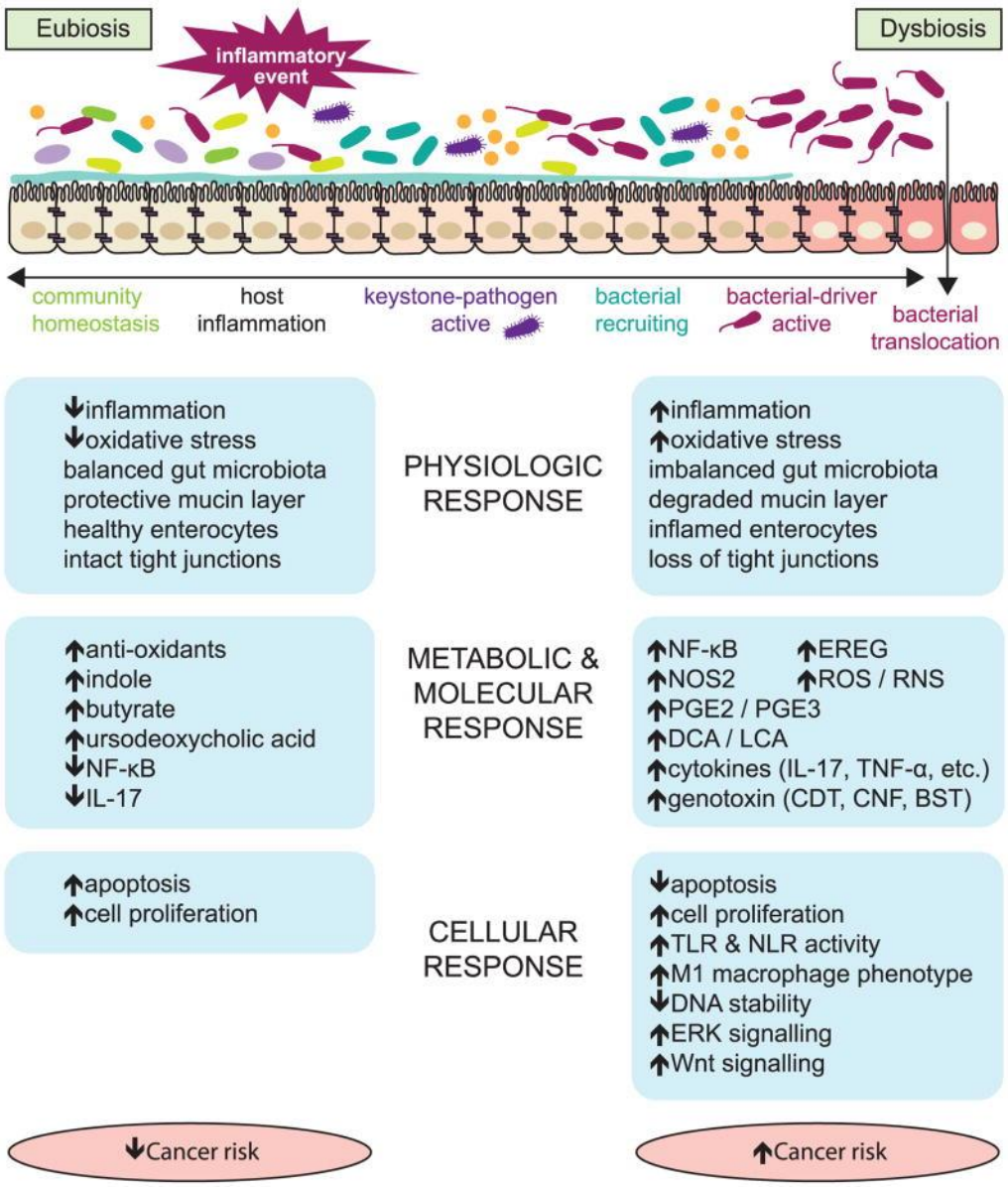

Figure 5. From balanced to imbalanced GM profile. The progression of the gut microbial community from a state of balance (eubiosis) to imbalance (dysbiosis) is associated with metabolic and cellular host responses that modulate cancer risk[202].

[202] Sheflin AM, Whitney AK, Weir TL. Cancer-promoting effects of microbial dysbiosis. *Curr Oncol Rep*. **2014**;16:406.

Beyond the direct involvement of the GM community in cancer development and progression, a new frontier in research is understanding the relationship between GM and drug metabolism (*i.e.*, pharmacomicrobiomics)[203], with the main focus on anti-cancer therapies. Along with chemotherapy and radiotherapy, a novel anti-cancer approach is the so-called targeted immunotherapy, bearing the dual role of both boosting the host anti-tumor immune response, and, at the same time, helping to hit cancer resistance and recurrence mechanisms[204,205]. In this field, the gut microbial community can modulate the host response to anti-cancer therapies through numerous mechanisms, including immune interactions and metabolism of xenobiotics[206]. In turn, these drugs can directly affect the GM-host mutualistic relationship[207]. For these reasons, it is important to identify the actors of the intricate GM-drugs relationship and find novel strategies to manipulate the gut microbial community in order to improve patients' therapeutic outcome, as final goal of this research. Targeted intervention on the gut microbial ecosystem may be pivotal to ameliorate the anti-cancer therapy-related toxicity, as well as to improve therapeutic efficacy[208,209].

The first step on microbiome in anti-cancer therapies has been done in 1890, when two heat-inactivated microorganisms belonging to *Streptococcus* were injected intratumorally as an attempt to cure cancer in human[210]. Several years later patients affected by bladder

---

[203] Rizkallah MR, Saad R, Aziz RK. The Human Microbiome Project, personalized medicine and the birth of pharmacomicrobiomics. *Curr Pharmacogenomics Pers Med*. **2010**;8:182-193.

[204] Emens LA, et al. Cancer immunotherapy: Opportunities and challenges in the rapidly evolving clinical landscape. *Eur J Cancer*. **2017**;81:116-129.

[205] Toh HC. Cancer immunotherapy-the end of the beginning. *Chin Clin Oncol*. **2018**;7:12.

[206] Alexander JL, et al. Gut microbiota modulation of chemotherapy efficacy and toxicity. *Nat Rev Gastroenterol Hepatol*. **2017;**14:356-365.

[207] Roy S, Trinchieri G. Microbiota: A key orchestrator of cancer therapy. *Nat Rev Cancer*. **2017**;17:271-285.

[208] Nayak RR, Turnbaugh PJ. Mirror, mirror on the wall: Which microbiomes will help heal them all?. *BMC Med*. **2016**;14:72.

[209] Fessler JL, Gajewski TF. The microbiota: A new variable impacting cancer treatment outcomes. *Clin Cancer Res*. **2017**;23:3229-3231.

[210] McCarthy EF. The toxins of William B. Coley and the treatment of bone and soft-tissue sarcomas. *IOWA Orthop J*. **2006**;26:154-158.

carcinoma were injected intratumorally with *Mycobacterium bovis* right after the tumor resection. In this study, it has been observed that in treated patients this microorganism was able to reduce tumor relapse by inducing a local immune response[211]. Moreover, the oral administration of the well-known probiotic *Lactobacillus casei* was associated with the decrease of superficial bladder carcinoma recurrence[212]. All these studies highlighted that the mechanism behind the anti-tumor responses was the microbial stimulation of host's natural killer cells and macrophages, two important immune system effectors[213]. Although these are old and rudimental studies, they paved the way for many published and ongoing clinical trials based on attenuated gut microorganisms to favor anti-cancer treatments. Recently, it has been observed in several refractory solid tumors that different microorganisms, such as *Mycobacterium obuense*[214,215] and genetically-modified *Salmonella typhimurium*[216,217], promote anti-cancer responses by both activating the host's immune system and exerting a cytotoxic effect on tumor cells. However, although very promising, many clinical trials are still needed to improve these therapies and limit bacterial-associated toxicity, mainly correlated with the long microbial half-life[218].

---

[211] Zbar B, et al. Tumor immunity produced by the intradermal inoculation of living tumor cells and living *Mycobacterium bovis* (strain BCG). *Science*. **1970**;170;1217-1218.

[212] Aso Y, Akazan H. Prophylactic effect of a *Lactobacillus casei* preparation on the recurrence of superficial bladder cancer. BLP Study Group. Urol. Int. 1992, 49, 125–129.

[213] Hoesl CE, Altwein JE. The probiotic approach: An alternative treatment option in urology. Eur. Urol. 2005, 47, 288–296.

[214] Stebbing J, et al. An intra-patient placebo-controlled phase I trial to evaluate the safety and tolerability of intradermal IMM-101 in melanoma. *Ann Oncol*. **2012**;23:1314-1319.

[215] Dalgleish AG, et al. Randomised, open-label, phase II study of gemcitabine with and without IMM-101 for advanced pancreatic cancer. *Br J Cancer*. **2016**;115:789-796.

[216] Toso JF, et al. Phase I study of the intravenous administration of attenuated *Salmonella typhimurium* to patients with metastatic melanoma. *J Clin Oncol*. **2002**;20:142-152.

[217] Nemunaitis J, et al. Pilot trial of genetically modified, attenuated *Salmonella* expressing the *E. coli* cytosine deaminase gene in refractory cancer patients. *Cancer Gene Ther*. **2003**;10:737-744.

[218] Kramer MG, et al. Bacterial therapy of cancer: Promises, limitations, and insights for future directions. *Front Microbiol*. **2018**;9:16.

Beyond the direct intratumoral role of specific microorganisms, the gut microbial community has recently been associated with the therapeutic outcome in different types of treatments[219]. Since the discovery of the cytotoxic effects of mustard gas during the Second World War, chemotherapeutic agents based on cytotoxic actions have been developed (*i.e.*, alkylating agents, platinum-based drugs, cytotoxic antibiotics) and are still the major staple of anti-cancer therapy[220]. However, several malignances are linked with the development of resistance to therapy that is considered the first cause of failure of available anti-cancer treatments, as well as subsequent tumor relapse. In order to fight these resistances, novel approaches are in continuous progress[221]. An example is given by the development of targeted immunotherapy[222]. The research focused on the GM involvement in anti-cancer therapies followed the same vein. The first studies highlighted the ability of intestinal microorganisms to affect drug pharmacokinetics, anti-cancer activity and toxicity in chemotherapy treatments at various levels[223] (**Figure 6**). Indeed, it has been shown that the anti-tumor effect of oxaliplatin or cisplatin treatment on subcutaneous transplantable tumors is dramatically decreased in germ-free mice or gut microbial-depleted mice by broad-spectrum antibiotics. The explanation of this platinum resistance can be found in the role of commensal microbiome members to promote oxidative stress and, afterwards, the apoptosis of tumor cells. As a direct consequence, in the absence of a healthy gut microbial ecosystem, there is a decreased GM-dependent reactive oxygen species (ROS) production, thus a less

[219] Schwabe RF, Jobin C. The microbiome and cancer. *Nat Rev Cancer*. **2013**;13:800-812.

[220] DeVita VT, Chu E. A history of cancer chemotherapy. *Cancer Res*. **2008**;68:8643-8653.

[221] McGranahan N, Swanton C. Biological and therapeutic impact of intratumor heterogeneity in cancer evolution. *Cancer Cell*. **2015**;27:15-26.

[222] Toh HC. Cancer immunotherapy-the end of the beginning. *Chin Clin Oncol*. **2018**;7:12.

[223] Dzutsev A, et al. The role of the microbiota in inflammation, carcinogenesis, and cancer therapy. *Eur J Immunol*. **2015**;45:17-31.

effective chemotherapeutic response[224]. Consistently, in mice affected by lung tumors and treated with antibiotic-coupled cisplatin therapy, long-term survival is decreased with the development of bigger tumors. In contrast, when cisplatin is combined with probiotic administration, such as *Lactobacillus acidophilus,* these animal models showed an improved response to therapy. Probiotics intake during chemotherapy promotes the activation of pro-apoptotic genes within the tumor mass and the enhancement of host's immune response[225]. Similar to platinum-derived drugs, the alkylating agent cyclophosphamide coupled with oral bacterial administration (*i.e.*, *Lactobacillus johonsoni* and *Enterococcus hirae*) leads to the conversion of T cells from naïve to pro-inflammatory T helper 17, with the final effect of improving cyclophosphamide efficacy in tumor-bearing mice[226,227]. The intestinal presence of *E. hirae* and *Barnesiella intestinihominis* correlated with a more favorable prognosis in patients with advanced lung or ovarian cancer treated with chemo-immunotherapy, confirming the role of the gut microbial community[228].

As the chemotherapy resistance has caught on, recent anti-cancer researches focused mostly on immunotherapy but still with limited results due to the variability of immune response in patients and the diverse susceptibility of tumor types[229]. In this scenario, the gut microbial ecosystem had a predominant role by pushing the scientific literature on novel aspects of the GM-anti-cancer relationship. Indeed, it has been shown that the administration

---

[224] Iida N, et al. Commensal bacteria control cancer response to therapy by modulating the tumor microenvironment. *Science*. **2013**;342:967-970.

[225] Gui QF, et al. Well-balanced commensal microbiota contributes to anti-cancer response in a lung cancer mouse model. *Genet Mol Res*. **2015**;14:5642-5651.

[226] Zitvogel L, et al. Mouse models in oncoimmunology. *Nat Rev Cancer*. **2016**;16:759-773.

[227] Ivanov II, et al. Specific microbiota direct the differentiation of IL-17-producing T-helper cells in the mucosa of the small intestine. *Cell Host Microbe* **2008**;4:337.

[228] Daillere R, et al. *Enterococcus hirae* and *Barnesiella intestinihominis* facilitate cyclophosphamide-induced therapeutic immunomodulatory effects. *Immunity*. **2016**;45:931-943.

[229] Mellman I, Coukos G, Dranoff G. Cancer immunotherapy comes of age. *Nature*. **2011**;480:480-489.

of CpG oligodeoxynucleotides, synthetic molecules mimicking bacterial DNA, can strongly stimulate the immune system, showing anti-tumor activity in several types of cancer[230]. It has been proved by performing *in-vivo* intra-tumoral injection of CpG oligodeoxynucleotides administered together with an anti-interleukin-10 receptor (IL-10R) antibody, an increase of TNF production from immune system cells at the tumor site, and, in turn, the tumor growth reduction by hemorrhagic necrosis. Moreover, in antibiotic-treated mice, the administration of specific microorganisms, such as *Alistipes shahii* and *Ruminococcus* genus, favored TNF production with notable improvement in the therapeutic outcome[231]. Gut microbiome members are also involved in the intrinsic efficacy of another class of immunotherapy drugs able to treat several types of solid tumors, known as immune checkpoint inhibitors. These novel anti-cancer agents consist of molecules able to block immune-inhibitory pathway, thus modulating T cells activation against tumor target cells[232,233,234]. The currently used checkpoint inhibitors are monoclonal antibodies targeting cytotoxic T lymphocyte-associated antigen 4 (CTLA4) or the programmed cell death 1 (PD1) located on T cell surfaces, as well as its ligand (*i.e.*, programmed cell death ligand 1, PD-L1)[235]. While anti-CTLA4 therapy is able to regulate the T cell proliferation early during the immune response within the lymph nodes, anti-PD1 suppresses the T cell activation later in the body

[230] Jahrsdörfer B, Weiner GJ. CpG oligodeoxynucleotides as immunotherapy in cancer. *Update Cancer Ther*. **2008**;3,:27-32.

[231] Iida N, et al. Commensal bacteria control cancer response to therapy by modulating the tumor microenvironment. *Science*. **2013**;342:967-970.

[232] Routy B, et al. Gut microbiome influences efficacy of PD-1-based immunotherapy against epithelial tumors. *Science*. **2018**;359:91-97.

[233] Gopalakrishnan V, et al. Gut microbiome modulates response to anti-PD-1 immunotherapy in melanoma patients. *Science*. **2018**;359:97-103

[234] Matson V, et al. The commensal microbiome is associated with anti-PD-1 efficacy in metastatic melanoma patients. *Science*. **2018**;359:104-108.

[235] Chen Q, et al. Delivery strategies for immune checkpoint blockade. *Adv Healthc Mater*. **2018**;7:e1800424.

periphery[236]. A recent study from Vetizou and colleagues demonstrated that subcutaneous tumor responds poorly to anti-CTLA4 therapy in antibiotic-treated or germ-free mice, but the response is significantly increased when the gut microbial community is enriched in *B. fragilis* and *Burkholderia cepacia*[237]. Furthermore, oral feeding with either *Bacteroides thetaiotaomicron* or *B. fragilis* to microbiota-depleted mice restores the therapeutic response to anti-CTLA4 by inducing immune cell response in tumor-draining lymph nodes. The feeding of mice with combined *B. fragilis* and *B. cepacia* also restores the therapeutic response to anti-CTLA4, but unlike single administration of *Bacteroides* taxa, the combined treatment also significantly decreases the extent of intestinal damage and colitis associated with the anti-tumor response[237]. These studies were confirmed in patients affected by melanoma and treated with anti-CTLA4, where the increased abundance of the Bacteroidetes phylum was associated with a reduction of therapy-associated colitis, while the underrepresentation of these bacterial taxa was associated with increased risk of colitis. By studying the gut bacterial profile of these patients, three different configurations have been found; the first one dominated by *Prevotella* spp., whereas the other two were mostly driven by different *Bacteroides* spp. When transferring the fecal microbiota from patients with each of the three configurations to germ-free mice, only the microbial profile characterized by an enrichment in *B. thetaiomicron* or *B. fragilis* resulted in a high responsiveness to anti-CTLA4 treatment. These observations strongly indicate that some members of the gut microbial community can affect the immunotherapy response and that altering non-responder compositions could favor the anti-tumor activity[237]. On the same line,

[236] Buchbinder EI, Desai A. CTLA-4 and PD-1 pathways: Similarities, differences, and implications of their inhibition. *Am J Clin Oncol.* **2016**;39:98-106.

[237] Vétizou M, et al. Anticancer immunotherapy by CTLA-4 blockade relies on the gut microbiota. *Science*. **2015**;350:1079-1084.

Sivan et al. discovered that in melanoma-bearing mice the PD-L1-targeted antibody efficacy is improved in the presence of an enriched gut microbial profile with different *Bifidobacterium* species, including *B. breve*, *B longum* and *B. adolescientis*. Indeed, the oral administration with a commercially available cocktail of probiotics (*i.e.*, *B. breve* and *B. longum*) combined with the anti-PD-L1 antibody, is able to boost the immune T cell response and stop the tumor growth[238]. Multiple translational studies have been performed from this moment onwards, supporting these findings. In particular, Routy et al. integrated the discoveries about the anti-PD-L1 therapy that were obtained only in animal models. They found that melanoma patients treated with antibiotics during the anti-PD-L1 immunotherapy had a lower survival rate. Importantly, metagenomics analysis has been performed on the patients' GM, showing a difference in the gut microbial profile between responders and non-responders to therapy. Anti-PD-L1 responders were enriched in two bacterial taxa (*i.e.*, *Akkermansia* and *Alistipes*). By performing fecal microbial transplantation (FMT) from patients to germ-free mice, the authors found that *Akkermansia muciniphila* (alone or in combination with *E. hirae*) was able to increase intra-tumoral cytotoxic T cell infiltrates, thus increasing the PD-1 blockade response in mice[239]. In parallel, the same compositional difference between responders and non-responders to anti-PD-L1 therapy was confirmed by Gopalakrishnan et al.[240]. The authors observed that melanoma-therapy responders were characterized by higher microbial diversity, as well as the increase of relative abundance of both *Ruminococcaceae* and *Faecalibacterium*, being associated with improved effector T cell function in the peripheral and intra-tumor microenvironment. In contrast, patients

[238] Sivan A, et al. Commensal *Bifidobacterium* promotes antitumor immunity and facilitates anti-PD-L1 efficacy. *Science*. **2015**;350:1084-1089.

[239] Routy B, et al. Gut microbiome influences efficacy of PD-1-based immunotherapy against epithelial tumors. *Science*. **2018**;359:91-97.

[240] Gopalakrishnan V, et al. Gut microbiome modulates response to anti-PD-1 immunotherapy in melanoma patients. *Science*. **2018**;359:97-103.

characterized by poor immunotherapy response showed a lower microbial diversity and higher relative abundance of Bacteroidales, correlating with impaired systemic and anti-tumor immune responses[240]. Along the same line, Matson et al. performed another gut microbial metagenomic characterization from melanoma patients treated with immune checkpoint inhibitors, further corroborating the finding that responders showed a different microbiome compared to those not responding to therapy. They identified and functionally proved *in-vivo* the importance of *B. longum*, *Enterococcus faecium* and *Collinsella aerofaciens* in ameliorating anti-PD-L1 efficacy[241]. Even if the last decade witnessed massive advances in unveiling the role of gut microbiome in cancer and other diseases, there are still many obstacles for translating basic microbiome research into therapeutic applications. Despite the novel studies reported above, these findings were performed only in small cohorts and in limited types of cancer, so each of these microbiome-targeted therapies still need to be carefully evaluated, leaving the road still open to new research outlets.

[241] Matson V, et al. The commensal microbiome is associated with anti-PD-1 efficacy in metastatic melanoma patients. *Science*. **2018**;359:104-108.

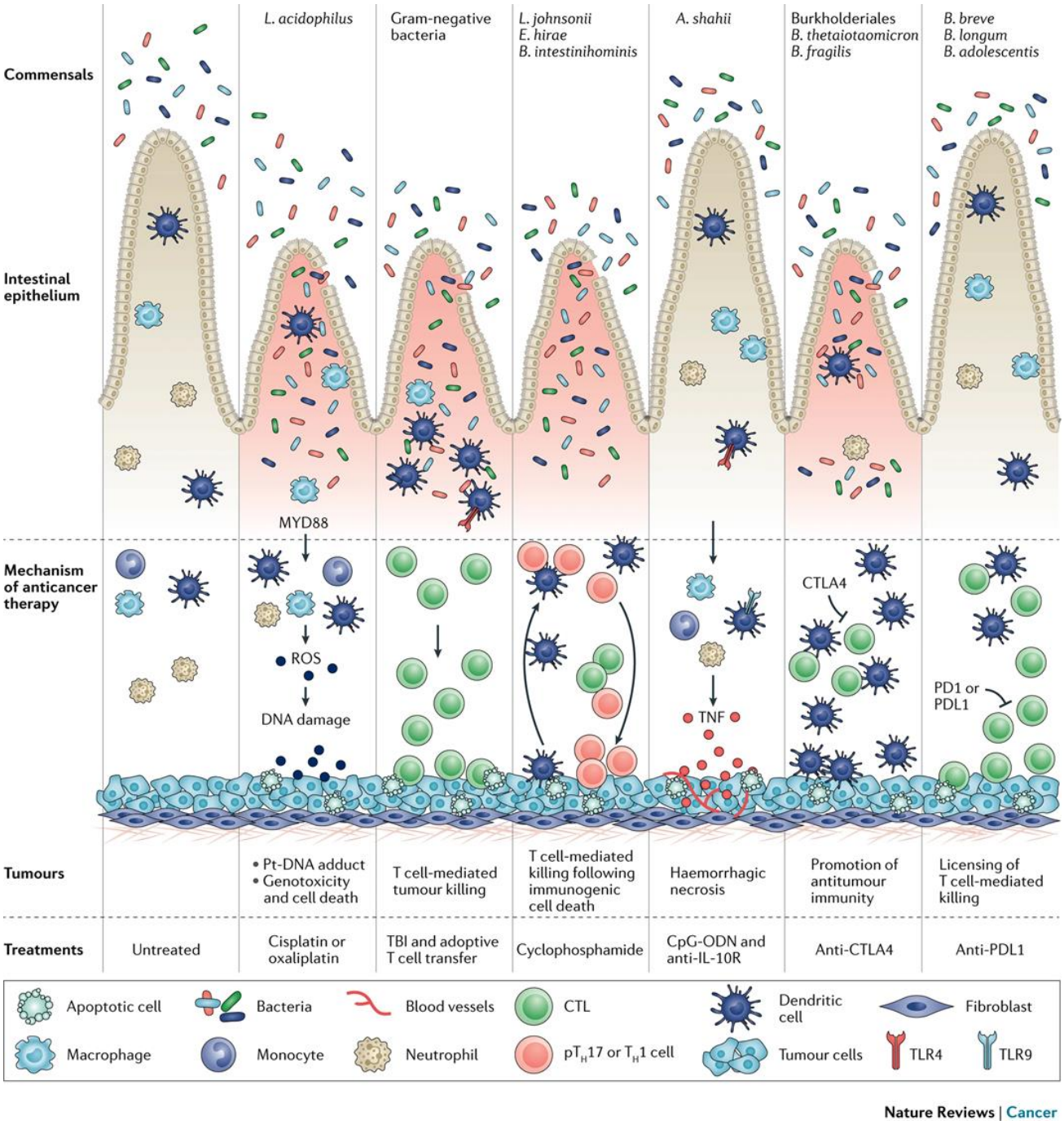

Figure 6. **How the GM regulates anti-cancer therapies**[242]. In physiological conditions, the commensals in the intestinal lumen are prevented from translocating through the intestinal mucosa by an intact epithelial barrier covered by a mucus layer that is poorly permeable to microorganisms. Treatment with platinum (Pt) drugs, total body irradiation (TBI), cyclophosphamide (CTX) and anti-cytotoxic T lymphocyte-associated antigen 4 (CTLA4) all cause damage to the mucus layer, which disrupts barrier integrity and enables bacteria to penetrate the lamina propria, which lies beneath the epithelium. Translocated bacteria activate innate immune cells and initiate local and systemic inflammation. Mechanisms of

[242] Roy S, Trinchieri G. Microbiota: A key orchestrator of cancer therapy. *Nat Rev Cancer*. **2017**;17:271-285.

gut-associated toxicity and tumor clearance vary based on treatment type, and the microbial species that have been demonstrated to affect these mechanisms are listed at the top of the figure. Gut commensals, through myeloid differentiation primary response 88 (MYD88)-associated receptors, prime myeloid cells for the generation of reactive oxygen species (ROS), which, in the presence of Pt–DNA adducts formed in response to cisplatin or oxaliplatin, cause DNA damage[243],[244]. TBI used to condition patients before they receive adoptive T cell therapy induces mucosal damage and translocation of commensals, which through Toll-like receptor 4 (TLR4) signaling activate dendritic cells to sustain proliferation and cytotoxic functions of the transferred T cells[245]. CTX induces immunological cell death of tumor cells, which elicits the generation of anti-tumor pathogenic T helper 17 (pTH17) cells, TH1 cells and cytotoxic T lymphocytes (CTLs); CTX also induces damage to the mucosa and translocation of commensal bacteria that activate tumor antigen-presenting dendritic cells, enhancing the anti-tumor immune response[246],[247]. During CpG-oligodeoxynucleotide (ODN)–anti-interleukin-10 receptor (IL-10R) therapy, the gut microbiota, through TLR4 signaling, primes tumor-infiltrating myeloid cells to respond to the TLR9 agonist CpG-ODN, producing tumor necrosis factor (TNF) and other inflammatory cytokines that induce hemorrhagic necrosis of the tumor and an anti-tumor immune response[243]. Anti-CTLA4 immunotherapy promotes both anti-tumor and anti-commensal immunity; the anti-commensal immunity against specific genera, such as Burkholderiales and Bacteroidales (*B. thetaiotaomicron* and *B. fragilis*), results in mucosal damage and bacterial translocation but also serves as an adjuvant for the anti-tumor response[248]. The efficacy of anti-programmed cell death protein 1 ligand 1 (PDL1) therapy in generating anti-tumor immunity by preventing programmed cell death protein 1 (PD1) interaction with PDL1 is enhanced by the presence in the GM of *Bifidobacterium* spp. (*B. breve*, *B. longum* and *B. adolescentis*)[249].

---

[243] Iida N, et al. Commensal bacteria control cancer response to therapy by modulating the tumor microenvironment. *Science*. **2013**;342:967-970.

[244] Gui Q F, et al. Well-balanced commensal microbiota contributes to anti-cancer response in a lung cancer mouse model. *Genet Mol Res*. **2015**;14:5642-5651.

[245] Paulos CM, et al. Microbial translocation augments the function of adoptively transferred self/tumorspecific CD8+ T cells via TLR4 signaling. *J Clin Invest*. **2007**;117:2197-2204.

[246] Viaud S, et al. The intestinal microbiota modulates the anticancer immune effects of cyclophosphamide. *Science*. **2013**;342:971–976.

[247] Daillere R, et al. *Enterococcus hirae* and *Barnesiella intestinihominis* facilitate cyclophosphamide-induced therapeutic immunomodulatory effects. *Immunity*. **2016**;45:931-943.

[248] Vetizou M, et al. Anticancer immunotherapy by CTLA-4 blockade relies on the gut microbiota. *Science.* **2015**;350:1079-1084.

[249] Sivan A, et al. Commensal *Bifidobacterium* promotes antitumor immunity and facilitates anti-PD-L1 efficacy. *Science*. **2015**;350:1084-1089.

All the novel findings just summarized were mostly focused on solid tumors and the role of gut microbial community on the clinical outcome. However, another branch regarding the relationship between GM and cancer treatments is mainly centered on hematologic malignances (*i.e.*, acute leukemia, lymphoma, myeloma). The first-line and life-saving therapy for patients affected by various blood tumors is considered hematopoietic stem cell transplantation (HSCT), a combination of stem cell therapy, conventional treatments (*i.e.*, chemotherapy, radiation) and immune therapy[250]. However, application of HSCT is characterized by several life-threating complications, such as graft-versus-host disease (*i.e.*, when alloreactive donor T cells attack host organs such as skin, liver, gut), tumor relapse and, not least, local and systemic infections[251]. In this regard, recent studies in mice and humans suggest important relationships between gut microbial community and outcomes in HSCT recipients. Indeed, HSCT practices significantly affect the gut microbial homeostasis with a reduction of microbial diversity and sometimes the monodominance by Proteobacteria members, *Enterococcus* or *Streptococcus*[252]. In a retrospective study, the reduction of biodiversity in patients who underwent HSCT was associated with a significantly increased mortality (52%) compared to patients with high-diversity GM profile (8%)[253]. Moreover, during the post-transplant period, anti-microbial treatments are commonly used to treat febrile neutropenia with the final consequence to affect microbial homeostasis, which in turn increases susceptibility to infections[254]. For example, an increased level of *Enterococcus*

---

[250] Jenq RR, van den Brink MR. Allogeneic haematopoietic stem cell transplantation: individualized stem cell and immune therapy of cancer. *Nature reviews Cancer*. **2010**;10:213-221.

[251] Zeiser R, Blazar BR. Acute graft-versus-host disease - biologic process, prevention, and therapy. *N Engl J Med*. **2017**;377:2167-2179.

[252] Taur Y, et al. Intestinal domination and the risk of bacteremia in patients undergoing allogeneic hematopoietic stem cell transplantation. *Clin Infect Dis*. **2012**;55:905-914.

[253] Taur Y, et al. The effects of intestinal tract bacterial diversity on mortality following allogeneic hematopoietic stem cell transplantation. *Blood*. **2014**;124:1174-1182.

[254] Jenq RR, et al. Regulation of intestinal inflammation by microbiota following allogeneic bone marrow transplantation. *J Exp Med*. **2012**;209:903-11.

spp. after antibiotic exposure is correlated with increased risk of developing bacteremia[252]. Similarly, an enrichment of *Enterobacteriaceae* members and other gram-negative microorganisms are associated with increased mortality[253]. Moreover, recent studies in animal models demonstrated that also GvHD (*i.e.*, graft-versus-host disease) development is associated with a specific gut microbial dysbiosis, characterized by an increase in *Enterobacteriaceae* and a reduction in obligate anaerobic bacteria belonging to the Clostridiales order. These findings were also confirmed in several clinical studies on both adult and pediatric patients[254,255,256]. Some of these clinical studies characterized the GM dynamics in HSCT showing a specific gut microbial profile, the so-called "anti-inflammatory Clostridia", *i.e.*, members of the families *Clostridiaceae*, *Lachnospiraceae*, *Ruminococcaceae* and *Eubacteriaceae*, that might be involved in the mechanism by which gut microbes exert a counteracting effect on GvHD onset and progression[257,258]. A partial confirmation of this observation has been provided by a study on a large cohort of adults, in which the relative abundance of *Blautia*, a well-known health-associated and SCFA-producing taxon belonging to *Lachnospiraceae* family, was correlated with reduced mortality from GvHD[259]. This finding further supports the hypothesis that also GM-derived metabolites, such as SCFAs and/or other signaling molecules, can influence the onset of GvHD. Indeed, it has been demonstrated in a mouse model that bacteria-derived butyrate improves the junctional integrity of intestinal epithelial cells, decreases apoptosis and mitigates GvHD

---

[255] Eriguchi Y, et al. Graft-versus-host disease disrupts intestinal microbial ecology by inhibiting Paneth cell production of alpha-defensins. *Blood*. **2012**;120:223-231.

[256] Biagi E, et al. Early gut microbiota signature of aGvHD in children given allogeneic hematopoietic cell transplantation for hematological disorders. *BMC Med Genomics*. **2019**;12:49.

[257] Mathewson ND, et al. Gut microbiome-derived metabolites modulate intestinal epithelial cell damage and mitigate graft-versus-host disease. *Nat Immunol*. **2016**;17:505-13.

[258] Atarashi K, et al. Treg induction by a rationally selected mixture of clostridia strains from the human microbiota. *Nature*. **2013**;500:232–6.

[259] Jenq RR, et al. Intestinal *Blautia* is associated with reduced death from graft-versus-host disease. *Biol Blood Marrow Transplant*. **2015**;21:1373-83.

severity[257]. All these findings corroborated the hypothesis of a strict relationship between HSCT outcomes and gut microbial homeostasis, but more studies on larger cohorts are still needed to support these assumptions. Moreover, most of these studies were conducted on adult patients, while only few data are available on pediatric subjects.

Aim of the studies

Due to the strong literature supporting the involvement of the gut microbial community in several aspects of tumor development and anti-cancer treatments, the first part of this thesis is focused on analyzing the role and trajectory of the GM in different tumors:

a) The first study shows the consequences of infection with *Salmonella enterica*, the only genotoxin-producing bacterium associated with an increased risk of developing hepatobiliary cancer and CRC, on the alteration of the DNA damage response and acquisition of genomic instability in normal and APC-deficient cells, using classical two-dimensional (2D) and a novel organotypic three-dimensional (3D) tissue models.

b) The second study profiled the gut microbial ecosystem in women with epithelial ovarian cancer over the course of chemotherapy, in relation to the therapeutic response (*i.e.*, platinum resistant vs. platinum sensitive).

c) The trajectory of the gut microbial community before and after HSCT in pediatric patients affected by different hematological malignances was analyzed according to different post-transplant outcomes, such as local and systemic infections, GvHD and veno-occlusive disease (SOS/VOD).

2.1 Infection with genotoxin-producing *Salmonella enterica* synergizes with loss of the tumor suppressor APC in promoting genomic instability via the PI3K pathway in colonic epithelial cells

Brief introduction

Colorectal cancer (CRC) is the third most common cancer and a leading cause of cancer death[260]. Approximately 15% to 30% of CRCs occur within families, and the occurrence of germline mutations in the hereditary nonpolyposis colorectal cancer syndromes and familial adenomatous polyposis (FAP) has been extensively studied. All FAP patients carry inactivating mutations of the *adenomatous polyposis coli* (*APC*) tumor suppressor gene, and the gene is also mutated in 70–80% of sporadic colorectal adenomas and carcinomas[261]. In addition to germline genetic alterations, different diets and lifestyles have a significant impact on colorectal carcinogenesis[262]. The introduction of NGS has highlighted significant alterations in the intestinal microbiota of CRC patients compared with healthy subjects[263]. However, it is still unknown whether the dysbiosis precedes or is a consequence of the tumor microenvironment and whether microbial products contribute to the carcinogenic process. An emerging property that may link the microbiota with the acquisition of carcinogenic traits is the enrichment in the CRC microbiome of bacterial families that produce genotoxins with the capacity to induce damage in the host cell DNA[263]. Three bacterial genotoxins, the

[260] Siegel R, Desantis C, Jemal, A. Colorectal cancer statistics, 2014. CA: *Cancer Journal for Clinicians*. **2014**;64:104-117.

[261] Fearon ER. Molecular genetics of colorectal cancer. *Annual Review of Pathology*. **2011**;6:479-507.

[262] Huxley RR, et al. The impact of dietary and lifestyle risk factors on risk of colorectal cancer: A quantitative overview of the epidemiological evidence. *International Journal of Cancer*. **2009**;125:171-180.

[263] Villeger R, et al. Microbial markers in colorectal cancer detection and/or prognosis. *World Journal of Gastroenterology*. **2018**;24:2327-2347.

cytolethal distending toxin (CDT), the typhoid toxin (TT), and colibactin[264,265] have been functionally characterized. CDT and TT are protein toxins that share the same CdtB active subunit, which is structurally and functionally homologue to the mammalian DNase I[266]. The delivery of CdtB to the nucleus of intoxicated cells is accompanied by the induction of DNA single- and double-strand breaks and triggering of an ATM-dependent DNA damage response (DDR) characterized by the formation of nuclear foci of phosphorylated histone 2AX (γH2AX), relocalization of the Mre11/Nbs1/Rad50 complex, and activation of CHK2 and p53[267,268]. As a consequence of DDR activation, the intoxicated cells are arrested in the G1 and/or G2 phases of the cell cycle, and upon failure to repair, the damage undergoes senescence or apoptosis in a cell type-dependent manner[269]. However, intoxicated cells may occasionally survive and overcome the DDR-induced tumorigenic barrier, leading to genomic instability and the acquisition of carcinogenic traits[270,271]. Thus, the genotoxic activity of these bacterial effectors may contribute to CRC development. To address this issue, the consequences of infection with *Salmonella enterica* the only genotoxin-producing bacterium associated with an increased risk of developing hepatobiliary and colon carcinoma in humans was characterized [272,273] on alteration of the DDR and acquisition of

---

[264] Guerra L, et al. The biology of the cytolethal distending toxins. *Toxins (Basel).* **2011**;3:172-190.

[265] Haghjoo E, Galan JE. *Salmonella typhi* encodes a functional cytolethal distending toxin that is delivered into host cells by a bacterial- internalization pathway. *Proc Natl Acad Sci USA.* **2004**;101:4614-4619.

[266] Song J, Gao X, Galan JE. Structure and function of the *Salmonella Typhi* chimaeric A(2)B(5) typhoid toxin. *Nature*. **2013**;499:350-354.

[267] Guerra L, et al. Bacterial genotoxin triggers FEN1-dependent RhoA activation, cytoskeleton remodeling and cell survival. *J Cell Sci.* 2**011**;124:2735-2742.

[268] Spano S, Ugalde JE, Galan JE. Delivery of a *Salmonella Typhi* exotoxin from a host intracellular compartment. *Cell Host Microbe*. **2008**;3:30-38.

[269] Blazkova H, et al. Bacterial intoxication evokes cellular senescence with persistent DNA damage and cytokine signalling. *J Cell Mol Med*. **2010**;14:357-367.

[270] Guidi R, et al. *Salmonella enterica* delivers its genotoxin through outer membrane vesicles secreted from infected cells. *Cell Microbiol*. **2013**;15:2034-2050.

[271] Hanahan D, Weinberg RA. Hallmarks of cancer: The next generation. *Cell*. **2011**;144:646-674.

[272] Dutta U, et al. Typhoid carriers among patients with gallstones are at increased risk for carcinoma of the gallbladder. *Am J Gastroenterol*. **2000**;5:784-787.

[273] Mughini-Gras L, et al. Increased colon cancer risk after severe *Salmonella* infection. *PLoS One*. **2018**;13:e0189721.

genomic instability in normal and APC-deficient cells, using classical two-dimensional (2D) and organotypic three-dimensional (3D) tissue models.

Material and Methods

Cell lines

The isogenic human colonic epithelial cell lines 1CT (APC wild type) and 1CTA (APC deficient) were previously described[274]. Cells were cultured in a high-glucose Dulbecco's Modified Eagle (DMEM) medium/medium 199 (Sigma-Aldrich Merck, Darmstadt, Germany, at ratio 4:1), supplemented with 2% fetal bovine serum (FBS; Gibco ThermoFisher Scientific), epidermal growth factor (EGF 20 ng/ml, Sigma-Aldrich), hydrocortisone (1 mg/ml, Sigma-Aldrich), insulin (10 mg/ml, Sigma-Aldrich), transferrin (2 mg/ml, Sigma-Aldrich Merck), sodium selenite (5 nM, Sigma-Aldrich Merck), and gentamycin sulfate (50 µg/ml, Sigma-Aldrich Merck): DMEM complete medium. The 1CTA cells were cultured in DMEM complete medium supplemented with puromycin (1 µg/ml, Invitrogen, Carlsbad, CA, USA). Human colonic fibroblasts (ATCC, Manassas, VA, USA) were maintained in Eagle's Minimum Essential Medium (ATCC) supplemented with 10% of FBS (Gibco) and 10 µg/ml of ciprofloxacin (Sigma-Aldrich Merck). The immortalized isogenic murine $Apc^{+/+}$ and $Apc^{+/Min}$ colon epithelial cells were previously described[275]. The cell lines harbor a temperature-sensitive mutation of the simian virus 40 large tumor antigen gene (tsA58), under the control of interferon-γ (IFN-γ) and express an active SV40 form at the permissive temperature

[274] Roig AI, et al. Immortalized epithelial cells derived from human colon biopsies express stem cell markers and differentiate in vitro. *Gastroenterology*. **2010**;138:1012-1021.

[275] Forest V, et al. Butyrate restores motile function and actin cytoskeletal network integrity in apc mutated mouse colon epithelial cells. *Nutr Cancer*. **2003**;45:84-92.

(33°C). Cells were routinely cultured at permissive temperature of 33°C in DMEM (Sigma-Aldrich Merck) supplemented with 10% FBS (Gibco), EGF (10 ng/ml, Sigma-Aldrich), IFN-γ (2 ng/ ml, BD Biosciences, Franklin Lakes, NJ, USA), and 2% penicillin/streptomycin (ThermoFisher Scientific). All cells were maintained in a humidified atmosphere with 5% CO2 at 37°C. When indicated, cells were preincubated for 1 h with inhibitors specific for the MAPK p38 (SB203580 10 μM, Sigma-Aldrich Merck) or PI3K (GDC-0941 1 μM, Abcam, Cambridge, UK) or DMSO (Sigma-Aldrich Merck) as vehicle, prior infection. Infection was performed in in the continuous presence of SB203580, whereas 1-h treatment with the GDC-0941 was repeated every 24 h after infection.

RT- qPCR

RNA was isolated using the RNeasy Mini kit (Qiagen, Hilden, Germany) following manufacturer's instructions. Briefly, after cell lysis, one volume of 70% ethanol was added to each solution and then transferred on the RNeasy spin column for the following purifications. RNA elution was performed with 50 μl of RNAse-free water. Subsequently, cDNA synthesis was performed using the High-capacity cDNA Reverse Transcription and RiboLock RNase Inhibitor kits (Thermofisher Scientific) with 1-μg RNA and a PTC-225 Thermal Cycler (MJ Research, Waltham, MA, USA), according to the instructions of the manufacturer. Quantitative PCR was performed using the following primers F: AGGCTGCATGAGAGCACTTGTG and R: CACACTTCCAACTTCTCGCAACG for APC and F: CTGGCACCCAGCACAATG and R: GCCGATCCACACGGAGTACTT for beta actin. Amplifications were carried out using an ABI PRISM® 7000 Sequence Detection System (Applied Biosystems, Foster City, CA, USA) as follows: a first one-hold stage at 95°C for 10 min followed by 41 cycles (95°C for 15 s, 60°C for 30 s, and 72°C for 30 s), and a final extending step (95°C for 10 s). All qPCR reactions were performed in triplicate, and the

threshold cycle (Ct) values were averaged. The fold change of the target gene relative to the internal control was calculated as 2−Δ(ΔCt), where ΔCt = Cttarget – Cthousekeeping and Δ (ΔCT) = ΔCttreated – ΔCtuntreated, according to the Minimum Information for Publication of Quantitative Real-Time PCR Experiments guidelines.

Organotypic 3D tissue models

Colonic tissue models were prepared based on a protocol for lung tissue model previously described[276,277], with minor modifications. Briefly, a six-well plate insert with 3.0-μm high-density membrane (VWR, Radnor, PA, USA) was coated with 1 ml of a solution of bovine type I collagen (PureCol, Cell systems, Kirkland, WA, USA) in DMEM at a final concentration of 0.72 mg/ml (collagen-DMEM) and incubated for 30 min at 37°C in 5% CO2. Eighty thousand human colonic fibroblasts were resuspended in 3 ml of the collagen–DMEM solution, overlaid on the polymerized collagen layer and incubated for 2 h at 37°C in 5% CO2. Following the polymerization, a 2-ml DMEM medium was added to the outer chamber, and the culture was kept for 24 h at 37°C in 5% CO2. The subsequent day, 2 ml of fresh DMEM medium were added to the inner chamber. The models were maintained for 7 days, and the medium was replaced every second day. Six hundred thousand 1CT or 1CTA cells, resuspended in 150-μl DMEM complete medium without puromycin and gentamycin, were overlaid on the fibroblast/collagen matrix and incubated for 4 h at 37°C in 5% CO2 after which 2-ml complete DMEM medium without antibiotics was gently added to the insert, and the models were cultivated for additional 24 h at 37°C in 5% CO2 prior infection.

[276] Mairpady Shambat S, et al. Modelling staphylococcal pneumonia in a human 3D lung tissue model system delineates toxin-mediated pathology. *Dis Models Mech*. **2015**;8:1413-1425.

[277] Sundstrom KB, et al. Andes hantavirus-infection of a 3D human lung tissue model reveals a late peak in progeny virus production followed by increased levels of proinflammatory cytokines and VEGF-A. *PLoS One*. **2016**;11: e0149354.

Bacterial strains

The *Salmonella typhimurium* strain MC1 used in this study was previously described[278]. The strain was transformed with the pEGFP-C1 plasmid carrying a cassette containing the TT genes pltB-pltA and cdtB (MC1 TT). As control, the MC1 strain was transformed with the pEGFP-C1 vector containing only the pltB-pltA genes (MC1 ΔcdtB). Cloning of the TT genes into the pEGFP-C1 plasmid was previously described[279].

Bacterial infection

Fifty thousand 1CT and 1CTA or sixty thousand $Apc^{+/+}$ and $Apc^{+/Min}$ cells were grown in six well plates (PrimariaTM, Gibco ThermoFisher Scientific), without or with 13-mm-diameter coverslips previously coated with FBS, in 3-ml complete medium. Epithelial cells were infected at a MOI of 100:1 in a gentamicin protection assay as previously described[280]. Cells were lysed in 1 ml of 0.5% sodium deoxycholate (Sigma-Aldrich) in PBS to evaluate bacterial load by CFU counting as previously described[280]. Cells grown on slides were fixed in 4% formaldehyde in phosphate-buffered saline (PBS) for 20 min at room temperature for immunofluorescence analysis. Human organotypic colonic models were infected at a MOI of 25:1 as previously described[280], except that the models were not subjected to centrifugation, and incubation with the bacterial suspension was prolonged to 2 h. After infection, cells were maintained in RPMI supplemented with 10% FBS and 10-µg/ml gentamicin for the indicated periods of time, when 2 ml of 2-M sucrose solution were added to both the inner and the outer chambers, and samples were incubated for 1 h at room

[278] Clements MO, et al. Polynucleotide phosphorylase is a global regulator of virulence and persistency in *Salmonella enterica*. *Proc Natl Acad Sci USA*. **2002**;99:8784-8789.

[279] Guidi R, et al. *Salmonella enterica* delivers its genotoxin through outer membrane vesicles secreted from infected cells. *Cell Microbiol.* **2013**;15:2034-2050.

[280] Bjur E, et al. Thioredoxin 1 promotes intracellular replication and virulence of *Salmonella enterica* serovar *Typhimurium*. *Infect Immun*. **2006**;74:5140-5151.

temperature. Subsequently, the models were embedded in O.C.T. (Sakura Finetek, Torrance, CA, USA), snap frozen and stored at −80°C. Six-µm sections were cut using a CryoStar™ NX70 Cryostat (Gibco ThermoFisher Scientific), and slides were fixed in 4% PFA in PBS for 20 min at room temperature for immunofluorescence analysis.

Repair assay

The capacity of the 1CT/1CTA and $Apc^{+/+}$/$Apc^{+/Min}$ cells to repair the DNA damage was assessed as previously described with minor modifications[281]. Briefly, 100,000 cells were grown on 13-mm-diameter coverslips in six well plates in 3-ml complete medium and treated with the indicated DNA-damaging agents. After 6 h, cells were either fixed in 4% formaldehyde in PBS (defined as 6 h) to assess the extent of the DNA damage or washed once with PBS and incubated with fresh medium in absence of the genotoxic agent for additional 18 h before fixation (defined as 24 h) to assess the residual DNA damage. DNA damage was assessed by immunofluorescence analysis as described below. The percentage of repair was calculated as follows: [1 − (% positive cells at 24 h/% positive cells at 6 h)] × 100, where cells with a defective repair will accumulate more DNA damage 24-h posttreatment, resulting in a lower repair percentage. The following genotoxic agents were used: the recombinant CDT from *Haemophilus ducreyi* (1 µg/ml)[282], etoposide (15 µM, Sigma-Aldrich Merck), camptothecin (5 µM, Selleckchem, Munich, Germany), and H_2O_2 (50 µM, Sigma-Aldrich-Merck).

[281] Graillot V, et al. Genotoxicity of cytolethal distending toxin (CDT) on isogenic human colorectal cell lines: Potential promoting effects for colorectal carcinogenesis. *Front Cell Infect Microbiol*. **2016**;6:34.

[282] Guerra L, et al. Cellular internalization of cytolethal distending toxin: a new end to a known pathway. *Cell Microbiol*. **2005**;7:921-934.

Immunofluorescence

Immunofluorescence was performed as previously described[283]. The following primary antibodies were used: rabbit antibodies anti-*S. enterica* OMA (1:500, Reagensia AB, Solna, Sweden), anti-phospho-KAP1 (1:100, Bethyl Laboratories Inc, TX, USA), anti-phospho-H2AX Ser139 (γH2AX), anti-phospho-CHK2 Thr68, and anti-Ki67 (1:100, Cell Signaling Technology, Boston, MA, USA); and mouse antibodies anti-γH2AX (1:100, Millipore), anti-53BP1 (1:100, BD), anti-phospho-p53 Ser15 (1:100, Cell Signaling Technology), anti-cyclin B1 (1:100, Santa Cruz Biotechnology, Dallas, TX, USA), and anti-p21 (Cip1/WAF1; 1:100, BD). The actin cytoskeleton was visualized by staining with TRITC or FITC-conjugated phalloidin (1 µg/ml, Sigma-Aldrich Merck) as previously described[284]. Images were acquired with a fluorescence microscope (Leica DM RA2, Leica Microsystems, Wetzlar, Germany) equipped with a CCD camera (C4742-95, Hamamatsu, Japan) or a confocal scanning microscope (Zeiss Confocal Microscope LSM510 META, Carl Zeiss Microscopy, Jena, Germany). The images were analysed using the ImageJ software, and at least 100 cells per slide were counted. Cells were scored positive for γH2AX and 53BP1 when they exhibited ≥5 foci/ cell. Cells were considered positive for phospho-Kap1, phospho-Chk2, phospho-p53, and Ki67 when the mean fluorescence intensity was higher than the mean fluorescence intensity of the uninfected cells plus two standard deviations.

Cell cycle analysis

Cells, harvested by trypsinization, were fixed for 20 min on ice with 1 ml of ice-cold 70% ethanol and subsequently resuspended in 0.3 ml of propidium iodide solution (3.8-mM

[283] Guerra L, et al. A bacterial cytotoxin identifies the RhoA exchange factor Net1 as a key effector in the response to DNA damage. *PLoS One*. **2008**;3:e2254.

[284] Frisan T, et al. The *Haemophilus ducreyi* cytolethal distending toxin induces DNA double-strand breaks and promotes ATM-dependent activation of RhoA. *Cell Microbiol*. **2003**;5:695-707.

sodium citrate, 0.3% NP40, 0.05-mg/ml propidium iodide; 0.02 mg/ml RNase) for 1 h at 4°C. Flow cytometry analysis was performed using a FACSCalibur flow cytometer (BD Biosciences). Pulse processing was used to exclude cell doublets from the analysis. Data from 1 × 104 cells were collected and analyzed using the CellQuest Pro software (BD Biosciences).

Colony assay

1CTA cells were preincubated for 1 h with the specific PI3K inhibitor (GDC-0941 1 μM), or DMSO as vehicle, prior infection, and exposed to purified CDT at 20 and 10 ng/ml for 2 weeks, 1-h treatment with the GDC-0941 was repeated every 24 h after infection for 1 week. Cells were fixed with 4% formaldehyde for 20 min, washed twice with 20% methanol, stained with 0.05% crystal violet (Sigma-Aldrich) in 25% methanol, and washed three times with PBS. Bound stain was extracted by incubation for 15 min in 2% SDS in water and quantified by reading the absorbance at 550 nm.

Statistical analyses

Results are expressed as mean ± SEM of at least three independent experiments. All the statistical analyses have been performed using the Prism 7, Graphpad Software. The significance of differences between two experimental groups was determined by a Student t test. The significance of differences between three experimental groups was determined by ANOVA with Fisher's LSD post-test. P values <.05 were considered significant.

Results

APC deficiency alters the DDR of cells infected with genotoxic Salmonella

Two cell models were used to investigate whether APC deficiency alters the outcome of infection with genotoxin-producing bacteria in eukaryotic cells: (a) the immortalized non transformed human colonic epithelial cell line 1CT that carries a functional APC gene[285] and the isogenic 1CTA cell line where a three-fold downregulation of the APC mRNA was obtained by stable transfection of specific shRNA[286] (**Figure 7a**); and (b) the SV40 large T antigen immortalized murine colonic epithelial cells that are either APC wild type ($Apc^{+/+}$) or APC haploinsufficient due to an allelic mutation leading to expression of a truncated inactive product ($Apc^{+/Min}$)[287]. In both cell types APC deficiency was associated with disruption of actin stress fibers (**Figure S1A**) and increased nuclear size (**Figure S1B**). Cells grown in standard 2D cultures were infected with *S. typhimurium* strain MC1 expressing a functional typhoid toxin (MC1 TT) or an isogenic strain that lacks the genotoxic activity due to deletion of the gene encoding for the active subunit (MC1 ΔcdtB) at a multiplicity of infection (MOI) of 100:1. Downregulation of the APC mRNA or APC haploinsufficiency did not influence *Salmonella* infection as assessed by the similar recovery of viable bacteria after infection (**Figure 7b**), and the presence of *Salmonella*-containing vacuoles within the infected cells, detected by LPS staining, 24-h post-infection (**Figure 7c**). As expected, only infection with the MC1 TT strain induced DNA damage as assessed by a significant increase in the percentage of cells expressing early (KAP1 phosphorylation) and late (CHK2 and p53 phosphorylation) markers

[285] Roig AI, et al. Immortalized epithelial cells derived from human colon biopsies express stem cell markers and differentiate in vitro. *Gastroenterology*. **2010**;138:1012–1021.

[286] Graillot V, et al. Genotoxicity of cytolethal distending toxin (CDT) on isogenic human colorectal cell lines: Potential promoting effects for colorectal carcinogenesis. *Front Cell Infect Microbiol*. **2016**;6:34.

[287] Forest V, et al. Butyrate restores motile function and actin cytoskeletal network integrity in apc mutated mouse colon epithelial cells. *Nutr Cancer*. **2003**;45:84-92.

of DDR activation (**Figures S2**), therefore, the data relative to infection with the control MC1 ΔcdtB strain will not be included in the subsequent figures.

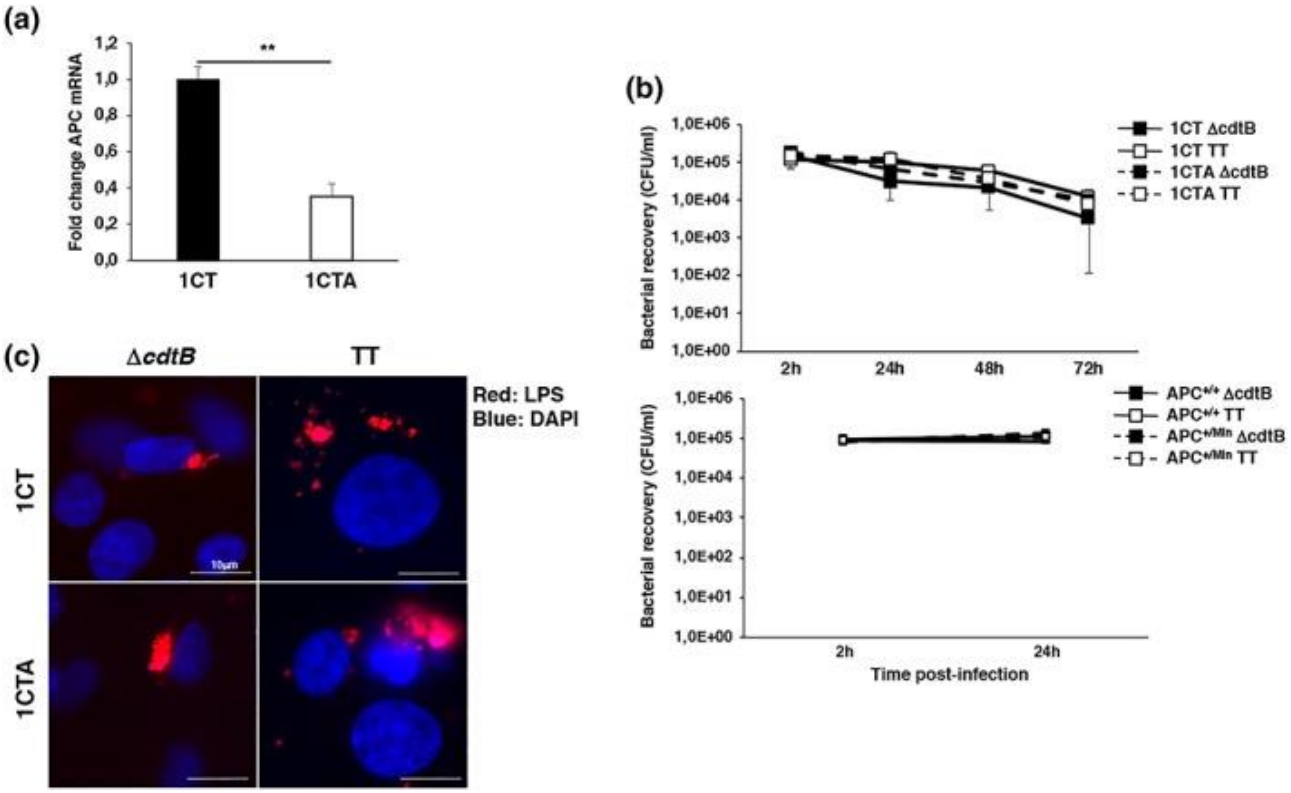

Figure 7. **Infection with the *Salmonella* MC1 TT and MC1ΔcdtB strains.** (**a**) Levels of APC mRNA assessed by qPCR in the 1CT and 1CTA cell lines. Mean ± SEM of three independent experiments. (**b**) 1CT and 1CTA cells (upper panel) and $Apc^{+/+}$ and $Apc^{+/Min}$ cells (lower panel) grown in 2D culture were infected with the MC1 cdtB (cdtB) or MC1 TT (TT) strains at MOI 100:1. The data are presented as number of CFU/ml of viable bacteria recovered at the indicated time points. Mean ± SEM of four to eight independent experiments. (**c**) Cells grown in 2D culture were infected with the MC1 cdtB or MC1 TT strains at MOI 100:1. Bacteria were visualized using a rabbit serum anti-LPS followed by a goat anti-rabbit secondary antibody conjugated to Alexa-568 (red). Nuclei were counterstained with DAPI (blue). Representative scanning confocal micrographs at magnification 63×.

Hereafter, it was assessed whether APC deficiency was associated with altered activation of the DDR upon infection with the genotoxic *Salmonella*. To this end, 1CT and 1CTA cells were infected with the MC1 TT strain, and the kinetics of expression of DNA damage sensor proteins (phospho-KAP1 and γH2AX) and transducer effectors (phospho-CHK2 and phospho-p53 on Ser 15) were monitored over a period of 72 h. Infection with the genotoxic *Salmonella* caused an increase of p-KAP1, γH2AX, p-CHK2, and p-p53 Ser15 positive cells in both APC-proficient and APC-deficient cells within the first 24 h after infection (**Figure 8**). However, whereas the levels of these proteins decreased or remained constant over time in the 1CT cells, the percentage of cells positive increased over time in the 1CTA cell line for most of the markers (**Figure 8**). The different kinetics profile of the DDR response was not dependent on a reduced proliferation rate of the 1CTA cells compared with the APC proficient line, as shown by the growth curve presented in **Figure S3A**. Similar results were observed when comparing the kinetics of the DDR activation in the $Apc^{+/+}$ and $Apc^{+/Min}$ cells (**Figure S4A**). Collectively, these data indicate that APC deficiency is associated with an altered response to the *Salmonella*-induced DNA damage, and the sustained DDR suggests a reduced capacity of the 1CTA cells to repair the damaged DNA.

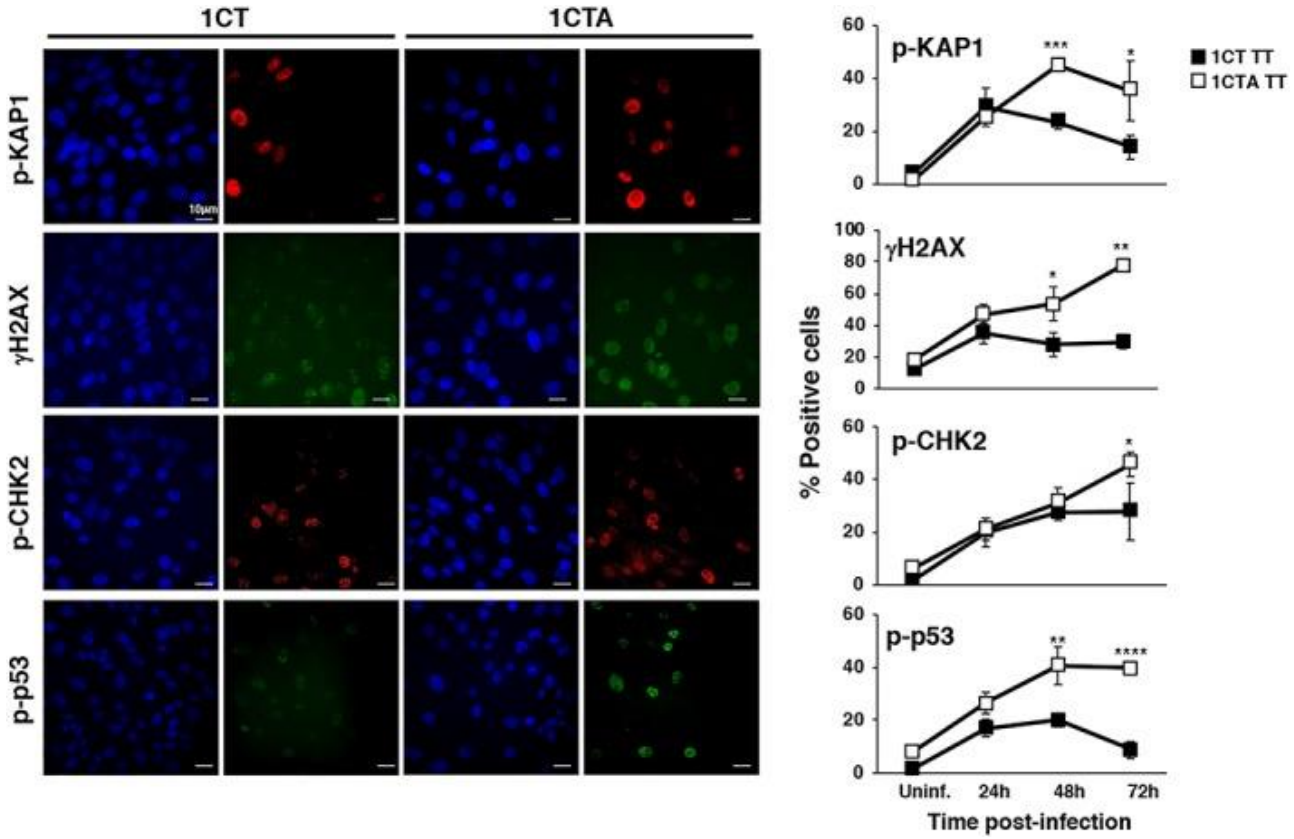

Figure 8. **APC-deficient cells show a sustained activation of the DNA damage response.** 1CT and 1CTA cells, grown in 2D culture, were left untreated (Uninf.) or infected with the MC1 TT strain (TT) at MOI 100:1 for the indicated period of time. Activation of the DNA damage response was assessed by immunofluorescence analysis, using antibodies specific for phosphorylated KAP1 (p-KAP1), phosphorylated H2AX(γH2AX), phosphorylated CHK2 (p-CHK2), Ser15 phosphorylated p53 (p-p53). Left panel: representative fluorescence micrographs; right panel: quantification of the positive cells. The percentage of positive cells in uninfected cells was similar during all the time kinetics experiment; here, were presented the values relative to the 24-h time point. Mean ± SEM of three independent experiments. One hundred cells were evaluated foreach experiment for each cell line. Statistical analysis comparing 1CT and 1CTA for each time point was performed using the Student t test, *p <.05; **p < .01; ***p < .001; ****p < .0001.

APC deficiency is associated with reduced DNA damage repair capacity

To address the effect of APC deficiency on the DNA repair capacity, 1CT and 1CTA cells were exposed to a panel of DNA-damaging agents known to cause DNA strand breaks (CDT, etoposide, and camptothecin) and oxidative damage (H_2O_2). The treated cells were either fixed after 6 h to assess the extent of DNA damage or further incubated for 18 h in fresh medium without the compounds to evaluate the residual damage by monitoring KAP1 and H2AX phosphorylation and the formation of 53BP1 foci. As shown in **Figure S5**, a similar response to the different DNA-damaging agents was observed for all the three markers analyzed 6-h posttreatment independently of the levels of APC expression. However, for all the genotoxic agents, the extent of repair was significantly lower in the 1CTA cells (**Figure 9**), indicating that APC deficiency reduces the capacity to repair the DNA damage induced by a broad spectrum of damaging agents. A comparable reduced capacity to repair DNA damage was obtained upon exposure of the APC haploinsufficient murine cells to etoposide, camptothecin, and H_2O_2 (**Figure S4B**).

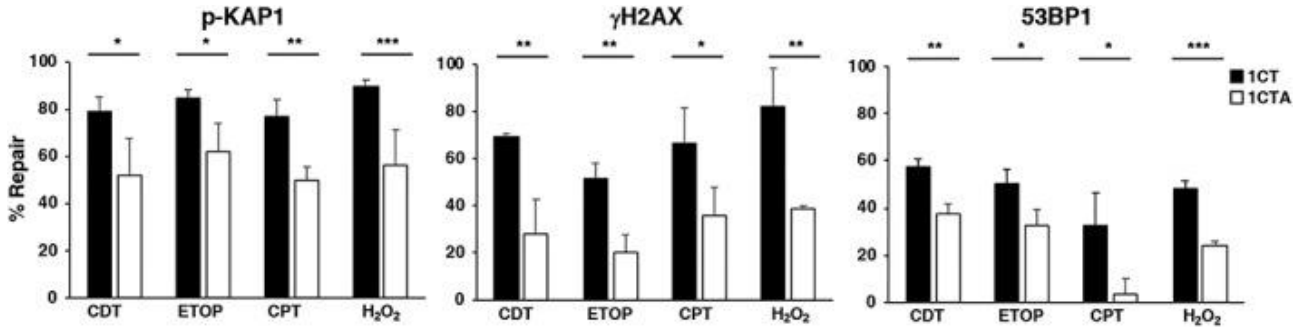

Figure 9. **APC deficiency reduces the repair of DNA damage induced by a broad spectrum of genotoxic stresses.** 1CT and 1CTA cells, grown in 2D culture, were left untreated (see Figure S5) or treated for 6 h with CDT (1 μg/ml), etoposide (ETOP, 15 μM), camptothecin (CPT, 5 μM), or H_2O_2 (50 μM), defined as 6 h. After 6-h incubation, cells were washed and maintained in medium without the genotoxic agents for additional 18 h, defined as 24 h. The percentage of repair was calculated as follows: [1 − (% positive cells at 24 h/% positive cells at 6 h)] × 100. One hundred cells were evaluated for each experiment for each cell line. Mean ± SEM of three independent experiments. Statistical analysis was performed using the Student t test, *$p < .05$; **$p < .01$; ***$p < .001$.

Infection with genotoxic Salmonella prevents cell cycle arrest in APC-deficient cells

To evaluate the effect of the sustained DDR and failure to repair the genotoxin-induced DNA damage on cell proliferation, the levels of Ki67 expression and the rate of cell growth in untreated, MC1 TT or MC1 ΔcdtB infected 1CT and 1CTA cells were monitored. As shown in **Figure 10a**, in the absence of bacterial infection or upon infection with the control MC1 ΔcdtB strain, both APC-proficient and APC-deficient cells exhibited contact inhibition over the course of the experiment, as assessed by a time-dependent decrease in the number of Ki67 positive cells and a significant accumulation of cells in the G1 phase of the cell cycle at 72-h post-infection (**Figure 10b**). The percentage of Ki67 positive cells also decreased in infected 1CT cells following activation of the DDR response, reaching more than 90% of the total population 72-h post-infection (**Figures 10a**). Cell cycle analysis showed that cells were

arrested both in G1 and G2 phases of the cell cycle (**Figure 10b**). In contrast, approximately 50% of the 1CTA cells remained Ki67 positive 72-h post-infection with the genotoxic *Salmonella* (**Figure 10a**), and this effect was not associated with accumulation of cells in the G2 phase of the cell cycle (**Figure 10b**). Growth curve analysis further showed that although 1CT cells infected with the MC1 TT strain show a significant reduced cell recovery compared with the uninfected cells 72-h post-infection, this effect was not observed in infected 1CTA cells, where the cell recovery was similar to that observed in uninfected controls (**Figure S3B**). The lower cell recovery in the infected 1CT cells was not due to increased rate of cell death, because the percentage of subG1 apoptotic cells was not significantly different in the two cell lines at any condition or time point tested (**Figure 10b**). Progression from G2 to mitosis in the 1CTA cells exposed to the genotoxic strain was further confirmed by nuclear translocation of cyclin B1[288] (**Figure 10c**) and was associated with failure to upregulate expression of the cyclin-dependent kinase inhibitor p21[289] (**Figure 511a**). It is noteworthy that the majority of the CT1A cells positive for Ki67 at 48-h and 72-h post-infection still maintained sustained levels of DNA damage, visualized by staining for γH2AX (**Figure 11b**), indicating failure to properly activate the cell cycle checkpoint response.

[288] Pines J, Hunter T. Human cyclins A and B1 are differentially located in the cell and undergo cell cycle-dependent nuclear transport. *J Cell Biol*. **1992**;115:1-17.

[289] Georgakilas AG, Martin OA, Bonner WM. p21: A two-faced genome guardian. *Trends Mol Med*. **2017**;23:310-319.

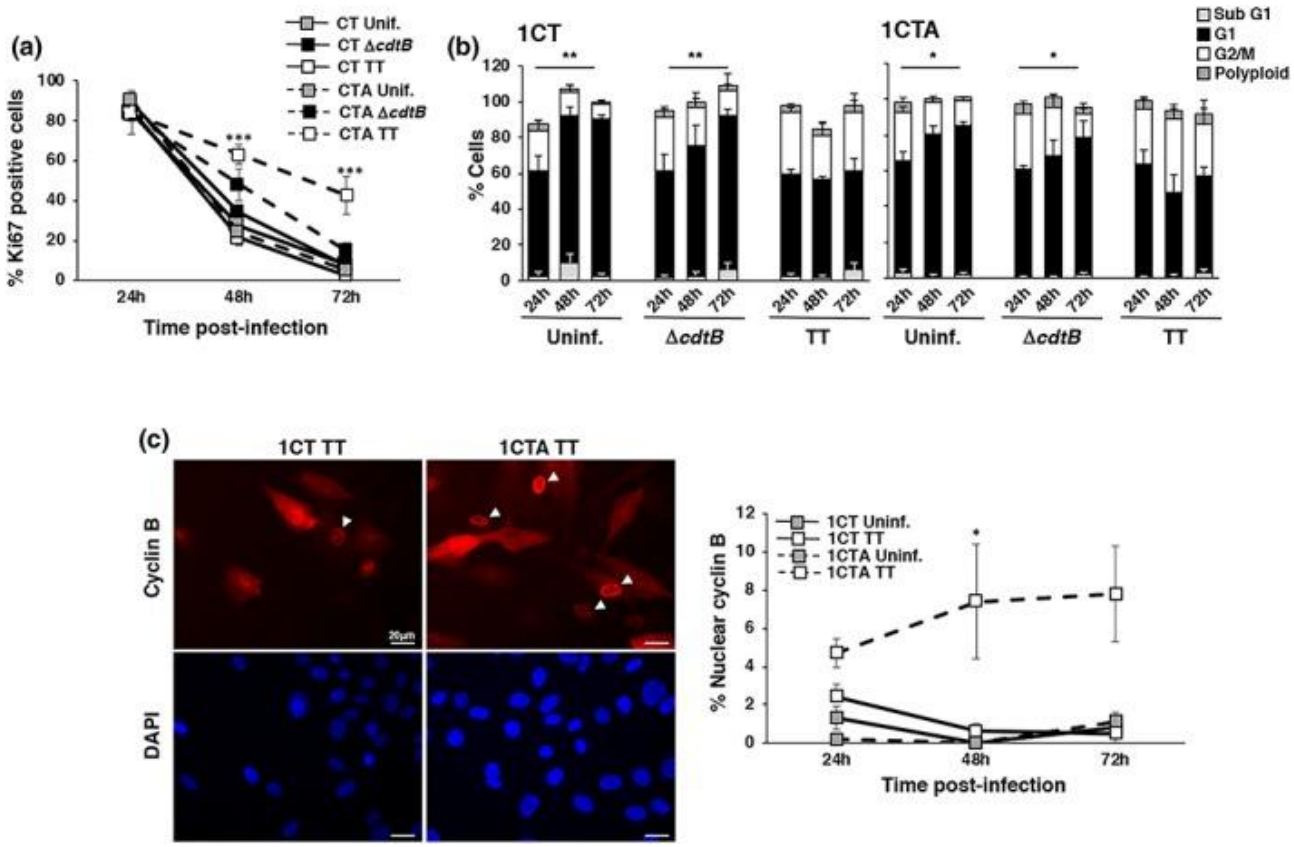

Figure 10. APC deficiency impairs activation of cell cycle arrest. 1CT and 1CTA cells grown in 2D culture were left uninfected or infected with the MC1 cdtB or MC1 TT strains as described in Figure 1. The proliferation status was assessed by immunofluorescence analysis, using antibodies specific for Ki67 and cyclin B1. (**a**) Quantification of cells positive for Ki67. Mean ± SEM of four independent experiments. (**b**) Cell cycle distribution assessed by PI staining followed by FASC analysis. Mean ± SEM of four independent experiments. Statistical analysis was performed using the Student t test *p < .05; **p < .01. Significant accumulation in the G1 phase of the cell cycle was observed in 1CT and 1CTA cells at 72-h post-infection compared with the 24-h time point. (**c**) Left panel: fluorescence micrographs showing the subcellular distribution of cyclin B1, white arrowheads indicated cells progressing to the M phase of the cell cycle, characterized by the nuclear translocation of cyclin B1. Right panel: quantification of cells with nuclear translocation of cyclin B1. Mean ± SEM of three independent experiments. One hundred cells were evaluated for each experiment for each cell line. Statistical analysis was performed using the Student t test, *p < .05; ***p < .001.

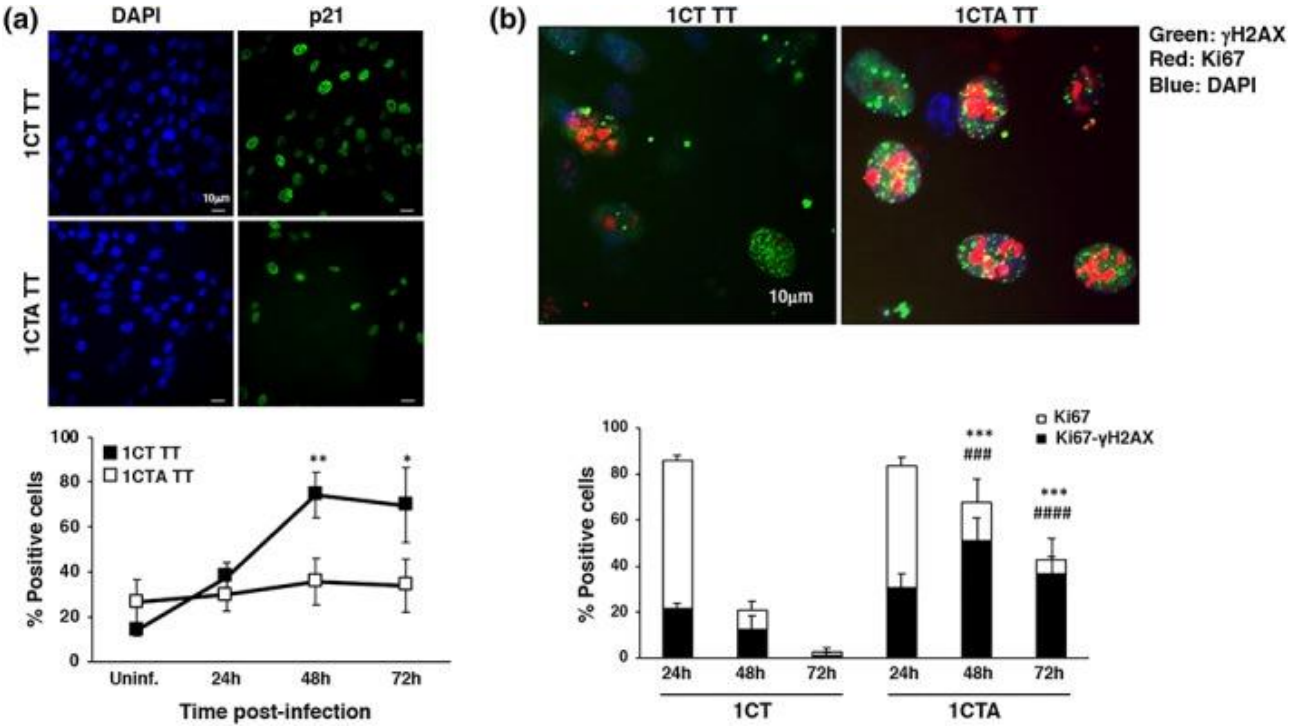

Figure 11. **APC deficient cells proliferate in spite of the presence of DNA damage**. 1CT and 1CTA cells grown in 2D culture were infected with the MC1 TT strain as described in Figure 1. (**a**) Upregulation of p21 expression was assessed by immunofluorescence analysis. Upper panel: representative fluorescence micrographs; lower panel: quantification of the positive cells. Mean ± SEM of three to four independent experiments. Statistical analysis comparing 1CT and 1CTA for each time point was performed using the Student t test: *p < .05; **p < .01. (**b**) Induction of proliferation status and DNA damage was assessed by immunofluorescence analysis, using antibodies specific for Ki67 and γH2AX, respectively. Upper panel: representative micrograph showing cells double positive for the proliferation (Ki67, red) and DNA damage (γH2AX, green) markers. Nuclei were counterstained with DAPI (blue). Lower panel: quantification of 1CT and 1CTA cells infected with the MC1 TT strain positive for Ki67 (white bar) and double positive for both Ki67 and γH2AX (black bar). Mean ± SEM of three to four independent experiments. Statistical analysis was performed using the Student t test. *,#$p < .05$; **,##$p < 0.01$; ***,###$p < .001$; ****,####$p < .0001$. *comparison Ki67 positive cells, #comparison Ki67-γH2AX double-positive cells.

APC loss enhances genomic instability upon infection with the genotoxic Salmonella

Hereafter, was assessed whether the reduced DNA repair capacity combined with the failure to halt cell proliferation observed in APC-deficient cells exposed to the genotoxic *Salmonella* was associated with enhanced genomic instability. To this end, 1CT and 1CTA cells were left uninfected, or infected with MC1 TT, or control MC1 ΔcdtB bacteria (data not shown), and genomic instability was assessed by the formation of micronuclei over a period of 72 h. As shown in **Figure 12a**, a marginal increase of micronuclei positive cells was detected in the 1CT cells infected with the MC1 TT strain, consistent with the fact that the majority of the cells stop proliferation in response to infection with the genotoxin-producing bacterium (**Figure 10**). In contrast, a significant higher percentage of cells carrying micronuclei was observed 24-h post-infection in 1CTA cells exposed to the genotoxic *Salmonella*, and the rate of micronuclei positive cells increased over time. Similar time-dependent increase in the formation of micronuclei was observed in infected murine $Apc^{+/Min}$ cells (**Figure S4C**). It was not detected a significant increase in the percentage of polyploid cells over the course of 72-h infection with the MC1 TT strain (**Figure 10b**). *Salmonella* infection induces activation of the PI3K/AKT axis and the mitogen-activated protein kinase (MAPK) p38[290,291], which have also been demonstrated to activate survival and proliferative signals critical in carcinogenesis[292,293]. To assess whether these pathways contribute to inhibit the checkpoint response upon MC1 TT infection in APC-deficient cells, leading to accumulation of genomic instability, 1CTA cells were preincubated with the inhibitors GDC-0941 (1 μM) and

[290] Hobbie S, et al. Involvement of mitogen-activated protein kinase pathways in the nuclear responses and cytokine production induced by *Salmonella typhimurium* in cultured intestinal epithelial cells. *J Immunol*. **1997**;159:5550-5559.
[291] Steele-Mortimer O, et al. Activation of Akt/protein kinase B in epithelial cells by the *Salmonella typhimurium* effector sigD. *J Biol Chem*. **2000**;275:37718-37724.
[292] Dolado I, Nebreda AR. Regulation of Tumorigenesis by p38α MAP Kinase. In F. Posas, & A. R. Nebreda (Eds.), Stress-Activated Protein Kinases. **2008**. (Vol. 20) (pp. 99–128). Berlin Heidelberg: Springer-Verlag.
[293] Liu P, et al. Targeting the phosphoinositide 3-kinase pathway in cancer. *Nat Rev Drug Discov.* **2009**;8:627-644.

SB203580 (10 μM) specific for PI3K and MAPK p38, respectively, prior infection. Treatment did not affect infection (data not shown) or the extent of the *Salmonella*-induced DNA damage 72-h post-infection as assessed by the similar levels of phosphorylation of γH2AX (**Figure 12b**). However, inhibition of the PI3K, but not MAPK p38, reduced the number of cells positive for the proliferative marker Ki67 in cells infected with the genotoxic *Salmonella* (**Figure 12b**, and data not shown) and cell outgrowth as assessed by colony assay in cells exposed to purified CDT (**Figure S6**). The reduced proliferative activity observed in 1CTA treated with the PI3K inhibitor was dependent on the upregulation of p21 expression (**Figure 12b**). Collectively, these data indicate that inhibition of the checkpoint responses is, at least partially, dependent on the PI3K/AKT axis. As a consequence of the reduced proliferative state, PI3K inhibition resulted in reduction of the percentage of cells carrying micronuclei (**Figure 12b**). Thus, the levels of Ki67 expression and micronuclei formation were significantly lower in 1CT cells infected with the toxigenic strain compared with the APC-deficient cells, and this phenotype was not affected by the inhibitors (data not shown).

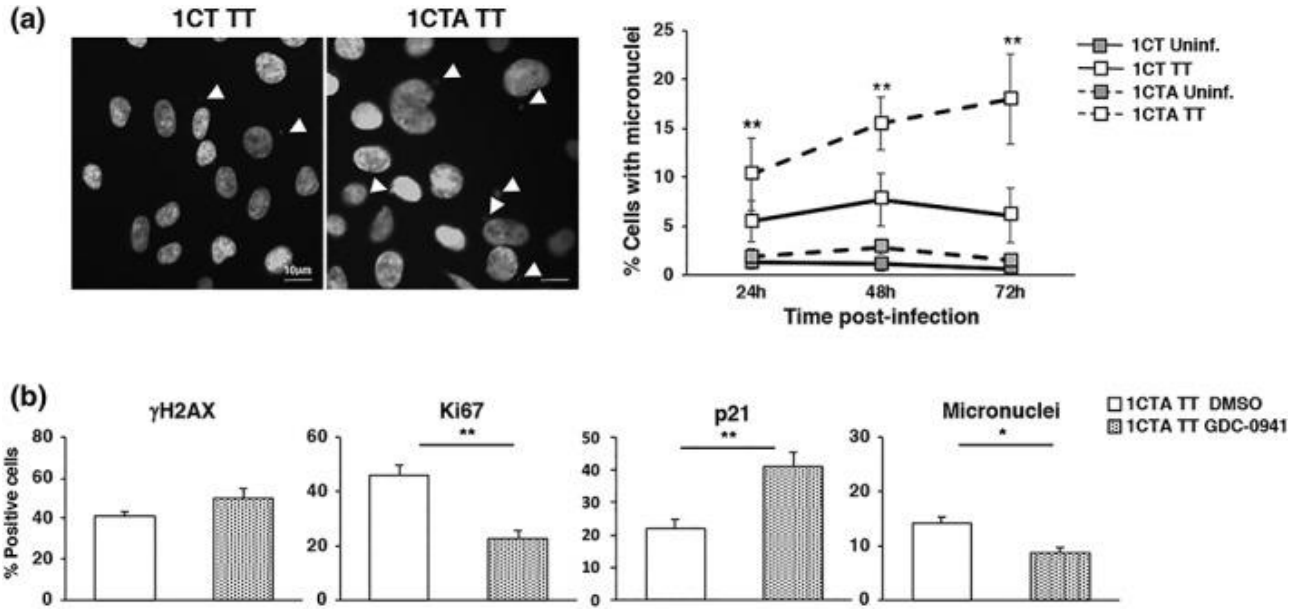

Figure 12. APC deficiency promotes acquisition of genomic instability upon infection with the genotoxic *Salmonella* in a PI3K dependent manner. (**a**) 1CT and 1CTA cells, grown in 2D culture, were left untreated (Uninf.) or infected with the MC1 TT (TT) strain at MOI 100:1 for the indicated period of time. The left panel shows representative fluorescence micrographs of the infected cells illustrating the presence of micronuclei (white arrowheads) detected by DAPI staining. The right panel shows the quantification of micronuclei positive cells. Mean ± SEM of four to eight independent experiments. (**b**) 1CTA cells were pretreated for 1 h with the specific PI3K inhibitor CDG-0941 (1 μM) for 1-h prior infection, which was carried on for 72 h. DMSO was used as vehicle control. Detection of DNA damage, proliferative capacity, and micronuclei formation were assessed by γH2AX, Ki67, p21, and DAPI staining. Mean ± SEM of three independent experiments. Statistical analysis was performed using the Student t test, *$p < .05$; **$p < .01$.

Sustained activation of the DDR was confirmed in an organotypic 3D-tissue model of colonic epithelium

Because the 2D monoculture system does not reproduce the microenvironment of the infected epithelium and its interaction with the connective tissue of the lamina propria, 3D organotypic culture was developed. Here, primary colonic fibroblasts embedded into a collagen matrix provided a lamina propria-like support for the colonic epithelial cell monolayer (**Figure S7A**). The data highlighted that epithelial cells grown in 3D conditions were more susceptible to *Salmonella* infection, as illustrated by bacterial overgrowth and destruction of the epithelial monolayer already 24-h post-infection at MOI 100:1 and 50:1 (**Figure S7B**). The infection of 1CT and 1CTA cells with MC1 TT or MC1 ΔcdtB bacteria at MOI 25:1 resulted in the formation of *Salmonella*-containing vacuoles, detected by LPS staining 24-h post-infection (**Figure S7C**), without major alteration of the epithelial layer and was therefore used in all the subsequent experiments. The 3D model confirmed the sustained activation of the DDR in infected APC-deficient 1CTA cells compared with the 1CT cell line (**Figure 13**). However, whereas the majority of 1CT and 1CTA cells grown in 2D culture expressed the Ki67 proliferation marker at the initial stages of the experimental set-up (**Figure 10a**), the 3D culture condition promoted a significant reduction in the percentage of Ki67 positive cells from approximately 80% to 25% in uninfected controls (**Figures 10a** and **14b**) due to formation of a confluent monolayer (**Figure S7A**). As expected, infection with MC1 TT induced a further decrease in the percentage of Ki67 positive cells in 1CT monolayers. In contrast, the percentage of 1CTA cells expressing the proliferative marker increased up to 50% 24-h post-infection and remained high for the entire observation period (**Figure 14b**), suggesting an exit from the quiescent state upon MC1 TT infection. This effect was specific for the genotoxic *Salmonella*, because it was not observed in cells infected with

the MC1 cdtB strain (**Figures 8b**). In addition, the majority of Ki67 positive cells showed signs of DNA damage, assessed by formation of the 53BP1 foci (**Figure 8c**).

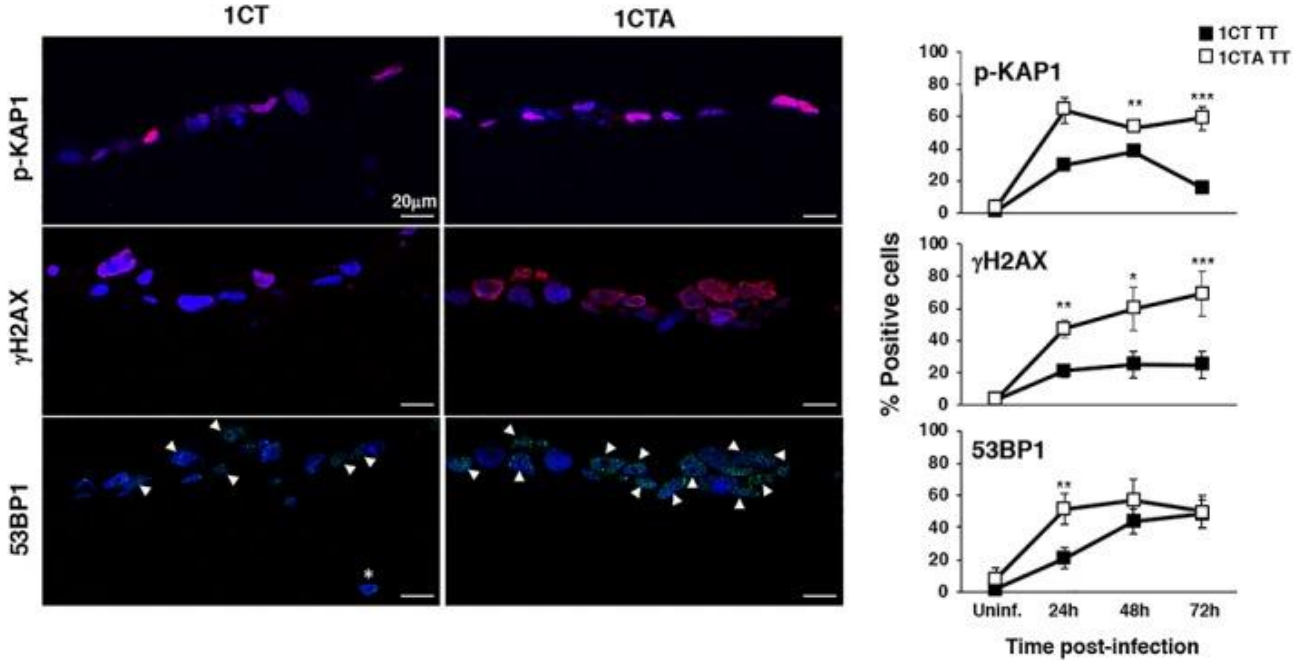

Figure 13. **APC-deficient cells show a sustained activation of the DNA damage response in 3D culture.** 1CT and 1CTA cells, grown in 3D culture, were left untreated (Uninf.) or infected with the MC1TT strain (TT) at MOI 25:1 for the indicated period of time. Activation of the DNA damage response was assessed as described in Figure 3. Left panel: representative scanning confocal micrographs; right panel: quantification of the positive cells. Mean ± SD of three to seven independent experiments. One hundred cells were evaluated for each experiment for each cell line. Statistical analysis was performed using the Student t test, *$p < .05$; **$p < .01$; ***$p < .001$.

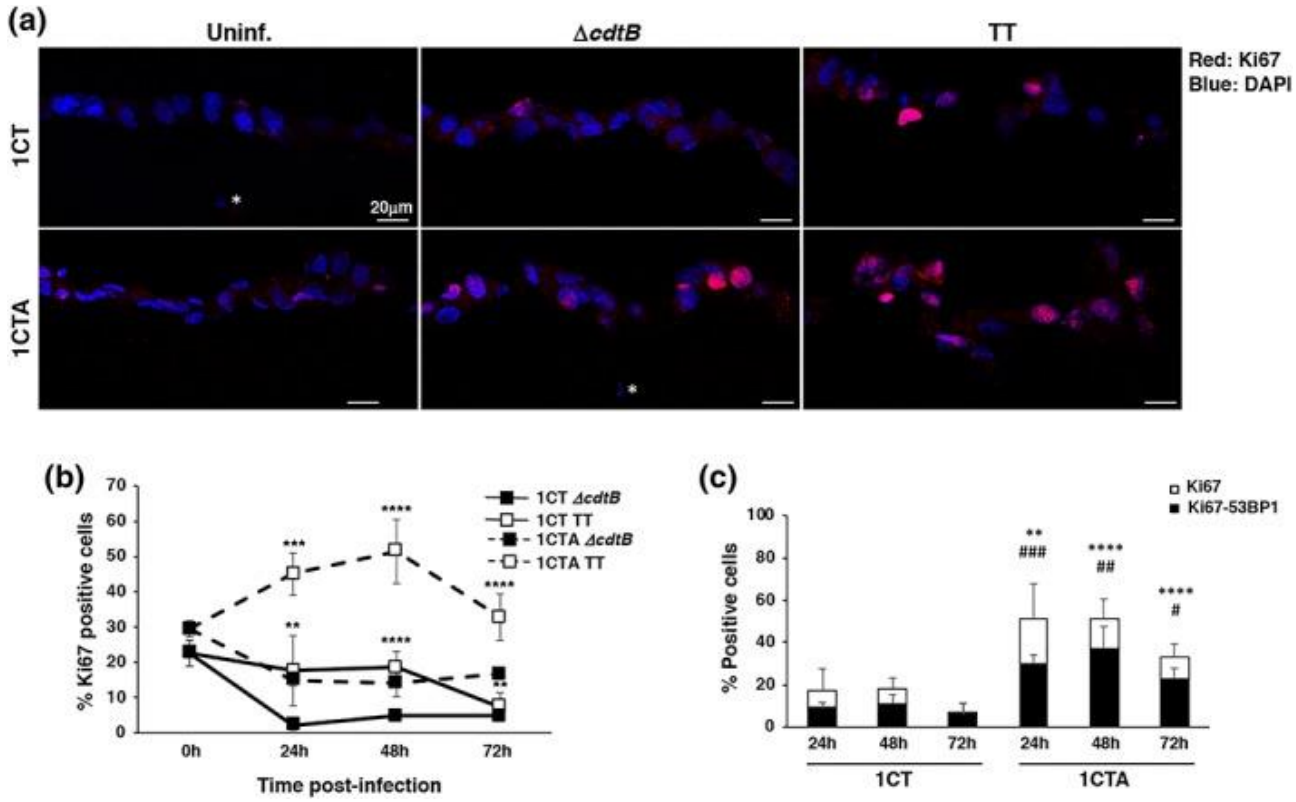

Figure 14. Infection with genotoxic *Salmonella* promotes exit from quiescence of the 1CTA cells. 1CT and 1CTA cells, grown in 3D culture, were infected with the MC1 TT or MC1 cdtB strain. Induction of proliferation status and DNA damage was assessed by immunofluorescence analysis, using antibodies specific for Ki67 and 53BP1, respectively, at the indicated time points. (**a**) Representative scanning confocal micrograph of infected 1CT and 1CTA cells grown in 3D culture stained with the anti-Ki67 specific antibody (red). Nuclei were counterstained with DAPI (blue). Magnification 40×. The white asterisk indicates nuclei of fibroblasts embedded in the collagen matrix. (**b**) Quantification of cells positive for Ki67. (**c**) Quantification of cells positive for Ki67 (white bar) and double positive for both Ki67 and 53BP1 foci (black bar). Mean ± SEM of three to four independent experiments. Statistical analysis was performed using the Student t test. *,#$p < .05$; **,##$p < .01$; ***,###$p < .001$; ****,####$p < .0001$.*comparison Ki67 positive cells, #comparison Ki67-γH2AX double-positive cells

Discussion

The GM of CRC patients has been shown to harbor an increased proportion of bacteria expressing bacterial genotoxins[294,295,296,297]. The pro-tumorigenic effect of these genotoxins has been shown in mouse models prone to develop cancer or dysplasia, such as the IL10 knock-out mice exposed to the pro-carcinogen AOM[298]. However, the context in which the infection/colonization with genotoxin-producing bacteria occurs may have a great impact on the outcome of the response to the toxins. Indeed, it has been shown that infection of immunocompetent mice with a TT producing *Salmonella* is associated with a strong suppression of the intestinal inflammatory response, and no sign of dysplasia or tumor development was observed in mice colonized with the bacterium for 6 months[299]. Thus, the pro-carcinogenic effect of these toxin families may be exerted under special circumstances, such as a proinflammatory environment or haploinsufficiency of tumor suppressor genes. According to these results, was demonstrated that the lack of the APC tumor suppressor gene, mutated in 80% of sporadic CRC and in 100% of FAP, contributed to the carcinogenic properties of the typhoid toxin, in colonic epithelial cells using both classical monolayer 2D culture and 3D organotypic model, by inhibiting concomitantly two key steps of the DDR: DNA repair and DNA damage-induced cell cycle arrest. The data highlighted that in response to infection with the TT-producing *Salmonella*, APC-deficient or haploinsufficient

---

[294] Buc E, et al. High prevalence of mucosa-associated *E. coli* producing cyclomodulin and genotoxin in colon cancer. *PLoS One*. **2013**;8:e56964.

[295] Candela M, et al. Human intestinal microbiota: Cross-talk with the host and its potential role in colorectal cancer. *Crit Rev Microbiol*. **2011**;37:1-14.

[296] Candela M, et al. Inflammation and colorectal cancer, when microbiota-host mutualism breaks. *World J Gastroenterol*. **2014**;20:908-922.

[297] Shen XJ, et al. Molecular characterization of mucosal adherent bacteria and associations with colorectal adenomas. *Gut Microbes*. **2010**;1:138-147.

[298] Arthur JC, et al. Intestinal inflammation targets cancer- inducing activity of the microbiota. *Science*. **2012;**338:120-123.

[299] Del Bel Belluz L, et al. The typhoid toxin promotes host survival and the establishment of a chronic asymptomatic infection. *PLoS Pathog*. **2016**;12:e1005528.

cells present (a) a sustained DDR response, (b) a reduced capacity to repair DNA damage in response to a broad panel of genotoxic agents, and (c) a failure to induce upregulation of the cyclin kinase inhibitor p21 and consequently to activate a proper cell cycle arrest leading to proliferation in spite of the presence of DNA damage. The inability to repair DNA and to completely halt the cell cycle is ultimately associated with an enhanced acquisition of genomic instability, thus synergizing with the APC deficiency in the carcinogenic process. The failure to activate a proper checkpoint response was dependent on activation of the PI3K pathway, as shown by the significant reduction in cells expressing the proliferation marker Ki67 and consequent reduction in micronuclei formation in cells pretreated with the specific PI3K inhibitor. *Salmonella* infection is associated with the activation of the PI3K/AKT axis[300]; however, in this experimental setup, the ability to inhibit the checkpoint responses and maintain Ki67 expression was predominantly observed in cells infected with the genotoxic strain compared with the effect induced by the control strain MC1 ΔcdtB, which is consistent with activation of PI3K and AKT observed in response to CDT or ionizing radiation[301,302]. The activation of the PI3K pathway is most likely dependent on the activation of the DDR, because it has been previously demonstrated that Nbs1, one of the three components of the Mre11-Rad50-Nbs1 complex, interacts through its conserved C-terminal motif with the p110α catalytic subunit of PI3K, stimulating the kinase activity[303], and the activation of this complex in cells exposed to CDT was previously shown by Guerra et al.[304].

---

[300] Steele-Mortimer O, et al. Activation of Akt/protein kinase B in epithelial cells by the *Salmonella typhimurium* effector sigD. *J Biol Chem*. **2000**;275:37718-37724.

[301] Frisan T, et al. The *Haemophilus ducreyi* cytolethal distending toxin induces DNA double-strand breaks and promotes ATM-dependent activation of RhoA. *Cell Microbiol*. **2003**;5:695-707.

[302] Seiwert N, et al. AKT2 suppresses pro-survival autophagy triggered by DNA double-strand breaks in colorectal cancer cells. *Cell Death Dis*. **2017**;8:e3019.

[303] Chen YC, et al. Activation of phosphoinositide 3-kinase by the NBS1 DNA repair protein through a novel activation motif. *J Mol Med*. **2008**;86:401-412.

[304] Guerra L, et al. Myc is required for activation of the ATM-dependent checkpoints in response to DNA damage. *PLoS One*. **2010**;5:e892.

However, in APC-deficient cells, this activation can be further potentiated because CKS2, a direct transcriptional target of the β catenin/TCF4, has been shown to activate the PI3K pathway in CRC cells[305]. As a consequence of the PI3K/AKT pathway activation, downregulation of p21, likely mediated by the AKT-dependent inhibition of the FoxO transcription family[306], overrides the checkpoint response, because cells exposed to the PI3K inhibitor showed reduced Ki67 levels and concomitant upregulation of p21 expression. In addition, colonization with the CDT producing *Campylobacter jejuni* has been shown to enhance tumor formation in the $Apc^{Min/+}$ mouse model upon dextran sulfate sodium-induced colitis, in a mechanistic target of rapamycin-dependent manner (mTOR)[307]. Interestingly, mTOR is a key target of the PI3K/AKT axis[308], highlighting the relevance of the activation of this pathway in bacterial genotoxin-induced carcinogenesis in the context of APC deficiency. It is noteworthy that a small but reproducible fraction of the APC-proficient 1CT cells grown in 3D culture presented a sign of DNA damage but were still positive for the proliferation marker Ki67. Thus, it is possible that under certain circumstances, also normal cells may escape the checkpoint response, which can lead to acquisition of genomic instability and transformation. These circumstances may be a chronic inflammatory condition or coinfection with other bacteria known to be associated with CRC, such as *Fusobacterium nucleatum*[309] and the enterotoxigenic *B. fragilis*[310]. Interestingly, recent data showed that the colonic mucosa of FAP patients is characterized by the presence of bacterial biofilms, where

---

[305] Qi J, et al. New Wnt/beta-catenin target genes promote experimental metastasis and migration of colorectal cancer cells through different signals. *Gut*. **2016**;65:1690-1701.

[306] Zhang X, et al. Akt, FoxO and regulation of apoptosis. *Biochim Biophys Acta*. **2011**;1813:1978-1986.

[307] He Z, et al. *Campylobacter jejuni* promotes colorectal tumorigenesis through the action of cytolethal distending toxin. *Gut*. **2011**;68:289-300.

[308] Fruman DA, et al. The PI3K pathway in human disease. *Cell*. **2017**;170:605-635.

[309] Kostic AD, et al. Genomic analysis identifies association of *Fusobacterium* with colorectal carcinoma. *Genome Res*. **2012**;22:292–298.

[310] Purcell RV, et al. Colonization with enterotoxigenic *Bacteroides fragilis* is associated with early-stage colorectal neoplasia. *PLoS One*. **2017**;12:e0171602.

E. coli and *B. fragilis* are predominant members and that the two bacteria synergized to promote cancer in an AOM-dependent CRC murine model[311]. Collectively, these data highlight the carcinogenic potential of the TT and provide a molecular mechanism to support the epidemiological observations linking chronic *Salmonella* infection with increased cancer risk not only in the hepatobiliary tract but also in the colon[312,313].

APC deficiency and DNA damage repair

All these data, demonstrating an altered DNA repair in the APC-deficient cells, are in agreement with previous results demonstrating that intoxication with sublethal doses of the *E. coli* CDT synergized with the APC deficiency in promoting genomic instability[314]. Here, the analysis was expanded by performing a detailed analysis of the DDR and further showed that APC deficiency is associated with failure to repair not only DNA single- and double-strand breaks but also oxidative damage, indicating that APC is involved in the regulation of multiple repairs pathways. This protein is well-characterized as negative regulator of β-catenin. The absence of a functional APC results in a constitutive translocation of β-catenin in the nucleus leading to transcriptional activation of the target genes, many of which promote cell cycle division (cMYC and Cyclin D1)[315]. However, there are evidences that APC can directly regulate DNA repair in a β-catenin independent manner. Kouzmenko and colleagues have shown that APC (aminoacids 1441-2077) contributes to the recruitment of DNA-PK, a key sensor and regulator of the non-homologous end joining repair and favors

[311] Dejea CM, et al. Patients with familial adenomatous polyposis harbor colonic biofilms containing tumorigenic bacteria. *Science*. **2018**;359:592-597.

[312] Dutta U, et al. Typhoid carriers among patients with gallstones are at increased risk for carcinoma of the gallbladder. *Am J Gastroenterol*. **2000**;95:784787.

[313] Mughini-Gras L, et al. Increased colon cancer risk after severe Salmonella infection. *PLoS One*. **2018;**13:e0189721.

[314] Graillot V, et al. Genotoxicity of cytolethal distending toxin (CDT) on isogenic human colorectal cell lines: Potential promoting effects for colorectal carcinogenesis. *Front Cell Infect Microbiol*. **2016**;6:34.

[315] Tortelote GG, et al. Complexity of the Wnt/betacatenin pathway: Searching for an activation model. *Cell Signal*. **2017**;40:30-43.

phosphorylation of histone H2AX (γH2AX) in response to DNA-damaging agents causing DNA DSB[316,317]. Interestingly, germline and somatic APC mutations resulting in a truncated form of the protein are localized within this region[318]. This effect seems to be specific for certain types of DNA damage, such as induction of DNA breaks, whereas APC does not interact with γH2AX in cells exposed to cisplatin, which promotes the formation of platinum-DNA adducts, mainly repaired by nucleotide- and base-excision repair[316,317]. Alternatively, failure to repair the damaged DNA may be dependent on the lack of p21 upregulation observed in APC-deficient cells, which has been shown to accumulate at the sites of laser-induced localized DNA breaks, colocalizing with γH2AX and Ku80, one of the components of the DNA-PK[319].

Genotoxin-producing bacteria and CRC

It is not clear whether the dysbiosis observed in CRC patients precedes the tumor development, contributing to the initiation, or is a consequence of the altered microenvironment, contributing to tumor progression. It has been shown that the GM of the APC $^{Min716/+}$ and APC $^{Min850/+}$ mice, widely used models for FAP, displays an enrichment in *E. coli* and *B. fragilis* compared with the wild-type control mice even prior the development of polyposis[320],[321], indicating that the tumor suppressor gene mutation causes the dysbiosis. Two major forms of genomic instability have been detected in CRC: chromosomal instability

316 Kouzmenko AP, et al. Truncation mutations abolish chromatin-associated activities of adenomatous polyposis coli. *Oncogene*. **2008**;27:4888–4899.

317 Wang D, Lippard SJ. Cellular processing of platinum anticancer drugs. *Nat Rev Drug Discov*. **2005**;4:307-320.

318 Kohler EM, et al. Functional definition of the mutation cluster region of adenomatous polyposis coli in colorectal tumours. *Hum Mol Genet*. **2008**;17:1978-1987.

319 Koike M, Yutoku Y, Koike A. Accumulation of p21 proteins at DNA damage sites independent of p53 and core NHEJ factors following irradiation. *Biochem Biophys Res Commun*. **2011**;412:39-43.

320 Dejea CM, et al. Patients with familial adenomatous polyposis harbor colonic biofilms containing tumorigenic bacteria. *Science*. **2018**;359:592-597.

321 Son JS, et al. Altered interactions between the gut microbiome and colonic mucosa precede polyposis in APCMin/+ Mice. *PLoS One*. **2015**;10:e0127985.

(CIN), associated with a poor prognosis and characterized by frequent deletions, amplifications, inversions, and translocations; and microsatellite instability, with a more favorable prognosis and characterized by a wide spread hypermethylation at promoter sites. CIN occurs more frequently in tumor showing APC and KRAS mutations, whereas the microsatellite instability phenotype is mainly associated with BRAF mutations[322]. Chronic exposure to sublethal dose of the *Helicobacter hepaticus* CDT induces genomic instability in rat fibroblasts, and approximately 20% of the alterations observed were deletions[323], suggesting that the presence of genotoxin-producing bacteria can contribute to the CIN observed in a subset of CRC patients.

Organotypic culture

In this study was compared the effects of the infection with the genotoxic *Salmonella* in classical 2D conditions and in 3D organotypic model. The two models showed a similar alteration of the DDR kinetics in APC-deficient cells. However, differently from the 2D model where both 1CT and 1CTA cells were replicating as indicated by the high percentage of Ki67 positive cells in control and infected cells at the 24-h time point, cells grown in 3D were approaching a quiescent stage when infection was performed. Interestingly, infection with the toxigenic strain promoted an increase in the percentage of 1CTA cells positive for Ki67 in the 3D model. This outcome was not detected in cells infected with the control MC1 cdtB *Salmonella*, excluding that the cell proliferation is due to a wound-healing response to the infection. The data strongly suggest that more complex culture settings may highlight aspects of the cellular responses to DNA damage that were previously not observed in

[322] Amaro A, Chiara S, Pfeffer U. Molecular evolution of colorectal cancer: From multistep carcinogenesis to the big bang. *Cancer Metastasis Rev*. **2016**;35:63-74.

[323] Guidi R, et al. Chronic exposure to the cytolethal distending toxins of Gram-negative bacteria promotes genomic instability and altered DNA damage response. *Cell Microbiol*. **2013**;15:98-113.

traditional monocellular systems. In conclusion, was demonstrated that infection with genotoxin-producing enteric bacteria, enriched in the microbiome of CRC patients, synergizes with the APC deficiency in the acquisition of genomic instability, the enabling characteristic of cancer, due to an altered DNA repair, activation of PI3K, and reduced capacity to implement an efficient cell cycle arrest. In addition, the use of organotypic 3D culture may represent a more suitable model than the classical 2D conditions to identify still unknown outcomes of the cell response to genotoxic stresses.

2.2 The gut microbiota dynamics during chemotherapy in epithelial ovarian cancer patients are closely related to the therapeutic response

Brief introduction

Epithelial ovarian cancer (EOC) is a relatively rare disease with the highest incidence rates in western countries such as Europe and North America (8 cases per 100,000)[324]. Currently, there is no established screening test for this disease and this cancer represents the most lethal and silent gynecological tumor, with diagnosis in advanced stages (III-IV) in about 65% of cases and a five-year relative survival of only 20-30%[325]. Recent advances in tumor molecular characterization correlated with findings from clinicopathologic and molecular characterizations of ovarian cancers have revealed that EOC can be divided in two distinct groups termed type I (*i.e.*, low grade serous carcinoma, endomerioid carcinoma, clear cells carcinoma, mucinous carcinoma, malignant Brenner tumors, serous mucinous carcinoma) and type II carcinomas (*i.e.*, high grade serous carcinoma, undifferentiated carcinoma and carcinosarcoma). High-grade serous ovarian cancers (HGSOC) represent the most frequent histological type. Primary tumors originate from the epithelium of the ovary, fallopian tube or peritoneum and then spread to the peritoneal surfaces and viscera of the pelvis and whole abdomen (*i.e.*, carcinosis), the cancer's spread by blood and lymphatic way is rare[326]. The standard therapeutic approach is surgical cytoreduction followed by first-line standard chemotherapy with platinum and taxane compounds. When surgery is not possible for

[324] Webb PM, Jordan SJ. Epidemiology of epithelial ovarian cancer. *Best Pract Res Clin Obstet Gynaecol.* **2017**;41:3-14.

[325] Baldwin LA, et al. Ten-year relative survival for epithelial ovarian cancer. *Obstet Gynecol.* **2012**;120:612-618.

[326] Wu R, et al. Type I to type II ovarian carcinoma progression: mutant Trp53 or Pik3ca confers a more aggressive tumor phenotype in a mouse model of ovarian cancer. *Am J Pathol.* **2013**;182:1391-1399.

disease extent, neoadjuvant chemotherapy is an option to reduce the burden of the disease and achieve cytoreduction in responders, in non-responders the prognosis is poor[327]. Despite optimal surgery and appropriate first-line chemotherapy, about 70–80% of patients with EOC will develop disease recurrence and patients are candidate to new therapeutic opportunities, such as novel drug classes combined to different combination of chemotherapy[328,329]. The literature data demonstrate that when EOC recurs, it should be considered a chronic and lethal disease with poor prognosis[330]. Recurrence occurs in about 23% of patients during 6 months after first-line chemotherapy (Platinum Resistant, PR), and 60% after 6 months (Platinum Sensitive, PS)[331]. Progressively PS patients experience shorter disease-free intervals, with the development of PR. Etiology of EOC is poorly understood[332]. Risk factors are represented by age, late menopause, genetic factors (BRCA mutation and Lynch syndrome) and environmental agents. The role of infections and inflammation in the pathogenesis of EOC are not completely elucidated, probably inflammation and changes in hormone levels lead to DNA damage by oxidative stress. Pelvic inflammatory disease, although not being a recognized risk factor, is associated with EOC in several publications[333]. The correlation between some agents such as *Chlamydia*, HPV and cytomegalovirus

[327] Chandra A, et al. Ovarian cancer: Current status and strategies for improving therapeutic outcomes. *Cancer Med*. **2019**;8:7018-7031.

[328] Thigpen JT, et al. Phase II trial of paclitaxel in patients with progressive ovarian carcinoma after platinum-based chemotherapy: a Gynecologic Oncology Group study. *J Clin Oncol*. **1994**;12:1748-1753.

[329] Perrone AM, Zamagni C, De Iaco P. Hyperthermic intraperitoneal chemotherapy in ephitelial ovarian cancer should be proposed in eight time points. *Eur J Surg Oncol*. **2014**;40:1028-1029.

[330] Cortez AJ, et al. Advances in ovarian cancer therapy. *Cancer Chemother Pharmacol*. **2018**;81:17-38.

[331] Perrone AM, et al. Potential Prognostic Role of 18F-FDG PET/CT in Invasive Epithelial Ovarian Cancer Relapse. A Preliminary Study. *Cancers (Basel)*. **2019**;11:713.

[332] Tomao F, et al. Overcoming platinum resistance in ovarian cancer treatment: from clinical practice to emerging chemical therapies. *Expert Opin Pharmacother*. **2017**;18:1443-1455.

[333] Guerra F, et al. Modulation of RAB7A Protein Expression Determines Resistance to Cisplatin through Late Endocytic Pathway Impairment and Extracellular Vesicular Secretion. *Cancers (Basel)*. **2019**;11:52.

infections has been investigated but it is difficult to make any firm conclusion[334]. Interestingly, recent studies by Banerjee et al. profiled the EOC oncobiome, showing distinct viral, bacterial and fungal signatures associated with EOC, including increased representation or unique detection of retroviridiae and HPV, several members of Proteobacteria and Firmicutes, and yeasts and zygomycetous fungi compared to the control group[335]. Indeed, it is known that commensal microorganisms from different body niches can be variously involved in oncogenesis and tumor progression (e.g., *Helicobacter pylori* for gastric cancer and *Fusobacterium nucleatum* in colorectal carcinogenesis)[336,337,338,339]. In this scenario, special attention is being paid to the GM, *i.e.*, the richest and most diverse microbial community of the human holobiont, closely linked to our health[340]. Due to its ability to modulate immune responses and interfere with drug metabolism[341], GM is indeed a very hot topic in cancer research[342,343,344]. Since the first landmark studies in animal models[345,346,347],

---

[334] Mert I, Walther-Antonio M, Mariani A. Case for a role of the microbiome in gynecologic cancers: Clinician's perspective. *J Obstet Gynaecol Res*. **2018**;44:1693-1704.

[335] Banerjee S, et al. The ovarian cancer oncobiome. *Oncotarget*. **2017**;8:36225-36245.

[336] Wroblewski LE, Peek RM Jr, Wilson KT. *Helicobacter pylori* and gastric cancer: factors that modulate disease risk. *Clin Microbiol Rev*. **2010**;23:713-739.

[337] Kostic AD, et al. Genomic analysis identifies association of *Fusobacterium* with colorectal carcinoma. *Genome Res*. **2012**;22:292-298.

[338] Yu T, et al. *Fusobacterium nucleatum* promotes chemoresistance to colorectal cancer by modulating autophagy. *Cell*. **2017**;170:548-563.e16.

[339] Bullman S, et al. Analysis of *Fusobacterium* persistence and antibiotic response in colorectal cancer. *Science*. **2017;**358:1443-1448.

[340] Gilbert JA, et al. Current understanding of the human microbiome. *Nat Med*. **2018**;24:392-400.

[341] Roy S, Trinchieri G. Microbiota: a key orchestrator of cancer therapy. *Nat Rev Cancer*. **2017**;17:271-285.

[342] Finlay BB, et al. Can we harness the microbiota to enhance the efficacy of cancer immunotherapy?. *Nat Rev Immunol*. **2020**;20:522-528.

[343] Cheng WY, Wu CY, Yu J. The role of gut microbiota in cancer treatment: friend or foe? *Gut*. **2020**;69:1867 1876.

[344] Roberti MP, et al. Chemotherapy-induced ileal crypt apoptosis and the ileal microbiome shape immunosurveillance and prognosis of proximal colon cancer. *Nat Med*. **2020**;26:919-931.

[345] Vétizou M, et al. Anticancer immunotherapy by CTLA-4 blockade relies on the gut microbiota. *Science*. **2015**;350:1079-1084.

[346] Sivan A, et al. Commensal *Bifidobacterium* promotes antitumor immunity and facilitates anti-PD-L1 efficacy. *Science*. **2015**;350:1084-1089.

[347] Routy B, et al. Gut microbiome influences efficacy of PD-1-based immunotherapy against epithelial tumors. *Science*. **2018**;359:91-97.

an ever-growing body of evidence indicates that peculiar GM profiles can improve the efficacy of anticancer therapy while reducing side effects. These “more favorable” profiles appear to share greater diversity and greater proportions of health-associated microorganisms, mainly producers of SCFAs[348,349]. However, most of the studies have been conducted in patients with hematological malignancies or melanoma, while no information is available to date regarding the possible role of GM in EOC. In an attempt to bridge this gap, here the GM of 24 women with EOC was profiled through 16S rRNA gene sequencing, and its trajectories were reconstructed over the course of chemotherapy, in relation to the therapeutic response (PR vs. PS). Specifically, patients received neoadjuvant or adjuvant therapy based on the severity of the disease. Fecal samples were collected at diagnosis and before and after each chemotherapeutic cycle until the follow-up.

[348] Gopalakrishnan V, et al. Gut microbiome modulates response to anti-PD-1 immunotherapy in melanoma patients. *Science*. **2018**;359:97-103.
[349] Helmink BA, et al. The microbiome, cancer, and cancer therapy. *Nat Med*. **2019**;25:377-388.

Materials and Methods

Patient enrollment and fecal sampling

Patients with EOC diagnosis referred to the Gynecologic Oncology Unit of the Sant'Orsola Malpighi University Hospital (Bologna, Italy) were enrolled for a longitudinal study on the GM from diagnosis (T0) through chemotherapy treatment (pre and post each cycle) until the follow up. The local Ethical Committee of Area Vasta Emilia Romagna approved the study. Written informed consent was obtained from each enrolled patient during the first access to the Gynecologic Oncology Unit. Inclusion criteria were: i) suspicious or confirmed first diagnosis of ovarian cancer; ii) patients who wanted to be treated in Gynecologic Oncology Unit; iii) patients available to collect stool samples at diagnosis, during treatments and at follow-up. Patients with carcinosis or metastasis to other organs, intestinal inflammatory diseases and characterized by a chronic intake of antibiotics were excluded from the study. All enrolled patients were clustered in two groups (12 vs. 12 subjects) depending on the chemotherapeutic program followed: i) women with moderate disease extent were treated with adjuvant approach characterized by surgical cytoreduction followed by first-line standard chemotherapy with platinum and taxane compounds; ii) patients characterized by an excessive disease extent with no possibility of proceeding with surgery followed neoadjuvant chemotherapy, with a first chemotherapeutic program before surgical cytoreduction. Right before and after surgery, all patients filled in a food and drug intake questionnaire. Evaluable data were age, body mass index (BMI), personal pathological history, histological subtype divided in type I and type II, International Federation of Gynecology and Obstetrics (FIGO) stage, chemotherapy schedules and number, and surgical information including peritoneal cancer index (PCI). At the end of both treatments (*i.e.*, adjuvant and neoadjuvant chemotherapy), follow-up was performed as follows in order

to detect relapse: CA 125 examination and clinical assessment every four months for the first two years and then every 6 months for five years, CT scan every six months. During the post-treatment revaluations, EOC subjects for both chemotherapeutic treatments were further divided into two main groups based on the time elapsed between the last platinum intake and the diagnosis of relapse. Platinum-resistant patients were defined as those who had relapsed before 6 months (non-responders; PR); the platinum-sensitive group was characterized by all subjects who did not relapse in the first 6 months of follow-up (responders; PS). Fecal samples were collected at diagnosis, and before and after each chemotherapy cycle. As for the follow-up, the samples were taken every three months in all patients with no sign of relapse. A total of 406 fecal samples were collected, stored at -80°C and shipped in dry ice to the Department of Pharmacy and Biotechnology, University of Bologna (Bologna, Italy), for the GM analysis.

Microbial DNA extraction

Total microbial DNA was extracted from 0.25 g of stool sample using the repeated bead-beating plus column method, as previously described in Yu and Morrison[350] with few modifications[351]. Briefly, all samples were suspended in 1 mL of lysis buffer (500 mM NaCl, 50 mM Tris-HCl, pH 8, 50 mM EDTA, and 4% SDS) followed by three bead-beating steps in the FastPrep instrument (MP Biomedicals, Irvine, CA) at 5.5 movements/s for 1 min, in presence of four 3-mm glass beads and 0.5 g of 0.1-mm zirconia beads (BioSpec Products, Bartlesville, OK). After 15-min incubation at 95°C, samples were centrifuged at 13,000 rpm for 5 min. Two hundred and sixty microliters of 10 M ammonium acetate were added to the

[350] Yu Z, Morrison M. Improved extraction of PCR-quality community DNA from digesta and fecal samples. *Biotechniques*. **2004**;36:808-812.

[351] D'Amico F, et al. Enteral nutrition in pediatric patients undergoing hematopoietic SCT promotes the recovery of gut microbiome homeostasis. *Nutrients*. **2019**;11:2958.

supernatant and a subsequent centrifugation of 10 min at 13,000 rpm was performed. Each sample was then incubated with one volume of isopropanol, followed by incubation in ice for 30 min. Precipitated nucleic acids were washed with 70% ethanol, re-suspended in 100 µL of TE buffer (10 mM Tris-HCl, 1 mM EDTA pH 8.0), and treated with 2 µL of 10 mg/mL DNase-free RNase at 37°C for 15 min. The nucleic acid purification was performed using the DNeasy Blood and Tissue Kit (QIAGEN, Hilden, Germany) following the manufacturer's instructions. DNA concentration and quality were evaluated using NanoDrop ND-1000 spectrophotometer (NanoDrop Technologies, Wilmington, DE, USA).

16S rRNA gene amplification and sequencing

The V3-V4 hypervariable regions of the 16S rRNA gene were amplified by using the 341F and 785R primers with linked Illumina adapter overhang sequences, as previously described in Klindworth et al.[352]. Fragment amplification was performed by using KAPA HiFi HotStart ReadyMix (Roche, Basel, Switzerland), setting the thermal cycle as follows: 3 min at 95°C, 25 cycles of 30 s at 95°C, 30 s at 55°C, and 30 s at 72°C, and a final 5-min step at 72°C. Library preparation consisted of a first purification with a magnetic bead-based clean-up system (Agencourt AMPure XP, Beckman Coulter, Brea, CA), a limited-cycle PCR to obtain the indexed library using Nextera technology, and a second AMPure XP magnetic bead-based clean-up step. Final libraries were prepared by pooling all samples to an equimolar concentration of 4nM; denaturation and dilution to 5 pM were carried out before performing the sequencing on an Illumina MiSeq platform with a 2 × 250 bp paired-end protocol according to manufacturer's instructions (Illumina, San Diego, CA).

[352] Klindworth A, et al. Evaluation of general 16S ribosomal RNA gene PCR primers for classical and next-generation sequencing-based diversity studies. *Nucleic Acids Res*. **2013**;41:e1.

Bioinformatics and statistics

All sequences were processed using a pipeline that combined PANDASeq[353] and QIIME2[354]. After length and quality filtering, reads were binned into amplicon sequence variants (ASVs) using DADA2[355]. Taxonomic assignment was carried out by using the VSEARCH algorithm[356] and the Greengenes database (May 2013 release). Chimeras were discarded during the analysis. Publicly available sequences of healthy women, matched to EOC patients for several covariates (*i.e.*, age, body mass index [BMI] and geography), were downloaded and used as a control. Sequences were from different cohorts to minimize study-related bias, specifically from: De Filippis et al.[357] (deposited in National Center for Biotechnology Information Sequence Read Archive (NCBI SRA): Bioproject ID SRP042234), Italian samples from Schnorr et al.[358] (MG-RAST database: project ID mgp12183) and elderly samples from Biagi et al.[359] (MG-RAST database: project ID mgp17761). Alpha-diversity was evaluated using the number of observed ASVs and Simpson inverse index. Bray-Curtis, weighted and unweighted UniFrac distances were used to construct Principal Coordinates Analysis (PCoA) graphs. All statistical analyses were performed using the R software. PCoA plots were generated using the "vegan"[360] and "Made4"[361] packages and data separation was tested by a permutation test with pseudo-F ratios (function "Adonis" in "vegan"). To assess

---

353 Masella AP. PANDAseq: paired-end assembler for Illumina sequences. *BMC Bioinformatics*. **2012**;13:31.

354 Bolyen E, et al. Reproducible, interactive, scalable and extensible microbiome data science using QIIME 2. *Nat Biotechnol*. **2019**;37:852-857

355 Callahan BJ, et al. DADA2: High-resolution sample inference from Illumina amplicon data. *Nat Methods*. **2016**;13:581-583.

356 Rognes T, et al. VSEARCH: a versatile open source tool for metagenomics. *PeerJ*. **2016**;4:e2584

357 De Filippis F, et al. High-level adherence to a Mediterranean diet beneficially impacts the gut microbiota and associated metabolome. *Gut*. **2016**;65:1812-1821.

358 Schnorr SL, et al. Gut microbiome of the Hadza hunter-gatherers. *Nat Commun*. **2014**;5:3654.

359 Biagi E, et al. Gut Microbiota and Extreme Longevity. *Curr Biol*. **2016**;26:1480-1485.

360 http://www.cran.r-project.org/package=vegan/

361 Culhane AC, et al. MADE4: an R package for multivariate analysis of gene expression data. *Bioinformatics*. **2005**;21:2789-2790.

differences in alpha diversity and GM composition at different taxonomic levels among groups, Kruskal–Wallis test followed by post-hoc Wilcoxon rank-sum test was used. Discriminating taxa between groups were identified through linear discriminant analysis (LDA) effect size (LEfSe) algorithm[362]. Only taxa with LDA score > 2 at $p < 0.05$ were considered discriminating. For the generation of Co-Abundance Groups (CAGs), only bacterial genera present in at least 10% of the samples were considered. As previously shown in Claesson et al.[363], associations among genera were evaluated using the Kendall correlation test, visualized using hierarchical Ward-linkage clustering based on the Spearman correlation coefficients and used to define co-abundant groups. Wiggum plot networks were created by using Cytoscape software[364,365], with the circle size proportional to bacterial abundance and the connection between nodes representing significant Kendall correlations between genera ($p < 0.05$). When necessary, p values were corrected for multiple comparisons using the Benjamini–Hochberg method. A false discovery rate (FDR) ≤ 0.05 was considered as statistically significant. FDR ≤ 0.1 was considered as a trend.

[362] Segata N, et al. Metagenomic biomarker discovery and explanation. *Genome Biol*. **2011**;12:R60.

[363] Claesson MJ, et al. Gut microbiota composition correlates with diet and health in the elderly. *Nature*. **2012**;488:178-184.

[364] http://www.cytoscape.org/

[365] Smoot ME, et al. Cytoscape 2.8: new features for data integration and network visualization. *Bioinformatics*. **2011;**27:431-432.

Results

Study cohort description

The 16S rRNA gene sequencing was performed on a total of 406 fecal samples from 24 women with EOC, yielding 12,399,150 high-quality reads (mean ± SD, 30,540 ± 21,518). For each patient, sampling took place at several time-points, starting from diagnosis (T0), before and after each chemotherapy cycle (C, pre and post), and at follow-ups, every 3 months from the end of therapy (**Figure 15**). Patients were divided in two groups based on the severity of the disease at diagnosis and, consequently, on the therapy administered thereafter. Specifically, 12 women were treated with adjuvant chemotherapy, *i.e.* the standard therapeutic approach involving surgical cytoreduction followed by first-line standard chemotherapy, while the other 12 patients were given neoadjuvant chemotherapy to reduce the extent of the disease before cytoreductive surgery. At the end of the therapies, all patients were clinically revaluated and categorized as platinum sensitive (PS) or platinum resistant (PR), based on the onset of relapses (later than or within 6 months of first-line chemotherapy, respectively). Specifically, for the neoadjuvant treatment, six patients were PS and six PR; for adjuvant chemotherapy, only three patients were classified as PR while the others responded positively to therapy (*i.e.,* 9 patients were in the PS group).

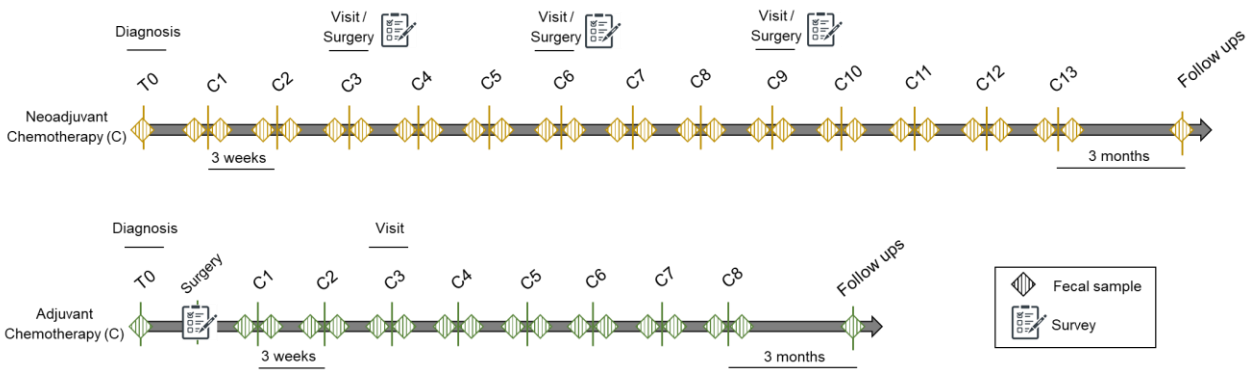

Figure 15. Study design. Schematic representation of fecal sampling for patients with epithelial ovarian cancer, given neoadjuvant (top) or adjuvant (bottom) chemotherapy. The diamonds indicate sampling time-points, *i.e.,* at diagnosis (T0), before and after each chemotherapy cycle (C), and at follow-ups, every 3 months from the end of therapy. Chemotherapy courses were repeated every 3 weeks, depending on the clinical picture. Patients were asked to complete a questionnaire on food and drug intake right before and after surgery.

The gut microbiota in EOC patients at diagnosis

The GM of 24 EOC patients at diagnosis (T0) was profiled and compared with that of 24 healthy women matched by several covariates (*i.e.,* age, BMI and geography) from previous studies[366,367,368]. No significant difference in alpha diversity was observed between two groups using the Simpson's inverse index (Wilcoxon test, $p = 0.3$). In contrast, Bray-Curtis distance-based PCoA showed significant segregation between the GM of EOC patients and that of healthy subjects (permutation test with pseudo-F ratios, $p = 0.001$) (**Figure 16A**). Regarding the taxonomic composition, the GM of both patients and controls was dominated by the phylum Firmicutes (mean relative abundance in patients vs. controls, 68.8% vs.

[366] De Filippis F, et al. High-level adherence to a Mediterranean diet beneficially impacts the gut microbiota and associated metabolome. *Gut*. **2016**;65:1812-1821

[367] Schnorr SL, et al. Gut microbiome of the Hadza hunter-gatherers. *Nat Commun*. **2014**;5:3654.

[368] Biagi E, et al. Gut Microbiota and Extreme Longevity. *Curr Biol*. **2016**;26:1480-1485.

73.9%), along with Bacteroidetes (11.2% vs. 15.1%), Actinobacteria (13.2% vs. 7.1%) and Proteobacteria (4.6% vs. 1.9%) (**Figure 16B**). Consistent with the typical adult-like GM profile[369] *Ruminococcaceae* (29.4% vs. 32.5%), *Lachnospiraceae* (18.3% vs. 32.5%) and *Bacteroidaceae* (6.3% vs. 11.7%) were the most abundant families. However, EOC patients were characterized by decreased proportions of *Lachnospiraceae* (Wilcoxon test, $p < 0.001$), as well as other families, such as *Bifidobacteriaceae*, *Clostridiaceae*, *Rikenellaceae* and *Porphyromonadaceae*, ($p \leq 0.01$). On the other hand, the EOC-related GM profiles were markedly enriched in *Coriobacteriaceae* ($p < 0.001$) (**Figure 16C**). Also at the genus level, several differences emerged between the two groups (**Figure 16D**). In particular, compared to healthy subjects, the GM of EOC patients was enriched in the *Coriobacteriaceae* members, *Adlercreutzia* and *Collinsella* ($p \leq 0.05$), as well as in *Lactococcus* and *Lachnobacterium* ($p \leq 0.002$). On the other hand, EOC patients showed a decrease in the relative abundance of *Lachnospiraceae* genera, such as *Coprococcus*, *Blautia*, *Dorea*, *Lachnospira* and *Roseburia*, along with *Bifidobacterium* ($p \leq 0.009$). When stratifying patients by disease severity and BRCA I and II mutations, no significant differences were found (**Figure S8**).

[369] The Integrative HMP (iHMP) Research Network Consortium, Proctor LM, et al. The Integrative Human Microbiome Project. *Nature*. **2019**;569:641-648.

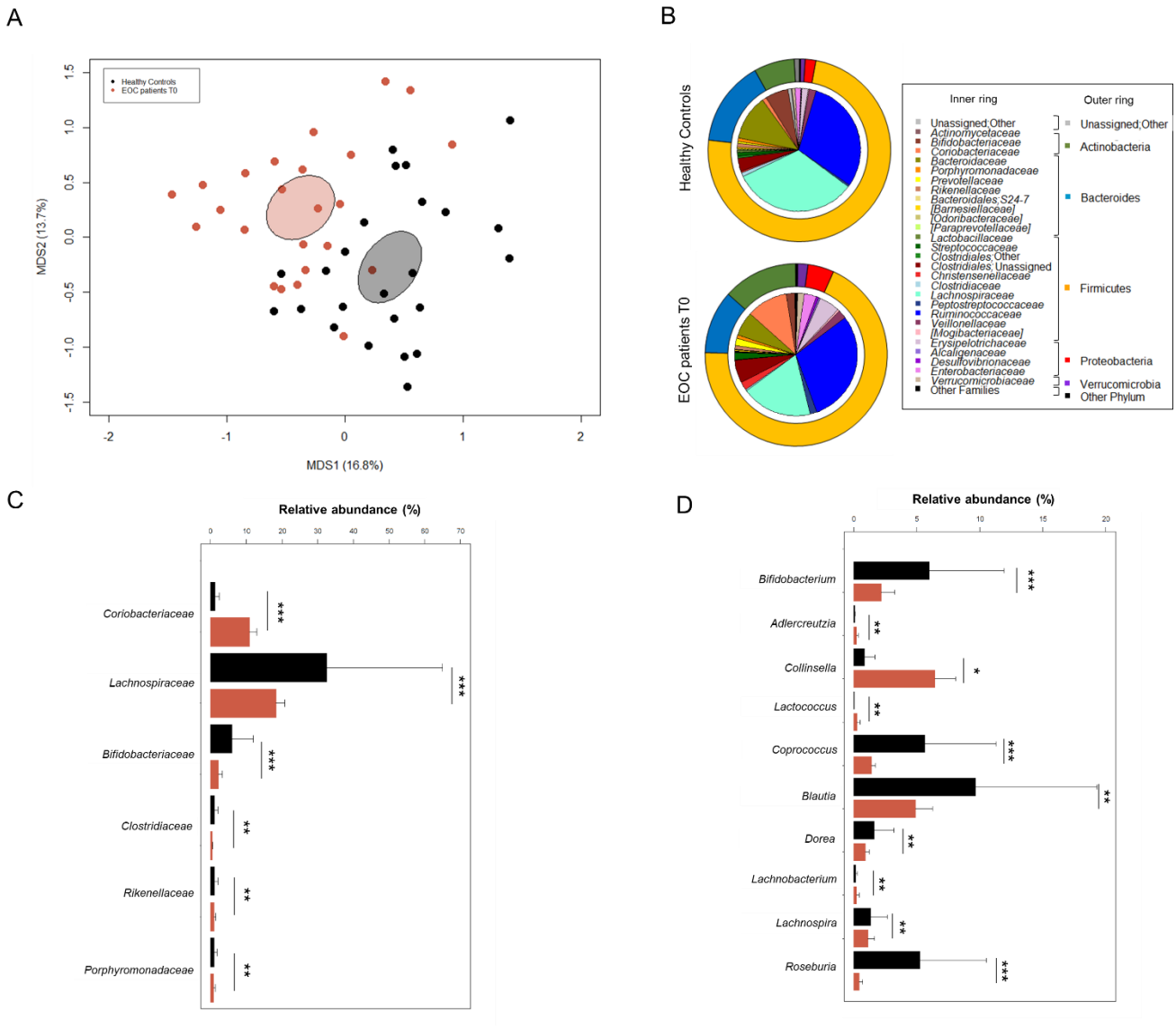

Figure 16. The gut microbiota of EOC patients at diagnosis compared to healthy women.

A, Principal Coordinates Analysis (PCoA) based on Bray-Curtis dissimilarity between the genus-level profiles of 24 EOC patients and 24 age/BMI-matched healthy women, living in the same geographical area (across Italy). Significant separation between groups was found (permutation test with pseudo-F ratios, p = 0.001). Ellipses include 95% confidence area based on the standard error of the weighted average of sample coordinates. **B**, Pie charts showing the average relative abundance of the major phyla (outer ring) and families (inner ring) in the gut microbiota of EOC patients and healthy women. Only taxa with relative abundance > 0.1% in at least 1 sample are shown. Relative abundance (mean ± SEM) of families (**C**) and genera (**D**) differentially represented between groups (Wilcoxon test, * for $p \leq 0.05$; ** for $p < 0.01$; *** for $p < 0.001$). Only families with mean relative abundance > 0.5% in at least one of the two groups are shown.

Gut microbiota dynamics in EOC patients during chemotherapy

The dynamics of GM in 24 women with EOC were reconstructed during adjuvant and neoadjuvant treatments (12 vs. 12 patients), from baseline (T0), through each chemotherapy cycle (C, pre and post) until follow-up. For both patient groups, alpha diversity was found to fluctuate over time with, in particular, a reduction from the baseline at the very beginning of chemotherapy treatments (preC3 and preC4) (Wilcoxon test, $p \leq 0.1$) (**Figure S9**). PCoA based on weighted UniFrac distances showed no differences over time (permutation test with pseudo-F ratios, $p = 0.889$) but strong individuality, with samples from the same subject clustering nearby for both treatment groups ($p = 0.001$). As previously shown at baseline, the GM was dominated by the phylum Firmicutes at all time-points considered, regardless of the chemotherapy treatment, with varying proportions of Bacteroidetes, Actinobacteria, Proteobacteria and Verrucomicrobia. Compared to T0, patients receiving neoadjuvant therapy showed a significant increase in Actinobacteria over time (samples preC4, postC6 and postC7), while those given adjuvant therapy showed an early reduction in Firmicutes (preC3 and postC4) (Wilcoxon test, $p < 0.05$). Consistent results were obtained at the family level, with an increase over time in the relative abundance of *Coriobacteriaceae* in patients undergoing neoadjuvant chemotherapy, accompanied by a reduction in *Ruminococcaceae*, almost after every chemotherapy cycle ($p < 0.05$). For patients given adjuvant therapy, it was mainly observed a reduction in *Lachnospiraceae* (preC5 and preC7, $p < 0.05$) (**Figure S9**).

Potential gut microbiota signatures of therapeutic response

Within each treatment group, patients were stratified by platinum sensitivity (PS) or resistance (PR), based on the time before relapses appeared (beyond or within 6 months of first-line chemotherapy, respectively), and their GM profiles were followed over time. As discussed above for the whole cohort, an overall trend towards reduced diversity in early treatment cycles was observed across all study groups (**Figure 17A**). This was particularly evident for PR patients receiving neoadjuvant therapy, for whom GM diversity dropped dramatically before the C7 cycle (Wilcoxon test, $p = 0.03$). Interestingly, these low levels tended to persist over time unlike what was observed for PS patients given neoadjuvant therapy, whose values remain substantially high until follow-up. A similar pattern (*i.e.,* almost no change in the PS group while greater fluctuations in the PR group) was observed in EOC patients receiving adjuvant treatment. In order to further explore the variation in GM structure that each woman underwent over time, we calculated the weighted UniFrac distances between each time-point and the respective T0, for all PS and PR patients during both chemotherapy treatments (*i.e.,* neoadjuvant vs. adjuvant) (**Figure 17B**). The GM was found to vary over the course of therapy, with more or less fluctuations depending on the study group. In particular, for PR patients undergoing neoadjuvant treatment, the distance from T0 increased considerably before the C7 cycle, then remaining above the baseline inter-individual variation, to drop only in the last time-points and in the follow-up. In contrast, the variations in the corresponding PS group were mostly lower than the inter-patient variability at T0. Similarly, for adjuvant treatment, the distance values for PR patients were often greater than the average inter-patient variation at baseline, while the GM variation in PS patients remained nearly constant over time.

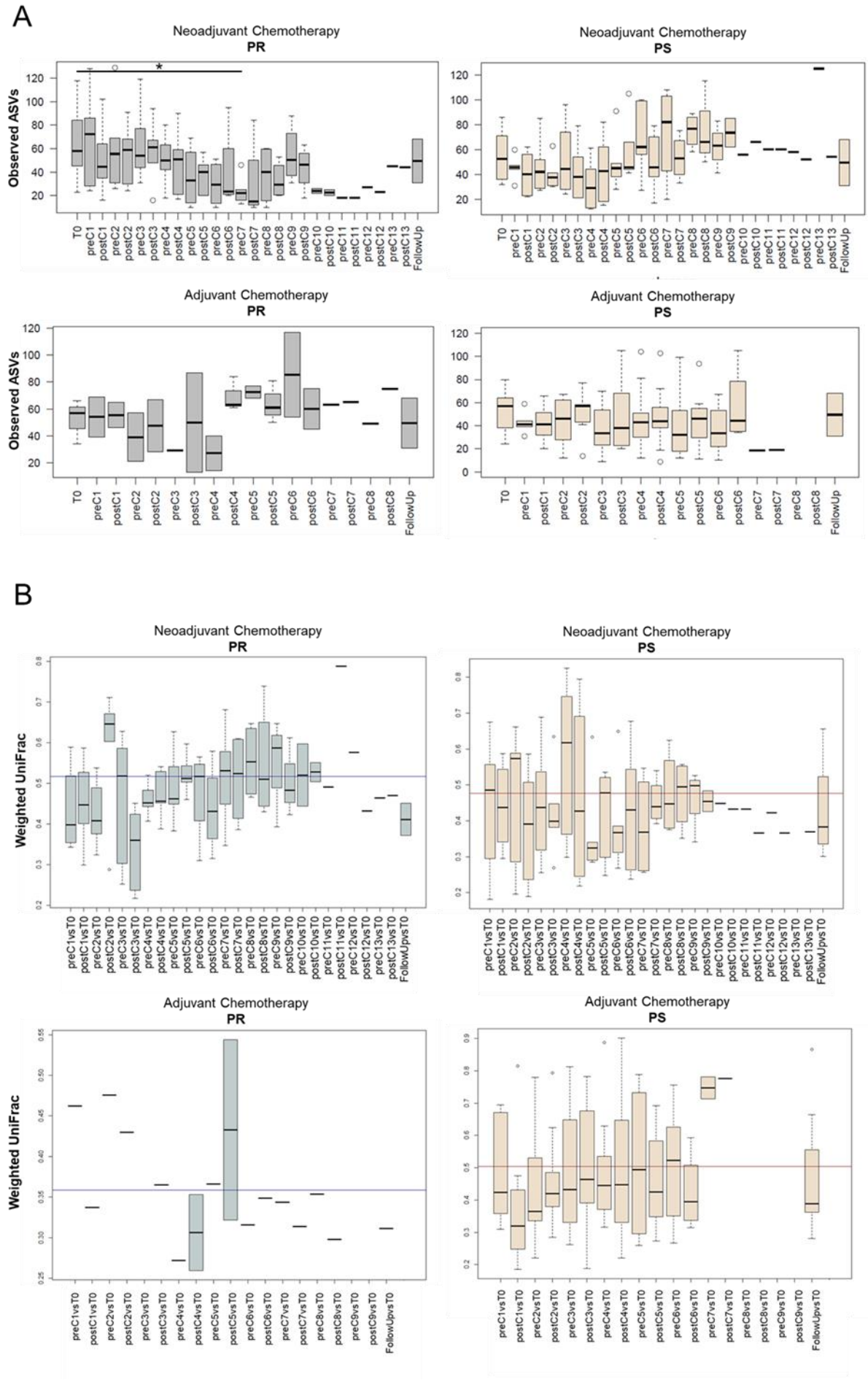
A
Neoadjuvant Chemotherapy
PR
Neoadjuvant Chemotherapy
PS
Adjuvant Chemotherapy
PR
Adjuvant Chemotherapy
PS
Observed ASVs
B
Neoadjuvant Chemotherapy
PR
Neoadjuvant Chemotherapy
PS
Adjuvant Chemotherapy
PR
Adjuvant Chemotherapy
PS
Weighted UniFrac

Figure 17. Dynamics of alpha and beta diversity in EOC patients during chemotherapy, based on the therapeutic response. Boxplots showing the distribution of the number of observed ASVs (**A**) and weighted UniFrac distances between each time-point and the respective T0 for each patient (**B**), during neoadjuvant (top) or adjuvant (bottom) chemotherapy. Patients were stratified by response to therapy: PR, platinum resistant vs. PS, platinum sensitive. C, chemotherapy cycle. For UniFrac distances, the average inter-patient variability at baseline (*i.e.*, T0) is depicted as a line in each plot. (* for $p < 0.05$).

In an attempt to identify potential taxonomic markers of platinum response, a linear discriminant analysis (LDA) effect size (LEfSe) was performed (**Figure 18**). Members of Actinobacteria, including the *Coriobacteriaceae* family with *Eggerthella* and unclassified genera, and *Bifidobacterium* were found to discriminate for PR patients regardless of chemotherapy treatment. On the other hand, the GM of PS patients was discriminated by *Veillonellaceae* members (*i.e.*, *Veillonella*, *Megasphaera* and *Dialister*) as well as by *Catenibacterium* and *Anaerotruncus*. As for peculiarities of each treatment group, Bacteroidetes members (*Bacteroides*, *Prevotella* and *Parabacteroides*), *Faecalibacterium* and *Acidaminococcus* were characteristic of PS patients undergoing adjuvant chemotherapy, while *Desulfovibrio*, *Paraprevotella*, *Anaerostipes*, *Sutterella* and *Pseudoramibacter_Eubacterium* of those receiving the neoadjuvant treatment. Furthermore, the GM of PR patients of the neoadjuvant group was specifically discriminated by *Serratia*, *Sarcina*, *Staphylococcus*, *Peptococcus*, *Haemophilus*, *Turicibacter*, *Streptococcus* and *Collinsella*, while that of PR patients receiving adjuvant therapy by *Coprobacillus*, *Coprococcus*, *[Eubacterium]*, *Dorea* and *Dehalobacterium*. The temporal dynamics of the main taxa identified as discriminating between PR and PS patients are reported in **Figure S10**. Among these, it is worth noting that the proportions of *Coriobacteriaceae*, especially *Eggerthella*, and *Bifidobacterium* were overall considerably higher in PR than in PS patients

throughout the course of treatment. In contrast, *Veillonellaceae* members, *Catenibacterium* and *Anaerotruncus* were poorly represented, if not absent, in the GM of PR patients at the different time-points, while reaching high relative abundance values in PS patients during therapy. It should also be noted that these taxa were not differentially represented at baseline between PR and PS patients receiving neoadjuvant or adjuvant therapy, and that some differences persisted in the follow-up, particularly the overabundance of *Eggerthella* in PR patients (Wilcoxon test, follow-up vs. baseline, neoadjuvant group: $p = 0.03$; adjuvant group: $p = 0.1$) and *Dialister* in PS patients (adjuvant group: $p = 0.1$).

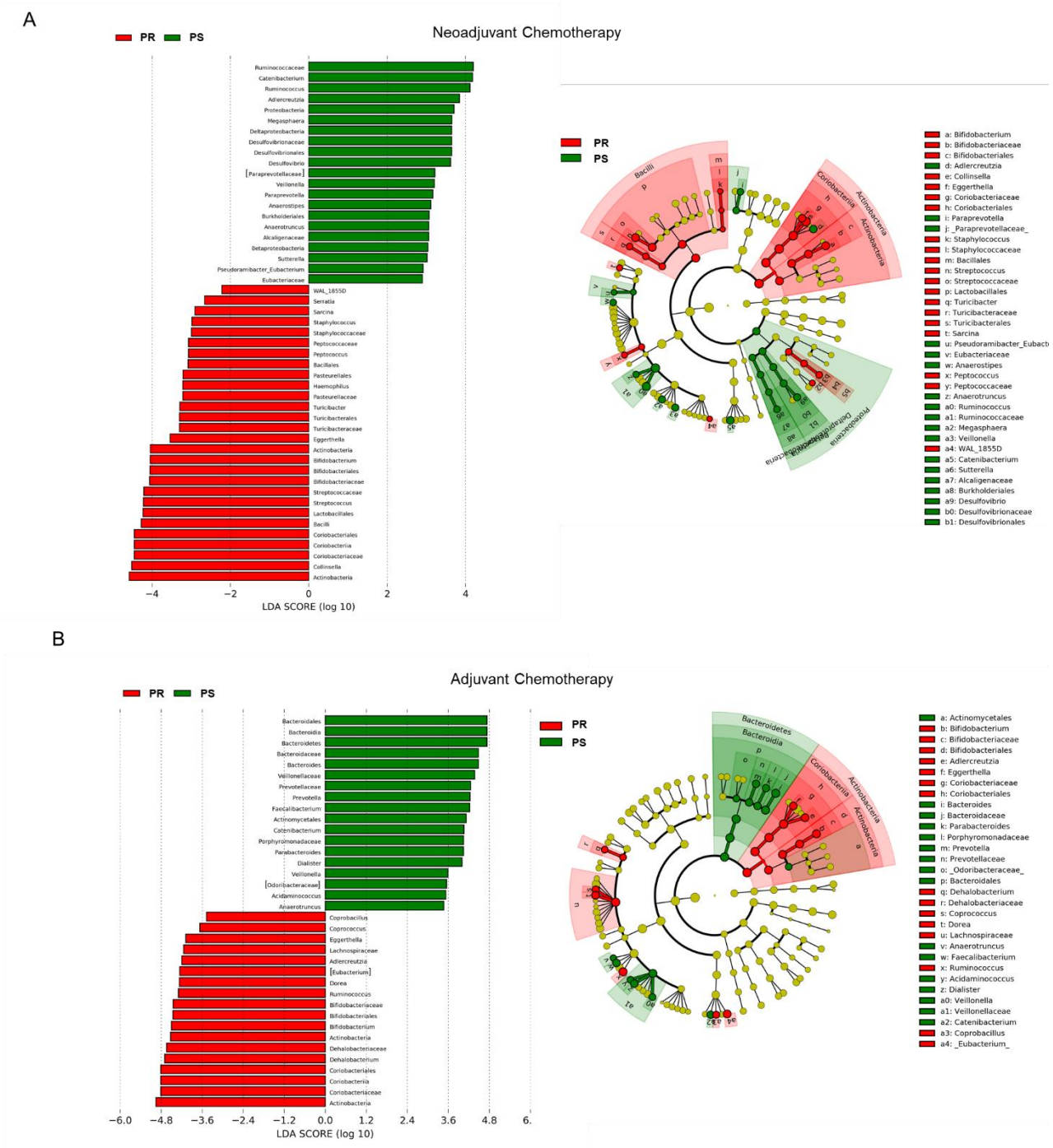

Figure 18. Potential taxonomic signatures of therapeutic response in EOC patients receiving neoadjuvant or adjuvant chemotherapy. Differentially represented taxa between platinum sensitive (*i.e.*, PS) and platinum resistant (*i.e.*, PR) patients receiving neoadjuvant (**A**) or adjuvant (**B**) chemotherapy were identified by linear discriminant analysis (LDA) effect size (LEfSe) analysis. Left, LDA scores; right, cladograms. The logarithmic threshold for discriminative features was set to 2.0.

To further explore the GM compositional variation pattern in relation to the therapeutic response, we established co-abundance associations of genera and then clustered correlated taxa into co-abundance groups (CAGs), describing the GM structures found across the whole dataset (permutation multivariate analysis of variance, $p < 0.05$; see **Figure S11**). Four CAGs were identified and named based on the dominant (*i.e.*, the most abundant) genus within each of them (*Bacteroides*, *Collinsella*, *[Ruminococcus]* and *Faecalibacterium*). The CAG relationships are shown as Wiggum plots in **Figure 19**. Regardless of the treatment group, PR patients were characterized by the *Collinsella* CAG (cyan), especially the co-abundance of *Bifidobacterium* and *Turicibacter*, as well as by *Eggerthella*, belonging to the *[Ruminococcus]* CAG (dark blue). The *Collinsella* CAG was also represented in PS patients but with mostly distinct genera, including *Veillonellaceae* members. On the other hand, PS patients shared an overrepresentation of the *Bacteroides* CAG (brown), with co-abundance of *Desulfovibrio*, *Odoribacter*, *Phascolarctobacterium* and *Methanobrevibacter*, along with other treatment-specific genera. Again, the *Bacteroides* CAG was also represented in PR patients, especially those receiving adjuvant therapy, but with much increased proportions of *[Eubacterium]* and *Dehalobacterium*. The *Faecalibacterium* CAG (green), with co-abundance of well-known SCFA producers, such as *Faecalibacterium*, *Lachnospira*, *Ruminococcus*, *Roseburia* and *Coprococcus*, was mostly represented in the neoadjuvant treatment group, regardless of response.

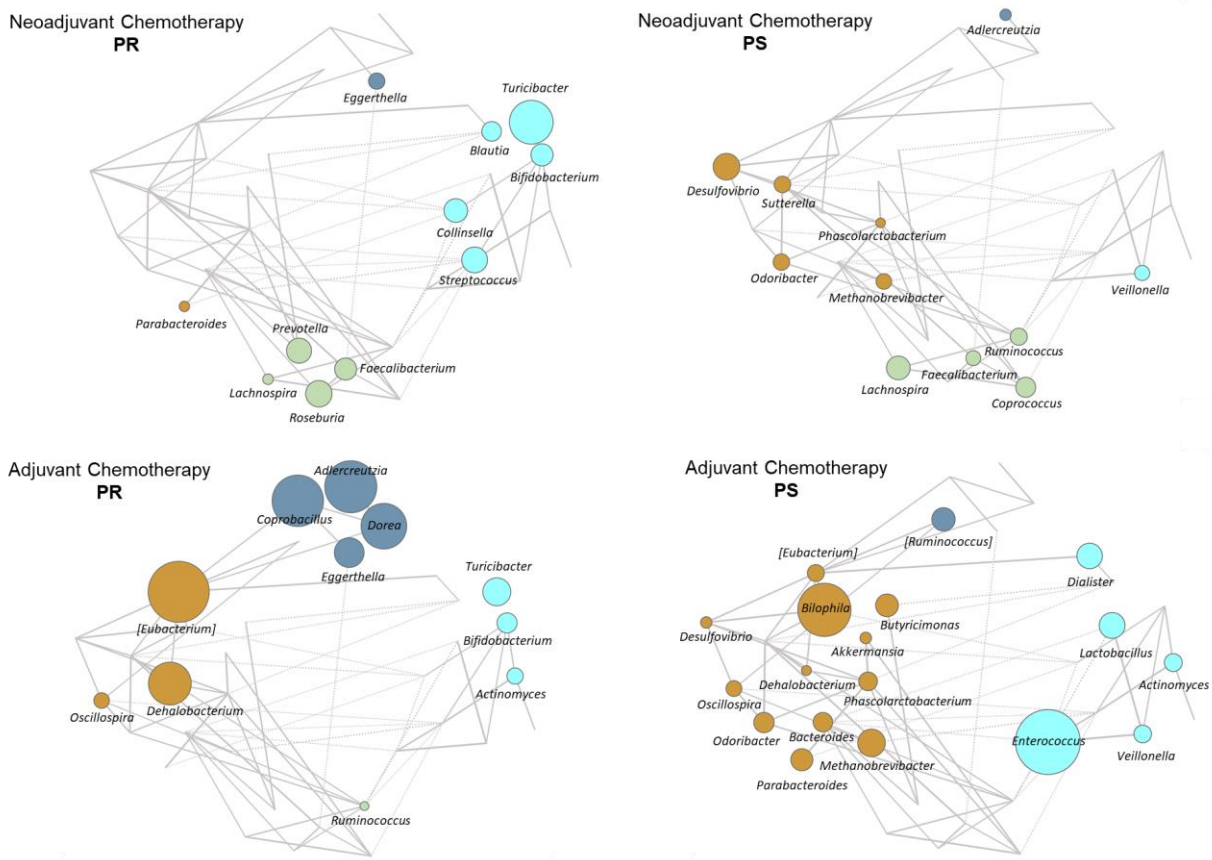

Figure 19. Co-abundance groups in the gut microbiota of EOC patients receiving neoadjuvant or adjuvant chemotherapy. Wiggum plots showing the pattern of variation of the four identified co-abundance groups (CAGs) in EOC patients receiving neoadjuvant (top) or adjuvant (bottom) chemotherapy. Patients were stratified by response to therapy: PR, platinum resistant (left) vs. PS, platinum sensitive (right). CAGs were named according to the most abundant genera and color coded as follows: *Bacteroides* (brown), *Collinsella* (cyan), *[Ruminococcus]* (dark blue) and *Faecalibacterium* (green). Each node represents a genus and its dimension is proportional to the over-abundance relative to background. Connections between nodes indicate positive and significant Kendall correlations between genera ($p < 0.05$). Line thickness is proportional to correlation strength. See also **Figure S11**.

Discussion

As far as we know, for the first time here we profiled the GM of women with EOC and reconstructed its trajectory over the course of chemotherapy, in relation to disease severity (and therefore treatment administered, neoadjuvant vs. adjuvant) and therapeutic response (PR vs. PS). As already observed in other tumor contexts[370,371,372,373], the GM of patients at baseline (*i.e.*, before anti-cancer treatments) showed some dysbiotic traits compared to healthy women matched for several confounding factors (*i.e.*, age, sex, BMI and geography). In particular, EOC patients were depleted of most of the typically health-associated GM members, such as *Blautia*, *Coprococcus*, *Lachnospira*, *Dorea* and *Roseburia*, all belonging to the *Lachnospiraceae* family. These microorganisms are well known to produce SCFAs, *i.e.*, key metabolites to maintain host metabolic, immunological and neurological homeostasis[374,375,376], and their decrease probably represents a non-specific, shared response to diseases, as recently discussed[377]. On the other hand, EOC patients were particularly enriched in *Collinsella* (*Coriobacteriaceae* family). *Collinsella* has recently been

[370] Castellarin M, et al. Fusobacterium nucleatum infection is prevalent in human colorectal carcinoma. *Genome Res*. **2012**;22:299-306.

[371] Feng Q, et al. Gut microbiome development along the colorectal adenoma-carcinoma sequence. *Nat Commun*. **2015**;6:6528.

[372] Yu J, et al. Metagenomic analysis of faecal microbiome as a tool towards targeted non-invasive biomarkers for colorectal cancer. *Gut*. **2017**;66:70-78.

[373] Bik EM, et al. Molecular analysis of the bacterial microbiota in the human stomach. *Proc Natl Acad Sci USA*. **2006**;103:732-7.

[374] Koh A, et al. From dietary fiber to host physiology: short-chain fatty acids as key 411 bacterial metabolites. *Cell*. **2016**;165:1332-1345.

[375] Gilbert JA, et al. Current understanding of the human microbiome. *Nat Med*. **2018**;24:392-400.

[376] Turroni S, et al. Microbiota-Host Transgenomic Metabolism, Bioactive Molecules from the Inside. *J Med Chem*. **2018**;61:47-61.

[377] Duvallet C, et al. Meta-analysis of gut microbiome studies identifies disease-specific and shared responses. *Nat Commun*. **2017**;8:1784.

associated with metabolic disorders[378,379,380] and suggested to play a role in altering intestinal permeability and contributing to a pro-inflammatory state, even in other pathological contexts, such as rheumatoid arthritis[381].

Strikingly, when reconstructing the GM dynamics during the chemotherapy treatment, it was found that the GM of EOC patients behaved differently over time in relation to the therapeutic response. Specifically, a progressive reduction of alpha diversity was observed for PR patients, while in PS patients, the diversity values remained mostly stable and generally higher. Moreover, unlike PS patients, the GM of PR patients underwent considerable fluctuations in terms of beta diversity, mostly higher than the baseline inter-patient variability, thus hinting at profound structural changes over time. From a taxonomic standpoint, the GM of PR women preserved the overabundance of *Coriobacteriaceae* members – especially *Egghertella* – and exhibited a peculiar overrepresentation of *Bifidobacterium* over time, regardless of chemotherapy treatment. It is worth noting that all of these microorganisms produce lactate as part of their metabolism[381,382,383]. On the other hand, *Veillonella, Megasphaera* and *Dialister,* all lactate utilizers belonging to the *Veillonellaceae* family, were distinctly associated with a more favorable platinum response (PS). Lactate is a key element in tumor metabolism. Tumor cells have the remarkable ability to adjust their energetic metabolism as part of their mechanisms for survival; this feature is now recognized as a

---

[378] Gomez-Arango LF, et al. Low dietary fiber intake increases *Collinsella* abundance in the gut microbiota of overweight and obese pregnant women. *Gut Microbes*. **2018**;9:189-201.

[379] Lambeth SM, et al. Composition, diversity and abundance of gut microbiome in prediabetes and type 2 diabetes. *J Diabetes Obes*. **2015**;2:1-7.

[380] Cancello R, et al. Effect of short-term dietary intervention and probiotic mix supplementation on the gut microbiota of elderly obese women. *Nutrients*. **2019**;11:3011.

[381] Chen J, et al. An expansion of rare lineage intestinal microbes characterizes rheumatoid arthritis. *Genome Med*. **2016**;8:43.

[382] Pokusaeva K, Fitzgerald GF, van Sinderen D. Carbohydrate metabolism in Bifidobacteria. *Genes Nutr*. **2011**;6:285-306.

[383] Chan RC, Mercer J. First Australian description of *Eggerthella lenta* bacteraemia identified by 16S rRNA gene sequencing. Pathology. **2008**;40:409-410.

hallmark of cancer[384]. In order to promote growth, high amounts of glucose are metabolized by the tumor cells, producing large volumes of lactate and thus favoring the acidification of the tumor microenvironment (the Warburg effect). In turn, acidosis is associated with several processes, such as metastasis, angiogenesis and most importantly, immunosuppression, leading to a worse clinical prognosis[385,386]. It is therefore tempting to speculate that the aforementioned GM signatures of therapeutic response are somehow related to the lactate cycle, altering its bioavailability and the levels of acidosis, thus affecting the efficacy of chemotherapy. This could also be favored by chemotherapy-related disruption of the gut epithelial barrier, creating an open passage for microbial-derived molecules (e.g., lactate) as well as pathobionts, which can variously influence tumor promotion. Interestingly, the increase of *Bifidobacterium* and the reduction of *Veillonella* have recently been shown in the GM of non-responder melanoma patients after fecal microbiota transplantation (FMT) from responder donor[387].

In conclusion, this pilot study highlighted distinct GM trajectories in EOC patients during chemotherapy treatment, closely related to the therapeutic response, regardless of disease severity. In particular, the potential GM signatures found suggest the involvement of certain GM members in regulating the levels of the oncometabolite lactate, therefore the levels of acidosis and tumor progression. This new evidence related to the GM-cancer relationship will need to be confirmed in a larger cohort, possibly with other approaches, including

---

[384] Hanahan D, Weinberg RA. Hallmarks of cancer: the next generation. *Cell*. **2011**;144:646-674.

[385] de la Cruz-López KG, et al. Lactate in the regulation of tumor microenvironment and therapeutic approaches. *Front Oncol*. **2019**;9:1143.

[386] San-Millán I, Brooks GA. Reexamining cancer metabolism: lactate production for carcinogenesis could be the purpose and explanation of the Warburg Effect. *Carcinogenesis*. **2017**;38:119–33.

[387] Baruch EN, et al. Fecal microbiota transplant promotes response in immunotherapy-refractory melanoma patients. *Science*. **2020**:eabb5920. [Epub ahead of print]. doi: 10.1126/science.abb5920.

functional analysis, to uncover the role of these microorganisms in favoring or vice versa worsening the clinical response to therapy.

2.3 Enteral nutrition in pediatric patients undergoing hematopoietic stem cell transplantation promotes the recovery of gut microbiome homeostasis

Brief introduction

Hematopoietic stem cell transplantation (HSCT) is a clinical practice routinely used to treat patients with high-risk hematopoietic malignancies and hematological and genetic diseases. The HSCT procedure includes a conditioning regimen, treatments with chemotherapy and/or immunotherapy, which aim to eliminate cancer cells while allowing patients to receive donor HSCs[388,389]. One of the most life-threating complications of these transplant procedures, which can lead to patient morbidity and mortality, is the acute graft versus host disease (aGvHD), characterized by the response of alloreactive donor T cells to host organs including skin, gut, liver, lungs and central nervous system[390]. The gut microbiome has been hypothesized to have a role in the aGvHD onset[391,392,393]. In particular, several studies have been realized in this field, indicating that the path of GM recovery following HSCT is closely related to the risk of developing aGvHD[382,394]. Indeed, HSCT conditioning regimens, in addition to damaging the intestinal epithelial barrier, induce the disruption of the GM structure, with the loss of all its probiotic properties. A prolonged GM dysbiosis following

[388] Jenq RR, van den Brink MRM. Allogeneic haematopoietic stem cell transplantation: individualized stem cell and immune therapy of cancer. *Nat Rev Cancer*. **2010**;10:213-221.

[389] Shono Y, van den Brink MRM. Gut microbiota injury in allogeneic haematopoietic stem cell transplantation. *Nat Rev Cancer*. **2018**;18:283-295.

[390] Zeiser R, Blazar BR. Acute graft-versus-host disease - biologic process, prevention, and therapy. *N Engl J Med*. **2017**;377:2167-2179.

[391] Biagi E, et al. Gut microbiota trajectory in pediatric patients undergoing hematopoietic SCT. *Bone Marrow Transplant*. **2015**;50:992-998.

[392] Biagi E, et al. Early gut microbiota signature of aGvHD in children given allogeneic hematopoietic cell transplantation for hematological disorders. *BMC Med Genomics*. **2019**;12:49.

[393] Zama D, et al. Gut microbiota and hematopoietic stem cell transplantation: where do we stand?. *Bone Marrow Transplant*. **2017**;52:7-14.

[394] Taur Y, et al. The effects of intestinal tract bacterial diversity on mortality following allogeneic hematopoietic stem cell transplantation. *Blood*. **2014**;124:1174-1182.

HSCT has in turn been demonstrated to expose the patient to an increased risk of innate immune system activation (*i.e.*, alloreactive T cells) and systemic infections, causing aGvHD development[395,396]. Conversely, the prompt recovery of a eubiotic GM layout may provide the host with health-promoting GM-dependent ecological services protective against the aGvHD onset, such as barrier effect and preservation of immune homeostasis[397]. These GM-dependent probiotic activities mainly rely on a balanced production of SCFAs, such as acetate, propionate and butyrate[398,399,400] which have well-known health-promoting activities, which are important to mitigate the aGvHD development risk[401], being potent anti-inflammatory and antimicrobial compounds, as well as strengthening the epithelial barrier and regulating the host metabolic homeostasis[402]. Patients who undergo HSCT are often suffering from nutritional deficiencies, with a decrease in oral food intake, weight loss and malnutrition due to treatment side effects (e.g., nausea, vomiting, diarrhea and oral mucositis)[403,404]. Therefore, nutritional support after the transplant, by enteral nutrition (EN) or parenteral nutrition (PN), has become a strategic aspect to be considered in HSCT-associated procedures. EN, also called "tube-feeding", is the method by which food is

---

[395] Hill GR, Ferrara JL. The primacy of the gastrointestinal tract as a target organ of acute graft-versus-host disease: rationale for the use of cytokine shields in allogeneic bone marrow transplantation. *Blood*. **2000;**95:2754-2759.

[396] Koyama M, et al. MHC Class II Antigen Presentation by the Intestinal Epithelium Initiates Graft-versus-Host Disease and Is Influenced by the Microbiota. *Immunity*. **2019**;S1074-7613(19)30362-0.

[397] Bäckhed F, et al. Host-bacterial mutualism in the human intestine. *Science*. **2005**;307:1915-1920.

[398] Rooks MG, Garrett WS. Gut microbiota, metabolites and host immunity. *Nat Rev Immunol*. **2016**;16:341–352.

[399] Tremaroli V, Bäckhed, F. Functional interactions between the gut microbiota and host metabolism. *Nature*. **2012**;489:242-249.

[400] Turroni S, et al. Microbiota-host transgenomic metabolism, bioactive molecules from the inside. *J Med Chem*. **2018**;61:47-61.

[401] Mathewson ND, et al. Gut microbiome-derived metabolites modulate intestinal epithelial cell damage and mitigate graft-versus-host disease. *Nat Immunol*. **2016**;17:505–513.

[402] Petersson J et al. Importance and regulation of the colonic mucus barrier in a mouse model of colitis. *Am J Physiol Gastrointest Liver Physiol*. **2011**;300:G327-G333.

[403] Fuji S, et al. Systematic nutritional support in allogeneic hematopoietic stem cell transplant recipients. *Biol Blood Marrow Transplant.* **2015**;21:1707-1713.

[404] Walrath M, et al. Gastrointestinal side effects and adequacy of enteral intake in hematopoietic stem cell transplant patients. *Nutr Clin Pract*. **2015;**30:305-310.

directly delivered inside the patient's gastrointestinal tract, while PN is an effective strategy of delivering nutrients directly into the bloodstream. Nowadays, it is well known that total PN, the first-line approach for HSCT patients, is associated with different clinical adverse effects such as infections[405,406,407] and metabolic disorders [408], as well as with gut mucosal atrophy[409], cell dysfunction[410], and alterations in GM composition[411]. Conversely, EN has been indicated as a possible solution to overcome all these adverse effects. Further, we believe that EN, by feeding the GM, besides providing nutritional benefit, can also favor the prompt recovery of a eubiotic and SCFA-producing GM layout, with ultimate benefits in terms of aGvHD protection. For all the reasons that link GM composition and its metabolites to post-HSCT outcomes, as well as in light of the importance of nutritional intake to maintain an "appropriate" GM–host relationship, here, the efficacy of EN, in comparison with the traditional PN, was evaluated in supporting the more rapid recovery of a eubiotic GM layout in pediatric patients undergoing HSCT. In particular, longitudinal fecal samples from twenty pediatric patients was analyzed to build GM and SCFA production trajectories from before to up to 120 days after the transplant; ten of them were fed with EN post-HSCT, while the other ten were fed with PN.

---

[405] Evans JC, Hirani SP, Needle JJ. Nutritional and post-transplantation outcomes of enteral versus parenteral nutrition in pediatric hematopoietic stem cell transplantation: A systematic review of randomized and nonrandomized studies. *Biol Blood Marrow Transplant*. **2019**;25:e252-e259.

[406] Guièze R, et al. Enteral versus parenteral nutritional support in allogeneic haematopoietic stem-cell transplantation. *Clin Nutr.* **2014**;33:533-538.

[407] Yilmaz G, et al. Risk factors of catheterrelated bloodstream infections in parenteral nutrition catheterization. *J Parenter Enteral Nutr*. **2007**;31;284-287.

[408] Lough M, et al. Parenteral nutrition in bone marrow transplantation. *Clin Nutr*. **1990**;9:97-101.

[409] Buchman AL, et al. Parenteral nutrition is associated with intestinal morphologic and functional changes in humans. *J Parenter Enteral Nutr*. **1995**;19:453-460.

[410] Wang J, et al. Gut Microbiota as a Modulator of Paneth Cells During Parenteral Nutrition in Mice. *JPEN J Parenter Enteral Nutr*. **2018**;42:1280-1287.

[411] Dahlgren AF, et al. Longitudinal changes in the gut microbiome of infants on total parenteral nutrition. *Pediatr Res.* **2019**;86:107-114.

Material and Methods

Subject enrollment and sample collection

A total of twenty patients that underwent HSCT were enrolled for a longitudinal study on fecal samples approved by Ethics Committee of the Sant'Orsola-Malpighi Hospital-University of Bologna (ref. number 19/2013/U/Tess). Written informed consent was obtained from each enrolled patient or parent/legal guardian. Study inclusion parameters were the availability of a pre-HSCT fecal sample and of at least two samples collected after HSCT. Patients were separated in two groups depending on the feeding procedure used the days immediately after the transplant, ten patients were fed by using EN (mean age 9.3 years) and ten patients were treated with the administration of total PN (mean age 10.1 years. Inclusion criteria for nutritional regimen clustered children that received EN nutrition for more than 7 days post HSCT in EN group and all patients that received total PN or EN feeding for less than 7 days after the transplant in PN group. Patients in the PN group were chosen based on matching the ones in the EN group regarding age, source of stem cell, type of disease and conditioning regimen. Before the transplant, all patients received once a week trimethoprim-cotrimoxazole for the prevention of *Pneumocystis jirovecii* infection and anti-fungal prophylaxis was also performed by using voriconazole or posaconazole. For both nutritional groups, five out of ten patients developed aGvHD at different grade of severity (**Table S1**). In all patients occurred febrile neutropenia and Ceftazidime was used in all of them as the first-line broad-spectrum antibiotic therapy. A total of 104 fecal samples were collected before HSCT and at different time-points after the transplant, up to 120 days post HSCT (**Figure 20**).

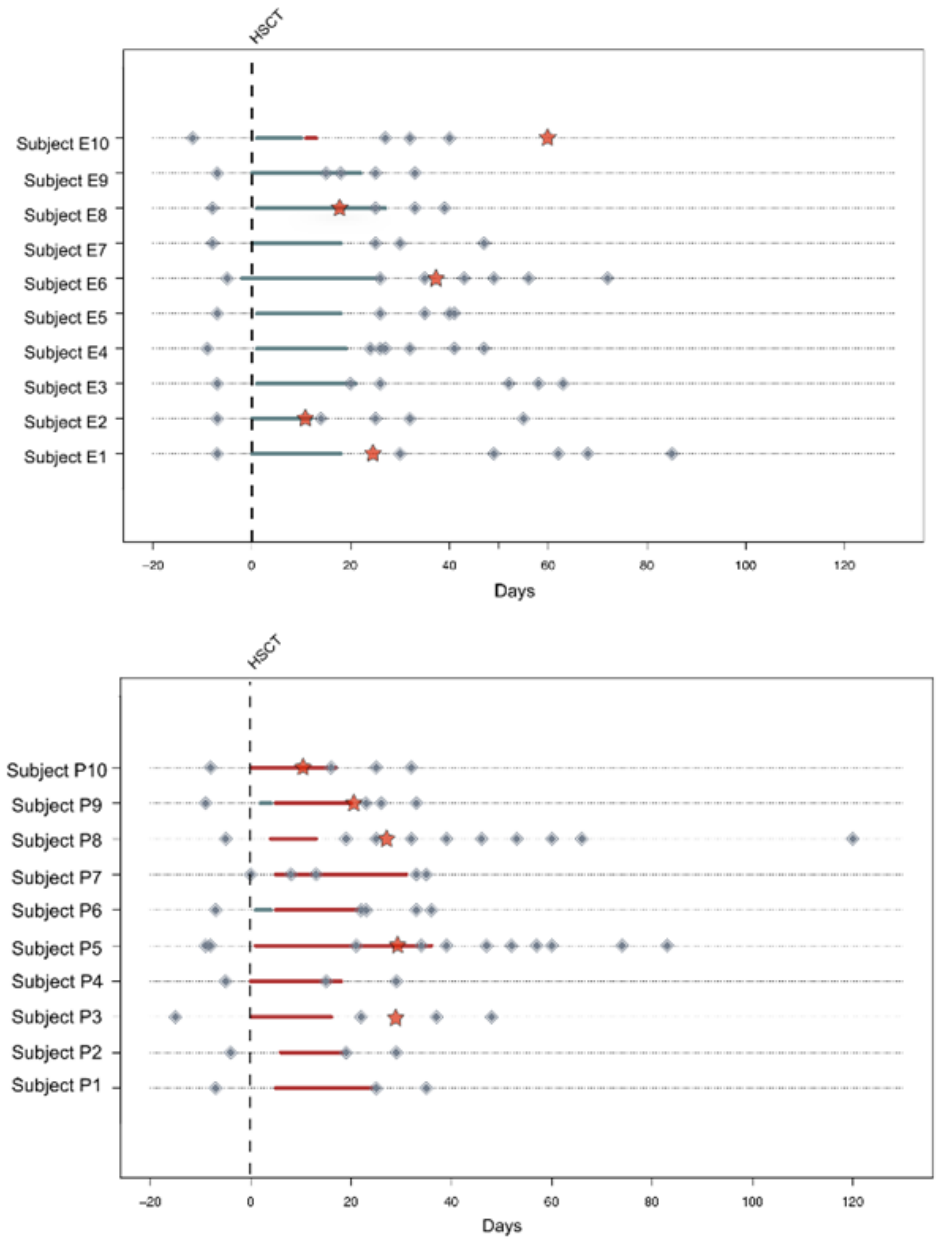

Figure 20. General representation of the fecal sampling for each enrolled subject. On the top of the figure are depicted the ten patients that followed EN (enteral nutrition), while at the bottom are highlighted the ten subjects treated with PN (parenteral nutrition). Diamonds indicate each individual fecal sample taken pre and post-transplant. Hematopoietic stem cell transplantation (HSCT) is indicated by the vertical line in the graph and the moment of the eventual acute graft-versus-host disease (aGvHD) occurrence is reported with a red star. The bars below each subject's timeline indicate the type and the length of the nutritional regimen followed: blue bars indicate EN and red bars indicate PN.

Microbial DNA extraction

Total microbial DNA was extracted from 250 mg of stool sample using the repeated bead-beating plus column method, as previously described with few modifications[412]. Briefly, all the samples were suspended in 1 ml of lysis buffer (500 mM NaCl, 50 mM Tris-HCl, pH 8, 50 mM EDTA, and 4% sodium dodecyl sulfate) and bead-beaten three times in a FastPrep instrument (MP Biomedicals, Irvine, CA) at 5.5 movements/s for 1 min, in the presence of four 3-mm glass beads and 0.5 g of 0.1-mm zirconia beads (BioSpec Products, Bartlesville, OK). After an incubation step at 95 °C for 15 min, samples were centrifuged at 13,000 rpm for 5 min. Two hundred and sixty microliters of 10 M ammonium acetate were added to the supernatant, followed by 5-min incubation in ice and 10-min centrifugation at 13,000 rpm. Each sample was incubated with one volume of isopropanol, followed by an incubation in ice for 30 min. Precipitated nucleic acids were washed with 70% ethanol, re-suspended in 100 µl of TE (10 mM Tris-HCl, 1 mM EDTA pH 8.0) buffer, and treated with 2 µl of 10 mg/ml DNase-free RNase at 37 °C for 15 min. DNA purification was performed using the DNeasy Blood and Tissue Kit (QIAGEN, Hilden, Germany) following the manufacturer's instructions. DNA concentration and quality were evaluated using NanoDrop ND-1000 spectrophotometer (NanoDrop Technologies, Wilmington, DE).

16S rRNA gene amplification and sequencing

The V3-V4 hypervariable region of the 16S rRNA gene was amplified by using the 341F and 785R primers with linked Illumina adapter overhang sequences, as previously described in Klindworth et al.[413]. Fragment amplification was performed by using KAPA HiFi HotStart

[412] Yu Z, Morrison M. Improved extraction of PCR-quality community DNA from digesta and fecal samples. *Biotechniques*. **2004**;36:808-812.

[413] Klindworth A, et al. Evaluation of general 16S ribosomal RNA gene PCR primers for classical and next-generation sequencing-based diversity studies. *Nucleic Acids Res*. **2013**;41:e1.

ReadyMix (Roche, Basel, CH) setting the thermal cycle as follows: 3 min at 95 °C, 25 cycles of 30 s at 95 °C, 30 s at 55 °C, and 30 s at 72 °C, and a final 5-min step at 72 °C. Library preparation followed a first purification with a magnetic bead-based clean-up system (Agencourt AMPure XP, Beckman Coulter, Brea, CA) and a limited-cycle PCR was performed to obtain the indexed library using Nextera technology, followed by a second AMPure XP magnetic beads clean-up step. Final libraries were prepared by pooling all samples to an equimolar concentration of 4nM; the denaturation and dilution to 5 pmol was carried out before performing the sequencing on an Illumina MiSeq platform with a 2 × 250 bp paired-end protocol according to manufacturer's instructions (Illumina, San Diego, CA). Raw sequence reads were deposited in the National Center for Biotechnology Information Sequence Read Archive (https://www.ncbi.nlm.nih.gov/bioproject/PRJNA592853).

Gas chromatography-mass spectrometry determination of SCFAs in fecal samples

When the amount of stool material was enough, an aliquot of each sample has been weighted (about 250 mg), for a total of 99 fecal samples, and analyzed for SCFAs determination. The analysis of acetic acid, propionic acid and butyric acid was performed as reported in several publications[414],[415]. Briefly, samples were homogenized in 10% perchloric acid and centrifuged at 15,000 rpm for 5 min at 4°C. Supernatants were diluted 1:10 in water and added with D8-butyric acid (internal standard) to 20 µg/mL. Headspace solid-phase micro extraction (HS-SPME) was carried out by using a 75-µm CarboxenTM/polydimethylsiloxane fiber (Supelco, Sigma-Aldrich, Milan, Italy) at 70°C with a 10 min equilibration and 30 min of extraction time. Analytes were desorbed into the gas chromatography (GC) injector and GC-

[414] Schnorr SL, et al. Gut microbiome of the Hadza hunter-gatherers. *Nat Commun*. **2014**;5:3654.

[415] Fiori J, et al. Simultaneous HS-SPME GC-MS determination of short chain fatty acids, trimethylamine and trimethylamine N-oxide for gut microbiota metabolic profile. *Talanta*. **2018**;189:573-578.

mass spectrometry analysis was carried out on a TRACE GC 2000 Series (Thermo Fisher Scientific, Waltham, MA, USA) gas chromatograph, interfaced with GCQ Plus (Thermo Fisher Scientific, Waltham, MA, USA) mass detector with ion-trap analyzer. Phenomenex ZB-WAX (30m× 0.25mm ID, 0.15-µm film thickness) capillary column was used. SCFA concentration was expressed as micromoles per gram (µmol/g) of feces. Limit of detection ranged from 4 to 68 nmol/g.

Bioinformatics and statistical analysis

A mean of 8043.9 ± 3632.5 (mean ± SD) high quality sequences per sample was obtained. Raw sequences were processed using a pipeline that combined PANDASeq[416] and QIIME2[417]. After length (minimum/maximum = 250/550 bp) and quality filtering (default parameters), reads were cleaned and binned into amplicon sequence variants (ASVs) using DADA2[418]. The latter is a recent method for resolving 16S rRNA gene region variants down to the level of single-nucleotide differences, without imposing the arbitrary dissimilarity thresholds that define operational taxonomic units[419]. Taxonomic assignment was carried out by using the VSEARCH algorithm[420] and the Greengenes database (May 2013 release). Chimeras were discarded during the analysis. Alpha-diversity was evaluated using two different metrics: Faith's Phylogenetic Diversity (PD whole tree) and observed ASVs. Weighted and Unweighted UniFrac distances were used to construct Principal Coordinates Analysis (PCoA) graphs. All statistical analyses were performed using the R software. PCoA

[416] Masella AP, et al. PANDAseq: paired-end assembler for Illumina sequences. *BMC Bioinformatics*. **2012**;13:31.
[417] Bolyen E, et al. Reproducible, interactive, scalable and extensible microbiome data science using QIIME 2. *Nat Biotechnol*. **2019**;37:852-857.
[418] Callahan BJ, et al. DADA2: High-resolution sample inference from Illumina amplicon data. *Nat Methods*. **2016**;13:581-583.
[419] Callahan BJ, McMurdie PJ, Holmes SP. Exact sequence variants should replace operational taxonomic units in marker-gene data analysis. *ISME J*. **2017**;11:2639-2643.
[420] Rognes T, et al. VSEARCH: a versatile open source tool for metagenomics. *PeerJ*. **2016**;4:e2584.

were generated using the "vegan"[421] and "Made4"[422] packages and data separation was tested by permutation test with pseudo-F ratios (function "Adonis" in "vegan"). To compare differences in microbiota composition among groups and covariates at all taxonomic levels and for alpha diversity metrics a preliminary analysis with Wilcoxon rank-sum test or Kruskal-Wallis test was carried out. When necessary, p values were corrected for multiple comparisons using the Benjamini-Hochberg method. False discovery rate (FDR) ≤ 0.05 was considered as statistically significant.

Results

The 16S rRNA gene sequencing and SCFAs determination were performed in a total of 104 and 99 samples, respectively, from twenty pediatric patients sampled before, during and after HSCT. Patients were divided into two groups of ten subjects depending on the type of feeding procedure received right after the transplant, EN or PN. Clinical and transplant characteristics are summarized in **Table S1**. Samples were grouped as "pre" (*i.e.*, samples taken before HSCT), "HSCT" (*i.e.*, the first samples taken after HSCT for all subjects, ranging from 8 to 30 days post-transplant), and "post" (*i.e.*, all other samples taken after HSCT). In order to better visualize the trajectory of GM recovery, post-HSCT samples were further divided into three groups: "post40" (*i.e.,* all samples taken from 31 to 40 days post-HSCT), "post60" (*i.e.,* samples taken from 41 to 60 days post-HSCT) and "post120" (*i.e.*, samples taken from 61 to 120 days after the transplant) (**Figure 20**).

[421] http://www.cran.r-project.org/package=vegan/

[422] Culhane AC, et al. MADE4: an R package for multivariate analysis of gene expression data. *Bioinformatics.* **2005**;21:2789-2790.

Variation in the Overall Bacterial Biodiversity in HSCT Patients during Enteral and Parenteral Feeding

The first analysis was conducted to compare the variation of the GM biodiversity from pre- to post-HSCT samples between EN and PN subjects. Different metrics were used to estimate alpha diversity, including phylogenetic diversity and observed ASVs. Both measures indicated, for EN and PN patients, a reduction of the GM diversity from pre-HSCT to HSCT samples. However, while PN patients maintained a low level of GM diversity also in post-HSCT samples (Wilcoxon rank-sum test; PRE_P vs. POST_P; observed_asvs: p = 0.05; PD_whole_tree: p = 0.13), patients fed with EN showed a post-HSCT recovery of a level of GM diversity comparable to that observed in pre-HSCT samples (PRE_E vs. POST_E; p = 0.44; p = 0.25). These data highlight a significantly different trajectory of GM diversity between EN and PN patients during the course of post-HSCT recovery (POST_E vs. POST_P; p = 0.01; p = 0.23) (**Figure 21A**).

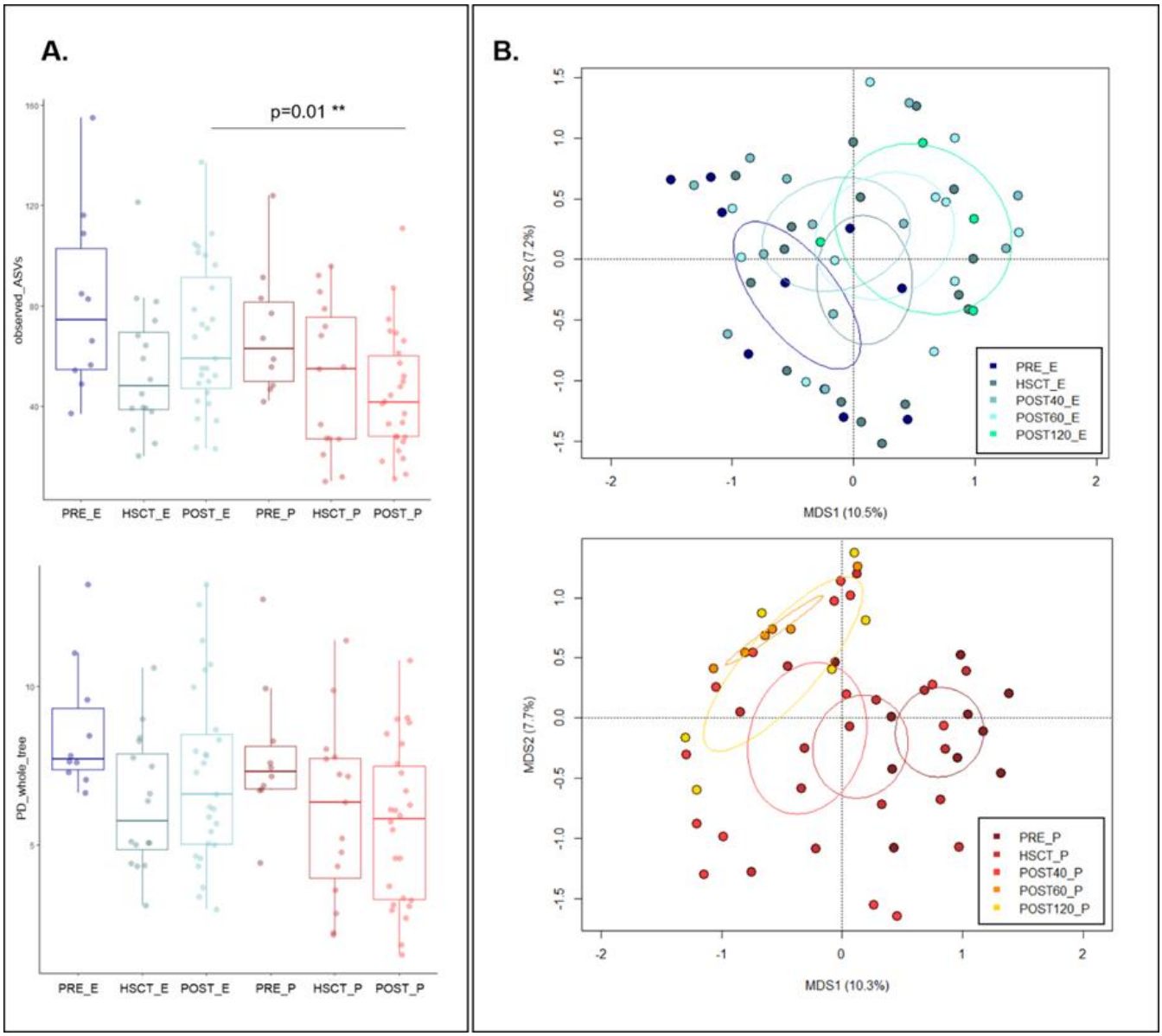

Figure 21. **Diversity of pre- and post-HSCT samples in patients treated with enteral and parenteral nutritional regimens**. (A.) Alpha diversity estimated with observed amplicon sequence variants (ASVs, top) and Faith's Phylogenetic Diversity (PD_whole_tree, bottom) metrics for samples taken at the baseline (PRE), during the transplant (HSCT) and up to 120 days post HSCT (POST) from patients treated with enteral (E) and parenteral (P) nutrition. Subjects treated with PN (in red) showed a significantly higher number of ASVs (Wilcoxon rank-sum test; POST_E vs. POST_P, p = 0.01). (B.) Principal Coordinates Analysis (PCoA) based on unweighted UniFrac distances between samples taken before (PRE) and after the transplant (HSCT, up to 30 days post-HSCT; POST40, up to 40 days post-HSCT; POST60, from 41 to 60 days post-HSCT; POST120, up to 120 days post-transplant) from patients treated with EN (top) and PN (bottom). A significant separation among groups was observed only in patients treated with PN (permutation test with pseudo-F ratios (Adonis), p = 0.001).

In order to explore the variation of the overall GM compositional structure from pre- to post-HSCT in EN and PN patients, a Principal Coordinates Analysis (PCoA) of unweighted UniFrac distances of the GM profiles in the whole sample set was performed. The data revealed a different GM response to the HSCT perturbation between PN and EN patients. In particular, while the post-HSCT samples from the firsts showed a significant shift of their GM structure (permutation test with pseudo-F ratios (Adonis); $p = 0.001$) that gradually moved away from the pre-HSCT composition to the one observed up to 120 days post HSCT (**Figure 21B**), for EN the overall GM configuration did not undergo to a significant dysbiotic shift following HSCT ($p = 0.063$).

Gut Microbiota Composition in Enteral and Parenteral Nutritional Regimen during the HSCT Recovery

The GM composition analysis conducted at both phylum and family level did not highlight any significant difference between EN and PN groups at the baseline (PRE_E vs. PRE_P), as well as the HSCT time-points (HSCT_E vs. HSCT_P). In agreement with what has been previously observed by Biagi et al.[423], both for EN and PN patients, HSCT samples were characterized by profound rearrangements of the GM structure, as a result of the HSCT stress (**Figure S12**). Conversely, in the post-HSCT time-points, EN and PN patients showed significant differences in the GM compositional structure. Specifically, while in PN subjects pre- and post-HSCT samples showed significant variations in core GM families and genera,

[423] Biagi E, et al. Gut microbiota trajectory in pediatric patients undergoing hematopoietic SCT. *Bone Marrow Transplant*. **2015**;50:992-998.

in EN patients the GM composition pre- and post-HSCT did not show any significant divergence (**Figure 22**).

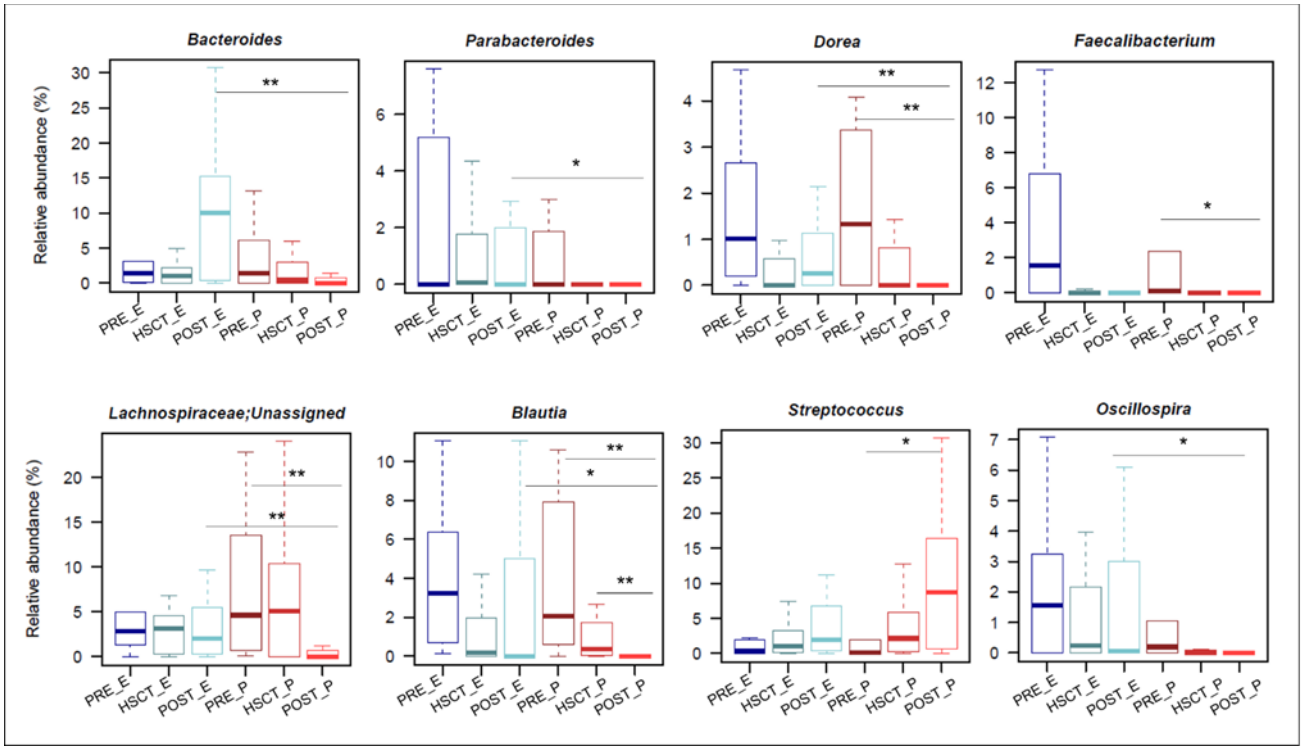

Figure 22. **Differences in the gut microbiota composition between HSCT patients following enteral and parenteral nutrition**. Boxplots representing the relative abundance distribution of genera that where significantly different between pre, HSCT and post-HSCT time-points in PN (in red) and EN patients (in blue). * $p \leq 0.05$; ** $p \leq 0.01$; Wilcoxon rank-sum test.

In particular, in EN patients, post HSCT the relative abundance of *Lachnospiraceae* remained stable over time, while it decreased in subjects treated with PN (POST_E vs. POST_P: $p = 0.003$). This difference was accounted for by increased representation of *Blautia* (POST_E vs. POST_P: $p = 0.036$) and *Dorea* ($p = 0.008$), both belonging to *Lachnospiraceae* family, in EN-fed subjects compared to PN patients (**Figure 22**). A similar increase post HSCT in EN- vs. PN-fed patients was observed in other genera, such as

Parabacteroides (p = 0.03) and *Oscillospira* (p = 0.03). Interestingly, *Faecalibacterium* significantly decreased in post-HSCT samples, compared to the baseline, only in PN patients (**Figure 22**). Finally, patients fed with EN were characterized by a post-HSCT increase in *Bacteroidaceae* compared to PN patients (POST_E vs. POST_P: p = 0.009), mostly attributable to the genus *Bacteroides* (p = 0.008). A significant difference was also highlighted for *Streptococcus*, whose relative abundance increased post-transplant in patients fed with PN (PRE_P vs. POST-P: p = 0.03), while no difference was observed in EN-fed subjects. Blood culture tests were performed on patients with febrile neutropenia. For EN patients none of them exhibited evidence of blood stream infection (BSI). On the other hand, seven PN-treated patients developed eleven documented BSI mainly attributed to *Staphylococcus* (36.4%), *Enterococcus* (18.2%) and *Streptococcus* (18.2%) genera, mostly identified from 5 to 30 days post HSCT.

Short-Chain Fatty Acid Production in EN and PN Patients Undergoing HSCT

A gas chromatograph-mass spectrometry (GC-MS) analysis of fecal SCFAs in HSCT patients fed with EN and PN was conducted from the baseline (pre-HSCT) to the transplant itself (HSCT samples), up to 120 days after transplant (post-HSCT). The results highlighted that patients who received PN were characterized by a significant decrease of SCFA levels in post-HSCT time-points compared to pre-HSCT samples (absolute amount (μmol/g) ± SEM, PRE_P vs. POST_P; 44.0 ± 6.2 vs. 16.2 ± 2.9; p = 0.006), while for EN subjects, the post-HSCT SCFA production levels were comparable to the baseline (PRE_E vs. POST_E, 35.0 ± 7.4 vs. 31.9 ± 3.1; p = 0.78) (**Figure 23**).

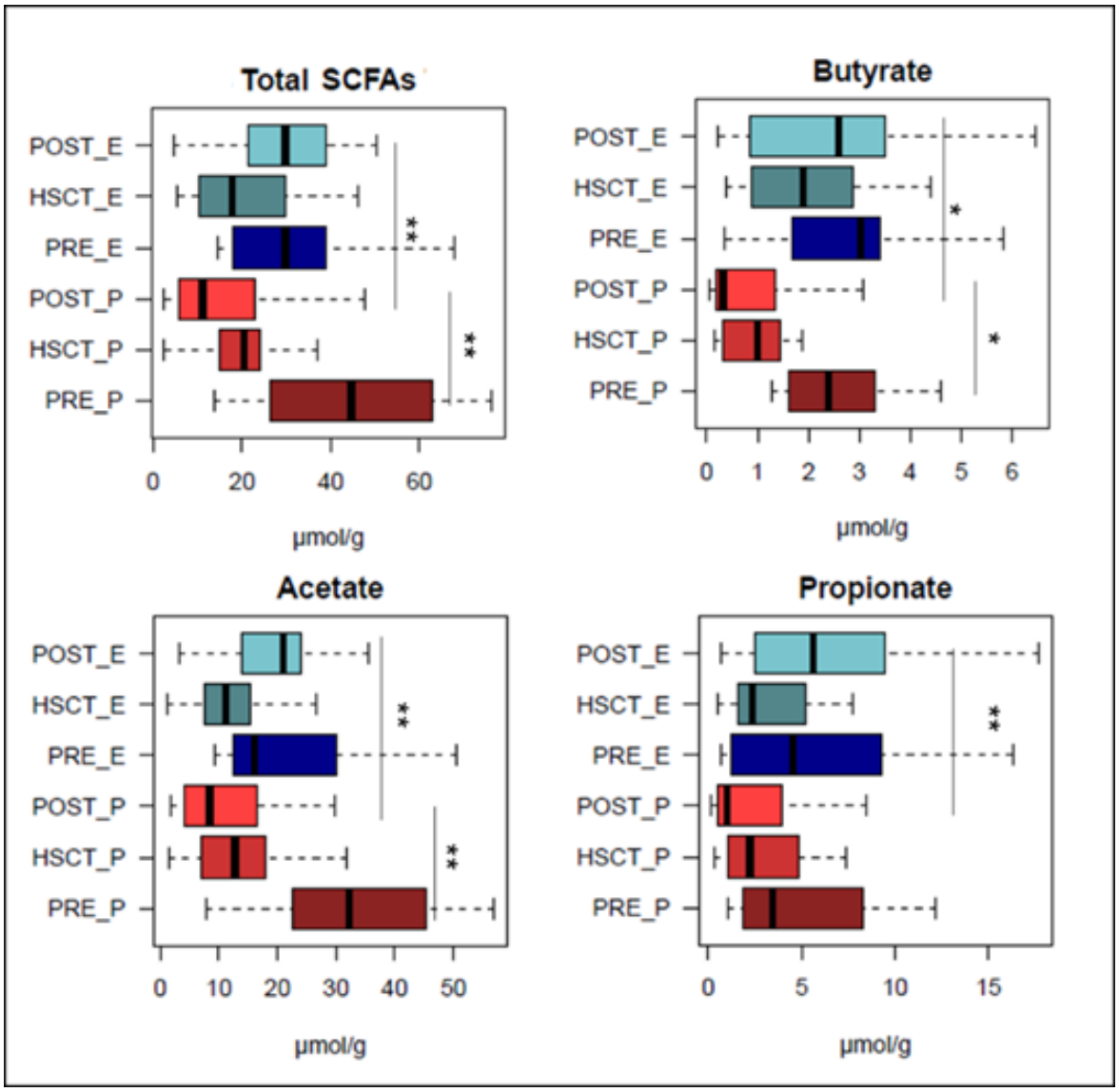

Figure 23. **Fecal levels of short-chain fatty acids in HSCT patients after enteral and parenteral nutritional regimens.** Boxplots showing the absolute amount distribution for short-chain fatty acids (SCFAs) measured in µmol/g. * $p \leq 0.05$; ** $p \leq 0.01$; Wilcoxon rank-sum test.

In detail, in post-HSCT samples EN patients were significantly enriched in butyrate (POST_E vs. POST_P: $p = 0.01$), acetate ($p = 0.005$) and propionate ($p = 0.005$) compared to subjects that received PN. Indeed, a significant decrease of all the major SCFAs, *i.e.,* butyrate (PRE_P vs. POST_P: $p = 0.01$), acetate ($p = 0.009$) and propionate ($p = 0.08$), was observed between pre- and post-HSCT samples of PN patients (**Figure 23**).

Discussion

Although post-HSCT enteral feeding is being increasingly recommended[424,425,426], intravenous nutrient intake (*i.e.*, PN) is still the first-line nutritional approach for the patients that received HSCT due to its compliance (*i.e.*, patient approval), but it has been associated with several clinical and microbiological adverse effects, including infections and GM dysbiosis[427,428]. So far, the central role of the GM composition and biodiversity in patients undergoing HSCT has been largely evaluated in several publications, highlighting the disruption of the gut microbial mutualistic asset after the transplant (*i.e.*, until 30 days post-HSCT) compared to the baseline, due to all HSCT conventional treatments that can alter the GM recovery possibilities post-HSCT[429]. Therefore, in this scenario was explored the potential of EN in supporting an eubiotic GM trajectory following HSCT. To this aim, the GM structure of twenty pediatric patients undergoing HSCT (ten treated with EN and ten with PN) was analyzed at the baseline, right after the transplant and in the post-HSCT recovery. In parallel, the GM functionality as SCFAs production by using GC-MS was evaluated. As shown in several publications[430,431], right after the transplant was observed the loss of the eubiotic GM configuration. However, the EN patients were characterized by a prompt

---

[424] Arends J, et al. ESPEN guidelines on nutrition in cancer patients. *Clin Nutr*. **2017**;36:11-48.

[425] Seguy D, et al. Better outcome of patients undergoing enteral tube feeding after myeloablative conditioning for allogeneic stem cell transplantation. *Transplantation*. **2012;**94:287-294.

[426] Azarnoush S, et al. Enteral nutrition: a first option for nutritional support of children following allo-SCT?. *Bone Marrow Transplant*. **2012**;47:1191-1195.

[427] Evans JC, Hirani SP, Needle JJ. Nutritional and post-transplantation outcomes of enteral versus parenteral nutrition in pediatric hematopoietic stem cell transplantation: A systematic review of randomized and nonrandomized studies. *Biol Blood Marrow Transplant*. **2019**;25:e252-e259.

[428] Wang J, et al. Gut Microbiota as a Modulator of Paneth Cells During Parenteral Nutrition in Mice. *JPEN J Parenter Enteral Nutr*. **2018**;42:1280-1287.

[429] Taur Y, et al. The effects of intestinal tract bacterial diversity on mortality following allogeneic hematopoietic stem cell transplantation. *Blood*. **2014;**124:1174-1182.

[430] Noor F, et al. The gut microbiota and hematopoietic stem cell transplantation: challenges and potentials. *J Innate Immun*. **2019**;11:405-415.

[431] Biagi E, et al. Early gut microbiota signature of aGvHD in children given allogeneic hematopoietic cell transplantation for hematological disorders. *BMC Med Genomics*. **2019;**12:49.

recovery of a diverse eubiotic GM layout, minimizing the dysbiotic shifts following the HSCT. Interestingly, Wilmanski et al.[432] recently found a connection between the eubiotic GM structure and the host blood metabolic profile. This suggests a possible feedback of the eubiotic GM trajectory in HSCT patients also in terms of blood metabolome, which have been connected with the GvHD risk[433]. At the compositional level, EN-fed subjects recovered a GM structural layout comparable to the one observed before the transplant starting from 30 days post HSCT, while in PN patients this end-point was never achieved. Particularly, we identified some genera including *Faecalibacterium*, *Dorea*, *Blautia*, *Bacteroides*, *Parabacteroides* and *Oscillospira*, whose relative abundance was restored in EN patients during the post-HSCT recovery, similar findings have been very recently observed in an adult cohort of 23 patients undergoing to HSCT by Andersen et al.[434]. Interestingly, most of these microorganisms for which we observed the restoring in EN-fed subjects are well-known health-promoting GM bacteria capable of producing SCFAs[435,436]. Consistently, the fecal levels of SCFAs, *i.e.*, propionate, butyrate and acetate, were restored only in EN patients between 30 and 120 days post HSCT. These findings are in line with a recent work showing increase levels of fatty acids in the blood of adult patients receiving mainly EN support post HSCT[437]. As a matter of fact, intestinal decrease of SCFA levels, especially butyrate, with a loss of GM diversity and SCFA-producers have been associated to post-

[432] Wilmanski T, et al. Blood metabolome predicts gut microbiome α-diversity in humans. *Nat Biotechnol*. **2019**;37:1217-1228.

[433] Reikvam H, et al. Patients with treatment-requiring chronic graft versus host disease after allogeneic stem cell transplantation have altered metabolic profiles due to the disease and immunosuppressive therapy: Potential implication for biomarkers. *Front Immunol*. **2017**;8:1979.

[434] Andersen S, et al. Pilot study investigating the effect of enteral and parenteral nutrition on the gastrointestinal microbiome post-allogeneic transplantation. *Br J Haematol*. **2020**;188:570-581.

[435] Lordan C, et al Potential for enriching next-generation health-promoting gut bacteria through prebiotics and other dietary components. *Gut Microbes*. **2019**;22;1-20.

[436] Morrison DJ, Preston T. Formation of short chain fatty acids by the gut microbiota and their impact on human metabolism. *Gut Microbes*. **2016**;7:189–200.

[437] Tvedt THA, et al. The systemic metabolic profile early after allogeneic stem cell transplantation: effects of adequate energy support administered through enteral feeding tube. *Biol Blood Marrow Transplant*. **2020**;26:380-391.

HSCT immunological complications. Recently, restoring by local administration the physiological levels of endogenous butyrate in *in-vitro* and *in-vivo* models has been shown to improve intestinal junctional integrity, decrease cellular apoptosis and mitigate GvHD severity[438]. These observations were also demonstrated in an adult cohort that received HSCT, where the increase of the relative abundance of the SCFA-producer *Blautia* was associated with the reduction of GvHD lethality and the improvement of overall patient survival[439]. In this scenario, the potential of EN in keeping an eubiotic and SCFA-producing GM configuration may have important post-HSCT clinical implications, as highlighted by the decrease of patient aGvHD severity and the reduction of local and systemic infections in EN compared to PN patients[440]. Indeed, for EN subjects, there are no evidence of BSI, probably supporting less impairment of the intestinal epithelial barrier. On the other hand, PN patients were found have blood culture positivity to several microorganisms (e.g., *Staphylococcus*, *Enterococcus* and *Streptococcus* genera), mainly from day 5 to 30 post-HSCT, leading to systemic infections and clinical complications. These results regarding the clinical outcomes of EN patients were generally in line with most of the previous studies in literature conducted on adult cohorts post HSCT[441]. However, it is important to mention that other studies provide conflicting results for what concern the clinical outcomes of EN assumption in HSCT adult patients[442,443]. In conclusion, in EN patients was observed prompt GM structural and

[438] Mathewson ND, et al. Gut microbiome-derived metabolites modulate intestinal epithelial cell damage and mitigate graft-versus-host disease. *Nat Immunol*. **2016;**17:505–513.

[439] Jenq, R.R.; et al. Intestinal Blautia is associated with reduced death from Graft-versus-Host Disease. *Biol Blood Marrow Transplant*. **2015**;21:1373-83.

[440] Zama D, et al. Enteral nutrition protects children undergoing allogeneic hematopoietic stem cell transplantation from blood stream infections. *Nutr J.* **2020**;19:29.

[441] Wang J, et al. Gut Microbiota as a Modulator of Paneth Cells During Parenteral Nutrition in Mice. *JPEN J Parenter Enteral Nutr.* **2018**;42:1280-1287

[442] Skaarud KJ, et al. Body weight, body composition and survival after 1 year: follow-up of a nutritional intervention trial in allo-HSCT recipients. *Bone Marrow Transplant*. **2019**;54:2102-2109.

[443] Skaarud KJ, et al. Effects of individualized nutrition after allogeneic hematopoietic stem cell transplantation following myeloablative conditioning; a randomized controlled trial. *Clin Nutr ESPEN*. **2018**;28:59-66.

functional recovery already starting from 30 days post-HSCT, featured by the restoration of health-promoting and SCFA-producing microorganisms and the reduction of full-blown infections. The data indicate that post-HSCT EN promotes the achievement of GM homeostasis, also including the production of immunomodulating metabolites, in a window frame that is strategic to educate the process of immunological reconstruction, possibly reducing the risk of local and systemic infections and aGvHD onset.

2.4 Early modifications of the gut microbiota in children with hepatic sinusoidal obstruction syndrome after hematopoietic stem cell transplantation

Brief introduction

Hepatic sinusoidal obstruction syndrome (SOS), also known as veno-occlusive disease (VOD) is a potentially life-threatening complication of HSCT. It is caused by the damage generated during the conditioning regimen to sinusoidal endothelial cells and hepatocytes in zone 3 of the hepatic acinus[444]. Pediatric patients are at higher risk of developing SOS/VOD than adults, showing an incidence of approximately 20% to 30%, compared to 9% to 14% in adults[445,446]. In a large pediatric cohort, the survival probability at 1 year for patients with or without severe and very severe SOS/VOD was 61% and 77%, respectively[446]. Mounting evidence has suggested that the GM is associated with HSCT outcomes[447] and may play a pivotal role in the pathophysiology of the main HSCT complications in children, namely blood stream infection (BSI) and graft-vs-host disease (GvHD)[448,449,450,451]. Preclinical studies suggest that microbial products translocated across impaired mucosal barriers may

[444] Mohty M, et al. Sinusoidal obstruction syndrome/veno-occlusive disease: Current situation and perspectives - A position statement from the European Society for Blood and Marrow Transplantation (EBMT). *Bone Marrow Transplant*. **2015**;50:781-789.

[445] Corbacioglu S, Jabbour EJ, Mohty M. Risk factors for development of and progression of hepatic Veno-Occlusive Disease/Sinusoidal Obstruction Syndrome. *Biol Blood Marrow Transplant*. **2019**;25:1271-1280.

[446] Faraci M, et al. Sinusoidal obstruction Syndrome/Veno-Occlusive Disease after autologous or allogeneic hematopoietic stem cell transplantation in children: a retrospective study of the Italian hematology-oncology association–hematopoietic stem cell transplantation group. *Biol Blood Marrow Transplant*. **2019**;25:313–320.

[447] Peled JU, al. Microbiota as predictor of mortality in allogeneic hematopoietic-cell transplantation. *N Engl J Med*. **2020**;382: 822–834.

[448] Kelly MS, et al. Gut Colonization Preceding Mucosal Barrier Injury Bloodstream Infection in Pediatric Hematopoietic Stem Cell Transplantation Recipients. *Biol Blood Marrow Transplant*. **2019**;25:2274–2280.

[449] Biagi E, et al. Early gut microbiota signature of aGvHD in children given allogeneic hematopoietic cell transplantation for hematological disorders. *BMC Med Genomics*. **2019;**12:1-11.

[450] Tamburini FB, et al. Precision identification of diverse bloodstream pathogens in the gut microbiome. *Nat Med*. **2018**;24:1809–1814.

[451] Zhai B, et al. High-resolution mycobiota analysis reveals dynamic intestinal translocation preceding invasive candidiasis. *Nat Med*. **2020**;26:59-64.

participate in the pathogenesis of endothelial damage[452,453,454], but, no data are available to date on the possible relationship between GM and SOS/VOD.

To address this issue, a retrospective single-institution case-control study was performed at the pediatric HSCT Unit of the University of Bologna, from 01/01/2015 to 31/12/2019. This study was approved by the Ethics Committee (ref. number 19/2013/U/Tess) and written informed consent was obtained from each enrolled patient or parent/legal guardian. Study inclusion criteria were the availability of a pre-HSCT fecal sample and of at least two samples collected after HSCT. Sample collection, storage, and DNA extraction procedures have been previously reported, as well as sequencing of V3-V4 regions of the 16S rRNA gene using Illumina technology[455].

[452] Eissner G, Multhoff G, Holler E. Influence of bacterial endotoxin on the allogenicity of human endothelial cells. *Bone Marrow Transplant*. **1998**;21:1286-1288.

[453] Falanga A, et al. Defibrotide reduces procoagulant activity and increases fibrinolytic properties of endothelial cells. *Leukemia*. **2003**;17:1636-1642.

[454] Kornblum N, et al. Defibrotide, a polydisperse mixture of single-stranded phosphodiester oligonucleotides with lifesaving activity in severe hepatic Veno-occlusive Disease: Clinical outcomes and potential mechanisms of action. *Oligonucleotides*. **2006**;16:105–114

[455] D'Amico F, et al. Enteral nutrition in pediatric patients undergoing hematopoietic SCT promotes the recovery of gut microbiome homeostasis. Nutrients. **2019**;11:2958.

Materials and Methods

Eighteen allo-HSCT pediatric recipients were selected among previously enrolled patients[449,455]. The cumulative incidence of SOS/VOD in our center is 15.38%. Three patients received haplo-HSCT with posttransplant cyclophosphamide. None of the patients received either Gemtuzumab or Inotuzumab prior to HSCT, or TBI-based therapy in the conditioning regimen. In the patients in which Busulfan pharmacokinetic monitoring was performed as part of routine clinical care**,** plasma concentrations at steady state were successfully therapeutically targeted (range: 700-900 ng/mL). Nine patients developed severe or very severe SOS/VOD according to the new EBMT (European Society for Blood and Marrow Transplantation) criteria for the diagnosis and grading of pediatric SOS/VOD[456]. All the patients developing VOD were treated with defibrotide from the date of diagnosis for at least 21 days and until resolution of signs and symptoms of SOS/VOD, and none of them died during transplant. Nine patients in the control group were selected by matching for age, sex, source of stem cells, type of disease, conditioning regimen, antibiotic prophylaxis and type of nutrition. In all patients, febrile neutropenia occurred, and ceftazidime was used as the first-line antibiotic therapy. A total of 74 fecal samples were available, collected before and after transplant, up to 72 days post-HSCT (**Figure 24**). Bioinformatic processing of the sequencing reads was carried out using a pipeline combining PANDAseq and QIIME2 as recently described[457]. 16S rRNA gene sequencing of these samples yielded a total of 3,805,437 reads, ranging from 5,246 to 233,603 per sample (mean 51,425, SD 39,961).

[456] Corbacioglu S, et al. Diagnosis and severity criteria for sinusoidal obstruction syndrome/veno-occlusive disease in pediatric patients: A new classification from the European society for blood and marrow transplantation. *Bone Marrow Transplant.* **2018**;53:138-145.

[457] Saresella M, et al. Alterations in circulating fatty acid are associated with gut microbiota dysbiosis and inflammation in multiple sclerosis. *Front Immunol.* **2020**;11:1390.

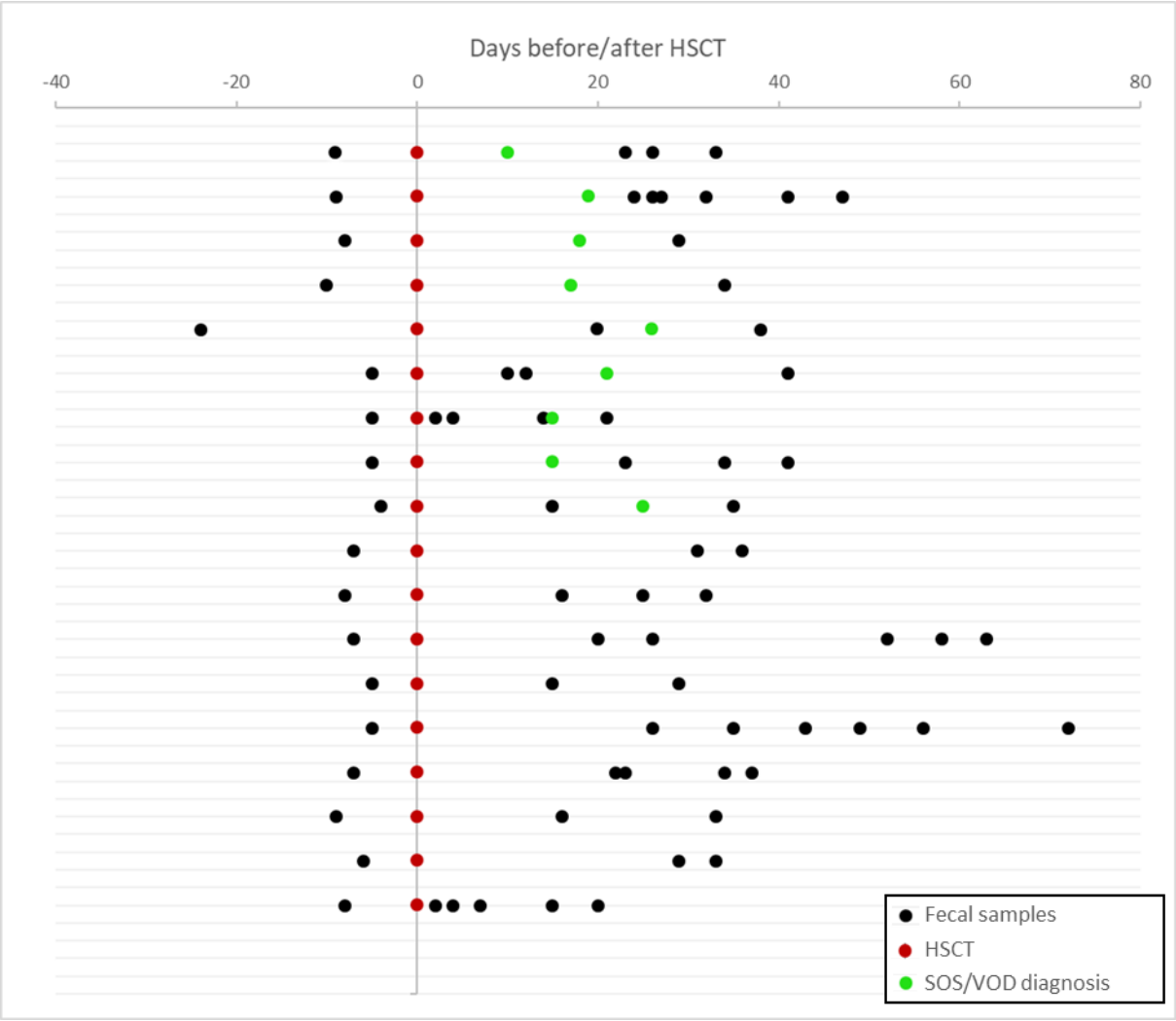

Figure 24. Schematic overview of the sampling time for each considered subject. HSCT (red dots), SOS/VOD diagnosis (green dots), and fecal sample collection (black dots) are plotted on timelines with distance from HSCT expressed in days.

Results and Discussion

Samples were grouped according to the sampling date relative to the HSCT as previously reported[458], *i.e.*, "PRE" (samples taken before HSCT within a maximum of 30 days before HSCT), "HSCT" (samples taken up to 30 days after HSCT), and "POST" (samples taken more than 30 days after HSCT). PRE samples from SOS/VOD patients showed significantly lower alpha diversity than controls even before HSCT, as measured by different biodiversity and richness metrics [*i.e.*, Faith's PD index, and number of observed amplicon sequence variants (ASVs)] ($p \leq 0.02$, Wilcoxon test with false discovery rate correction for multiple testing). During the first 30 days after HSCT, all subjects showed comparable low levels of GM diversity. The diversity of the POST samples was again significantly lower in SOS/VOD-diagnosed patients than in controls ($p \leq 0.02$, Wilcoxon test with false discovery rate correction for multiple testing), the latter showing overall diversity levels comparable to those calculated for PRE samples (**Figure 25A**). This observation is consistent with the recent scenario in which a high level of GM diversity, a common signature of a so-called "healthy" GM, has been associated with decreased mortality after HSCT. Greater alpha diversity is linked as well to a decreased probability of developing another post-HSCT complication, GvHD in pediatric patients[449]. A combined index of evenness and richness (inverse Simpson index) did not show an equal trend, even if decreased average values are visible for SOS/VOD patients in samples taken before transplant (**Figure 25A**).

Weighted and unweighted UniFrac distances between GM profiles were computed and used for Principal Coordinates Analysis (PCoA) on samples taken in the three defined time frames (**Figure 26**). According to a permutation test with pseudo-F ratios (Adonis), PRE samples

[458] Biagi E, et al. Gut microbiota trajectory in pediatric patients undergoing hematopoietic SCT. *Bone Marrow Transplant*. **2015**;50:992-998.

from SOS/VOD patients and controls significantly separated in the PCoA based on weighted UniFrac distances (p = 0.005), confirming that early compositional differences might characterize the GM of pediatric patients who subsequently develop SOS/VOD. In order to identify the discriminating taxa, we plotted the bacterial genera contributing most to the ordination space, using the function envfit in the vegan package of R statistical software. It was therefore possible to ascertain that PRE samples in control subjects were characterized by higher proportions of symbiotic bacteria belonging to the Clostridiales, *Ruminococcaceae* and *[Mogibacteriaceae]* groups and the *Bacteroides* genus (**Figure 25B**).

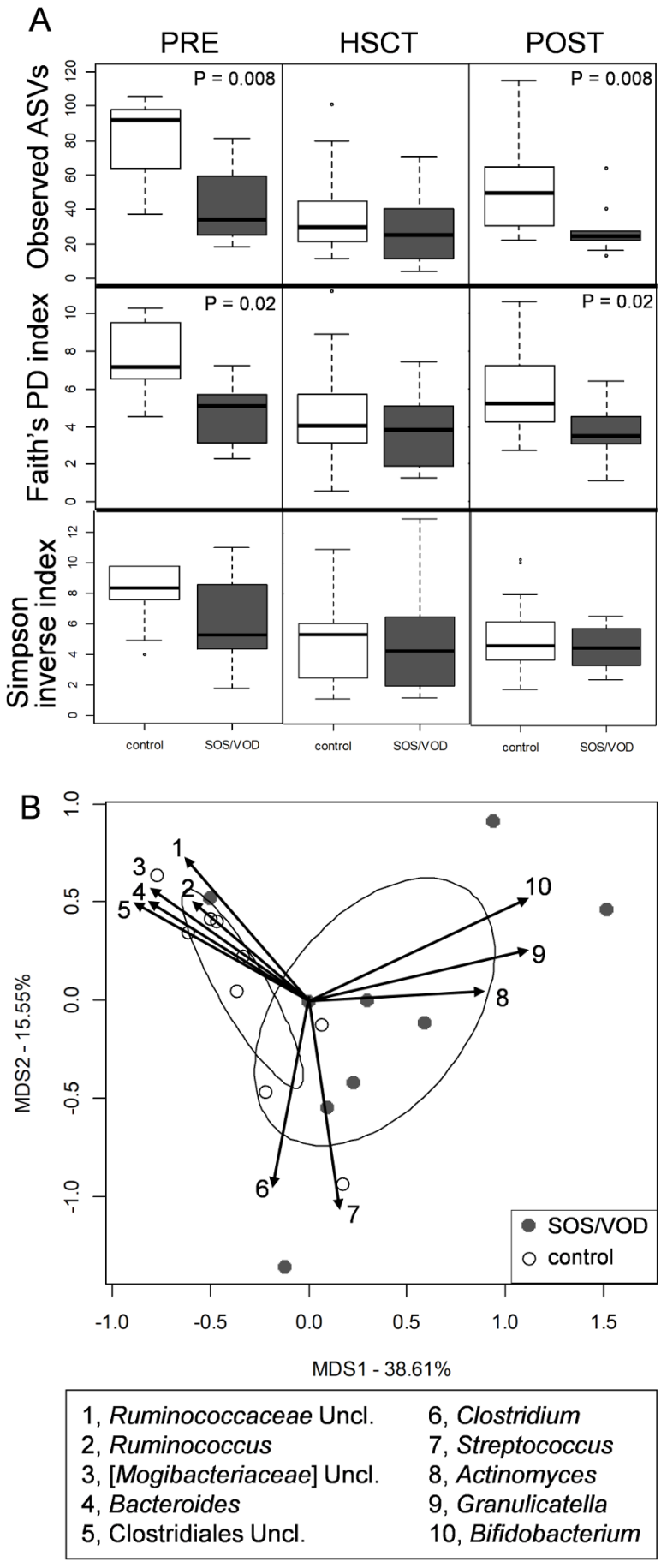
A
PRE
HSCT
POST
Observed ASVs
Faith's PD index
Simpson inverse index
P = 0.008
P = 0.008
P = 0.02
P = 0.02
control
SOS/VOD
control
SOS/VOD
control
SOS/VOD
B
MDS2 - 15.55%
MDS1 - 38.61%
SOS/VOD
control
1, Ruminococcaceae Uncl.
2, Ruminococcus
3, [Mogibacteriaceae] Uncl.
4, Bacteroides
5, Clostridiales Uncl.
6, Clostridium
7, Streptococcus
8, Actinomyces
9, Granulicatella
10, Bifidobacterium

Figure 25. The gut microbiota of SOS/VOD patients before HSCT shows less diversity and a different compositional structure compared to control subjects. (**A**) Alpha diversity of fecal microbiota in samples taken before transplant (PRE), up to 30 days after transplant (HSCT) and more than 30 days after transplant (POST), calculated for controls (white) and SOS/VOD patients (dark grey) using three different metrics, *i.e.*, number of observed amplicon sequence variants (ASVs), Faith's PD index, and inverse Simpson index. P values calculated using the Wilcoxon rank sum test are reported in the event of a significant difference ($p \leq 0.05$). (**B**) PCoA based on weighted UniFrac distances between microbiota profiles of samples collected before transplant from patients who subsequently developed SOS/VOD (dark grey circles) and controls (empty circles). First and second principal components (MDS1 and MDS2) are plotted, accounting for 38.61% and 15.55% of variance in the dataset, respectively. The separation between the two groups of samples (Adonis; $p = 0.008$) is highlighted by plotting the SEM-based ellipse around the centroid. The biplot of the average bacterial coordinates weighted by the corresponding relative abundance per sample was superimposed on the PCoA plot for the 10 genera contributing to the ordination space, as calculated using the function envfit in the vegan package of R (black arrows). The number associated with each arrow identifies the bacterial group contributing to the ordination space; the legend is shown at the bottom. Uncl = unclassified.

Interestingly, other authors have previously shown that higher relative abundances of *Ruminococcus* were associated with better clinical outcomes, mainly reduced GvHD incidence and severity[459]. In contrast, no clearly defined group of bacteria appeared to characterize the patients who subsequently developed SOS/VOD, whose samples are actually more dispersed in the PCoA plot, indicating greater inter-sample variability. For instance, only the PRE samples belonging to two patients aged less than 2 years in the SOS/VOD group were particularly enriched in *Bifidobacterium*, but this effect could be partially explained by the higher presence of these bacteria in toddlers, especially in those breastfed as all our patients under the age of two[460]. After transplant, HSCT samples from the SOS/VOD patients and controls overlapped in the PCoA, and only after 30 days from HSCT was it possible to see again a separation, albeit slight, between the two groups using the unweighted UniFrac metric (**Figure 26**).

[459] Ingham AC, et al. Specific gut microbiome members are associated with distinct immune markers in pediatric allogeneic hematopoietic stem cell transplantation. *Microbiome*. **2019**;7:131.

[460] Masetti R, et al. The gut microbiome in pediatric patients undergoing allogeneic hematopoietic stem cell transplantation. *Pediatr Blood Cancer*. **2020**;e28711.

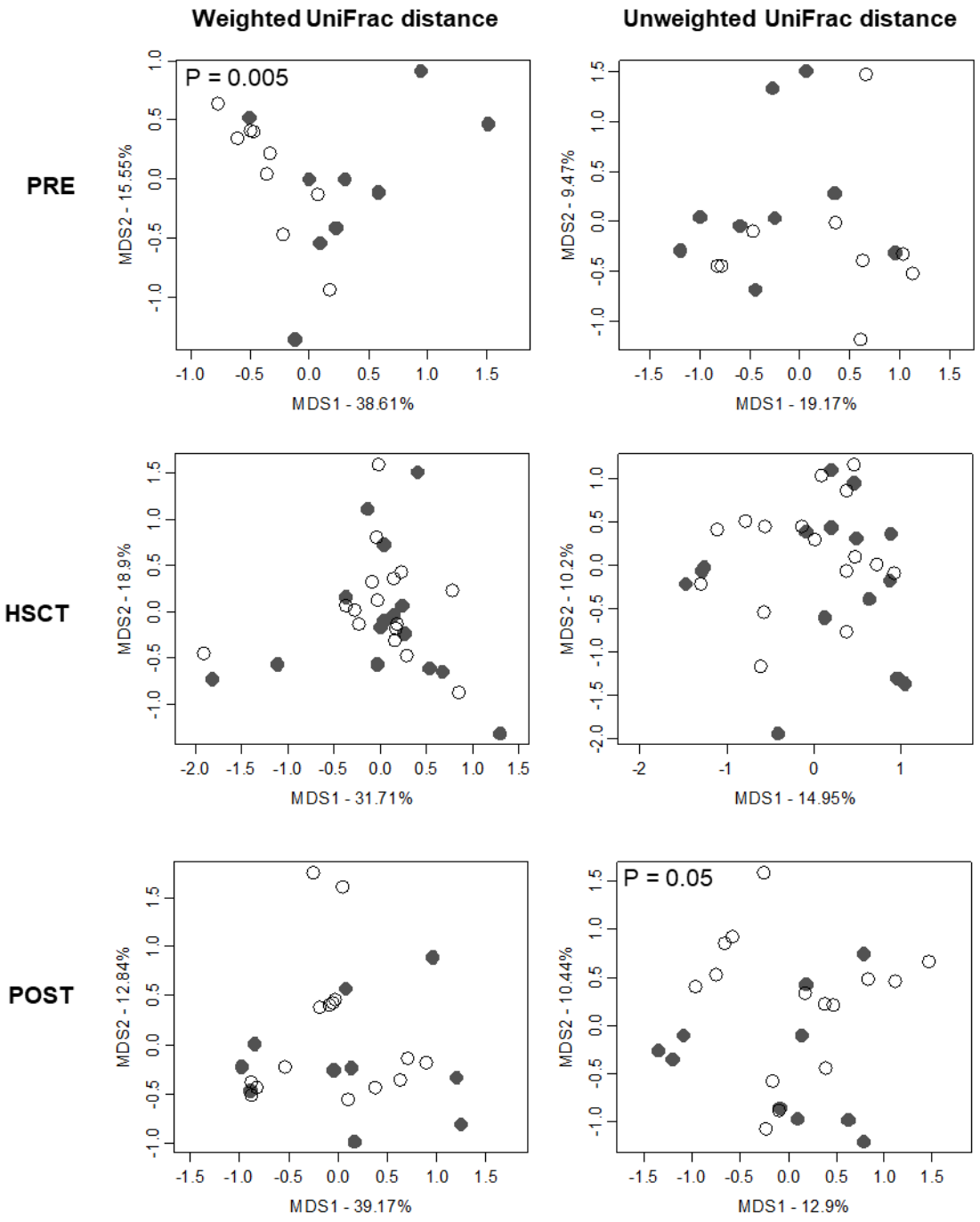

Figure 26. PCoA plots based on weighted (left) and unweighted (right) Unifrac distances of microbiota profiles of samples collected (from top to bottom) before transplant (PRE), during the first 30 days after transplant (HSCT) and >30 days after transplant (POST) from patients who subsequently developed SOS/VOD (dark grey cirles) and controls (empty white circles). First and second principal components (MDS1 and MDS2) are plotted for each analysis. Percentages of variance in the dataset accounted to MDS1 and MDS2 are reported. Permutation tests with pseudo-F ratios (Adonis function in vegan package of R software) were carried on for each analysis to test the significance of the separation between patients and control samples; p values <0.05 are reported (top left).

This pilot study reports for the first time a possible association between GM and the onset of SOS/VOD. In particular, the data seem to indicate that a rich and diverse GM before HSCT could be associated with a decreased probability of developing SOS/VOD. The protective signature identified, rich in Clostridiales, *Ruminococcaceae* and *Bacteroides,* shares some similarity to the protective configuration observed in studies regarding aGvHD[461,462,463]. The positive effect exerted by this specific pre-HSCT GM composition in both SOS/VOD and aGvHD could be related to the common endothelial damage that characterizes both diseases. As for the other complications, the mechanistic explanation for this effect remains poorly understood. Based on previous preclinical studies[464,465,466], the hypothesis is that an altered intestinal ecosystem, depleted of health-associated taxa and with low production of short-chain fatty acids, could lead to greater translocation of microbial molecules through the damaged intestinal mucosa. These bacterial products, and in particular LPS, could reach the liver sinusoid through the portal vein and participate in endothelial damage. This study presents some limitations mainly due to its retrospective design. The number of patients is relatively small because of the low incidence of this complication. Moreover, the timing of fecal sample collection, which depends on patients' bowel movements, is not fully matched between the two groups. The contribution of the relative unbalance in prophylactic levofloxacin and different types of antibiotics administered in the two groups was directly

[461] Biagi E, et al. Early gut microbiota signature of aGvHD in children given allogeneic hematopoietic cell transplantation for hematological disorders. *BMC Med Genomics*. **2019;**12:1-11.

[462] Masetti R, et al. The gut microbiome in pediatric patients undergoing allogeneic hematopoietic stem cell transplantation. *Pediatr Blood Cancer*. **2020**;e28711.

[463] Markey KA, et al. The microbe-derived short-chain fatty acids butyrate and propionate are associated with protection from chronic GVHD. *Blood*. **2020**;136:130-136.

[464] Eissner G, Multhoff G, Holler E. Influence of bacterial endotoxin on the allogenicity of human endothelial cells. *Bone Marrow Transplant*. **1998**;21:1286-1288.

[465] Falanga A, et al. Defibrotide reduces procoagulant activity and increases fibrinolytic properties of endothelial cells. *Leukemia*. **2003**;17:1636-1642.

[466] Kornblum N, et al. Defibrotide, a polydisperse mixture of single-stranded phosphodiester oligonucleotides with lifesaving activity in severe hepatic Veno-occlusive Disease: Clinical outcomes and potential mechanisms of action. *Oligonucleotides*. **2006**;16:105–114.

addressed with a specific sub-comparison. The total number of antibiotics and of specific antimicrobial molecules do not significantly differ between the two groups (**Figure S13**). A specific microbiological sub-analysis of GM composition before transplant reveled no differences between patients receiving and non-receiving prophylaxis with levofloxacin, using both weighted and unweighted UniFrac distances for the PCoA. Another unbalance worth underlining, which may be a confounding variable, is the number of BSI in the two groups (1 for SOS/VOD patients vs. 4 for controls), even if the higher incidence of bacterial infections was seen in the control group. The present results should prompt additional studies to better investigate the possible interplay between GM dysbiosis, endothelial cell injury and alloreactivity occurring in the pathogenesis of SOS/VOD. Studies involving larger cohorts of patients are warranted to explore whether the GM could serve as a predictive biomarker for clinicians to assess the risk, onset and progression of SOS/VOD.

Chapter 3 – CHARACTERIZATION OF INTESTINAL MICROBIAL COMMUNITY DURING ANTIBIOTIC EXPOSURE

As it is already known, the gut microbial community includes a wide variety of microorganisms, such as bacteria, archaeabacteria, fungi and viruses[467]. Of course, the balance between all these different microorganisms is complex and several defense mechanisms are established, such as secretion of antibiotic or synthesis of products conferring anti-microbial resistance[468]. These defense strategies can be intrinsic to commensal bacteria or acquired by transitional microorganisms, which need protection in a hostile ecosystem[469]. The presence of antibiotic-resistance genes (ARGs) in the genome of gut microorganisms is an obvious feature for at least two reasons: i) the gut microbial niche contains an enormous concentration of microorganisms in a relatively small environment; ii) this close environment predisposes to gene transfer by several different mechanisms[470]. Just think that ARGs have been around for a very long time, much longer than the "antibiotic era" that started in the 1930s with sulfamide introduction[471]. Some genes encoding for resistance to β-lactams, tetracycline and glycopeptides were found in 30,000-year-old Beringian permafrost sediments[472]. By comparing ancient and modern resistance genes and protein structures, it was found that the environment had an impact on the spread of ARGs already

[467] Lagier J-C, et al. Culture of previously uncultured members of the human gut microbiota by culturomics. *Nat Microbiol*. **2016**;1:16203.
[468] Relman DA, Lipsitch M. Microbiome as a tool and a target in the effort to address antimicrobial resistance. *Proc Natl Acad Sci U S A*. **2018**;115:12902-12910.
[469] Rolain J-M. Food and human gut as reservoirs of transferable antibiotic resistance encoding genes. Front Microbiol **2013**;4:173.
[470] Baron SA, Diene SM, Rolain J-M. Human microbiomes and antibiotic resistance. *Human Microbiome Journal*. **2018;**10:43-52.
[471] Santiago-Rodriguez TM, et al. Microbiome of an 11th century A.D. Pre-Columbian Andean Mummy. *PLoS One*. **2015**;10:e0138135.
[472] D'Costa VM, et al. Antibiotic resistance is ancient. *Nature*. **2011**;477:45-61.

in ancient times[473]. Moreover, some β-lactamases have been found in samples aged more than 2 billion years, even in plasmids, not only suggesting that horizontal gene transfer existed before antibiotic selective pressure but also explaining why some bacterial pathogens are more predisposed to acquire resistance[474]. Indeed, an ancient sequence sharing only 30% similarity with a known β-lactamase was expressed in an *E. coli* strain found in a medieval sample and showed high-level penicillinase activity, supporting the hypothesis that β-lactamases existed and were functional long before the antibiotics introduction[475,476]. However, in recent years, strong and continuous antibiotic exposure in both clinical practice and animal breeding has led to an alarming accumulation of ARGs. Antibiotic resistance has become a global public health concern and recognizing the ARG reservoirs could facilitate the control of their dissemination. In this regard, it is now well established that the human gut resistome, defined as the whole set of antibiotics, antiseptic and heavy metal resistance genes inside the gastrointestinal tract[477], is one of the best-known reservoirs of ARGs. Several different studies have targeted the selection of ARGs inside the gut microbial ecosystem, with the resulting number varying from less than 50[478,479] to thousands[480], and disparate genes were selected to represent the resistance to a given antibiotic class[481]. The

---

[473] Doyle D, et al. Characterization of an oxytetracycline- resistance gene, otrA, of *Streptomyces rimosus*. *Mol Microbiol*. **1991**;5:2923–33.

[474] Allen HK, et al. Call of the wild: antibiotic resistance genes in natural environments. *Nat Rev Microbiol*. **2010**;8:251-259.

[475] Rascovan N, et al. Exploring divergent antibiotic resistance genes in ancient metagenomes and discovery of a novel beta-lactamase family. *Environ Microbiol Rep*. 2016;8:886-895.

[476] Lugli GA, et al. Ancient bacteria of the Ötzi's microbiome: a genomic tale from the Copper Age. *Microbiome*. **2017**;5:5.

[477] D'Costa VM, et al. Antibiotic resistance is ancient. *Nature*. **2011**;477:457-461.

[478] Hasler R, et al. The antibiotic resistome and microbiota landscape of refugees from Syria, Iraq, and Afghanistan in Germany. *Microbiome*. **2018**;6:37.

[479] Sinha T, et al. Analysis of 1135 gut metagenomes identifies sex-specific resistome profiles. *Gut Microbes*. **2018**;29:1-9.

[480] Pehrsson EC, et al. Interconnected microbiomes and resistomes in low-income human habitats. *Nature*. **2016**;533:212-216.

[481] Buelow E, et al. Comparative gut microbiota and resistome profiling of intensive care patients receiving selective digestive tract decontamination and healthy subjects. *Microbiome.* **2017**;5:88.

gut resistome contains a wide variety of ARGs, but those most frequently reported are directed against the same antibiotic classes, such as tetracyclines, β-lactams, aminoglycosides and glycopeptides[482,483,484,485], as well as chloramphenicol and macrolides[486,487]. Different studies have been performed to highlight the antibiotic effect on the gut microbial profile; the first sign is the reduction of diversity, namely the decrease of the number and the relative abundance of several microorganisms, as well as the increase of the number of ARGs detected. Indeed, a study performed on Finnish pre-school children showed that macrolide assumption was correlated with a decrease of Actinobacteria, counterbalanced by an enrichment in Bacteroidetes and Proteobacteria[488]. In adult subjects, clindamycin exposure decreased the relative abundance of anaerobic microorganisms (e.g., *Bacteroides*) with an increase of *Enterobacteriaceae* members[489]. As for ARGs, as a matter of fact, all researches conducted on this topic came with the same conclusion: the pattern of ARG abundance and diversity varies with antibiotic use among populations. A multi-cohort study of individuals living in USA, Denmark and Spain revealed that resistance genes were more abundant for antibiotics used in animal husbandry than those not used for animal purposes. Moreover, a focus on antibiotics used in clinical practice highlighted that ARGs

---

[482] Hu Y, et al. Metagenome-wide analysis of antibiotic resistance genes in a large cohort of human gut microbiota. *Nat Commun*. **2013**;4:2151.

[483] Yang Z, et al. Preliminary analysis showed country-specific gut resistome based on 1,267 feces samples. *Gene*. **2016**;581:178-82.

[484] Sommer MOA, Dantas G, Church GM. Functional characterization of the antibiotic resistance reservoir in the human microflora. *Science*. **2009**;325:1128-31.

[485] Cheng G, et al. Functional screening of antibiotic resistance genes from human gut microbiota reveals a novel gene fusion. *FEMS Microbiol Lett*. **2012**;336:11-6.

[486] Gibson MK, Forsberg KJ, Dantas G. Improved annotation of antibiotic resistance determinants reveals microbial resistomes cluster by ecology. *ISME J*. **2015**;9:207-16.

[487] Moore AM, et al. Pediatric fecal microbiota harbor diverse and novel antibiotic resistance genes. *PLoS One*. **2013**;8:e78822.

[488] Korpela K, et al. Intestinal microbiome is related to lifetime antibiotic use in Finnish pre-school children. *Nat Commun*. **2016**;7:10410.

[489] Pérez-Cobas AE, et al. Differential effects of antibiotic therapy on the structure and function of human gut microbiota. *PLoS One*. **2013**;8:e80201.

were more abundant for those introduced into the commercial market earlier than those commercialized in recent years[490], confirming the hypothesis that a double stimulus from both agricultural and clinical practice is causing the current dramatic ARG accumulation. It is therefore not surprising that ARG abundance appears to be correlated with country-specific patterns of antibiotic consumption. Comparisons across culturally and genetically distinct populations suggest that the gut resistome changes not only in richness and evenness of ARGs, but also in the genetic diversity within ARG classes. The gut resistome of Chinese people has more ARG types and greater abundances of specific types than the resistome of Danes and Spaniards[491,492]. Hence, antibiotic exposure has clear and profound effects on the gut microbial community. Such effects are also age-dependent with an accumulation of ARGs over time as the number of exposures increases, even though the confounding effects of aging and illness are difficult to disentangle. An interesting study of a 5-day ciprofloxacin cycle on three healthy subjects with no prior antibiotic exposure for at least one year, highlighted immediate changes on the GM structure, including a dramatic decrease of health-associated microorganisms, such as *Bacteroides* and members of *Ruminococcaceae* and *Lachnospiraceae* families[493,494]. However, strong inter-individual variation was observed in some of these GM changes and also in microbial recovery, with complete recovery after several weeks in one subject and slow directional change over months toward an interim state in the latter two. Six months after this first antibiotic exposure,

---

[490] Forslund K, et al. Country-specific antibiotic use practices impact the human gut resistome. *Genome Res*. **2013**;23:1163-1169.

[491] Hu Y, et al. Metagenome-wide analysis of antibiotic resistance genes in a large cohort of human gut microbiota. *Nat Commun*. **2013**;4:2151.

[492] Yang Z, et al. Preliminary analysis showed country-specific gut resistome based on 1,267 feces samples. *Gene.* **2016**;581:178–182.

[493] Dethlefsen L, et al. The pervasive effects of an antibiotic on the human gut microbiota, as revealed by deep 16S rRNA sequencing. *PLoS Biol*. **2008**;6:e280.

[494] Dethlefsen L, Relman DA. Incomplete recovery and individualized responses of the human distal gut microbiota to repeated antibiotic perturbation. *Proc Natl Acad Sci USA*. **2011**;108:4554-4561.

the same subjects were treated with a second 5-day cycle of ciprofloxacin, resulting in a new GM shift in all subjects that persisted for at least two months. Therefore, despite a mild yet long-lasting imprint following antibiotic exposure, the GM profile of healthy young adults is overall resilient to a short-term antibiotic intervention and its ARG carriage, as well as the ecological interactions among community members, seem to modulate the recovery process[495]. Other studies on the experimental use of antibiotics in healthy volunteers have revealed similar basic findings: evidence for both shared (e.g., decreased overall taxonomic diversity, gain of pathobionts, loss of health-associated members) and individualized responses, with very different kinds and durations of effects, varying as a function of body site and antibiotic classes[496,497]. Some of these features, but not all, could be predicted based on the gut microbial composition before exposure[498]. However, a predictive understanding of microbiome stability and the impact of antibiotic disturbance on microbial ecosystem function is still an unmet need. The roles of past exposures to antibiotics, clinical story, as well as the age of the treated subjects are still not well understood. What is clear is that part of the gut resistome is acquired early in life. Some of the ARGs that characterize the healthy gut resistome appear during infancy, soon after birth[499,500,501]. Similar ARGs have been found in both infant and maternal gut, suggesting maternal influence in the appearance of the infant

---

[495] Paine RT, Tegner MJ, Johnson EA. Compounded perturbations yield ecological surprises. *Ecosystems*. **1998**;1:535-545.

[496] Zaura E, et al. Same exposure but two radically different responses to antibiotics: Resilience of the salivary microbiome versus long-term microbial shifts in feces. *MBio*. **2015**;6:e01693-15.

[497] Palleja A, et al. Recovery of gut microbiota of healthy adults following antibiotic exposure. *Nat Microbiol*. **2018**;3:1255-1265.

[498] Raymond F, et al. The initial state of the human gut microbiome determines its reshaping by antibiotics. *ISME J.* **2016**;10:707-720.

[499] Moore AM, et al. Gut resistome development in healthy twin pairs in the first year of life. *Microbiome*. **2015**;3:27.

[500] Moore AM, et al. Pediatric fecal microbiota harbor diverse and novel antibiotic resistance genes. *PLoS One*. **2013**;8:e78822

[501] Gueimonde M, Salminen S, Isolauri E. Presence of specific antibiotic (tet) resistance genes in infant faecal microbiota. *FEMS Immunol Med Microbiol*. **2006**;48:21-5.

resistome[499,501]. Indeed, it has been shown that intrapartum antibiotics for preventing group B streptococcal disease in newborns have consequences not only for the baby GM structure and function but also in terms of ARG content during the first months of the infants' life[502]. Furthermore, the control of the intake of antibiotics as the child grows is also noteworthy. Exposure to macrolides, more than β-lactams, has a lasting effect on the child gut microbial community, leading to a greater chance to develop immune-associated diseases, such as asthma and allergies[503]. Indeed, prospective studies offered a more robust base for causal inferences about antibiotic effects on GM development, function and resistance acquisition. Gibson and colleagues studied the GM of premature infants, highlighting reduced species richness and diversity after antibiotic exposure, also associated with enrichment of ARGs for several antibiotic classes, probably due to selection of multidrug-resistant strains (usually members of *Enterobacteriaceae* family)[504]. These conclusions were confirmed in post-term infants from Yassour at al., showing that the GM profile of antibiotic-treated children was less diverse in terms of both bacterial species and strains, with some species often dominated by single strains. In addition, ARGs carried on microbial chromosomes showed a peak in abundance right after the antibiotic exposure, followed by a sharp decline, whereas some genes carried on mobile elements persisted longer after antibiotic therapy ended[505]. In conclusion, for healthy adults a short-term antibiotic exposure usually does not lead to a lasting variation in GM structure and function due to the intrinsic resilience and plasticity of

[502] Nogacka A, et al. Impact of intrapartum antimicrobial prophylaxis upon the intestinal microbiota and the prevalence of antibiotic resistance genes in vaginally delivered full-term neonates. *Microbiome*. **2017**;5:93.
[503] Korpela K, et al. Intestinal microbiome is related to lifetime antibiotic use in Finnish pre-school children. *Nat Commun*. **2016**;7:10410.
[504] Gibson MK, et al. Developmental dynamics of the preterm infant gut microbiota and antibiotic resistome. *Nat Microbiol*. **2016**;1:16024.
[505] Yassour M, et al. Natural history of the infant gut microbiome and impact of antibiotic treatment on bacterial strain diversity and stability. *Sci Transl Med*. **2016**;8:343ra81.

the gut microbial community[506]. On the other hand, short-term or long-term antibiotic exposure during the fundamental period of the child's development could dramatically modify the GM balance, leading to a series of immune-associated complications (*i.e.,* asthma, allergies, IBD)[507], as well as a dramatic burst in ARG acquisition. A direct consequence of this bloom of ARGs, especially within the gastrointestinal tract, could be a greater susceptibility to multidrug-resistant pathogen overgrowth. This is one of the most relevant concerns in the hospital setting, where antibiotic use and exposure to antibiotic-resistant pathogens are common and patients often have a compromised immune system. Many nosocomial infections arise from the gastrointestinal tract, starting with profound microbial dysbiosis, including increased abundance of pathogens, and given their resistance to several antibiotic classes, the treatment of these patients is often very challenging. Particular attention is paid to immunosuppressed patients receiving chemotherapy or undergoing HSCT, who have an increased risk of developing local and systemic infections originating from the gastrointestinal tract[508,509]. These patients are characterized by an impaired immune system due to the combination of chemotherapy, immunotherapy, irradiation and antibiotic exposure, which can compromise the intestinal epithelial barrier and ultimately allow gut microbial members to disseminate systemically. The best-known intestinal microorganisms that are able to translocate and lead to bloodstream infection (BSI) are oxygen-tolerant and/or multidrug-resistant pathobionts, including vancomycin-resistant *Enterococcus*, members of *Enterobacteriaceae* family (*i.e., E. coli*, *Klebsiella* spp.) and

---

[506] Candela M, et al. Intestinal microbiota is a plastic factor responding to environmental changes. *Trends Microbiol.* **2012**;20:385-391.

[507] Kronman MP, et al. Antibiotic exposure and IBD development among children: A population-based cohort study. *Pediatrics.* **2012**;130:e794-e803.

[508] Velasco E, et al. Comparative study of clinical characteristics of neutropenic and non-neutropenic adult cancer patients with bloodstream infections. *Eur J Clin Microbiol Infect Dis*. **2006**;25:1-7.

[509] Kim S, Covington A, Pamer EG. The intestinal microbiota: Antibiotics, colonization resistance, and enteric pathogens. *Immunol Rev*. **2017**;279:90-105.

viridans streptococci[510,511,512]. According to all these findings, long-term antibiotic prophylaxis could have a profound impact on the early-life GM development, as well as on the acquisition of ARGs. Thus, the burden of ARGs is of strategic importance in several aspects of human life, from the child development to the mortality of hospitalized patients. The GM has been identified as one of the most prominent sources and reservoirs of ARGs and thus, the gut resistome needs to be characterized and monitored in all these risk situations, as well as in infants with a clinical history of long-term antibiotic exposure.

Aim of the studies:

a) The trajectory of the gut resistome in pediatric patients that underwent HSCT was characterized in relation to the clinical outcomes, such as BSI and GvHD development.

b) The gut microbial composition of infant patients affected by vesico-ureteral reflux (VUR) and treated with continuous low-dose antibiotic prophylaxis was profiled in order to prevent recurrent urinary tract infections.

[510] Taur Y, Pamer EG. Microbiome mediation of infections in the cancer setting. Microbiome mediation of infections in the cancer setting. *Genome Med*. **2016**;8:40.

[511] Kamboj M, et al. The changing epidemiology of vancomycin-resistant Enterococcus (VRE) bacteremia in allogeneic hematopoietic stem cell transplant (HSCT) recipients. *Biol Blood Marrow Transplant*. **2010**;16:1571-1581.

[512] Weinstock DM, et al. Colonization, bloodstream infection, and mortality caused by vancomycin-resistant *enterococcus* early after allogeneic hematopoietic stem cell transplant. *Biol Blood Marrow Transplant*. **2007**;13:615-621.

3.1 Gut resistome plasticity in pediatric patients undergoing hematopoietic stem cell transplantation

Brief introduction

The rate of infection by antibiotic-resistant bacteria (ARB) is continuously raising worldwide, particularly because of the selective pressure resulting from the increasing usage of broad-spectrum antibiotics[513]. This burden of ARB is of particular relevance for hematological patients, who undergo frequent antimicrobial prophylaxis and treatments[514]. The prolonged exposure to health care settings may indeed favor the progressive accumulation of ARG in the GM of patients[515]. Consequently, opportunistic ARB can accumulate in intestinal niches, where they can take advantage of the chemotherapy-induced damage to the gut epithelium and the overlapping neutropenia, spreading through the gut wall and causing life-threating systemic infections[516,517]. In patients who have received an HSCT, systemic infections with ARB have indeed been associated with a non-relapse mortality rate from 36 to 95%[518,519]. Furthermore, gut colonization by ARB and associated systemic infections may strongly influence the process of immune system recovery following HSCT, thus affecting the

[513] Roca, I. et al. The global threat of antimicrobial resistance: science for intervention. *New Microbes New Infect*. **2015**;6:22-29.

[514] Mikulska M, et al. Aetiology and resistance in bacteraemias among adult and paediatric haematology and cancer patients. *J Infect*. **2014**;68,321-331.

[515] Macesic N, et al. Changing microbial epidemiology in hematopoietic stem cell transplant recipients: increasing resistance over a 9-year period. *Transpl Infect Dis*. **2014**;16:887-896.

[516] Shono Y, van den Brink MRM. Gut microbiota injury in allogeneic haematopoietic stem cell transplantation. *Nat Rev Cancer*. **2018**;18:283-295.

[517] Girmenia C, et al. Infections by carbapenem-resistant *Klebsiella pneumoniae* in SCT recipients: a nationwide retrospective survey from Italy. *Bone Marrow Transplant*. **2015**;50:282-288.

[518] Caselli D, et al. Multidrug resistant *Pseudomonas aeruginosa* infection in children undergoing chemotherapy and hematopoietic stem cell transplantation. *Haematologica*. **2010**;95:1612-1615.

[519] Kim SB, et al. Incidence and risk factors for carbapenem- and multidrug-resistant *Acinetobacter baumannii* bacteremia in hematopoietic stem cell transplantation recipients. *Scand J Infect Dis*. **2014**;46:81-88.

incidence of acute Graft-versus-Host Disease (aGvHD)[520,521]. Although the relevance of ARB in HSCT is well recognized, to date the search for ARB in HSCT patients has been exclusively carried out by means of routine culture-dependent tests on rectal swabs[522,523,524]. Even if this represents a robust diagnostic approach, culture-dependent assessments of antibiotic resistance do not allow the evaluation of the whole gut resistome, defined as the overall pattern of ARGs and the corresponding ARB present in the GM[525]. The gut resistome has recently been recognized as an important and dynamic reservoir of ARGs, which can no longer be ignored when assessing antibiotic resistance[526,527,528]. In fact, it represents a basin of ARGs that can be transferred to passenger pathogens or opportunistic bacteria by horizontal gene transfer, with serious repercussions on human health[529,530,531]. In this scenario, the molecular assessment of the structure, ecology and evolution of the gut resistome in HSCT patients has become of strategic importance, allowing to understand the

---

[520] Sadowska-Klasa A, et al. Colonization with multidrug-resistant bacteria increases the risk of complications and a fatal outcome after allogeneic hematopoietic cell transplantation. *Ann Hematol*. **2018**;97:509-517.

[521] Andermann TM, Bhatt AS. Antibiotics in hematopoietic hell transplantation: adversaries or allies? *Biol Blood Marrow Transplant*. **2016**;22:972-974.

[522] Ferreira AM, et al. Epidemiology, risk factors and outcomes of multi-drug-resistant bloodstream infections in haematopoietic stem cell transplant recipients: importance of previous gut colonization. J Hosp Infect. 2018;100:83-91.

[523] Rashidi A, et al. Pretransplant gut colonization with intrinsically vancomycin-resistant enterococci (*E. gallinarum* and *E. casseliflavus*) and outcomes of allogeneic hematopoietic cell transplantation. *Biol Blood Marrow Transplant*. **2018**;2:1260-1263.

[524] Bilinski J, et al. Impact of Gut Colonization by antibiotic-resistant bacteria on the outcomes of allogeneic hematopoietic stem cell transplantation: a retrospective, single-center study. *Biol Blood Marrow Transplant*. **2016**;22:1087-1093.

[525] van Schaik W. The human gut resistome. *Philos Trans R Soc Lond B Biol Sci*. **2015**;370:20140087.

[526] Shono Y. et al. Increased GvHD-related mortality with broad-spectrum antibiotic use after allogeneic hematopoietic stem cell transplantation in human patients and mice. *Sci Transl Med*. **2016**;8:339ra71.

[527] Holler E. et al. Metagenomic analysis of the stool microbiome in patients receiving allogeneic stem cell transplantation: loss of diversity is associated with use of systemic antibiotics and more pronounced in gastrointestinal graft-versus-host disease. *Biol Blood Marrow Transplant*. **2014**;20:640-645.

[528] Gibson MK, Pesesky MW, Dantas G. The yin and yang of bacterial resilience in the human gut microbiota. *J Mol Biol*. **2014**;426:3866-3876.

[529] Gibson MK, Forsberg KJ, Dantas G. Improved annotation of antibiotic resistance determinants reveals microbial resistomes cluster by ecology. *ISME J*. **2015**;9:207-16.

[530] Forslund K, et al. Country-specific antibiotic use practices impact the human gut resistome. *Genome Res*. **2013**;23, 1163-1169.

[531] Pehrsson EC, et al. Novel resistance functions uncovered using functional metagenomic investigations of resistance reservoirs. *Front Microbiol*. **2013**;4:145.

dynamics that govern the ARB establishment in such patients. Particularly, the gut resistome characterization by shotgun metagenomics has been indicated as a unique and sensitive approach to understanding the genetic and biological effects of ARGs in HSCT, and studies in this direction have recently been encouraged[532]. Another previous research, provided the 16S rDNA-based phylogenetic description of the GM trajectory in 10 pediatric patients undergoing allo-HSCT[533]. Based on these findings, peculiarities of the structure and temporal dynamics of the GM – such as the presence and abundance of mutualistic short-chain fatty acid producers are a relevant factor for the success of HSCT. Here, a whole-genome shotgun (WGS) metagenome sequencing of the fecal DNA from eight subjects (four developing aGvHD and four aGvHD-negative) from Biagi et al. was performed[533]. This work provides – to the current knowledge for the first time – some glimpses on the gut resistome structure and its evolutionary trajectory in HSCT pediatric patients, before and after transplantation.

[532] Andermann TM, Bhatt AS. Antibiotics in hematopoietic hell transplantation: adversaries or allies?. *Biol Blood Marrow Transplant*. **2016**;22:972-974.

[533] Biagi E, et al. Gut microbiota trajectory in pediatric patients undergoing hematopoietic SCT. *Bone Marrow Transplant*. **2015**;50:992-998.

Materials and Methods

Sample collection

Genomic DNA was extracted from fecal samples of eight pediatric patients (mean age, 9.9 years) from Biagi et al.[533], who underwent allo-HSCT for high risk acute leukemia. Four patients out of the eight developed moderate (I-II grade) to severe (III-IV stage) aGvHD (**Table S2**). Sample collection, storage and DNA extraction procedures are fully reported in Biagi et al.[533]. Fecal samples were collected before HSCT and at different time points after the transplant, up to about 85 days post-HSCT, for a total of 32 samples (**Figure 27**). Because episodes of febrile neutropenia occurred after the chemotherapy, patients received an empirical treatment based on a third-generation cephalosporin with activity against *Pseudomonas* before HSCT. Informed consent was obtained for all the subjects enrolled by parents and/or legal guardians. The study was approved by the Ethics Committee of the Sant'Orsola-Malpighi Hospital-University of Bologna (ref. number 19/2013/U/Tess). All methods were performed in accordance with the relevant guidelines and regulations. Publicly available shotgun metagenomic sequencing data from fecal samples of 10 healthy Italian subjects (mean age, 31.9 years) from Rampelli et al.[534] were retrieved for comparative purposes and processed as described below. WSG sequencing DNA libraries were prepared using Illumina TruSeq DNA PCR-Free Low throughput Library Preparation Kit, following the manufacturer's instructions with few modifications. 100 nanograms of each genomic DNA was fragmented using a Covaris S2 sonication device in order to obtain 350 bp inserts. After sonication, DNA fragments were end-repaired and the appropriate library size was selected using different ratios of the Sample Purification Beads, then the samples

[534] Rampelli S, et al. Metagenome sequencing of the Hadza hunter-gatherer gut microbiota. *Curr Biol*. **2015**;25:1682-1693.

were A-tailed and ligated to adapters. Because of the low qualities of the library obtained, an "Enrich DNA Fragments" step was introduced according to the manufacturer's instructions (Illumina TruSeq DNA Sample Preparation Kit). Finally, size and concentration of DNA fragments were assessed using KAPA Library Quantification Kits (Kapa Biosystems) specific for the Illumina libraries. Approximately 8 pM libraries were paired-end sequenced (2 × 100 bp) on Illumina GAIIx platform: three samples were simultaneously sequenced in each line.

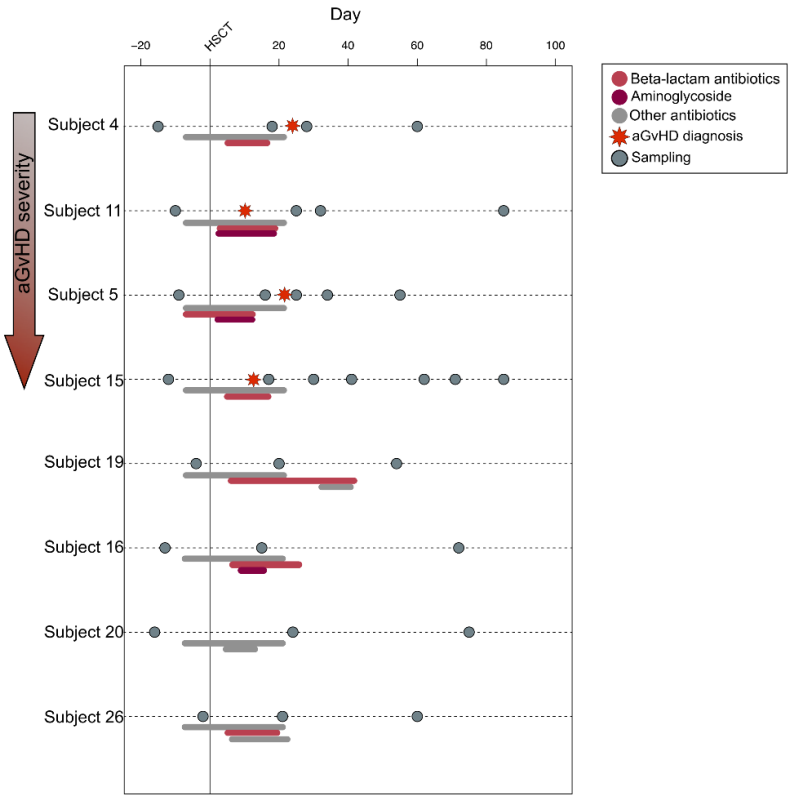

Figure 27. **Schematic representation of the sampling time for each enrolled patient**. HSCT is represented as a vertical line in the graph, while the occurrence of aGvHD is highlighted with a red star on the subject timeline. The bars below each timeline indicate the individual antimicrobial treatments by antibiotic class (see the legend at the top right).

Gut resistome analysis

Functional annotation of the sequences was performed as previously described in Rampelli et al.[534]. Briefly, shotgun reads were quality filtered using the human sequence removal pipeline from the Human Microbiome Project[535], and filtered reads were assembled in contigs using the MetaVelvet tool[536]. Raw sequence reads were deposited in the National Center for Biotechnology Information Sequence Read Archive (https://www.ncbi.nlm.nih.gov/bioproject/PRJNA525982). Protein sequences from the Antibiotic Resistance Genes Database (ARDB)[537] were screened against the assembled metagenomes using TBLASTN[538]. Only alignments with identity ≥80% and alignment length of at least 200 residues were retained for further analysis. When multiple hits were present, the best one was selected according to three criteria with the following priority: (i) percentage of identity and length of the alignment, (ii) function showing the highest number of hits, and (iii) presence of the corresponding microorganism in the respective gut ecosystems. For further analysis, the target resistance genes were normalized using the number of reads in the corresponding sample. Taxonomic classification of the identified sequences was retrieved from the results of TBLASTN. The amino acid sequences of the select proteins were clustered into Antibiotic Resistance Units (ARUs) at 30% identity level using UCLUST[539] (**Table S3**). The most abundant sequence of each ARU was selected as a representative sequence and re-classified using BLASTP and ARDB. ARU table containing

[535] Turnbaugh PJ, et al. The human microbiome project: exploring the microbial part of ourselves in a changing world. *Nature*. **2007**;449:804-810.

[536] Namiki T, et al. MetaVelvet: An extension of Velvet assembler to de novometagenome assembly from short sequence reads. *Nucleic Acids Res*. **2012**;40:e155.

[537] Liu B, Pop M. ARDB-Antibiotic Resistance Genes Database. *Nucleic Acids Res*. **2009**;37:D443–D447.

[538] Altschul SF, et al. Basic local alignment search tool. *J Mol Biol*. **1990**;215:403-410.

[539] Edgar RC. Search and clustering orders of magnitude faster than BLAST. *Bioinformatics*. **2010**;26:2460-2461.

resistance abundance across the samples was built using the script "make_otu_table.py" in QIIME[540] and used for further analysis as described below.

Bioinformatics and statistical analysis

The ARU table was used as input for a Principal Coordinates Analysis (PCoA) based on Bray-Curtis distances between samples. PCoA graphs were generated using the "vegan" package[541] in R studio, and data separation was tested by permutation test with pseudo-F ratios (function "Adonis" in "vegan"). The ARU table was also used to build a heat map of the normalized ARU abundances before and after transplantation for all patients ("ggplot2" package[542]). ARUs were superimposed on the bidimensional space using the function "envfit" of the "vegan" package and only ARGs showing a significant correlation were plotted. Significant differences in ARU table between pre-HSCT patients and healthy controls were assessed by Wilcoxon signed rank-sum test. False discovery rate (FDR) < 0.05 was considered as statistically significant.

[540] Caporaso JG, et al. QIIME allows analysis of high-throughput community sequencing data. *Nat Methods*. **2011**;7:335-336.

[541] http://www.cran.r-project.org/package=vegan

[542] Wickham H. ggplot2: elegant graphics for data analysis. *Springer-Verlag New York*. **2009**.

Results

Gut resistome structure in pediatric patients undergoing HSCT and healthy controls

By means of shotgun metagenomics analysis of fecal DNA, the resistome configuration in eight pediatric patients undergoing HSCT was characterized because of the importance of antibiotic treatments during the patient clinical path. Fecal collection was performed before transplantation and at different time points (at least 3 per subject) post HSCT, for a total of 32 fecal samples (**Figure 27**). A total of 66,738,475 high-quality reads were generated after the sequencing (mean ± SEM, 2,085,577 ± 333,987). Reads were analyzed following the same bioinformatic procedure described by Rampelli et al.[534]. Antibiotic resistance reads were clustered into 45 ARUs (Antibiotic Resistance Units), each characterized by amino acid sequence identity of at least 30%. The most abundant sequence of each ARU was selected as representative and used for functional assignment. In order to highlight peculiarities in pre-HSCT pediatric patients, their resistome configuration was compared with that of 10 healthy Italian adults[534]. Bray-Curtis distance-based PCoA shows significant segregation in the gut ARG composition between pre-HSCT patients and healthy controls (permutation test with pseudo-F ratios, $p = 0.001$) (**Figure 28**). In particular, the GM of pre-HSCT patients was found to be enriched in ARGs coding for resistance to macrolides (ARU38). On the other hand, tetracycline (ARUs4 and 24) and beta-lactam (ARU26) ARGs were found to be more represented in healthy controls. In **Figure S14**, the relative abundance of each ARU in pre-HSCT patients and healthy controls is provided. For each ARU, the p value of the difference in abundance between patients and controls is also reported.

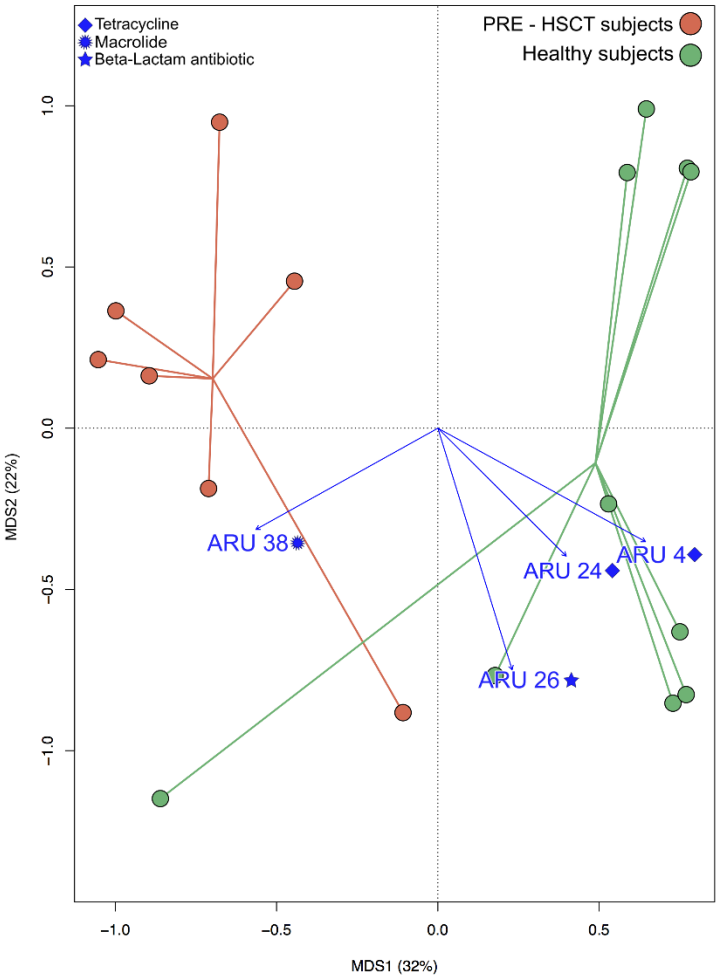

Figure 28. **Gut resistome structure of pre-HSCT pediatric patients and healthy subjects**. Bray-Curtis distancebased Principal Coordinates Analysis showing separation between the gut resistome of pre-transplant pediatric patients and healthy controls. Permutation test with pseudo-F ratios (Adonis), $p = 0.001$. Antibiotic Resistance Units (ARUs) with a significant correlation with the bidimensional space are represented with a blue arrow.

Gut resistome dynamics in pediatric patients after HSCT

The temporal dynamics of the gut resistome in the pediatric patients undergoing HSCT was analyzed by building a heat map showing the ARUs abundance in all pre- and post-transplant samples collected (**Figure 29**). During the sampling period, four patients developed aGvHD with different grade of severity (from I to IV, **Table S2**). According to these findings, most of the detected ARGs code for multidrug resistance as well as resistance to tetracyclines, macrolides, beta-lactams and aminoglycosides. Interestingly, patients developing aGvHD show a peculiar resistome trajectory, being enriched in ARGs compared to non-aGvHD patients. In particular, aGvHD patients show higher abundance and diversity of genes belonging to multidrug, macrolide and aminoglycoside resistance classes. All these resistance classes are represented by multiple ARUs, all of which seem to be acquired post-HSCT. For 3 out of 4 aGvHD patients (n. 4, 11 and 5) was observed a bloom of ARGs after HSCT. Interestingly, this rise in antibiotic resistance was attributable to multiple bacterial species and thus the resistance acquisition occurred at the ecosystem level. In particular, for patients n. 4, 11 and 5, ARGs were attributed to 5, 6 and 11 different microbial species, respectively. With regard to single ARGs was observed an increasing trend for ARU4 – present in almost all pre-HSCT samples and coding for a tetracycline inhibitor – in aGvHD-positive patients compared to non-aGvHD patients, in whom the abundance of this ARU remains overall stable during the sampling period. It is worth noting that subjects 5 and 15, developing grade III and IV aGvHD, show a high abundance of two ARUs, belonging to different ARG classes: ARU26, assigned to beta-lactamase CFXA3 and ARU38, coding for resistance to erythromycin, belonging to the macrolide resistance group. As observed for ARU4, both of these resistance genes were detected in pre-HSCT samples and found to persist with higher gene counts up to more than two months after transplant.

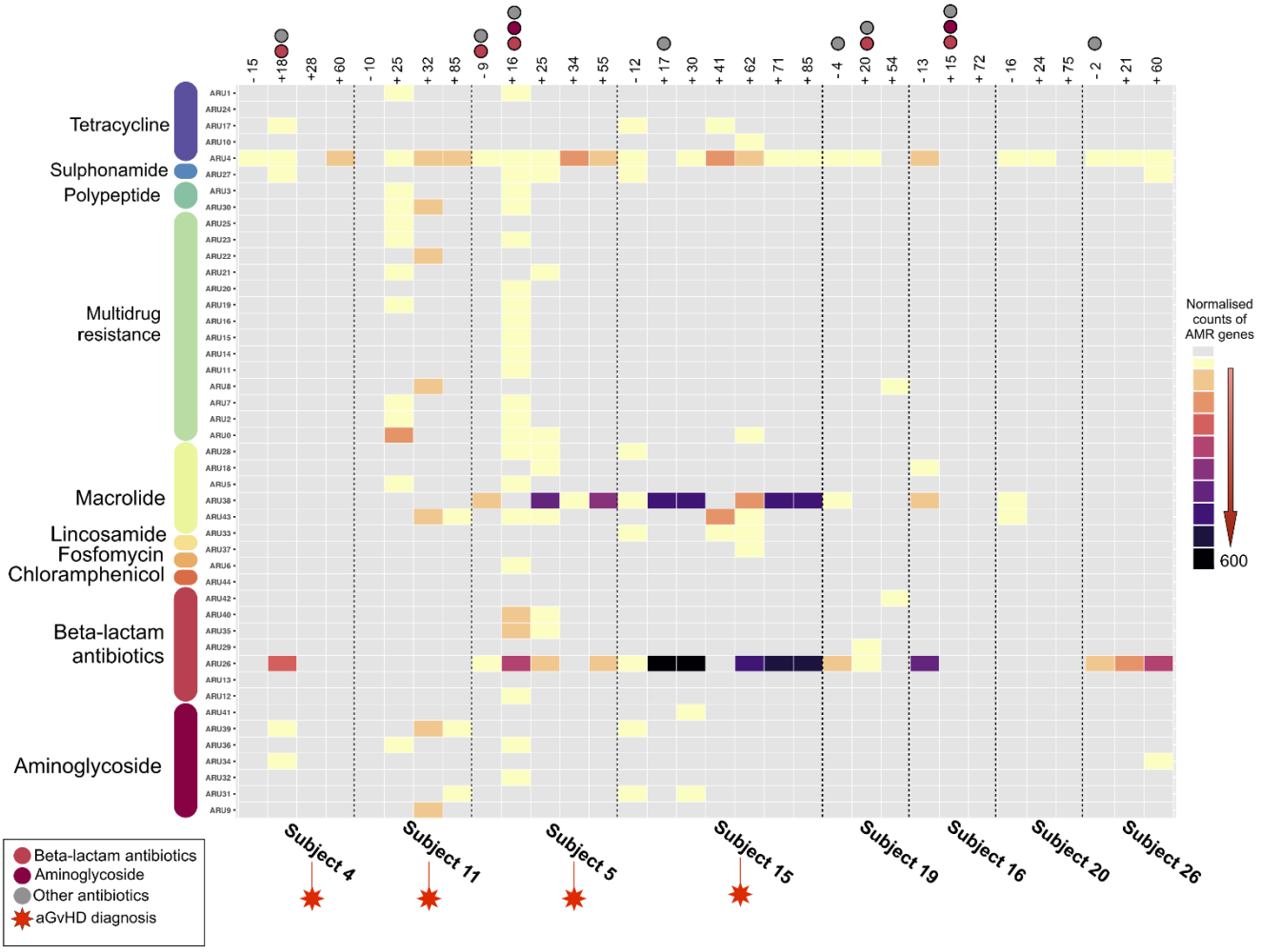

Figure 29. ARUs trajectory over time in pediatric patients undergoing HSCT. Rectangles indicate the distribution of ARU abundances across time points for each subject, normalized by ARG count and represented with different colors, from gray (0 count) to black (600 counts). A black dotted vertical line is used to separate the sample sets of patients. aGvHD-positive subjects are highlighted with a red star. The presence of colored circles indicates the antibiotic intake during the specific time point (light red for beta-lactam antibiotics, dark red for aminoglycosides and gray for other antibiotics). Antibiotic Resistance Units (ARUs) are grouped by class of antibiotic, based on the assigned protein function.

Microbial ecology of the ARG classes in HSCT pediatric patients.

In order to explore the taxonomy of the gut resistome, each of the 45 previously detected ARUs was assigned at the higher taxonomic level in order to have the phylogenetic information (*i.e.,* family level) (**Figure 30**). The results highlight a wide distribution of ARGs at this taxonomic level, including both environmental and intestinal microorganisms. Particularly, when focusing on ARGs characterizing aGvHD patients, was observed that those acquired post-HSCT (*i.e.*, those coding for multidrug, macrolide and aminoglycoside resistances) were assigned to bacterial families of putative intestinal origin, such as *Bacteroidaceae*, *Enterobacteriaceae*, *Enterococcaceae*, *Eubacteriaceae* and *Streptococcaceae*[543], as well as to more environmental and cosmopolitan microorganisms, such as *Pseudomonadaceae* and *Sphingobacteriaceae*[544]. Conversely, for what concerns the ARUs that were already present in pre-HSCT samples - and whose abundance was found to increase post-HSCT – *i.e.*, ARU4 (tetracycline inhibitor), ARU26 (β-lactamase CFXA3) and ARU38 (erythromycin resistance), a prevalent intestinal origin was determined. In particular, ARU4 is common to several GM components, including *Bifidobacteriaceae*, *Bacteroidaceae*, *Clostridiaceae*, *Enterobacteriaceae*, *Enterococcaceae*, *Eubacteriaceae*, *Lachnospiraceae* and *Streptococcaceae*, among others. Differently, ARU26 and ARU38 show a limited taxonomic diversity, with the first being assigned to three intestinal groups, *Bacteroidaceae*, *Eubacteriaceae* and *Prevotellaceae*, and the second only to *Bacteroidaceae*. These last ARUs, which characterize higher grade aGvHD, were also assigned at the species level. Particularly, the ARU26 was assigned to *Bacteroides* sp. *D1*, *Prevotella intermedia*,

[543] Lloyd-Price J, Abu-Ali G, Huttenhower, C. The healthy human microbiome. *Genome Med*. **2016**;8:51.

[544] Thomas F, et al. Environmental and gut Bacteroidetes: The food connection. *Front Microbiol*. **2011**;2:93.

Capnocytophaga ochracea and *B. fragilis* species; conversely the ARU38 was assigned to *B. fragilis* and *Bacteroides* sp. (**Figure S15**).

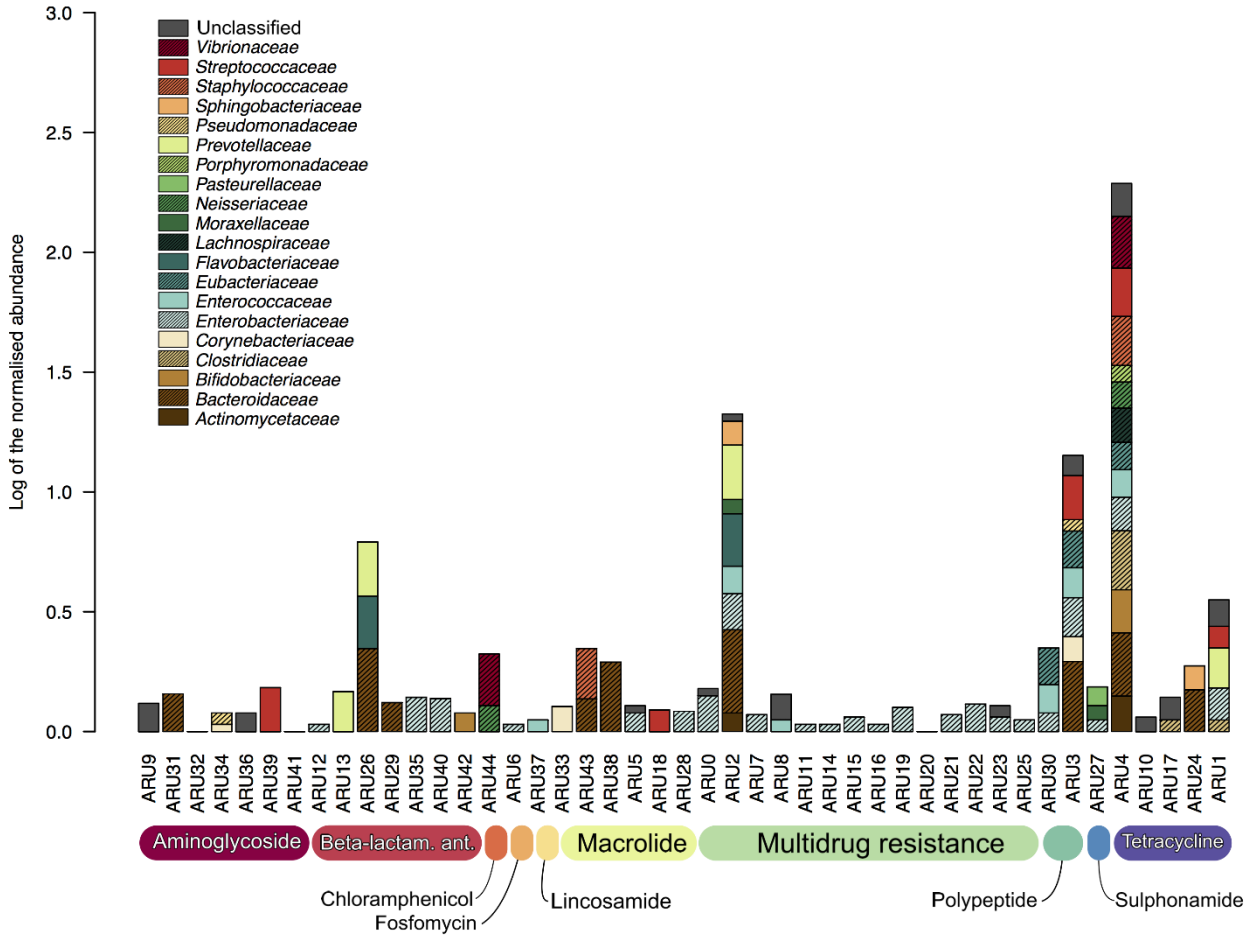

Figure 30. **Microbial ecology of Antibiotic Resistance Units (ARUs).** For each ARU, total abundance and family-level distribution are represented. ARUs are grouped by class of antibiotic, based on the assigned protein function. The reported values were normalized using a logarithmic scale. Ant., antibiotics.

Discussion

In order to highlight the impact of previous therapeutic treatments on the gut resistome of HSCT pediatric patients, the pre-HSCT gut resistome configuration was compared with the ARGs composition of 10 healthy Italian subjects[534]. According to these findings, pre-transplant pediatric patients possess an overall gut resistome structure different from that of healthy individuals, possibly shaped by the previous prolonged exposure to health care settings and being enriched in ARGs providing for macrolide resistance[545,546]. However, it should be stressed that the comparison of the ARG composition was performed between children and adults, and therefore the data need to be taken with adequate caution as the gut microbiome structure is known to change with age. Afterward, the analysis was focused on temporal variations of the gut resistome in the pediatric patients undergoing HSCT. Interestingly, the data highlight a distinctive gut resistome trajectory in patients developing aGvHD, involving not only the consolidation of ARGs already present before transplanting, but also the acquisition of a vast number of new ARGs following HSCT. Coding for multidrug, macrolide and aminoglycoside resistance classes, these newly acquired ARGs were assigned to different bacterial families, including microorganisms of intestinal origin as *Bacteroidaceae*, *Enterobacteriaceae*, *Enterococcaceae*, *Eubacteriaceae* and *Streptococcaceae*[547], as well as cosmopolitan bacteria, such as *Pseudomonadaceae* and *Sphingobacteriaceae*[548]. The gut resistome of aGvHD-positive patients was also found to be characterized by the increase in abundance of ARGs already present before HSCT. In

[545] Gibson MK, Forsberg KJ, Dantas G. Improved annotation of antibiotic resistance determinants reveals microbial resistomes cluster by ecology. *ISME J*. **2015**;9:207-16.

[546] Forslund K. et al. Country-specific antibiotic use practices impact the human gut resistome. *Genome Res*. **2013**;23:1163-1169.

[547] Lloyd-Price J, Abu-Ali G, Huttenhower C. The healthy human microbiome. *Genome Med*. **2016**;8:51.

[548] Thomas F, et al. Environmental and gut Bacteroidetes: The food connection. *Front Microbiol*. **2011**;2:93.

particular, a consistent post-HSCT bloom was detected only in aGvHD cases for ARGs coding for a tetracycline inhibitor, β-lactamase CFXA3 and erythromycin resistance. Interestingly, these ARGs were assigned to GM components, including *Bacteroidaceae*, *Prevotellaceae*, *Lachnospiraceae* and *Streptococcaceae*. It is also worth noting that the bloom of β-lactamase CFXA3 and erythromycin resistance – prevalently attributed to the major GM species of *Bacteroides* sp. and *B. fragilis* – was found to be associated with higher aGvHD severity (grade III and IV). In conclusion, this assessment of the gut resistome dynamics in eight pediatric patients undergoing HSCT allowed – to our knowledge for the first time - to shed some light on the microbial ecology of ARB in HSCT, going beyond the limit of the traditional culture-dependent studies. Despite the low number of subjects, an evidence that aGvHD onset is associated with a peculiar trajectory of the personal gut resistome following HSCT was provided. Even if all patients received fluoroquinolone antibiotic prophylaxis from day −9 to day 21 and anti-infective therapy based on beta-lactam antibiotics after transplant, only aGvHD subjects showed an extremely diversified and rich gut resistome, with a pattern of ARGs far exceeding the selective pressure due to the administered antibiotics. In particular, after HSCT, the resistome of pediatric patients developing aGvHD acquires a new and diversified pattern of ARGs, either from enteric and environmental microorganisms, and including multidrug resistance, as well as resistances to macrolide and aminoglycoside antibiotic classes. However, in parallel with the acquisition of new ARGs, the aGvHD development is also associated with a bloom of internal ARGs, already present in the individual gut resistome before the HSCT, and provided by major gut microbiome components such as *Bacteroides* sp. Particularly, this last element leads to the consolidation of ARGs such as tetracycline inhibitor, β-lactamase CFXA3 and erythromycin resistances, the latter two associated with a high aGvHD severity grade. Taken together,

these data indicate that the individual GM of HSCT patients can thus act as a dynamic reservoir of ARB, with the potential to implement the ARG pattern following HSCT. According to these findings, the aGvHD-associated magnification process of the individual gut resistome involve variations in the abundance of endogenous gut microbiome ARB, as well as the acquisition of allochthonous ARB, of enteric or environmental nature. Even if these data must be confirmed on a larger cohort, in a recently published research[549], it has been assessed the gut resistome dynamics in 12 subjects exposed to an antibiotic therapy. Results highlighted a plastic resistome response which partially resembled the observations carried out with this analysis. Indeed, according to the authors, four days post treatment it was observed an enrichment of ARGs, not limited to the ones targeted to the administered antibiotics. The inherently plastic behavior of the human gut resistome supports the importance of WGS-based resistome surveys in pediatric HSCT patients, allowing a better comprehension of the ecological dynamics of antibiotic resistance in aGvHD-positive cases, with the final goal of allowing a better refinement of antibacterial therapies.

[549] Palleja A, et al. Recovery of gut microbiota of healthy adults following antibiotic exposure. *Nat Microbiol*. **2018**;3:1255-1265.

3.2 Low-dose antibiotic prophylaxis alters the gut microbiota of infants with vesicoureteral reflux

Brief introduction

The human gastrointestinal tract harbors an individual-specific plethora of microorganisms that live in a mutualistic relationship with the host, strongly contributing to the maintenance of its homeostasis[550,551] and being essential for metabolic, immunologic and neurological functions[552]. Established soon after birth, the GM describes a characteristic developmental trajectory during infancy, reaching an almost stable phase that approximates the adult-like profile at around 3 years of age[553,554]. In particular the first months of life are considered a critical time window for GM maturation[555]. During this period various factors can affect its eubiotic state and trajectory, such as mode of delivery, formula or breast milk and, more importantly, the administration of drugs[556,557]. These modifications, albeit transient, may have short- and long-term consequences for health, as strongly suggested by extensive literature[550,551,556,557,558]. In particular, GM changes induced by early antibiotic exposure have been linked to weight gain and subsequent development of asthma, allergy, eczema, hay

---

[550] Candela M, et al. Dynamic efficiency of the human intestinal microbiota. *Crit Rev Microbiol*. **2015**;41:165-171.

[551] Gilbert J, et al. Current understanding of the human microbiome. *Nat Med*. **2020**;24:392-400.

[552] Turroni S, et al. Microbiota−host transgenomic metabolism, bioactive molecules from the inside. *J Med Chem*. **2018**;61:47-61.

[553] Stewart CJ, et al. Temporal development of the gut microbiome in early childhood from the TEDDY study. *Nature*. **2018**;562.

[554] Bäckhed F, et al. Dynamics and stabilization of the human gut microbiome during the first year of life. *Cell Host Microbe*. **2015**;17:690-703

[555] Bokulich NA, et al. Antibiotics, birth mode, and diet shape microbiome maturation during early life. *Sci Transl Med*. **2016**;8:343ra82.

[556] Tamburini S, et al. The microbiome in early life: implications for health outcomes. *Nat Med*. **2016**;22:713-722.

[557] Gibson MK, Crofts TS, Dantas G. Antibiotics and the developing infant gut microbiota and resistome. *Curr Opin Microbiol*. **2015**;27:51-56.

[558] Cotten MC. Adverse consequences of neonatal antibiotic exposure. *Curr Opin Pediatr*. **2016**;28:141-149.

fever, wheeze, atopy and inflammatory bowel disease[556,557,559,560]. Moreover, the GM of antibiotic-exposed infants can become an important reservoir of antibiotic-resistance genes, potentially leading to life-threatening complications[559,561]. Vesico-ureteral reflux (VUR) is one of the most common congenital abnormalities of the kidneys and urinary tract (CAKUT) in infants[562]. Impaired urine flow poses children with VUR at risk for recurrent urinary tract infections (UTIs). Although controversial, continuous antibiotic prophylaxis (CAP) administered at a sub-therapeutic daily dose, is currently considered the standard of care for infants with high-grade VUR in order to prevent recurrent UTIs, renal scarring and chronic kidney damage[563,564]. Altogether, antibiotic prophylaxis for various conditions may account for up to 28.6% of prescribed antibiotics in hospitalized children[565]. The ongoing randomized PREDICT trial was designed in the context of the controversial CAP cost-benefit ratio (EudraCT 2013-000309-21), aiming to clarify the efficacy of CAP in preventing the first symptomatic UTIs in infants with high-grade VUR. A nested study was planned to evaluate the GM trajectory during the first years of life, comparing patients randomized to CAP or not. Here, was performed an analysis of stool samples collected from 87 infants during the pre-trial screening phase, to assess the effect of short-term exposure to a sub-therapeutic dose of antibiotics on the GM composition and function in very young children.

---

[559] Cox LM, et al. Altering the intestinal microbiota during a critical developmental window has lasting metabolic consequences. *Cell*. **2014**;158:705-721.

[560] Kim DH, Han K, Kim SW. Effects of antibiotics on the development of asthma and other allergic diseases in children and adolescents. *Allergy, Asthma Immunol Res*. **2018**;10:457-465.

[561] Gasparrini AJ, et al. Persistent metagenomic signatures of early-life hospitalization and antibiotic treatment in the infant gut microbiota and resistome. *Nat Microbiol*. **2019**;4:2285-2297.

[562] Tullus K. Vesicoureteric reflux in children. *Lancet*. **2014**;385:371-379.

[563] Morello W, et al. Acute pyelonephritis in children. *Pediatr Nephrol*. **2015**;31:1253-1265.

[564] Montini G, Tullus K, Hewitt I. Febrile urinary tract infections in children. *N Engl J Med*. **2011**;365:239-250.

[565] Hufnagel M, et al. High rates of prescribing antimicrobials for prophylaxis in children and neonates: Results from the antibiotic resistance and prescribing in European children point prevalence survey. *J Pediatric Infect Dis Soc*. **2019**;8:143-151.

Materials and Methods

Patient selection

A cross-sectional study analyzing the GM composition and fecal levels of short- and branched-chain fatty acids (SCFAs and BCFAs, respectively) in a cohort of patients screened for the PREDICT trial from October 2014 to November 2018 was performed. The trial enrolls infants <5 months of age with high-grade VUR (III-V), without previous UTIs and with gestational age ≥35 weeks, who are randomized to prophylaxis or not and followed for five years. We identified all screened patients with a viable stool sample and available data regarding CAP exposure before randomization. Selected patients were divided in two groups: CAP-naïve vs. CAP-treated patients (**Figure S16**). The use of CAP before stool collection was only related to local practice and did not interfere with subsequent patient randomization. This study was approved by the Institutional Review Board of all participating centers and written informed consent was provided by all parents or legal guardians.

Samples and data collection

Stool samples were collected for each patient and immediately frozen at -80°C without processing. Samples were shipped in dry ice to the HolobioME unit (Dept. Pharmacy and Biotechnology, University of Bologna, Bologna, Italy) for GM and SCFA/BCFA analysis. From the PREDICT trial database, data regarding patients (age, gender, VUR), previous antibiotic prophylaxis (agent, dose and duration) and other potential GM-perturbing factors (*i.e.*, feeding modality, mode of delivery, gestational age, drug consumption and use of probiotics) were extracted.

Microbial DNA extraction, library preparation and sequencing

Microbial DNA was extracted from feces using the repeated bead-beating plus column method, as previously described.17 In brief, 0.25 g of fecal sample were resuspended in 1 mL of lysis buffer (500 mM NaCl, 50 mM Tris-HCl pH 8, 50 mM EDTA, 4% SDS) with four 3-mm glass beads and 0.5 g of 0.1-mm zirconia beads (BioSpec Products, Bartlesville, OK, USA), and homogenized three times in a FastPrep instrument (MP Biomedicals, Irvine, CA, USA) at 5.5 movements/sec for 1 min. After 15-min incubation at 95°C and centrifugation at 13,000 rpm for 5 min, samples were added with 260 µL of 10 M ammonium acetate. After a further centrifugation step, sample were incubated on ice for 30 min with one volume of isopropanol. Precipitated nucleic acids were washed with 70% ethanol, resuspended in TE buffer (10 mM Tris-HCl, 1 mM EDTA pH 8.0) and treated with 2 µL of 10 mg/mL DNase-free RNase at 37°C for 15 min. DNA purification was performed using the DNeasy Blood and Tissue Kit (QIAGEN, Hilden, Germany) following the manufacturer's instructions. DNA concentration and quality were assessed with NanoDrop ND-100 (NanoDrop Technologies, Wilmington, DE, USA). For library preparation, the V3-V4 hypervariable region of the 16S rRNA gene was amplified using 341F and 785R primers with added Illumina adapter overhang sequences, as previously described[566]. Amplification was performed using KAPA HiFi HotStart ReadyMix (Roche, Basel, Switzerland). PCR products were purified using a magnetic bead-based clean-up system (Agencourt AMPure XP, Beckman Coulter, Brea, CA, USA). A limited-cycle PCR was performed to obtain the indexed library using Nextera technology, followed by a second AMPure XP magnetic bead-based purification. Final libraries were pooled at equimolar concentration (4 nM), denatured with 0.2 N NaOH, and

[566] D'Amico F, et al. Enteral nutrition in pediatric patients undergoing hematopoietic SCT promotes the recovery of gut microbiome homeostasis. *Nutrients*. **2019**;11:1-12.

diluted to 5 pM with a 20% PhiX control before sequencing on an Illumina MiSeq platform with a 2 x 250 bp paired-end protocol according to the manufacturer's instructions (Illumina, San Diego, CA, USA).

GC–MS determination of fecal SCFAs and BCFAs

Approximately 0.25 g of feces were analyzed for levels of SCFAs (*i.e.,* acetic, propionic, butyric and valeric acids) and BCFAs (*i.e.,* isobutyric and isovaleric acids). Sample preparation was performed by head space-solid phase microextraction (HS-SPME), followed by gas chromatography–mass spectrometry (GC-MS) analysis to detect volatile metabolites, as previously described[567]. The chromatogram acquisition was obtained with Total Ion Current (TIC) and Single Ion Monitoring (SIM) scan modes.

Bioinformatics and statistics

Between-group differences in patient characteristics were assessed using the Chi-square test, to rule out potential confounders in the GM analysis. For GM, raw sequences were processed using a combined pipeline of PANDASeq[568] and QIIME2[569]. After length and quality filtering (default parameters), reads were binned into amplicon sequence variants (ASVs) using DADA2[570]. Taxonomic assignment was carried out using the VSEARCH algorithm[571] and Greengenes database (May 2013 release). Chimeras were discarded during analysis. Alpha diversity was calculated with different metrics, such as number of observed ASVs and Faith's Phylogenetic Diversity, while beta diversity was estimated by computing

[567] Schnorr SL, et al. Gut microbiome of the Hadza hunter-gatherers. *Nat Commun*. **2014**;5:3654.

[568] Masella AP, et al. PANDAseq: Paired-end assembler for Illumina sequences. *BMC Bioinformatics*. **2012**;13:31.

[569] Bolyen E, et al. Reproducible, interactive, scalable and extensible microbiome data science using QIIME 2. *Nat Biotechnol*. **2019**;37:852-857.

[570] Callahan BJ, et al. DADA2: High-resolution sample inference from Illumina amplicon data. *Nat Methods*. **2016**;3:581-583.

[571] Rognes T, et al. VSEARCH: a versatile open source tool for metagenomics. *PeerJ.* **2016**;4:e2584.

UniFrac distances, which were used as input for Principal Coordinates Analysis (PCoA). All statistical analysis was performed using R project. PCoA plots were generated using the "vegan"[572] and "Made4"[573] packages, and data separation was tested by a permutation test with pseudo-F ratios (function "Adonis" in "vegan"). The bacterial genera most contributing to the ordination space were identified using the function "envfit" of "vegan". Wilcoxon test was used to assess significant differences in alpha diversity, taxon relative abundance and SCFA/BCFA levels between groups. A p-value ≤ 0.05 was considered statistically significant, while a p-value between 0.05 and 0.1 as a trend.

[572] http://www.cran.r-project.org/package-vegan/

[573] Culhane AC, et al. MADE4: an R package for multivariate analysis of gene expression data. *Bioinformatics*. **2005**;21:2789-2790.

Results

Population

Eighty-seven patients aged 1-5 months were enrolled. The main demographic and clinical characteristics are listed in **Table S4**. Regarding CAP exposure, 51/87 patients did not receive any CAP before enrollment (hereafter referred to as CAP-naïve), while 36/87 patients were taking CAP (*i.e.*, CAP-treated). The median duration of CAP at the time of analysis was 47 days (range: 16 - 140 days). The use of different classes of antibiotics in the latter group of patients was as follows: amoxicillin or amoxicillin+clavulanic acid 21 (58.3%), trimethoprim 7 (19.4%), oral cephalosporins 6 (8.3%) and nitrofurantoin 2 (16.7%).

Comparison of potential confounding factors

No short cycles of antibiotics for any acute infection were reported in the selected population. The groups did not differ according to gender, feeding modality, gestational age and consumption of probiotics (**Table S4**). All patients were between 1 and 5 months of age, *i.e.*, within the development phase of GM maturation as recently established[574]. The predominant mode of delivery differed between the groups, with a higher proportion of children born by cesarean section in the CAP-naïve group than in the CAP-treated group (27/51 vs. 6/36, $p = 0.001$).

Gut microbiota of CAP-treated vs. CAP-naïve infants

The 16S rRNA gene-based NGS yielded a total of 908,524 high-quality reads, with an average of 10,443 ± 2,920 sequences per sample, binned into 3,075 ASVs. No differences in alpha diversity were observed between CAP-treated and CAP-naïve patients ($p \geq 0.2$;

[574] Stewart CJ, et al. Temporal development of the gut microbiome in early childhood from the TEDDY study. *Nature*. **2018**;62:583-588.

Wilcoxon test) (**Figure 31A**). Principal Coordinates Analysis (PCoA) of inter-individual variation, based on weighted UniFrac distances, revealed significant separation between groups (p = 0.015, permutation test with pseudo-F ratios) (**Figure 31B**). By contrast, no significant differences were detected according to the unweighted UniFrac metrics (**Figure S17**). Interestingly, no separation was observed with regards to any of the potential confounders listed above (**Figure S18**).

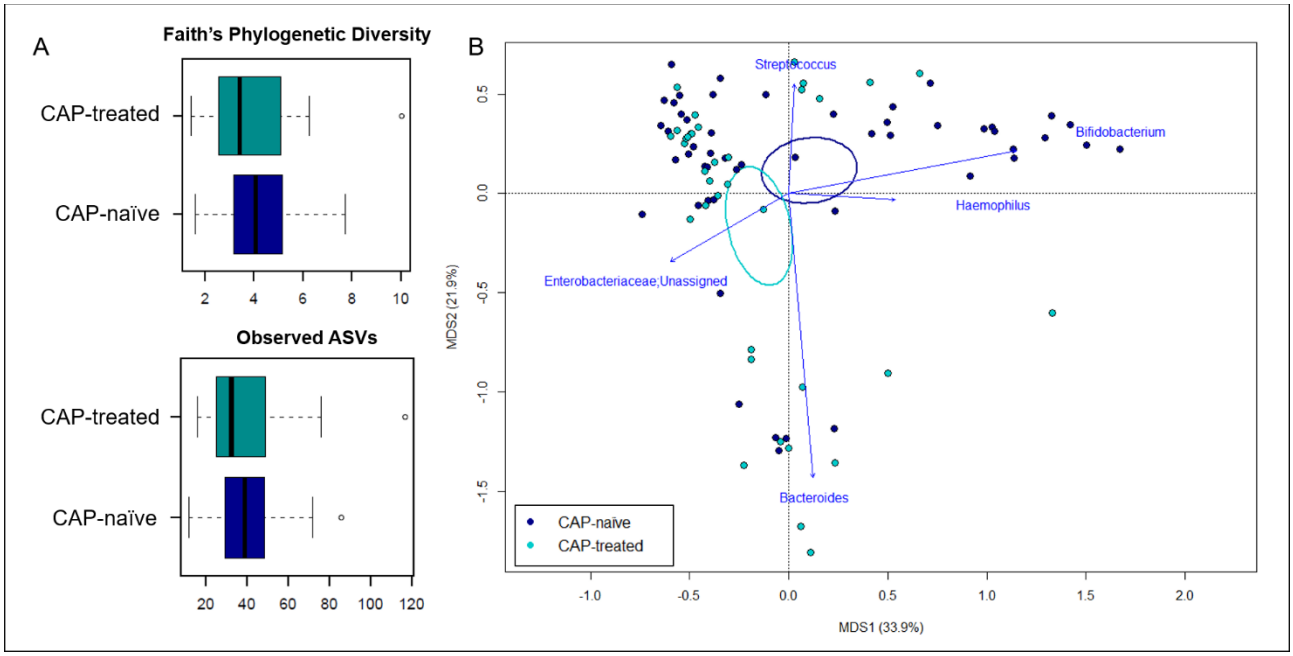

Figure 31. The gut microbiota of infants exposed to CAP segregates from that of naïve infants. (A) Alpha diversity estimated according to Faith's Phylogenetic Diversity and the number of observed ASVs. No significant differences were found ($p \geq 0.02$, Wilcoxon test). (B) Principal Coordinates Analysis (PCoA) based on weighted UniFrac distances between fecal samples. A significant separation between groups was observed (p = 0.015, permutation test with pseudo-F ratios). Ellipses include 95% confidence area based on the standard error of the weighted average of sample coordinates. Bacterial genera with the largest contribution to the ordination space are indicated with blue arrows ($p < 0.05$, permutational correlation test, "envfit" function).

In line with the available literature[574,575,576] the GM of both CAP-treated and CAP-naïve infants was dominated by the phyla Actinobacteria (mean relative abundance ± SEM, 27.7% ± 4.0% vs. 37.9% ± 3.6%), Proteobacteria (42.1% ± 4.4% vs. 31.3% ± 4.2%) and Firmicutes (20.1% ± 2.9% vs. 27.6% ± 3.1%). However, CAP-treated patients were significantly enriched in Bacteroidetes compared to CAP-naïve subjects ($p = 0.03$) (**Figure 32A**). Although the family-level GM layout of both groups was generally characterized by a preponderance of *Bifidobacteriaceae* (22.8% ± 4.0% vs. 31.5% ± 3.5%) and *Enterobacteriaceae* (41.7% ± 4.5% vs. 30.1% ± 4.3%) (**Figure 32B**), significant differences emerged. Specifically, compared to CAP-naïve infants, those exposed to CAP showed significant enrichment in *Bacteroidaceae* ($p = 0.03$) and *Enterobacteriaceae* members ($p = 0.05$), as well as a trend towards reduced proportions of *Bifidobacteriaceae* ($p = 0.09$). As expected, the ratio of *Enterobacteriaceae* to *Bifidobacteriaceae*, a validated index to measure intestinal health and microbial colonization resistance, with a higher value reflecting a compromised ecosystem[577], was significantly higher in the CAP-treated group than in the control group ($p = 0.05$) (**Figure 32C**).

[575] Candela M, et al. Dynamic efficiency of the human intestinal microbiota. *Crit Rev Microbiol*. **2015**;41:165-171.

[576] Bäckhed F, et al. Dynamics and stabilization of the human gut microbiome during the first year of life resource. *Cell Host Microbe*. **2015**;17:690-703

[577] Muleviciene A, et al. Iron deficiency anemia-related gut microbiota dysbiosis in infants and young children: a pilot study. *Acta Microbiol Immunol Hung*. **2018**;65:551-564.

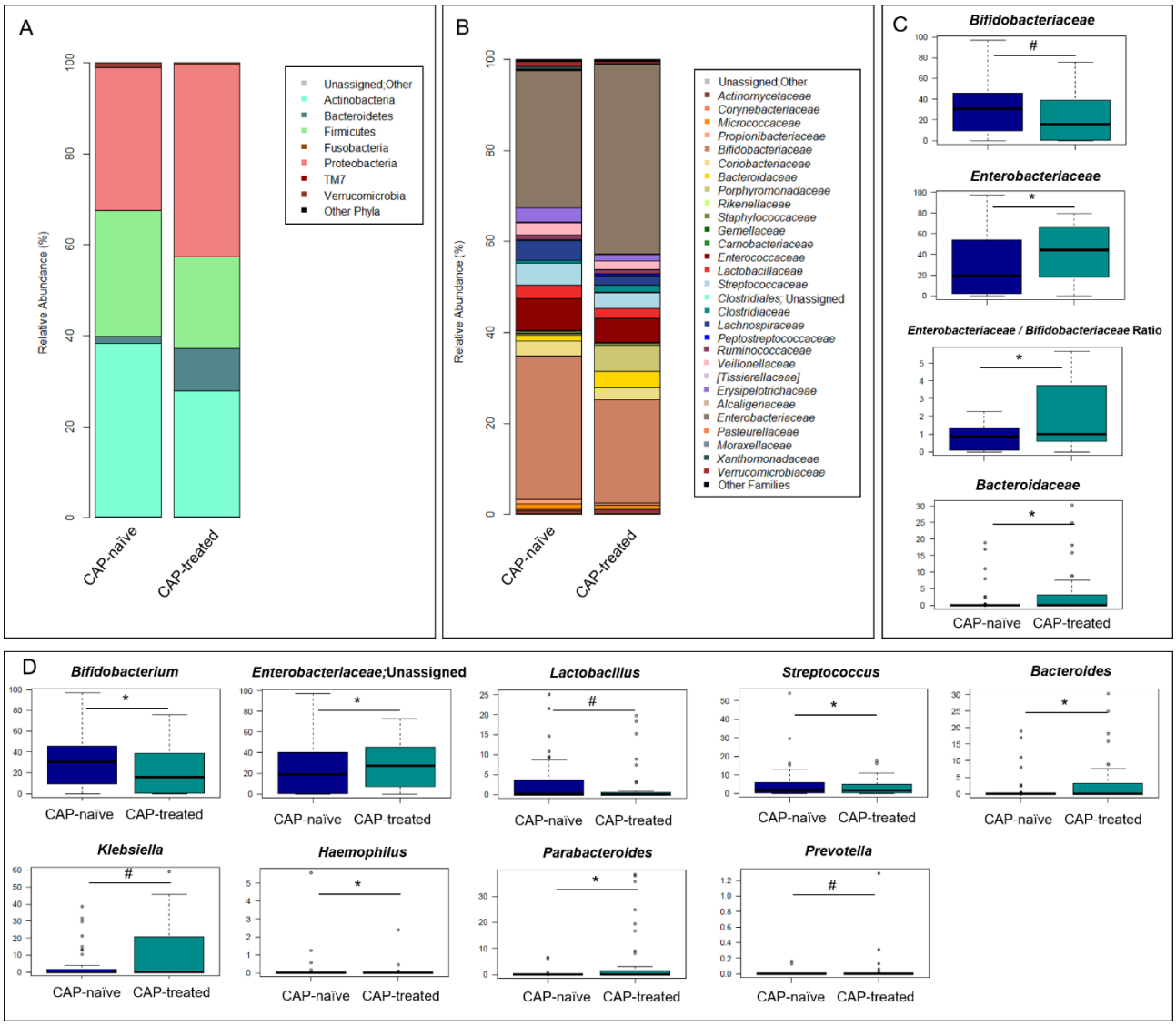

Figure 32. **Gut microbiota structure in CAP-treated vs. CAP-naïve infants.** Bar plots representing the relative abundance of the major phyla (A) and families (B) in the GM of CAP-naïve and CAP-treated infants. Boxplots showing the relative abundance distribution of bacterial families (C) and genera (D) with a significant difference ($p \leq 0.05$, Wilcoxon test; asterisk) or a trend ($0.05 < p \leq 0.1$; hashtag) between the two groups. Only taxa with relative abundance > 0.1% in at least 2 samples were considered.

In order to identify the bacterial genera responsible for the separation between the GM structures of CAP-treated and CAP-naïve infants, relative abundance vectors with a statistically significant contribution were identified and overlaid onto the weighted UniFrac ordination space of **Figure 31B** ($p \leq 0.05$, "envfit" function). Interestingly, several taxa drive the clustering pattern, *i.e.*, *Bacteroides* and unclassified genera of *Enterobacteriaceae*, which were associated with CAP, and *Bifidobacterium*, *Haemophilus* and *Streptococcus*, which were associated with controls ($p \leq 0.05$) (**Figure 32D**). Furthermore, the GM profile of CAP-treated patients was characterized by increased proportions of *Parabacteroides* ($p = 0.05$), as well as by a tendency towards increased amounts of *Klebsiella* and *Prevotella* and reduced amounts of *Lactobacillus* ($p \leq 0.1$) (**Figure 32D**).

Fecal levels of SCFAs and BCFAs

SCFA and BCFA fecal levels were determined on 52/87 infants, of whom 29 were not taking prophylaxis whereas 23 were currently under CAP. No significant differences were found between the groups in the total amount of SCFAs, as well as in the individual amounts of acetic, butyric, propionic and valeric acid ($p > 0.05$). Similarly, total BCFA levels and those of isobutyric and isovaleric acid were not different according to CAP exposure ($p > 0.05$) (**Figure 33**).

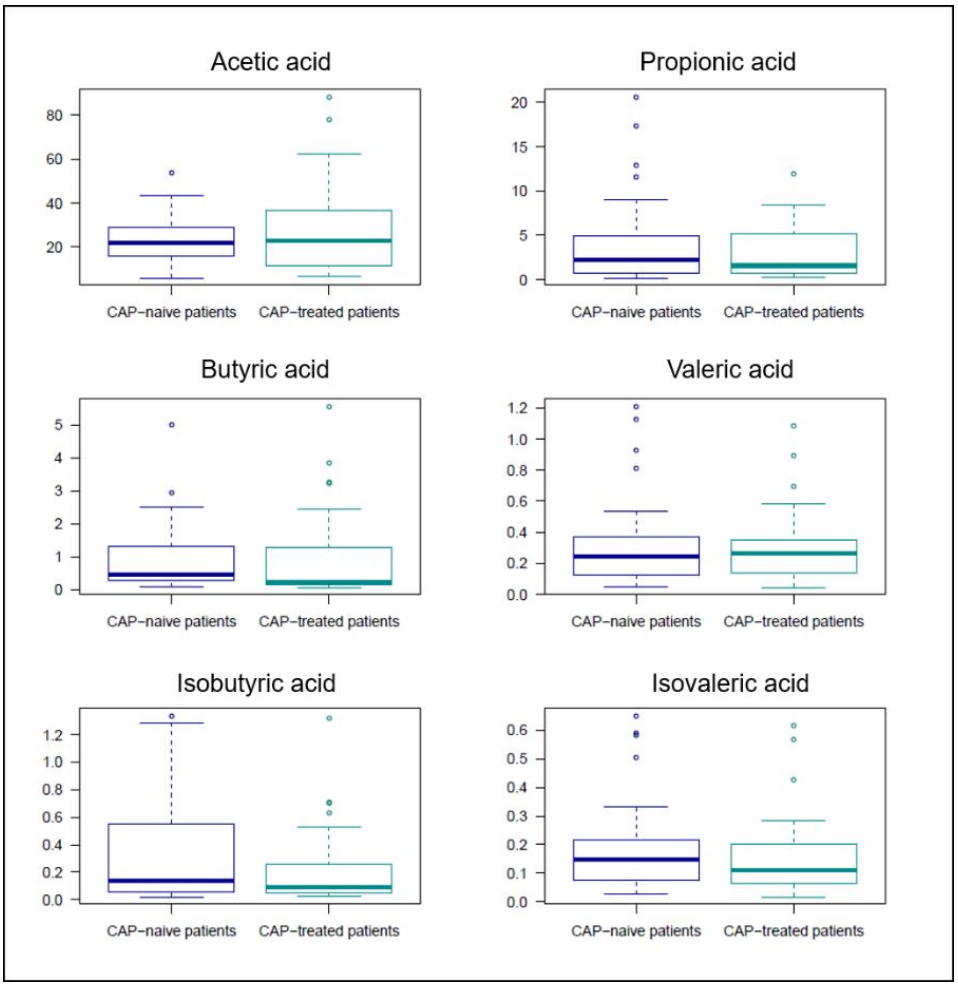

Figure 33. **Fecal levels of SCFAs and BCFAs in infants exposed or naïve to CAP**. Boxplots showing the absolute amount distribution for SCFAs (acetic, propionic, butyric and valeric acids) and BCFAs (isobutyric and isovaleric acids) measured in μmol/g. No significant differences were found (p-value > 0.05, Wilcoxon test).

Discussion

GM maturation is a fine process shaped by various environmental factors[578] which, in turn, influences a multitude of physiological host processes, including the development of the immune system and metabolic programming[579,580]. The first months of life are recognized as a critical time window during which GM-host cross-talk lays the foundations for future health[581]. In early life, the GM has a peculiar ecological structure, with distinct compositional differences from the profile typically observed in adults. The infant-type GM is characterized by the dominance of *Bifidobacterium* together with facultative anaerobes, including *Enterobacteriaceae* members, as well as a high level of plasticity over time[582,583]. Current evidence supports possible interferences of early-life antibiotic exposure on the GM maturation dynamics, with potential long-term health implications[584,585,586]. While GM alterations following antibiotic therapies are well established in adults, concerns are rising about the influence of antibiotics on the highly dynamic infantile GM[585]. Infants with VUR often receive extended CAP to prevent UTIs, but the beneficial effects of this intervention have to be balanced against potential long-term side effects. Comparing infants with VUR previously treated with CAP and those naïve, our study showed an altered GM composition

---

[578] Forsgren M, et al. Late preterm birth has direct and indirect effects on infant gut microbiota development during the first six months of life. *Acta Paediatr*. **2017**;106:1103-1109.

[579] Tamburini S, et al. The microbiome in early life: implications for health outcomes. *Nat Med*. **2016**;22:713-722.

[580] Cox LM, et al. Altering the intestinal microbiota during a critical developmental window has lasting metabolic consequences. *Cell*. **2014**;158:705-721.

[581] Bokulich NA, et al. Antibiotics, birth mode, and diet shape microbiome maturation during early life. *Sci Transl Med*. **2016**;8:343ra82.

[582] Stewart CJ, et al. Temporal development of the gut microbiome in early childhood from the TEDDY study. *Nature*. **2018**;562:583-588.

[583] Bäckhed F, et al. Dynamics and stabilization of the human gut microbiome during the first year of life resource. *Cell Host Microbe*. **2015**;17:690-703.

[584] Bokulich NA, et al. Antibiotics, birth mode, and diet shape microbiome maturation during early life. *Sci Transl Med*. **2016**;8:343ra82.

[585] Gibson MK, Crofts TS, Dantas G. Antibiotics and the developing infant gut microbiota and resistome. *Curr Opin Microbiol*. **2015**;27:51-56.

[586] Nogacka AM, et al. Early microbiota, antibiotics and health. *Cell Mol Life Sci*. **2018**;75:83-91.

even after short (less than 7 weeks) exposure to antibiotics administered at sub-therapeutic dosage. Interestingly, GM changes involved the loss of typical features of the eubiotic infant-type ecosystem. In particular, CAP-exposed patients showed decreased proportions of *Bifidobacterium*, a keystone taxon in the infant GM which dominates the ecosystem at least until breastfeeding ceases[587]. *Bifidobacterium* spp. are indeed are able to thrive on human milk oligosaccharides and associated with many health-promoting functions, including a critical role in the development of the child's immune system[588]. Conversely, compared to naïve patients, the GM of CAP-exposed infants was enriched in the genera *Bacteroides*, *Prevotella* and *Parabacteroides*. According to the TEDDY study, which followed the GM trajectory in 903 children from 3 to 46 months of age[587], *Bacteroides* is associated with increased gut microbial diversity and faster maturation during early life, regardless of the birth mode. Analogously, *Prevotella* is another well-known marker of the adult human GM, although differentially represented in relation to host variables, including diet and geography[589]. It is also worth noting that three enterotype-like clusters dominated by *Bacteroides*, *Prevotella* and *Bifidobacterium*, have recently been detected in the microbiota of school-aged children and suggested to represent stratified developmental trends of GM towards the adult configuration, with the *Bifidobacterium* enterotype being the less mature[590]. It can be hypothesized that CAP exposure may induce a non-eubiotic, accelerated maturation of the infant GM towards an adult-like profile. Moreover, the GM of patients receiving CAP was enriched in *Enterobacteriaceae* members, specifically *Klebsiella*, a well-

[587] Stewart CJ, et al. Temporal development of the gut microbiome in early childhood from the TEDDY study. *Nature*. **2018**;62:583-588.

[588] Laforest-Lapointe I, Arrieta M. Patterns of early-life gut microbial colonization during human immune development: An ecological perspective. *Front Immunol*. **2017**;8:788.

[589] Schnorr SL, et al. Gut microbiome of the Hadza hunter-gatherers. *Nat Commun*. **2014**;5:3654.

[590] Zhong H, et al. Impact of early events and lifestyle on the gut microbiota and metabolic phenotypes in young school-age children. *Microbiome*. **2019**;7:2.

known clinically relevant nosocomial pathogen, associated with several intestinal and systemic infections, including UTIs, and often resistant to multiple antibiotics[591]. In addition to indicating ineffectiveness of prophylaxis in controlling its spread, the high amounts of *Klebsiella* in the CAP-treated group represent a non-negligible risk factor for the development of more difficult-to-treat UTIs in this highly vulnerable population. While several potential confounders such as feeding modality or probiotics consumption did not differ between the groups, more CAP-naive infants had undergone Cesarian section. Although this may have partially biased our results, particularly regarding *Bacteroides*, which has sometimes been found enriched in infants born vaginally[592], a significant impact of the delivery mode on GM variation was not found, suggesting that CAP-related dysbiosis could be robust to this as well as to all other confounding variables considered. Previous reports have analyzed the impact of antibiotics on infantile GM, but in different settings, with less homogeneous populations. In 2014, a study on preterm infants demonstrated decreased bacterial diversity after 5-7 days of empiric antibiotic therapy with either ampicillin or gentamicin, resulting in compositional imbalances, such as increased *Enterobacter*[593]. In 2016, Bokulich and coworkers showed in a study of 43 healthy infants that prenatal and postnatal antibiotic exposure to different classes and doses of antibiotics delays GM maturation and suppresses important pathobionts[594]. A study on 39 children aged 0-3 years observed lower GM diversity and a peak of resistance genes after multiple courses (9-15) of

[591] Holt KE, et al. Genomic analysis of diversity, population structure, virulence, and antimicrobial resistance in *Klebsiella pneumoniae*, an urgent threat to public health. *Proc Natl Acad Sci USA*. **2015**;112:E3574-81.

[592] Stinson LF, Payne MS, Keelan JA. A critical review of the bacterial baptism hypothesis and the impact of cesarean delivery on the infant microbiome. *Front Med*. **2018**;5:135.

[593] Greenwood C, et al. Early empiric antibiotic use in preterm infants is associated with lower bacterial diversity and higher relative abundance of *enterobacter*. *J Pediatr*. **2014**;165:23-9.

[594] Bokulich NA, et al. Antibiotics, birth mode, and diet shape microbiome maturation during early life. *Sci Transl Med*. **2016**;8:343ra82.

full-dose antibiotic therapy[595]. More recently, persistent GM differences, not prevented by probiotics consumption, were demonstrated in 149 newborns exposed to perinatal (prenatal and/or postnatal) antibiotics compared to controls[596]. Our analysis sheds further light on the impact of antibiotics on GM, revealing that even short exposure to a sub-therapeutic dose of antibiotics results in detectable GM modification, in such a delicate moment for GM maturation. In particular, the observed deviation probably implies an impairment of the GM barrier effect, as supported by the increase in *Klebsiella*. Although the CAP-associated dysbiosis did not lead to imbalanced SCFA and BCFA production, a delayed effect in the following months/years of life cannot be excluded, when a more fermentative ecosystem is being established. Indeed, it has been demonstrated that early deviations from an eubiotic GM layout can provide long-lasting pathophysiological problems, as a result of a compromised GM-host dialogue that fails in GM-dependent immunological and metabolic programming[597,598]. The GM dysbiosis observed after a short exposure to CAP points to potentially even deeper alterations that may be caused by the extended, typically 2-year courses commonly prescribed to VUR patients. Long-term effects after children's exposure to antibiotics are still under investigation. Some authors suggest that GM disruption during a critical age contributes to an increased risk of diseases such as asthma, obesity and allergies[597,599,600,601]. Two different studies including over 23,000 children proved that

---

[595] Yassour M, et al. Natural history of the infant gut microbiome and impact of antibiotic treatment on bacterial strain diversity and stability. *Sci Transl Med*. **2016**;8:343ra81.

[596] Tapiainen T, et al. Impact of intrapartum and postnatal antibiotics on the gut microbiome and emergence of antimicrobial resistance in infants. *Sci Rep*. **2019**;9:10635.

[597] Tamburini S, et al. The microbiome in early life: implications for health outcomes. *Nat Med*. **2016**;22:713-722.

[598] Cox LM, et al. Altering the intestinal microbiota during a critical developmental window has lasting metabolic consequences. *Cell*. **2014**;158:705-721.

[599] Gibson MK, Crofts TS, Dantas G. Antibiotics and the developing infant gut microbiota and resistome. *Curr Opin Microbiol*. **2015**;27:51-56.

[600] Nogacka AM, et al. Early microbiota, antibiotics and health. *Cell Mol Life Sci*. **2018**;75:83-91.

[601] Reinhardt C, Reigstad CS, Bäckhed F. Intestinal microbiota during infancy and its implications for obesity. *J Pediatr Gastroenterol Nutr*. **2009**;48:249-256.

antibiotic exposure before 6 months is linked to increased body mass later in infancy[602,603]. This association is believed to be related to GM modifications[604]. Mouse models have provided clear evidence for a role of the GM for growth regulation, metabolism and fat storage[605,606]. Furthermore, GM dysbiosis has been linked to cardiovascular morbidity in children with chronic kidney disease[607]. Finally, antibiotic pressure increases drug-resistance genes in GM microorganisms ("resistome"), with potential horizontal transfer[608]. In conclusion, this study has demonstrated that even a short exposure to CAP can distinctly alter the GM composition in infants with VUR, with increased relative abundance of opportunistic pathogens, as well as decreased proportions of health-promoting taxa. Although antibiotic exposure is not the only predictor of the GM composition[604], the profound impact observed prompts reconsideration of the CAP cost-benefit ratio for infants with VUR. The ongoing randomized controlled PREDICT trial will longitudinally monitor GM profiles of CAP-exposed and unexposed infants in parallel to collecting clinical information. If persistent and/or associated with pathological conditions, such as obesity, allergies or multidrug-resistant infections, the impact of CAP on GM alterations might trigger a re-assessment of the role of CAP in the management of VUR.

---

602 Trasande L, et al. Infant antibiotic exposures and early-life body mass. *Int J Obes*. **2013**;37:16-23.

603 Saari A, et al. Antibiotic exposure in infancy and risk of being overweight in the first 24 months of life. *Pediatrics*. **2015**;135:617-626.

604 Bokulich NA, et al. Antibiotics, birth mode, and diet shape microbiome maturation during early life. *Sci Transl Med*. **2016**;8:343ra82.

605 Cox LM, et al. Altering the intestinal microbiota during a critical developmental window has lasting metabolic consequences. *Cell*. **2014**;158:705-721.

606 Ridaura VK, et al. Gut microbiota from twins discordant for obesity modulate metabolism in mice. *Science*. **2013**;341:1241214.

607 Hsu CN, et al. Blood pressure abnormalities associated with gut microbiota-derived Short Chain Fatty Acids in children with congenital cnomalies of the kidney and urinary tract. *J Clin Med*. **2019**;8:1090.

608 Gibson MK, Crofts TS, Dantas G. Antibiotics and the developing infant gut microbiota and resistome. *Curr Opin Microbiol*. **2015**;27:51-56.

Chapter 4 – THE GUT MICROBIOTA OF CRITICALLY ILL PATIENTS WITH COVID-19

Brief introduction

Severe acute respiratory syndrome coronavirus 2 (SARS-CoV-2)-associated coronavirus disease 2019 (COVID-19) has gripped the world in a pandemic, challenging its culture, economy and healthcare infrastructure[609,610]. Although it is primarily considered an influenza-like respiratory disease with a global mortality rate of 2.4%[611], SARS-CoV-2 RNA has also been detected in the stools of infected patients causing severe gastrointestinal symptoms, such as diarrhea, nausea, vomiting and abdominal pain, in up to 1 in 5 infected patients[612,613,614]. Surveys from Wuhan (China), where the outbreak began, showed that 23% of COVID-19 patients had only gastrointestinal symptoms, 33% of patients had both respiratory and gastrointestinal problems while the remaining 44% were only respiratory ill[615,616]. This is due to the ability of SARS-CoV-2 to enter human cells via the ACE2 (angiotensin-converting enzyme 2) receptor, which is highly expressed also on ileal and

---

[609] Huang C, et al. Clinical features of patients infected with 2019 novel coronavirus in Wuhan, China. *Lancet*. **2020**;395:497-506.

[610] Zhu N, et al. China novel Coronavirus investigating and research team. A novel coronavirus from patients with pneumonia in China, 2019. *N Engl J Med*. **2020**;382:727-733.

[611] WHO. Coronavirus disease (COVID-2019) situation reports. Available online: https://www.who.int/emergencies/diseases/novel-coronavirus-2019/situation-reports.

[612] Cheung KS, al. Gastrointestinal manifestations of SARSCoV-2 infection and virus load in fecal samples from the Hong Kong cohort and systematic review and meta-analysis. *Gastroenterology*. **2020**;159:81-95.

[613] Tariq R, et al. Prevalence and mortality of COVID-19 patients with gastrointestinal symptoms: a systematic review and meta-analysis. Mayo Clin Proc. **2020**;95:1632-1648.

[614] Wan Y, et al. Enteric involvement in hospitalised patients with COVID-19 outside Wuhan. *Lancet Gastroenterol Hepatol*. **2020**;5:534-535.

[615] Han C, et al. Digestive symptoms in COVID-19 patients with mild disease severity. *Am J Gastroenterol*. **2020**;115:916-923.

[616] Scaldaferri F, et al. Impact of COVID-19 pandemic on the daily management of biotechnological therapy in inflammatory bowel disease patients: Reorganisational response in a high-volume Italian inflammatory bowel disease centre. *United European Gastroenterol J*. **2020**;8:775-781.

colonic cells[617], thus leading to enteric manifestations through virus-induced immune-mediated damage[609,610,614,618]. As expected, the loss of intestinal homeostasis resulting from viral infection does not spare the gut microbial community that is universally recognized as a key element for host physiology[619,620]. The first reports in small cohorts of COVID-19 patients from China documented the presence of a dysbiotic state, also affecting the fungal component[621,622,623,624]. This dysbiosis is featured by reduced diversity, depletion of beneficial commensals, mainly SCFA producers from *Lachnospiraceae* and *Ruminococcaceae* families, and enrichment in opportunistic pathogens or pathobionts. Interestingly, these alterations appear overall distinct from other viral infections as H1N1[621], more severe in patients with high SARS-CoV-2 infectivity[624], and partly persist over time, even after viral clearance and symptom resolution[622]. These microbial signatures are likely to contribute to further impaired immune responses, even through the gut-lung axis, with breakdown of mucosal barriers and translocation of microbial components or microbes themselves, thus potentially fueling systemic hyperinflammation (*i.e.*, "cytokine storm"), as found in patients at risk of fatal outcome[625]. In this regard, it is worth mentioning that Zhou et al.[626] reported

---

617 Lamers MM, et al. SARS-CoV-2 productively infects human gut enterocytes. *Science*. **2020**;369:50-54.

618 Guan WJ, Ni ZY, Hu YHY, Liang W, Ou C, He J, et al. Clinical characteristics of Coronavirus disease 2019 in China. *N Engl J Med*. **2020**;382:1708-1720.

619 Turroni S, et al. Microbiota-host transgenomic metabolism, bioactive molecules from the inside. *J Med Chem*. **2018**;61:47-61.

620 Gilbert JA, et al. Current understanding of the human microbiome. *Nat Med*. **2018**;24:392-400.

621 Gu S, et al. Alterations of the gut microbiota in patients with COVID-19 or H1N1 influenza. *Clin Infect Dis*. **2020**;4:ciaa709.

622 Zuo T, et al. Alterations in gut microbiota of patients with COVID-19 during time of hospitalization. *Gastroenterology*. **2020**;159:944-955.

623 Zuo T, et al. Alterations in fecal fungal microbiome of patients with COVID-19 during time of hospitalization until discharge. *Gastroenterology*. **2020**;159:1302-1310.

624 Zuo T, et al. Depicting SARS-CoV-2 faecal viral activity in association with gut microbiota composition in patients with COVID-19. *Gut*. **2020**;gutjnl-2020-322294.

625 Ye Q, Wang B, Mao J. The pathogenesis and treatment of the `Cytokine Storm' in COVID-19. *J Infect*. **2020**;80:607-613.

626 Zhou F, et al. Clinical course and risk factors for mortality of adult inpatients with COVID-19 in Wuhan, China: a retrospective cohort study. *Lancet*. **2020**;395:1054-1062

that half of non-surviving COVID-19 patients experienced secondary bacterial and fungal infections. Although these estimates do not appear to be confirmed worldwide[627], secondary invasion by opportunistic pathogens is recognized as critically important during the disease course, thus requiring careful monitoring for improved antimicrobial stewardship[628]. In an attempt to further extend this knowledge, was characterized, by high-throughput 16S rRNA gene-based sequencing, the GM of 69 COVID-19 patients from three different hospitals from the metropolitan area of Bologna, in Emilia Romagna region (Italy), one of the most affected by the pandemic. Fecal samples were collected in the midst of the COVID-19 outbreak, from April to May 2020. GM profiles were compared with publicly available profiles of healthy age- and gender-matched Italians, as well as those of other critically ill non-COVID-19 patients.

[627] Rawson TM, Wilson RC, Holmes A. Understanding the role of bacterial and fungal infection in COVID-19. *Clin Microbiol Infect*. **2021**;27:9-11.

[628] Cox MJ, et al. Co-infections: potentially lethal and unexplored in COVID-19. *Lancet Microbe*. **2020**;1:e11.

Materials and Methods

Study design

The study was approved by the Ethics Committee of the promoting center (Comitato Etico Indipendente di Area Vasta Emilia Centro, n. 283/2020/Oss/AOUBo). Adult patients (≥18 years) diagnosed of SARS-CoV-2 virus infection hospitalized from April 21 to May 9, 2020, in two teaching hospitals (St. Orsola and Bellaria Hospital) and one tertiary non-teaching hospital (Maggiore Hospital) from the metropolitan area of Bologna (Italy) were enrolled. Subjects were excluded if they had not a laboratory confirmed diagnosis of SARS-CoV-2 infection, and/or clinical data were unavailable. Underlying conditions were recorded according to Charlson comorbidity index[629]. As for SARS-CoV-2 infection, we collected: i) date of symptoms onset; ii) date and symptoms at hospitalization; iii) vital signs, laboratory tests and imaging findings at hospitalization; iv) clinical severity at hospitalization classified according to sequential organ failure assessment; and v) all administered antiviral and immunomodulatory treatments. Admission to intensive care unit (ICU), management of respiratory failure, renal replacement therapy and inotropic support, as well as don't resuscitate order established by attending physician were recorded. Occurrence of bacterial superinfection was assessed according to Centers for Disease Control and Prevention (CDC) criteria[630]. A fecal sample was collected at the time of infectious disease consultation.

[629] Charlson ME, et al. A new method of classifying prognostic comorbidity in longitudinal studies: development and validation. *J Chronic Dis*. **1987**;40:373-383.

[630] Horan TC, Andrus M, Dudeck MA. CDC/NHSN surveillance definition of health care-associated infection and criteria for specific types of infections in the acute care setting. *Am J Infect Control*. **2008**;36:309-332.

SARS-CoV-2 diagnosis

Microbiological diagnosis of SARS-CoV-2 infection was performed by detection of SARS-CoV-2 RNA in respiratory samples (oropharyngeal-nasopharyngeal swab, bronchoalveolar lavage or broncoaspirate), as previously described[631]. Briefly, total DNA/RNA was extracted from samples by QiaSymphony (QIAGEN) and detection of SARS-CoV-2 was performed by real-time RT-PCR targeting regions in the N gene following the US CDC protocol.

Microbial DNA extraction, library preparation and sequencing

All fecal samples were processed in a biosafety level 3 laboratory (Centro di riferimento regionale per le emergenze microbiologiche (CRREM), St. Orsola Hospital, Bologna, Italy). Microbial DNA was extracted using the repeated bead-beating plus column method, as previously described[632]. For library preparation, the V3-V4 hypervariable region of the 16S rRNA gene was amplified by using the 341F and 785R primers[633]. The final libraries, indexed and purified, were sequenced on an Illumina MiSeq platform, with a 2 × 250 bp paired-end protocol according to the manufacturer's instructions (Illumina).

Bioinformatics and statistics

Raw sequences were processed using a combined pipeline of PANDASeq[634] and QIIME2[635]. Length and quality-filtered reads were binned into amplicon sequence variants (ASVs) using

[631] Bartoletti M, et al. Development and validation of a prediction model for severe respiratory failure in hospitalized patients with SARS-Cov-2 infection: a multicenter cohort study (PREDI-CO study). *Clin Microbiol Infect*. **2020**;26:1545-1553.

[632] Turroni S, et al. Temporal dynamics of the gut microbiota in people sharing a confined environment, a 520-day ground-based space simulation, MARS500. *Microbiome*. **2017**;5:39.

[633] D'Amico F, et al. Enteral nutrition in pediatric patients undergoing hematopoietic SCT promotes the recovery of gut microbiome homeostasis. *Nutrients*. **2019**;11:2958.

[634] Masella AP, et al. PANDAseq: Paired-end assembler for Illumina sequences. BMC *Bioinformatics*. **2012**;13:31.

[635] Bolyen E, et al. QIIME 2: Reproducible, interactive, scalable, and extensible microbiome data science. *Nat Biotechnol*. **2019**;37:852-857.

DADA2[636]. Taxonomic assignment was performed using VSEARCH[637] against the Greengenes database (May 2013 release). Chimeras were discarded during analysis. Publicly available 16S rRNA gene sequences of 69 healthy subjects matched by age (mean ± SD, 67.6 ± 22.7 years), sex (39 females, 30 males) and geography (across Italy) were downloaded from databases and processed as above (33 subjects: NCBI SRA, Bioproject ID SRP042234[638]; 36 subjects: MG-RAST ID mgp17761[639]). Sequences of patients admitted to ICU after undergoing liver transplantation in October 2019-February 2020, were also used for comparative purposes (unpublished data). Alpha diversity was calculated using the number of observed ASVs and the inverse Simpson index, while beta diversity was estimated by computing UniFrac and Bray-Curtis distances between the genus-level profiles, which were then used as input for Principal Coordinates Analysis (PCoA). All statistical analysis was performed in R. PCoA plots were generated using the "vegan"[640] and "Made4"[641] packages, and data separation was tested by a permutation test with pseudo-F ratio (function "Adonis" in "vegan"). The bacterial genera most contributing to the ordination space were identified using the function "envfit" of "vegan". Linear discriminant analysis (LDA) effect size (LEfSe) algorithm with LDA score threshold of 3 (on a log10 scale) was applied on genus-level tables to identify discriminating taxa[642]. Group differences in alpha diversity and taxon relative abundance were assessed by Wilcoxon test or Kruskal-Wallis test followed by post-hoc comparisons. P values were corrected for multiple comparisons

---

636 Callahan BJ, et al. DADA2: High-resolution sample inference from Illumina amplicon data. *Nat Methods*. **2016**;13:581-583.

637 Rognes T, et al. VSEARCH: A versatile open source tool for metagenomics. *PeerJ*. **2016**;4:e2584.

638 De Filippis F, et al. High-level adherence to a Mediterranean diet beneficially impacts the gut microbiota and associated metabolome. *Gut*. **2016**;65:1812-21.

639 Biagi E, et al. Gut Microbiota and Extreme Longevity. *Curr Biol*. **2016**;26:1480-1485.

640 http://www.cran.r-project.org/package-vegan/

641 Culhane AC, et al. MADE4: An R package for multivariate analysis of gene expression data. *Bioinformatics*. **2005**;21:2789-2790.

642 Segata N, et al. Metagenomic biomarker discovery and explanation. *Genome Biol*. **2011**;12:R60.

using the Benjamini–Hochberg method. A false discovery rate (FDR) ≤0.05 was considered statistically significant. Sequences assigned to *Enterococcus* were aligned to the NCBI 16S rRNA database (September 2019 release) using BLASTn[643]; only hits with ≥80% identity were considered. As for clinical data, categorical variables are presented as absolute numbers and relative frequencies; continuous variables are presented as mean and standard deviation if normally distributed or as median and interquartile range (IQR) if non-normally distributed. The incidence rate of bloodstream infection (BSI) due to *Enterococcus* spp. (*i.e.*, E-BSI) was calculated as the number of E-BSIs divided by the total number of 10,000 person-days at risk in ICU at St. Orsola Hospital in Bologna. The incidence rate was calculated for the first 4 months of 2020 (during the COVID-19 pandemic) and for the last three years over the same period (January-April). These values were compared by Poisson regression.

[643] Altschul SF, et al. Basic local alignment search tool. *J Mol Biol.* **1990**;215:403-410.

Results

Study cohort description

Of the 76 enrolled patients, 5 were excluded due to unavailable clinical data and 2 because of unconfirmed SARS-CoV-2 diagnosis, thus 69 were analyzed. Most of them were hospitalized at Bellaria hospital (N=51), 16 at Sant'Orsola and 2 at Maggiore hospital. The general characteristics of the study population are shown in **Table 1**.

	N=69
Demographics	
Age (years) (median, IQR)	73, 59-85
Male	38 (55.1)
Underlying diseases	
Obesity	11 (15.9)
BMI (median, IQR)	24, 22-27
Hypertension	44 (63.8)
Diabetes mellitus	12 (17.6)
Coronary disease	5 (7.4)
Congestive heart failure	6 (8.8)
Cerebrovascular disease	12 (17.6)
Peripheral vascular disease	4 (5.9)
Chronic kidney disease	11 (15.9)
COPD	15 (22.1)
Immunosuppression	7 (10.1)
Charlson index (median, IQR)	5, 2-7
Time from symptoms onset to hospitalization (days) (median, IQR)	3, 1-7
Symptoms at hospitalization	
Fever ≥38°C	21 (30.4)
Cough	28 (40.6)
Dyspnoea	36 (52.2)
Vital signs at hospitalization	
GCS (median, IQR)	15, 15-15
MAP (median, IQR)	90, 81-100
PR (median, IQR)	87, 75-98
RR (median, IQR)	20, 16-25
SatO2 on ambient air (median, IQR)	96, 95-98
Laboratory tests at hospitalization	
Lymphocytes (10^9/L) (median, IQR)	1.06, 0.68-1.46
CRP (mg/dl) (median, IQR)	6.2, 2.7-13
LDH (IU/L) (median, IQR)	264, 213-379
Imaging study	
Lung consolidation	31 (44.9)
Ground glass	50 (72.5)
COVID-19 severity at hospitalization	

SOFA (median, IQR)	2, 1-3
Therapeutic management of COVID-19	
DRV/r	3 (4.4)
DRV/cobi	5 (7.2)
LMWH	58 (84.1)
Hydroxycloroquine	58 (84.1)
Tocilizumab	25 (36.2)
Steroids	1 (1.5)
Supportive management of COVID-19	
ICU admission	16 (23.2)
Mechanical ventilation	10 (14.5)
Inotropic support	7 (10.3)
Renal replacement therapy	4 (5.8)
ECMO	0
Analysis of the gut microbiota	
Time from hospitalization to fecal sample collection (days) (median, IQR)	14, 6-23
Exposure to antibiotics in the 2 weeks prior fecal sampling	61 (88)
Bacterial infection after fecal sample collection	6 (8.7)
DTR infection after fecal sample collection	2 (2.9)
Outcome	
Severe respiratory failure	23 (33.3)
after collection of fecal sample	5 (7.2)
In-hospital mortality	9 (13)
Length of hospital stay (days) (median, IQR)	25, 13-33

Table 1. **Characteristics of study population.** BMI, body mass index; COPD, chronic obstructive pulmonary disease; CRP, C-reactive protein; DRV/cobi, darunavir/cobicistat; DRV/r, darunavir/ritonavir; DTR, difficult-to-treat resistance; ECMO, extracorporeal membrane oxygenation; GCS, Glasgow Coma Scale; IQR, interquartile range; LDH, lactate dehydrogenase; LMWH, low-molecular-weight heparin; MAP, mean arterial pressure; PR, pulse rate; RR, respiratory rate; SOFA, sequential organ failure assessment. Immunosuppression included neutropenia (neutrophil count <500/mm3), solid organ transplantation, hematopoietic stem cell transplantation, corticosteroid therapy at a dosage higher than or equivalent to prednisone 16 mg/day ≥15 days, uncontrolled HIV infection (<200 CD4/mm3). Unless otherwise specified, number and percentage (in brackets) are reported.

The gut microbiota of COVID-19 patients as compared to healthy subjects

The GM of COVID-19 patients was profiled by 16S rRNA gene-based NGS and compared with that of age- and sex-matched healthy Italians, whose sequences are publicly available[644,645]. A total of 2,792,602 high-quality reads (mean ± SD, 40,472 ± 11,243) were obtained and clustered into 12,889 Amplicon Sequence Variants (ASVs). A significant reduction in alpha diversity was observed in COVID-19 patients compared to healthy controls (p = 0.0008; Wilcoxon test) (**Figure 34A**). The PCoA of inter-individual variation, based on Bray-Curtis dissimilarity between the genus-level profiles, showed a significant separation between the groups (p = 0.001, permutation test with pseudo-F ratio) (**Figure 34B**).

644 De Filippis F, et al. High-level adherence to a Mediterranean diet beneficially impacts the gut microbiota and associated metabolome. *Gut*. **2016**;65:1812-1821.

645 Biagi E, et al. Gut Microbiota and Extreme Longevity. *Curr Biol*. **2016**;26:1480-1485.

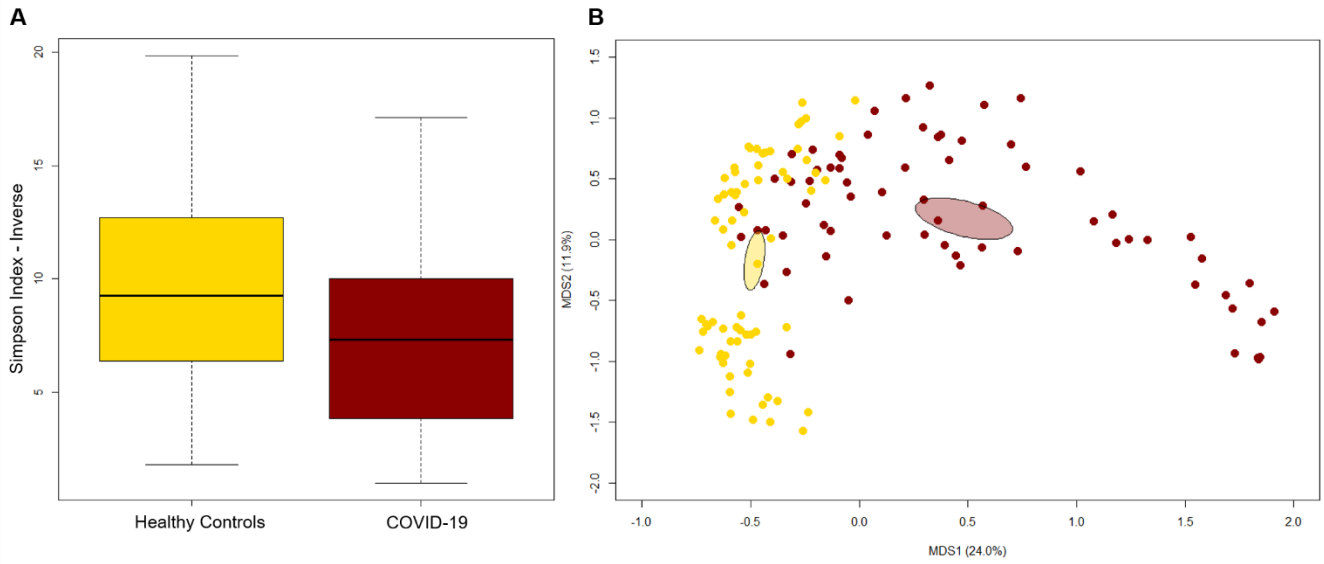

Figure 34. T**he gut microbiota of COVID-19 patients segregates from that of healthy subjects. A**, Alpha diversity estimated according to the inverse Simpson index. A significant reduction was observed in COVID-19 patients (p = 0.0008; Wilcoxon test). **B**, Principal Coordinates Analysis (PCoA) based on Bray-Curtis dissimilarity between the genus-level profiles. A significant separation between groups was found (p = 0.001, permutation test with pseudo-F ratio). Ellipses include 95% confidence area based on the standard error of the weighted average of sample coordinates.

As regards the composition, the GM of COVID-19 patients showed extensive destructuring even at high phylogenetic levels (**Figure 35A**). It was in fact characterized by alterations affecting the two dominant phyla, Firmicutes and Bacteroidetes, as well as subdominant components, mainly Actinobacteria and Synergistetes ($p \leq 0.02$; Wilcoxon test). At the family level, COVID-19 patients showed an enrichment in generally subdominant taxa, such as *Enterococcaceae*, *Coriobacteriaceae*, *Lactobacillaceae*, *Veillonellaceae*, *Porphyromonadaceae* and *Staphylococcaceae* ($p \leq 0.03$). On the other hand, their GM was characterized by a reduction of the dominant families *Bacteroidaceae*, *Lachnospiraceae* and *Ruminococcaceae*, as well as *Prevotellaceae* and *Clostridiaceae* ($p \leq 0.001$) (**Figure 35B**).

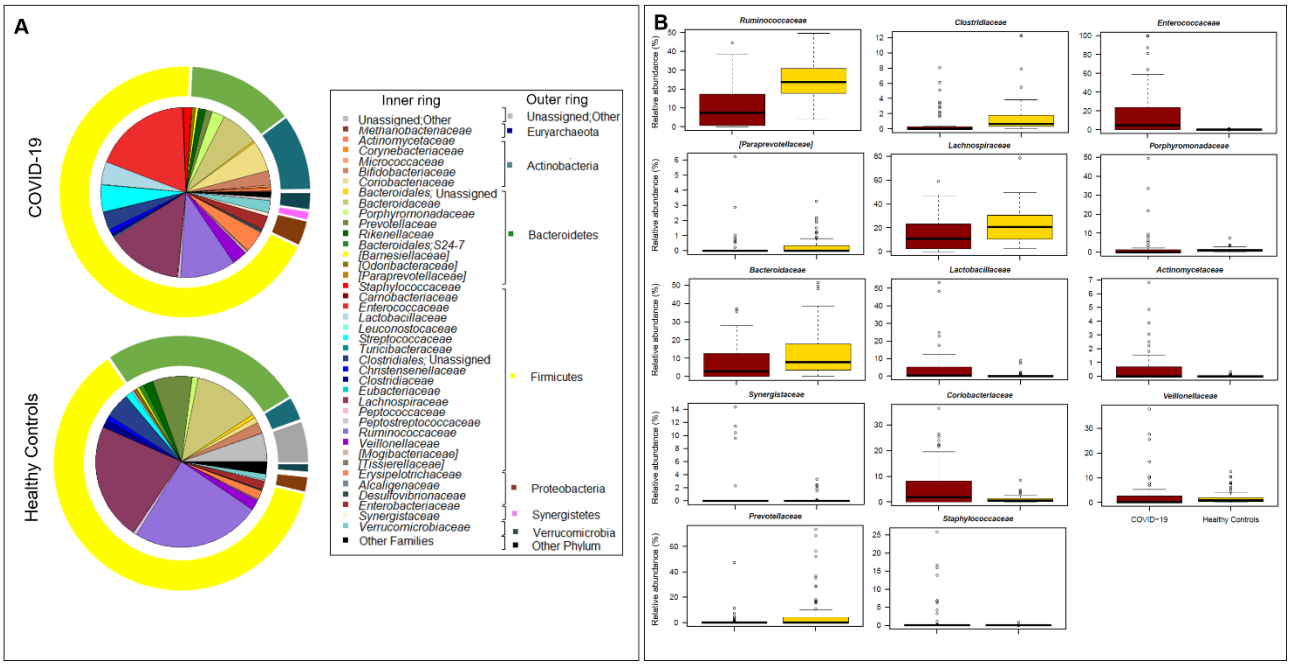

Figure 35. **Phylum and family-level structure of the gut microbiota of COVID-19 patients. A**, Pie charts showing the relative abundance of the major families in the gut microbiota of COVID-19 patients and healthy subjects. Outer rings depict phylum-level distribution. Only taxa with relative abundance >0.1% in at least 2 samples were considered. **B**, Boxplots showing the relative abundance distribution of families differentially represented between groups ($p \leq 0.05$, Wilcoxon test).

In order to identify discriminating genera, a linear discriminant analysis (LDA) effect size (LEfSe) was performed (**Figure 36A**). As expected, genera belonging to *Bacteroidaceae* (*i.e.*, *Prevotella* and *Bacteroides*), *Lachnospiraceae* (*i.e.*, *Coprococcus*, *Blautia*, *Roseburia* and *Lachnospira*) and *Ruminococcaceae* (*i.e.*, *Faecalibacterium*, *Ruminococcus*, *Oscillospira* and *Anaerofilum*) were the main discriminants of the GM of healthy subjects ($p \leq 0.008$). On the other hand, the GM of COVID-19 patients showed a distinctive pattern, with the enrichment of known or potential opportunistic pathogens, such as *Enterococcus*, *Staphylococcus*, *Serratia* and *Collinsella*, as well as *Lactobacillus*, *Parabacteroides*, *Lactococcus*, *Phascolarctobacterium*, *Odoribacter*, *Actinomyces*, *Methanobrevibacter* and

Akkermansia ($p \leq 0.02$) (see **Figure S19**). According to a species-level analysis, the sequences assigned to *Enterococcus*, *i.e.*, the dominant genus in the GM of COVID-19 patients (mean relative abundance in COVID-19 patients vs. healthy controls, 18.5% vs. 0.05%), were mostly attributable to *E. faecium* (8.4%) along with *E. hirae* (5.5%), *E. faecalis* (1.8%) and *E. villorum* (1.1%) (**Figure 36B**).

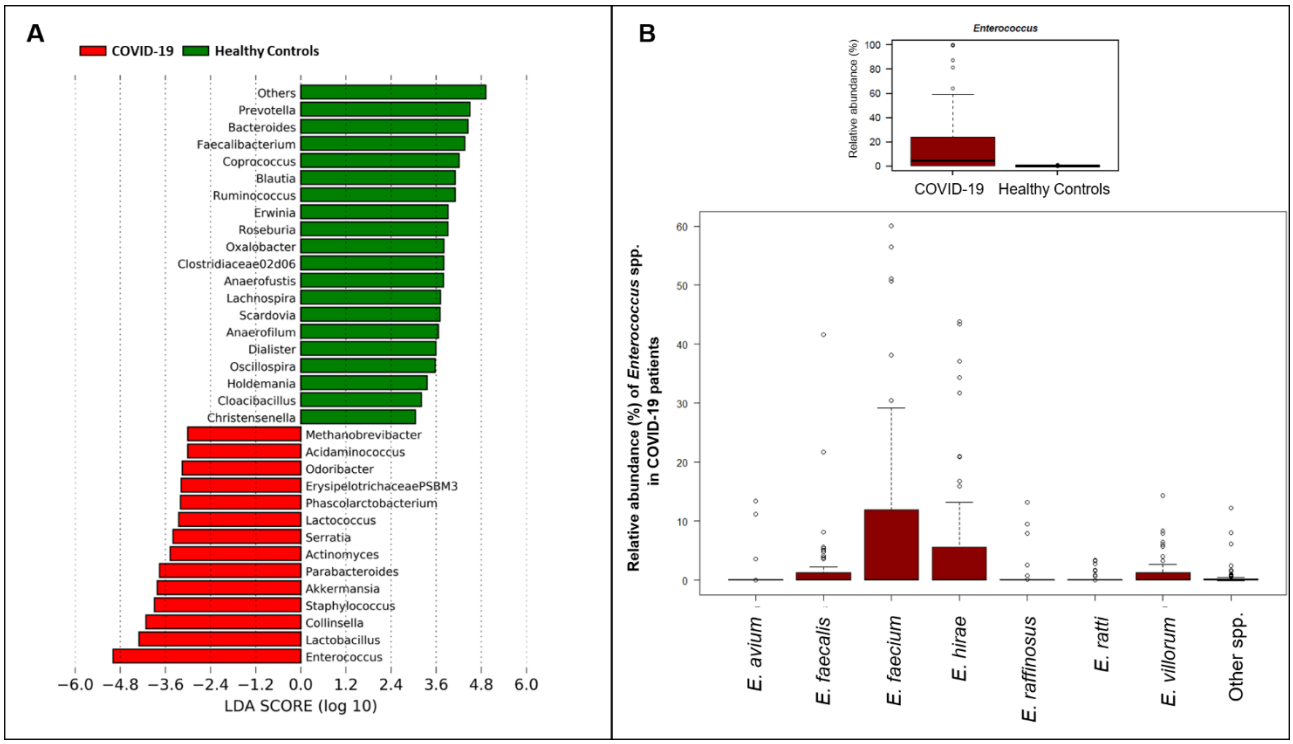

Figure 36. Genus-level gut microbiota signatures of COVID-19. A, Linear discriminant analysis (LDA) effect size (LEfSe) analysis. LDA scores indicate differentially represented genera between groups (the logarithmic threshold for discriminative features was set to 3.0). **B**, Boxplots showing the relative abundance distribution of the genus *Enterococcus* (upper panel) and its species (lower panel).

Gut microbiota dysbiosis of COVID-19 patients according to clinical severity and development of bloodstream infection

PCoA analysis based on weighted UniFrac distances between GM profiles of COVID-19 patients showed no segregation by age, sex, antibiotic intake in the 2 weeks prior to fecal sampling, length of hospital stay, time interval between fecal sampling and hospital admission, and outcome (death/discharge) ($p > 0.05$, permutation test with pseudo-F ratio) (see **Figure S20**). On the other hand, the GM profiles were found to stratify by ICU admission and occurrence of BSI ($p \leq 0.05$) (**Figure 37**). When looking for the bacterial genera driving the clustering patterns, was found that the same taxa were consistently depleted or enriched in relation to the two covariates ($p \leq 0.001$, "envfit" function). Specifically, ICU patients and those developing BSI were characterized by the over-representation (sometimes mono-dominance) of *Enterococcus* compared to the respective counterparts ($p \leq 0.001$). On the other hand, unclassified members of *Ruminococcaceae* and several *Bacteroidetes* genera, including *Bacteroides* and unclassified taxa of *Rikenellaceae* and *S24-7* families, were associated with COVID-19 patients who had not entered ICU and those who had not developed BSI ($p \leq 0.001$) (**Figure 37**). The severe destructuring of ICU and BSI-related GM profile was also evidenced by the further loss of alpha diversity ($p \leq 0.004$) (**Figure 37**). It should be noted that of the 16 COVID-19 patients who had entered ICU, 14 (87.5%) had developed BSI.

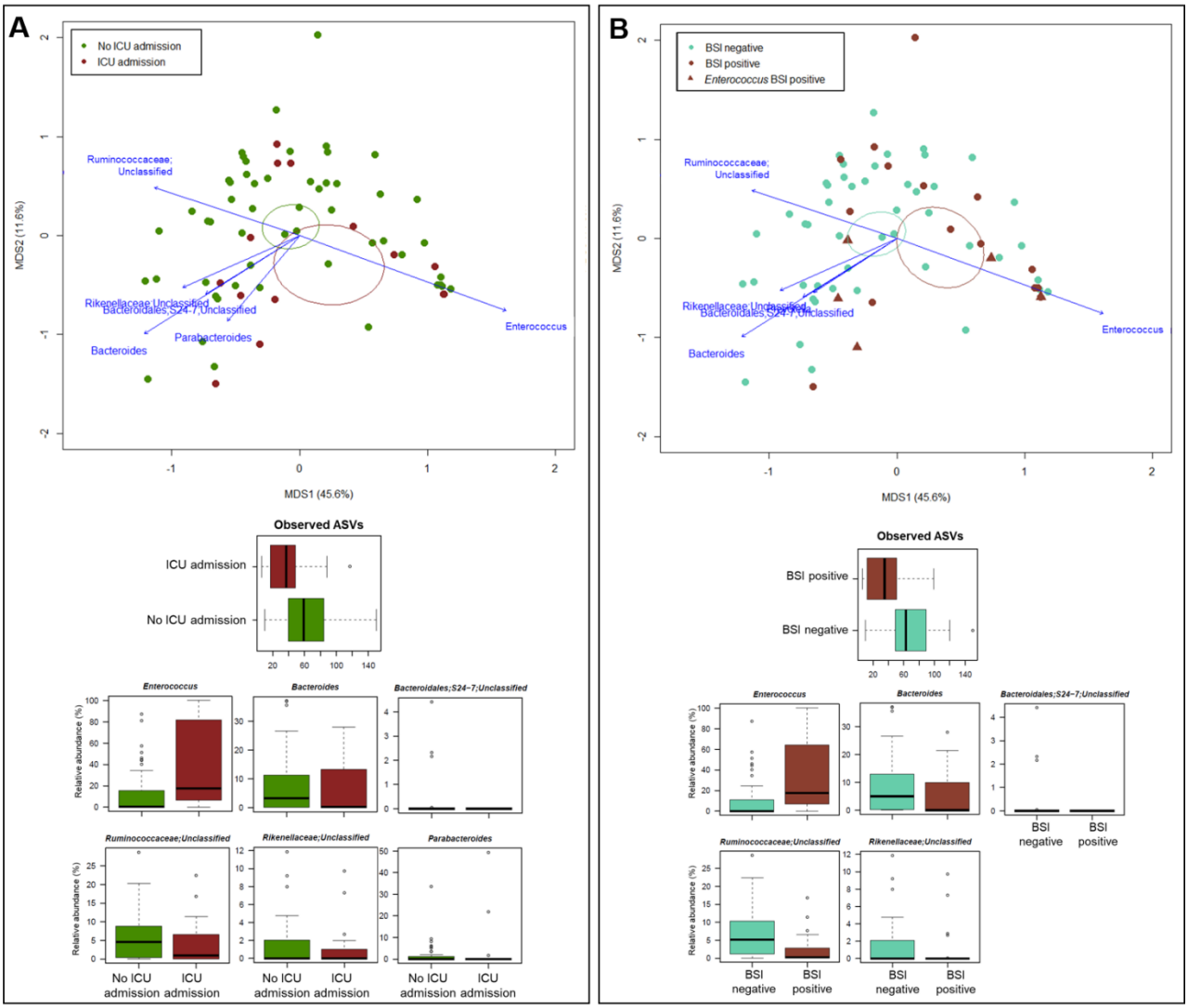

Figure 37. The gut microbiota dysbiosis of COVID-19 patients is exacerbated by ICU admission and development of BSI. Top, Principal Coordinates Analysis (PCoA) based on weighted UniFrac distances between the microbiota profiles of COVID-19 patients, stratified by ICU admission (**A**) and occurrence of BSI (**B**). A significant separation was found for both variables ($p \leq 0.05$, permutation test with pseudo-F ratio). Ellipses include 95% confidence area based on the standard error of the weighted average of sample coordinates. Bacterial genera with the largest contribution to the ordination space are indicated with blue arrows ($p \leq 0.001$, permutational correlation test, "envfit" function). Bottom, Boxplots showing the distribution of alpha diversity, estimated according to the number of observed ASVs, and the relative abundance of genera differentially represented between groups (*i.e.*, COVID-19 patients admitted or not to the ICU, panel A; COVID-19 patients developing BSI or not, panel B) ($p \leq 0.05$, "envfit" function).

The gut microbiota of critically ill COVID-19 vs. non-COVID-19 patients

In an attempt to further explore the GM dysbiosis of COVID-19 patients, the sequences in this study were compared with those of 16 critically ill non-COVID-19 patients who had been admitted to the ICU in October 2019-February 2020 following liver transplantation. Regardless of underlying disease, patients admitted to ICU showed comparable alpha diversity levels, lower than COVID-19 patients who had not entered ICU ($p = 0.0003$, Kruskal-Wallis test) (**Figure 38A**). In contrast, the GM structures of the three patient groups (*i.e.*, COVID-19 patients admitted or not to ICU and other ICU patients) clearly segregated in the Bray-Curtis-based PCoA space ($p = 0.001$, permutation test with pseudo-F ratio). Several genera were found to drive this separation ($p \leq 0.001$, "envfit" function). Notably, *Enterococcus* was far overrepresented in both groups of COVID-19 patients compared to other ICU patients, but closely associated with COVID-19 patients admitted to ICU ($p = 0.0001$, Wilcoxon test). Similarly, *Ruminococcus* was enriched in COVID-19 patients but associated with those who had not entered ICU ($p = 0.0003$), as well as *Oscillospira*, *Dorea* and *Coprococcus* ($p \leq 0.01$). Critically ill non-COVID-19 patients were mainly discriminated by *Enterobacteriaceae* genera, particularly *Klebsiella* ($p \leq 0.03$) (**Figure 38B**).

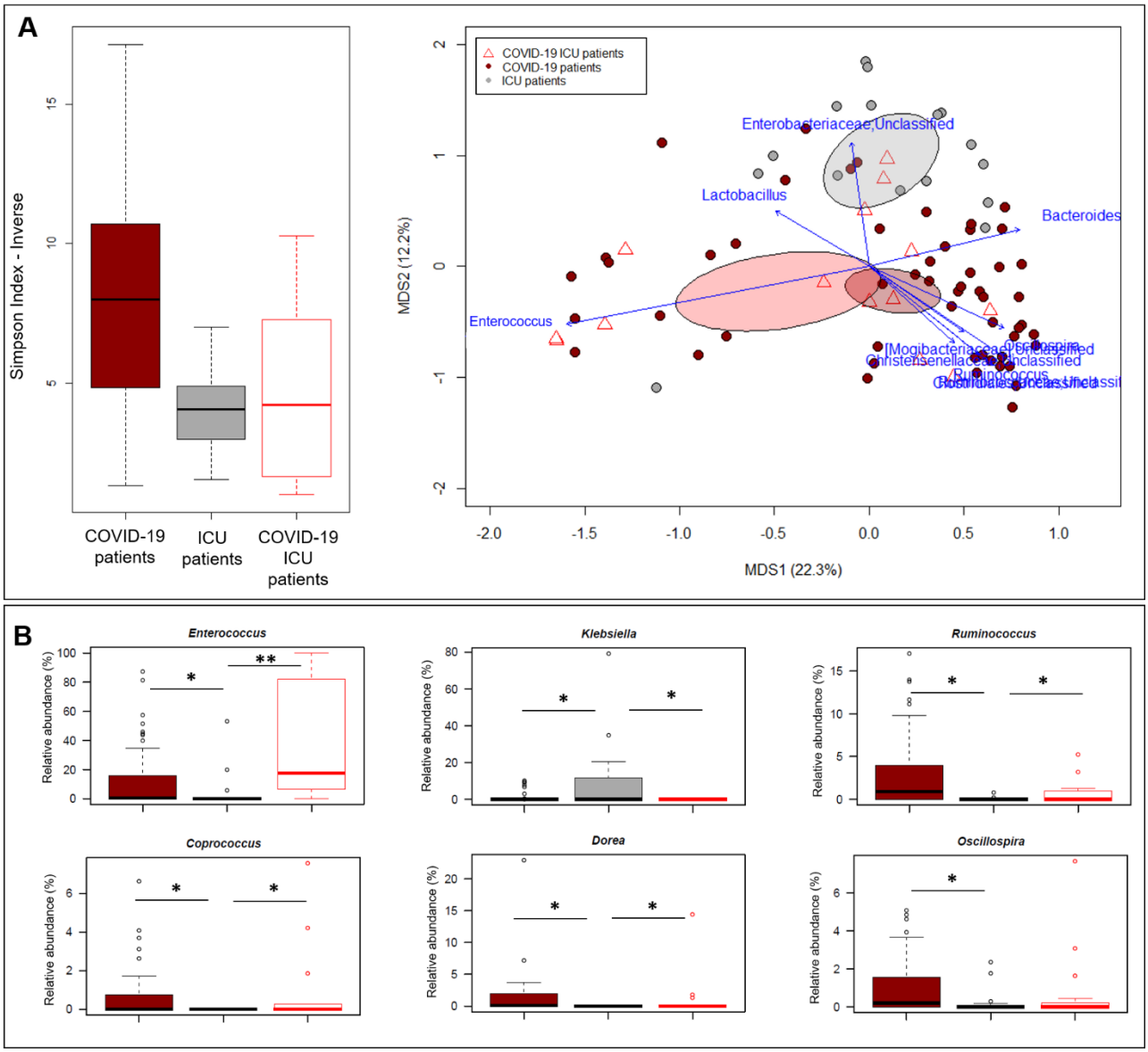

Figure 38. The gut microbiota dysbiosis of COVID-19 patients is distinct from that of critically ill non-COVID-19 patients. A, Left, Alpha diversity estimated according to the inverse Simpson index, for COVID-19 patients admitted or not to ICU and other critically ill patients admitted to the same ICU just before the COVID-19 outbreak. A significant reduction was observed in all patients admitted to ICU regardless of the underlying disease (p = 0.0003, Kruskal-Wallis test). Right, Principal Coordinates Analysis (PCoA) based on Bray-Curtis dissimilarity between the genus-level profiles. A significant separation was found among the study groups (p = 0.001, permutation test with pseudo-F ratio). Ellipses include 95% confidence area based on the standard error of the weighted average of sample coordinates. Bacterial genera with the largest contribution to the ordination space are indicated with blue arrows ($p \leq 0.001$, permutational correlation test, "envfit" function). **B**, Boxplots showing the relative abundance distribution of genera differentially represented between groups ($p \leq 0.05$, Wilcoxon test).

Incidence of bloodstream infection by Enterococcus spp. during the COVID-19 outbreak

In order to evaluate the dynamic change in BSI due to *Enterococcus* spp. (E-BSI) during the COVID-19 pandemic, we compared the E-BSI incidence in critically ill patients over the same period (January-April) since 2017 to 2020 (**Figure 39**). During the first 4 months of 2020, 1,317 patients were admitted to the ICU with a mean length of stay of 5.3 days and a total patient days of 6,924. The incidence rate of ICU-acquired E-BSI reached 27.4 (95% CI, 1.75-4.29) per 10,000 patient-days during the COVID-19 outbreak. In detail, 19 episodes of E-BSI were observed in the first 4 months of 2020 among patients recovered in ICU, mainly due to *E. faecium* (57.9%). A significant increase in the incidence rate of E-BSI was observed between 2017 and 2020 (p = 0.01, Poisson regression). This incidence rate was 14.8 (95% CI, 0.74–2.96) in 2019 and 15.2 (95% CI, 0.79–2.92) in 2018. The relative risk of ICU-acquired E-BSI during the first 4 months of 2020 was 1.84/3.14-fold higher than in previous years.

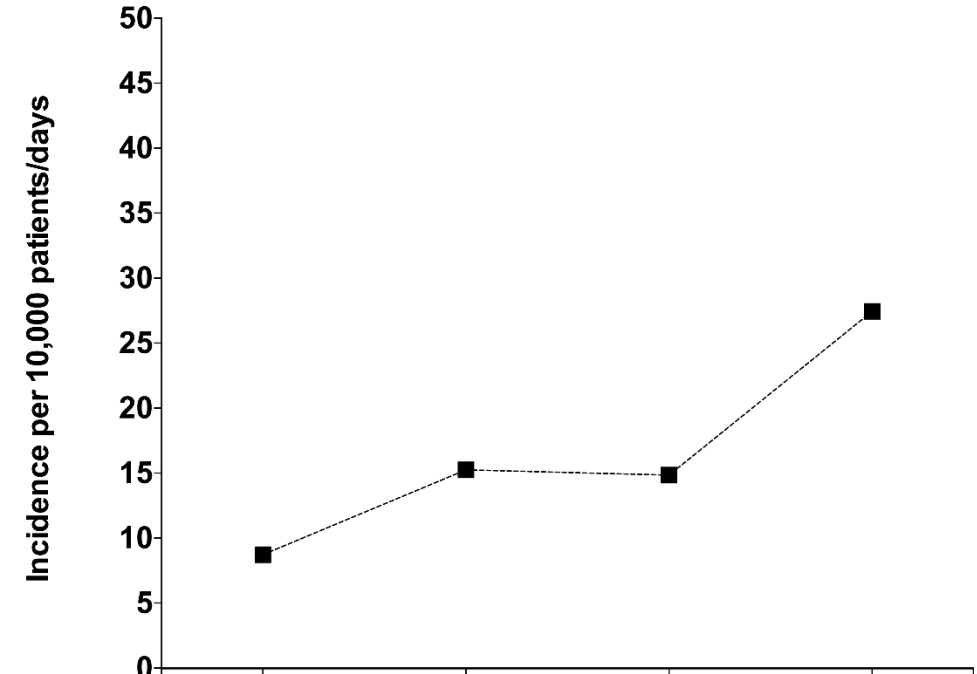

E-BSI	5	9	8	19
E. faecalis	0	2 (22.2%)	3 (37.5%)	8 (42.1%)
E. faecium	5 (100%)	5 (55.5%)	5 (62.5%)	11 (57.9%)
Others *spp.*	0	2 (11.2%)	0	0

Figure 39. Incidence of bloodstream infection due to *Enterococcus* spp. in critically ill patients during the COVID-19 pandemic and in the previous 3 years. Top, Incidence rate of ICU-acquired enterococcal-BSI (E-BSI) per 10,000 patient-days during the COVID-19 pandemic and in the previous 3 years. The incidence rate was evaluated over the same 4-month period (January-April) since 2017 to 2020. Bottom, Number of cases of BSI due to *E. faecium*, *E. faecalis* and others (*Enterococcus* spp.) over the studied periods.

the GM of 69 Italian patients affected by COVID-19 was profiled during the first wave in Italy. Consistent with previous reports on relatively small cohorts of Chinese patients[646,647,648], their GM appears severely dysbiotic, with distinct signatures compared to healthy subjects. In addition to a loss of diversity, COVID-19 patients show profound GM destruction, with drastic reduction in the relative abundance of the dominant families *Bacteroidaceae*, *Lachnospiraceae* and *Ruminococcaceae*, well known to be associated with health and to produce SCFAs, *i.e.*, microbial metabolites with a key, multifaceted role in human metabolic and immunological homeostasis[649]. On the other hand, we found increased proportions of potential pathobionts, mostly belonging to *Enterococcaceae*, *Coriobacteriaceae* and *Staphylococcaceae*. Among these, it is worth noting the presence of *Collinsella* and *Actinomyces*, both recently found enriched in fecal samples from Chinese COVID-19 patients, with the latter supposed to derive from extra-intestinal sites, such as the oral cavity or upper respiratory tract[646,647,648]. Although some of the aforementioned microbial traits are common to other disorders, both intestinal and systemic[650], the remarkable enrichment of *Enterococcus* appears to represent a distinctive GM footprint of our cohort. In some patients, GM was even almost mono-dominated by *Enterococcus* spp., mostly *E. faecium*, *E. hirae*, *E. faecalis* and *E. villorum*. A high abundance of *Enterococcus* in the GM of critically ill patients is likely to be clinically relevant given its pathogenic potential, intrinsic resistance to many

---

[646] Gu S, et al. Alterations of the gut microbiota in patients with COVID-19 or H1N1 influenza. *Clin Infect Dis.* **2020**;4:ciaa709.

[647] Zuo T, et al. Alterations in gut microbiota of patients with COVID-19 during time of hospitalization. *Gastroenterology.* **2020**;159:944-955.

[648] Zuo T, et al. Depicting SARS-CoV-2 faecal viral activity in association with gut microbiota composition in patients with COVID-19. *Gut.* **2020**;gutjnl-2020-322294.

[649] Koh A, et al. From dietary fiber to host physiology: short-chain fatty acids as key bacterial metabolites. *Cell.* **2016**;165:1332-1345.

[650] Duvallet C, et al. Meta-analysis of gut microbiome studies identifies disease-specific and shared responses. *Nat Commun.* **2017**;8:1784.

commonly used antimicrobials, and the ability to rapidly acquire resistance determinants against virtually all antibiotics[651]. Regardless of the source of enterococcal strains, the GM of COVID-19 patients may act as a reservoir of opportunistic, potentially antibiotic-resistant pathogens, with the potential to translocate across compromised epithelial barriers into circulation. The severity of COVID-19-related dysbiosis was found to be strongly associated with clinical severity, namely development of BSI and ICU admission. In particular, the GM of BSI positive and ICU COVID-19 patients was even less diverse, and showed a further increase in *Enterococcus* along with a reduction in *Ruminococcaceae* and *Bacteroidetes* taxa. Interestingly, *Bacteroidetes* members have been shown to negatively correlate with the fecal load of SARS-CoV-2 in COVID-19 patients and suggested to be involved in the regulation of ACE2 expression[652]. In an attempt to further unravel the impact of ICU stay, the GM of COVID-19 patients was compared with that of patients admitted to the ICU just before the COVID-19 outbreak. According to these findings, *Enterococcus* was far overrepresented in the GM of COVID-19 patients, especially those admitted to ICU, while almost absent in critically ill non-COVID-19 patients. Conversely, the latter were discriminated by higher proportions of *Enterobacteriaceae* members, especially *Klebsiella*. Further strengthening the hypothesis that high proportions of enterococci are unrelated to healthcare infrastructure but closely associated with COVID-19, the percentage of patients who developed E-BSI was significantly higher during the COVID-19 pandemic than in the previous 3 years.

Several limitations of this study should be mentioned: small sample size, stool collection at different time intervals, non-standardized bacterial superinfection diagnosis and therapy

[651] Gilmore MS, et al, editors. Enterococci: From Commensals to Leading Causes of Drug Resistant Infection [Internet]. Boston: Massachusetts Eye and Ear Infirmary; **2014**-.

[652] Zuo T, et al. Alterations in gut microbiota of patients with COVID-19 during time of hospitalization. *Gastroenterology*. **2020**;159:944-955.

protocols, and hospitalization in several ICUs (however close to each other). In conclusion, while confirming the existence of severe GM dysbiosis in COVID-19 patients, our work highlights a distinctive overrepresentation of *Enterococcus*, closely related to clinical severity and development of BSI. Future studies in independent and much larger cohorts from varied geographical contexts, possibly longitudinal and with multi-omics approaches, are needed to validate these findings, and deepen GM-host relationships and their contribution to the disease course. As recently discussed[653], GM monitoring in critically ill patients, including COVID-19 ones, could help clinical management, by predicting the onset of medical complications such as sepsis and mortality, thus allowing timely adoption of countermeasures aimed at alleviating the already weakened condition of these subjects.

[653] Agudelo-Ochoa GM, et al. Gut microbiota profiles in critically ill patients, potential biomarkers and risk variables for sepsis. *Gut Microbes*. **2020**;12:1707610.

Chapter 5 – CONCLUDING REMARKS

The present work focused on the role of the gut microbial community in different pathological contexts, from cancer development to chemotherapy treatments in relation to the clinical outcomes of patients.

In order to understand the carcinogenic role of *Salmonella enterica,* a subdominant genotoxic microorganism that can colonize the human gut ecosystem, *in-vitro* 2D and organotypic 3D models carrying a CRC-associated mutation (*i.*e., APC gene) were developed. According to our results, APC deficiency promoted the activation of the DNA damage response, reduced the ability to repair different types of damage, including DNA breaks and oxidative damage, and failed to induce cell cycle arrest. Moreover, this reduction in DNA repair capacity and the inability to activate adequate checkpoint responses were associated with increased genomic instability in APC-deficient cells exposed to the genotoxic *Salmonella* strain. These findings highlight the synergistic effect of the loss of APC gene and infection with genotoxin-producing *Salmonella* in promoting a microenvironment conducive to malignant transformation.

In addition to the role of specific gut microbial colonizers in cancer development and progression, it is now well recognized that a disruption of the gut microbial ecosystem (*i.e.,* dysbiosis) is involved in several life-threatening clinical outcomes in cancer patients. In this context, the gut microbial trajectory during chemotherapy treatments in women affected by epithelial ovarian cancer was profiled in relation to their therapeutic response. Patients with relapse within 6 months of first-line chemotherapy were classified as platinum resistant (PR), while the rest were platinum sensitive (PS). Both PR and PS patients were characterized by

a strong fluctuation in GM diversity but showed distinct compositional profiles over time. PR women were characterized by enrichment in pathobionts, mainly belonging to *Coriobacteriaceae* family (*i.e.*, *Collinsella* and *Eggerthella*), and unexpectedly by a rise of *Bifidobacterium*. On the other hand, the PS gut microbial profile was mainly characterized by the presence of lactate-degrading *Veillonella* and some typically health-associated microorganisms (*i.e., Faecalibacterium* and *Ruminococcus*). In line with recent literature, these results stress the existence of a more favorable GM profile, associated with improved therapeutic responses. However, more in-depth compositional and functional analysis is needed to fully uncover the GM role.

Similarly, the GM trajectory of pediatric patients was analyzed before and up to 120 days after hematopoietic stem cell transplantation (HSCT) (*i.e.,* involving chemotherapy, radiation and antibiotic prophylaxis). According to our results, the maintenance of a "healthy-like" GM profile before and after transplant is of vital importance for the prognosis of these patients. Indeed, a rich and diverse GM was associated with a decreased probability of developing veno-occlusive disease (SOS/VOD), a well-known complication of HSCT. The pre-HSCT protective GM signature included enrichment of Clostridiales, *Ruminococcaceae* and *Bacteroides*, similar to the protective configuration observed in studies regarding another HSCT-associated clinical problem, graft-versus-host disease (GvHD). The positive effect exerted by this peculiar pre-HSCT GM composition in both SOS/VOD and GvHD could be related to the common endothelial damage that characterizes both diseases. The hypothesis advanced is that an altered intestinal ecosystem, depleted of health-associated taxa and with low production of short chain fatty acids, could lead to greater translocation of microbial molecules through the damaged intestinal mucosa, leading to several systemic complications (*i.e.*, SOS/VOD, GvHD and bloodstream infections). In order to maintain a

balanced GM layout, the introduction of enteral feeding (EN) instead of intravenous nutrition (PN) right after the transplant gave promising results. EN-treated patients showed a prompt recovery of a structural and functional eubiotic GM profile post-HSCT, with increased proportions of health-associated microorganisms (*i.e.*, *Faecalibacterium*, *Blautia*, *Bacteroides* and *Oscillospira*) and subsequent production of health-promoting molecules (*i.e.,* SCFAs). The maintenance of GM homeostasis in these patients also promoted the reduction of full-blown infections and was associated with a lower risk of developing GvHD.

With specific regard to GvHD, patients developing this complication were also characterized by post-HSCT expansion of their gut resistome, involving the acquisition of new resistances, as well as the consolidation of those already present before HSCT. Interestingly, the GvHD-associated bloom in resistome diversity was not limited to genes coding for resistance to the antibiotics administered along the therapeutic course, but rather involved a broad pattern of different resistance classes, including multidrug resistance, as well as resistance to macrolides, aminoglycosides, tetracyclines and beta-lactams. The severe impact of antibiotics on the intestinal ecosystem of pediatric patients was confirmed by analyzing the GM profile of infants affected by vesico-ureteral reflux (VUR) and treated with continuous low-dose antibiotic prophylaxis (CAP). In fact, even a short exposure to CAP distinctly altered the GM composition, with increased relative abundance of opportunistic pathogens (*i.e.*, *Enterobacteriaceae* members), as well as decreased proportions of health-promoting taxa (*i.e., Bifidobacterium*). The first months of life are recognized as a critical time window during which GM-host cross-talk lays the foundations for future health. The loss of a health GM-host relationship could lead to development of pathological conditions, such as obesity, allergies or multidrug-resistant infections. Although antibiotic exposure is not the only predictor of GM

composition, the profound impact observed prompts reconsideration of the CAP cost-benefit ratio for VUR-affected infants.

Finally, the GM profile was evaluated in another cohort of critically ill patients undergoing multiple chemotherapy treatments, *i.e.*, hospitalized subjects affected by COVID-19. The GM structure of these patients appeared severely dysbiotic, with reduced diversity, loss of health-associated microorganisms and enrichment of potential pathogens, particularly *Enterococcus,* commonly associated with BSI development. Interestingly, the percentage of patients with BSI due to *Enterococcus* spp. was significantly higher during the COVID-19 pandemic than in the previous 3 years. These results confirmed the common thread that ties chemotherapeutic treatments, including antibiotic exposure: the profound impact on GM homeostasis, potentially leading to severe side effects.

Taken together, these data stress the relevance of mapping the gut microbial composition as well as the gut resistome, in order to aid clinical management of patients. Indeed, chemotherapeutic treatments can affect the GM balance by decreasing health-associated microorganisms while increasing antibiotic-resistant pathobionts, thus creating a dysbiotic loop that can be particularly harmful in subjects requiring clinical care (e.g., HSCT-receiving patients, VUR-affected infants, COVID-19 patients).

In conclusion, the gut microbial homeostasis is a focal element involved in different aspects of host health. Only with a deeper study of the total GM landscape, we could fully understand its role in disease and then develop new precision therapeutic approaches in order to manipulate the GM layout towards the best.

Chapter 6 – ACKNOWLEDGMENTS

Firstly, I would like to thank my PhD supervisor Prof. Patrizia Brigidi, who believed in me from the first day of my bachelor internship and for giving me the opportunity to learn so much.

A special thanks goes to Silvia, my mentor and, in time of need, also a good friend. She helped me in several moment of this period with scientifically-related (and non) obstacles that I had to face during these years.

Again, thanks for all the support, help and laughs to all my lab group members – Marco, Simo, Elena, Matte, Monica, Giorgia, Marghe, Daniel and Teresa. This journey would not have been the same without you.

To my "Swedish research family" – Teresa, Javier, Anna and Maria – a special thanks for welcoming me every time.

To all the students that I advised for the thesis preparation during these years, because I tried to teach them at my best but I was also learning a lot from them, thank you!

To my family - mum, dad and Franci - that always supported me in this choice and over this period, thank you from the bottom of my heart.

To Giacomo, thank you is never enough.

Chapter 7 – LIST OF PUBBLICATIONS FROM THE AUTHOR

1. **D'Amico F.*,** Perrone A.M.*, Rampelli S., Coluccelli S., Barone M., Fabbrini M., Brigidi P., De Iaco P. and Turroni S. Gut microbiota dynamics during chemotherapy in epithelial ovarian cancer are closely related to therapeutic outcome. *Submitted to Journal of Clinical Investigation*.

2. Turroni S., Petracci E., Edefonti V., Giudetti A.M., **D'Amico F.,** Paganelli L., Giovannetti G., Del Coco L., Fanizzi F.P., Rampelli S., Guerra D., Rengucci C., Bulgarelli J., Tazzari M., Ferraroni M., Nanni O. and Serra P. Effects of a diet based on foods from symbiotic agriculture on the gut microbiota of subjects at risk for metabolic syndrome. *Submitted to Nutrients.*

3. Morello W.*, **D'Amico F.*,** Serafinelli J., Turroni S., Abati I., Fiori J., Baskin E., Yalcinkaya F., Jankauskiene A., Pennesi M., Zurowska A., Becherucci F., Drozdz D., Mekahli D., Krzemien G., La Scola C., Taranta-Janusz K., Mehls O., Schaefer F., Candela M. and Montini G. Low-dose antibiotic prophylaxis alters the gut microbiota of infants with vesicoureteral reflux. *Submitted to Frontiers in Pediatrics*.

4. Gaibani P.*, **D'Amico F.*,** Bartoletti M., Lombardo D., Rampelli S., Fornaro G., Coladonato S., Siniscalchi A., Re MC., Viale P., Brigidi P., Turroni S. and Giannella M. The gut microbiota of critically ill patients with COVID-19. *Submitted to Frontiers in Cellular and Infection Microbiology*.

5. Masetti R., Biagi E., Zama D., Muratore E., **D'Amico F.,** Leardini D., Turroni S., Prete A., Brigidi P. and Pession A. Early modifications of the gut microbiota in children with SOS/VOD after hematopoietic stem cell transplantation. *Submitted to Scientific Reports*.

6. Bazzocchi G., Turroni S., Bulzamini M.C., **D'Amico F.**, Bava A., Castiglioni M., Cagnetta V., Losavio E., Cazzaniga M., Terenghi L., De Palma L., Frasca G., Aiachini B., Cremascoli S., Massone A., Oggerino C., Onesta M.P., Rapisarda L., Pagliacci M.C., Biscotto S., Scarazzato M., Giovannini T., Balloni M., Candela M., Brigidi P. and Kiekens C. Gut microbiota in patients during the acute phase after spinal cord injury: A multicenter studi in Italian spinal units. *Submitted to Scientific Reports*.

7. Pelusio N.F., Scicchitano D., Parma L., Dondi F., Brini E., **D'Amico F.,** Candela M., Yúfera M., Gilannejad N., Moyano F.J., Gatta P.P. and Bonaldo A. Interaction between dietary lipid level and seasonal temperature changes in gilthead sea bream *Sparus aurata*: effects on growth, fat deposition, plasma biochemistry, digestive enzyme activity and gut bacterial community. *Submitted to Frontiers in Marine Science*.

8. Palladino G., Biagi E., Rampelli S., Musella M., **D'Amico F.,** Turroni S., Brigidi P., Luna G.M. and Candela M. Seasonal changes in microbial communities associated with the jewel anemone *Corynactis viridis*. *Front Mar Sci*. **2021**;8:627585. doi:10.3389/fmars.2021.627585.

9. Ravegnini G., Fosso B., Di Saverio V., Sammarini G., Zanotti F., Rossi G., Ricci M., **D'Amico F.,** Valori G., Ioli A., Turroni S., Brigidi P., Hrelia P. and Angelini S. Gastric Adenocarcinomas and signet-ring cell carcinoma: Unraveling gastric cancer complexity through microbiome analysis-deepening heterogeneity for a personalized therapy. *Int J Mol Sci*. **2020**;21:9735. doi:10.3390/ijms21249735.

10. Busti S., Rossi B., Volpe E., Ciulli S., Piva A., **D'Amico F.,** Soverini M., Candela M., Gatta P.P., Bonaldo A., Grilli E. and Parma L. Effects of dietary organic acids and nature identical compounds on growth, immune parameters and gut microbiota of European sea bass. *Sci rep*. **2020**;10:21321. doi:10.1038/s41598-020-78441-9.

11. Pelusio N.F., Rossi B., Parma L., Volpe E., Ciulli S., Piva A., **D'Amico F.,** Scicchitano D., Candela M., Gatta P.P., Bonaldo A. and Grilli E. Effects of increasing dietary level of organic acids and nature-identical compounds on growth, intestinal cytokine gene expression and gut microbiota of rainbow trout (*Oncorhynchus mykiss*) reared at normal and high temperature. *Fish Shellfish Immunol.* **2020**;107:324-335. doi:10.1016/j.fsi.2020.10.021.

12. Rampelli S., Soverini M., **D'Amico F.,** Barone M.,Tavella T., Monti D., Capri M., Astolfi A., Brigidi P., Biagi E., Franceschi C., Turroni S., and Candela M. Shotgun metagenomics of gut microbiota in humans with up to extreme longevity and the increasing role of xenobiotic degradation. *mSystems*. **2020**;5:e00124-20. doi:10.1128/mSystems.00124-20.

13. Mondo E., Barone M., Soverini M., **D'Amico F.,** Cocchi M., Petrulli C., Mattioli M., Marliani G., Candela M. and Accorsi P.A. Gut microbiome structure and adrenocortical activity in dogs with aggressive and phobic behavioral disorders. *Heliyon*. **2020**;6:e03311. doi:10.1016/j.heliyon.2020.e03311.

14. Parma L., Pelusio N.F., Gisbert E., Estebanc M.A., **D'Amico F.,** Soverini M., Candela M., Dondi F., Bonaldo A. Effects of rearing density on growth, digestive conditions, welfare indicators and gut bacterial community of gilthead sea bream (*Sparus aurata*, L. 1758) fed different fishmeal and fish oil dietary levels. *Aquaculture*. **2020**;518:734854. doi:10.1016/j.aquaculture.2019.734854.

15. **D'Amico F.,** Biagi E., Rampelli S., Fiori J., Zama D., Soverini S., Barone M., Leardini D., Muratore E., Prete A., Gotti R., Pession A., Masetti R., Brigidi P., Turroni S. and Candela M. Enteral nutrition in pediatric patients undergoing hematopoietic SCT

promotes the recovery of gut microbiome homeostasis. *Nutrients*. **2019**;11:2958. doi:10.3390/nu11122958.

16. Martin O.C.B., Bergonzini A., **D'Amico F.,** Chen P., Shay J.W., Dupuy J., Svensson M., Masucci M., and Frisan T. Infection with genotoxin-producing Salmonella enterica synergises with loss of the tumour suppressor APC in promoting genomic instability via the PI3K pathway in colonic epithelial cells. *Cell microbiol*. **2019**;21:e13099. doi:10.1111/cmi.13099.

17. Parma L., Yúfera M., Navarro-Guillén C., Moyano F.J., Soverini M., **D'Amico F.,** Candela M., Fontanillas R., Gatta P.P. and Bonaldo A. Effects of calcium carbonate inclusion in low fishmeal diets on growth, gastrointestinal pH, digestive enzyme activity and gut bacterial community of European sea bass (*Dicentrarchus labrax L.*) juveniles. *Aquaculture*. **2019**;510:283-292. doi:10.1016/j.aquaculture.2019.05.064.

18. **D'Amico F.,** Soverini M., Zama D., Consolandi C., Severgnini M., Prete A., Pession A., Barone M., Turroni S., Biagi E., Brigidi P., Masetti R., Rampelli S. and Candela M. Gut resistome plasticity in pediatric patients undergoing hematopoietic stem cell transplantation. *Sci rep*. **2019**;9,5649. doi:10.1038/s41598-019-42222-w.

19. Barone M., Turroni S., Rampelli S., Soverini M., **D'Amico F.,** Biagi E., Brigidi P., Troiani E. and Candela M. Gut microbiome response to a modern Paleolithic diet in a Western lifestyle context. *PlosOne*. **2019**;14:e0220619. doi:10.1371/journal.pone.0220619.

20. Biagi E.*, **D'Amico F.***, Soverini M., Angelini V., Barone M., Turroni S., Rampelli S., Pari S., Brigidi P. and Candela M. Faecal bacterial communities from Mediterranean loggerhead sea turtles (*Caretta caretta*). *Env microbiol rep*. **2019**;11:361-371. doi:10.1111/1758-2229.12683.

21. Muleviciene A., **D'Amico F.,** Turroni S., Candela M. and Jankauskiene A. Iron deficiency anaemia-related gut microbiota dysbiosis in infants and young children: a pilot study. *Acta Microbiol Immunol Hung.* **2018**;65:551-564. doi:10.1556/030.65.2018.045.

22. **D'Amico F.,** Candela M., Turroni S., Biagi E., Brigidi P., Bega A., Vancini D. and Rampelli S. The rootstock regulates microbiome diversity in root and rhizosphere compartments of *Vitis vinifera* cultivar Lambrusco. *Front microbiol*. **2018**;9:2240. doi:10.3389/fmicb.2018.02240.

*These authors contributed equally to the work.

2.1 Infection with genotoxin-producing *Salmonella enterica* synergizes with loss of the tumor suppressor APC in promoting genomic instability via the PI3K pathway in colonic epithelial cells

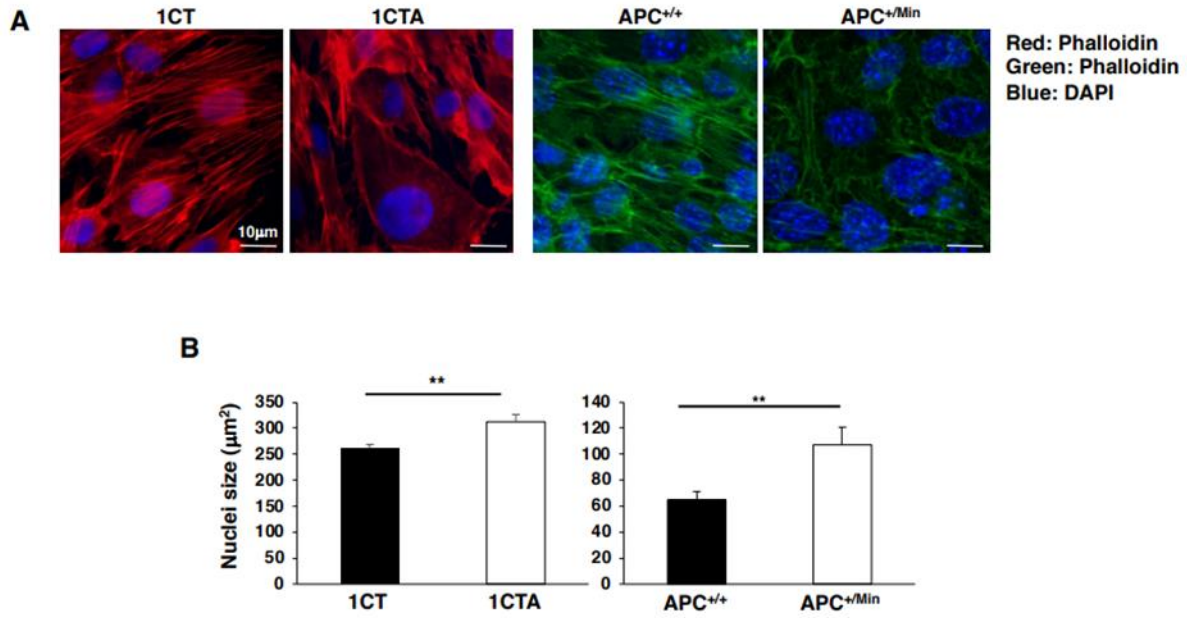

Figure S1. Phenotypic characterization of APC deficient and proficient cells. A. Representative scanning confocal micrographs showing the staining with TRITC (red)- or FITC (green)-conjugated phalloidin to visualize the actin stress fibers. Nuclei were counterstained with DAPI (blue). Magnification 63X. B. B. Nuclear size was assessed using the ImageJ software from micrograph pictures showed in A. Mean ± SEM of three independent experiments. One hundred cells were evaluated for each experiment for each cell line. Statistical analysis was performed using the Student t test, ** $p < 0.01$; *** $p < 0.001$; **** $p < 0.0001$.

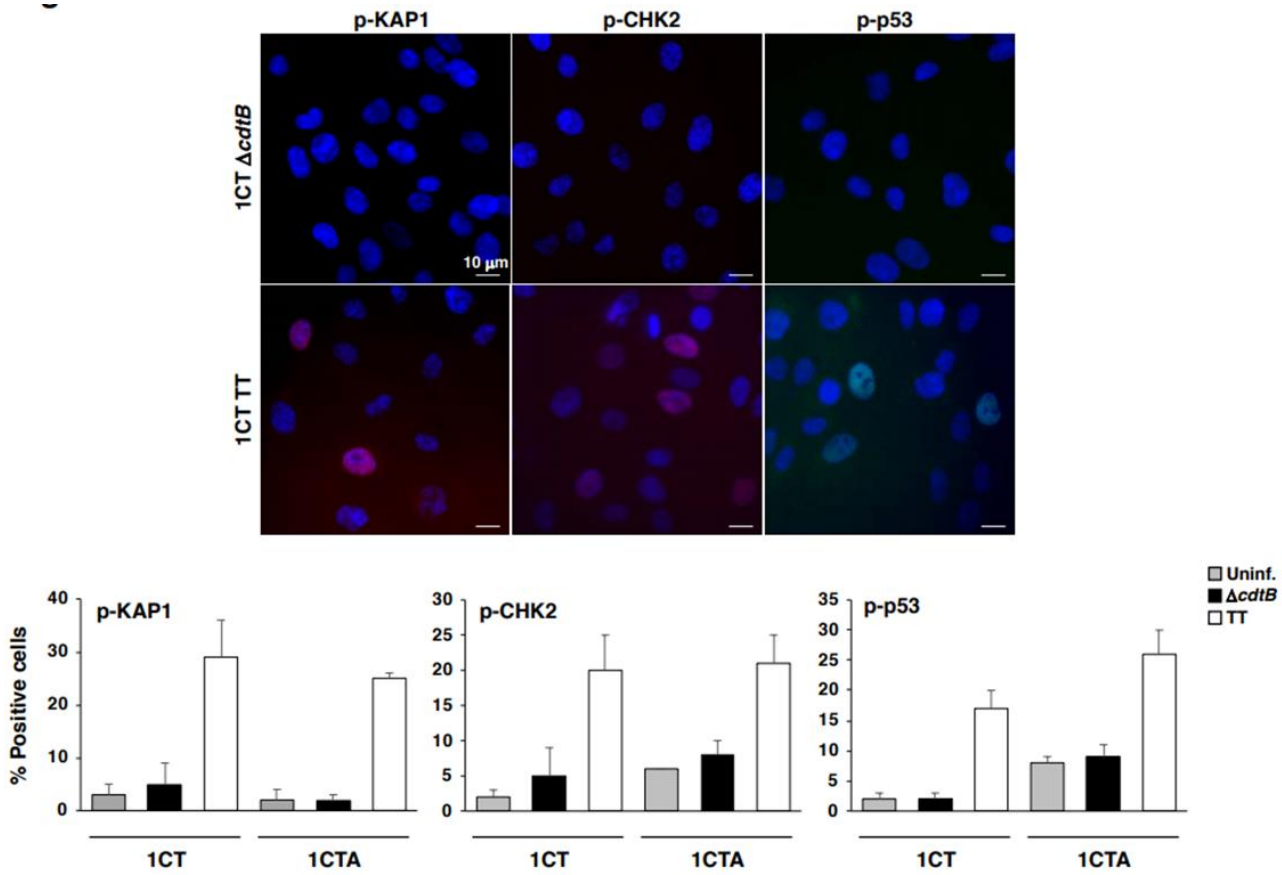

Figure S2. **Infection with the genotoxic *Salmonella* strain induces activation of the DDR.** 1CT and 1CTA cells, grown in 2D culture, were left uninfected (Uninf.) or infected with the MC1ΔcdtB (ΔcdtB) or the MC1TT (TT) strains for 24 h. Activation of the DDR was assessed by immunofluorescence analysis, using antibodies specific for phosphorylated KAP1 (p-KAP1), phosphorylated CHK2 (p-CHK2), Ser15 phosphorylated p53 (p-p53). The upper panel shows representative micrographs of the 1CT cells infected with MC1ΔcdtB or the MC1TT strains, while the lower panel shows the quantification of positive cells. Mean ± SEM of three to five independent experiments. One hundred cells were evaluated for each experiment for each cell line.

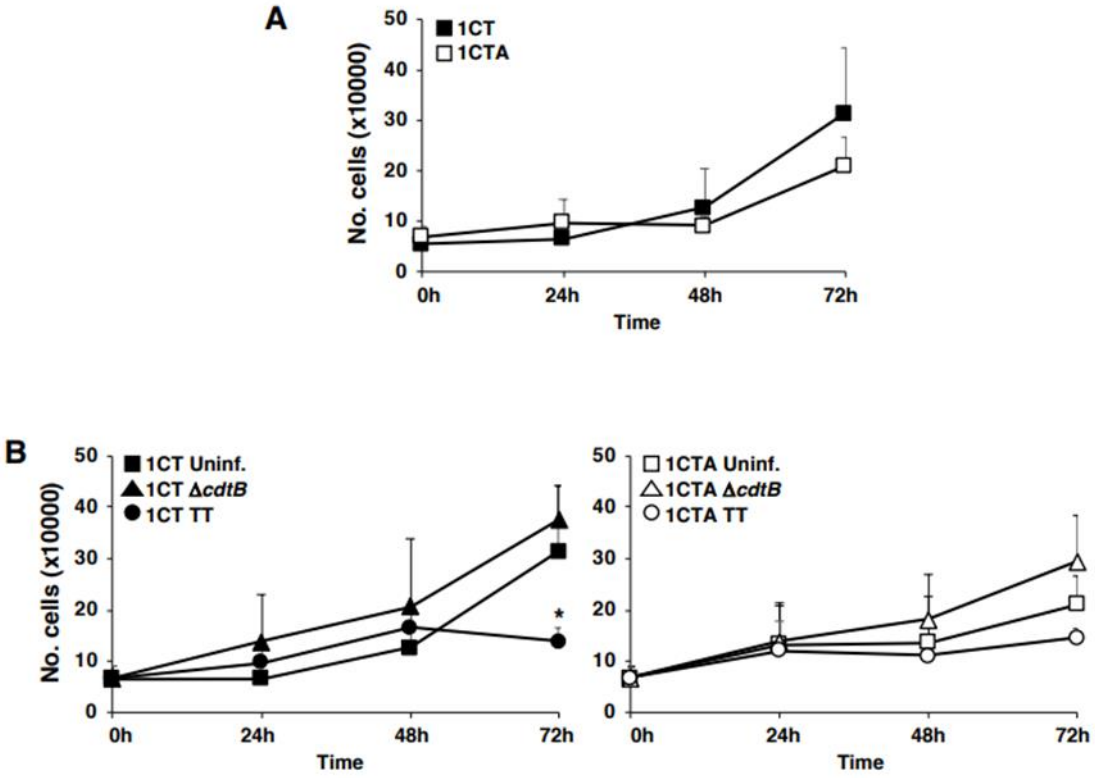

Figure S3. 1CT and 1CTA growth curve. Eighty thousand 1CT and 1CTA cells were plated in 10 cm culture dishes to avoid contact inhibition and left uninfected (Uninf.) or infected with the MC1ΔcdtB (ΔcdtB) or the MC1TT (TT) strains. At the indicated time points cells were counted by trypan blue exclusion. Mean ± SEM of five independent experiments. Statistical analysis was performed using the Student t test, * $p < 0.05$.

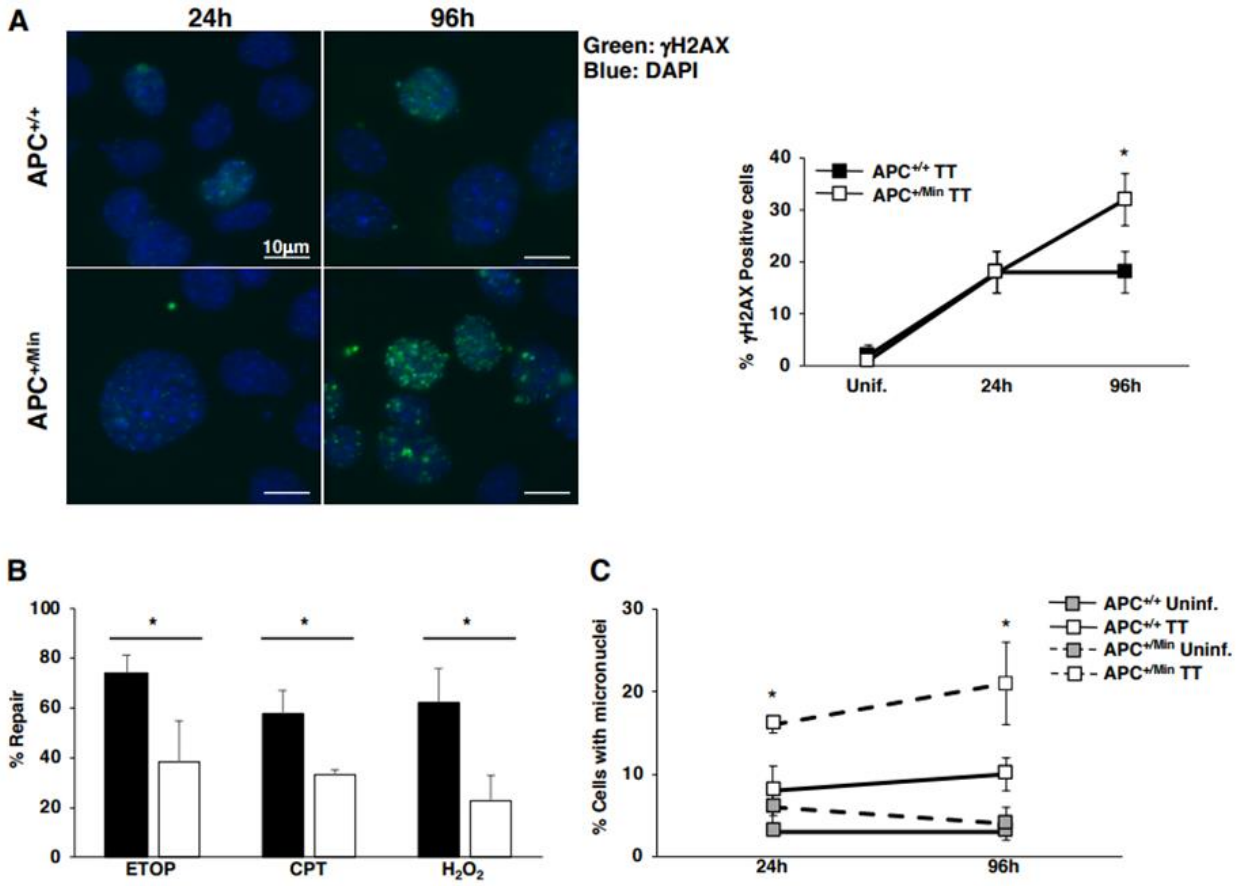

Figure S4. **APC deficiency reduces DNA repair and promotes acquisition of genomic instability in murine cells infected with the genotoxic *Salmonella* strain**. **A.** $APC^{+/+}$ and $APC^{+/Min}$ cells were left uninfected (Uninf.) or infected with the MC1 TT (TT) strain for the indicated period of times. Left panel: representative fluorescence micrographs of infected cells illustrating the induction of DNA damage assessed by γH2AX immunofluorescence (green). Nuclei were counterstained with DAPI (blue). Right panel: quantification of the γH2AX positive infected cells. **B.** $APC^{+/+}$ and $APC^{+/Min}$ cells were treated for 6 h with etoposide (ETOP, 15 µM), camptothecin (CPT, 5 µM) or H_2O_2 (50 µM) and the percentage of repair was assessed as described in Figure 4, using γH2AX as marker for the DDR. C. $APC^{+/+}$ and $APC^{+/Min}$ cells were infected as described in A, and micronuclei were detected by DAPI staining. Mean ± SEM of three to four independent experiments. Statistical analysis was performed using the Student's t test, * $p < 0.05$.

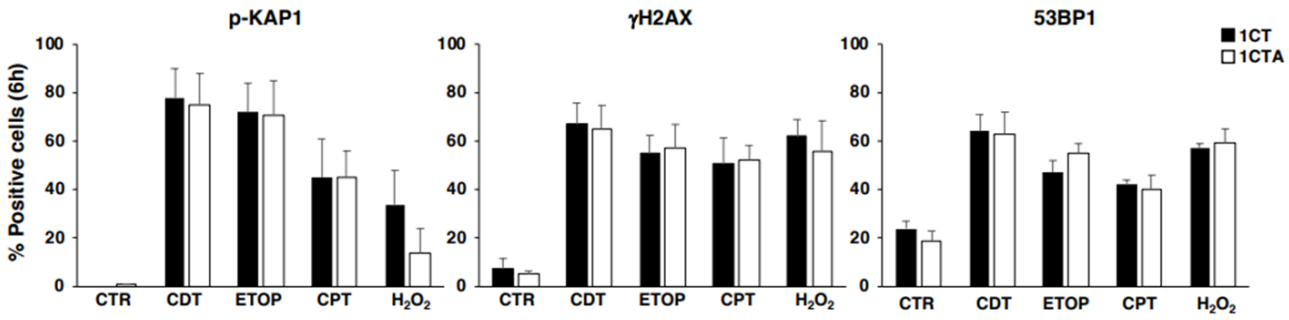

Figure S5. Early activation of the DDR response to a broad spectrum of genotoxic stresses. 1CT and 1CTA cells, grown in 2D culture, were left untreated (CTR) or treated for 6 h with CDT (1 µg/ml), etoposide (ETOP, 15 µM), camptothecin (CPT, 5 µM) or H_2O_2 (50 µM). Activation of the DDR was assessed by immunofluorescence analysis, using antibodies specific for phosphorylated KAP1 (p-KAP1), phosphorylated H2AX (γH2AX) or 53BP1. Mean ± SEM of three to five independent experiments.

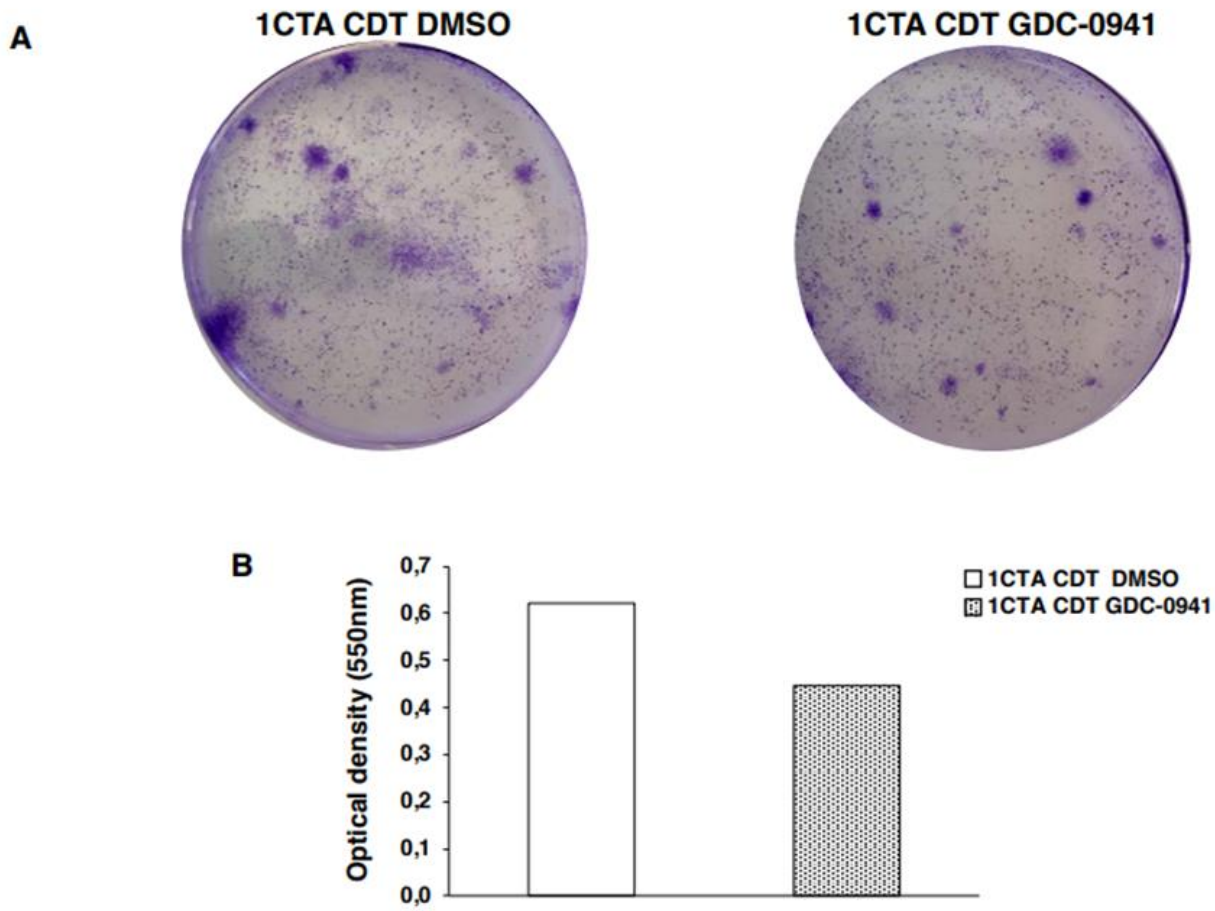

Figure S6. Colony assay. 1CTA cells were pretreated with the PI3K inhibitor CDG-0941 (1 µM) or DMSO as vehicle control for 1 h prior intoxication with CDT (10 ng/ml) in duplicate. Treatment with the inhibitor was repeated every 24 h after intoxication for a week. Colonies were stained with crystal violet 2 weeks post-intoxication. **A.** Representative picture of the crystal violet staining. **B.** Quantification of the incorporated crystal violet extracted with 2% SDS as described in Experimental procedures. Mean of duplicates.

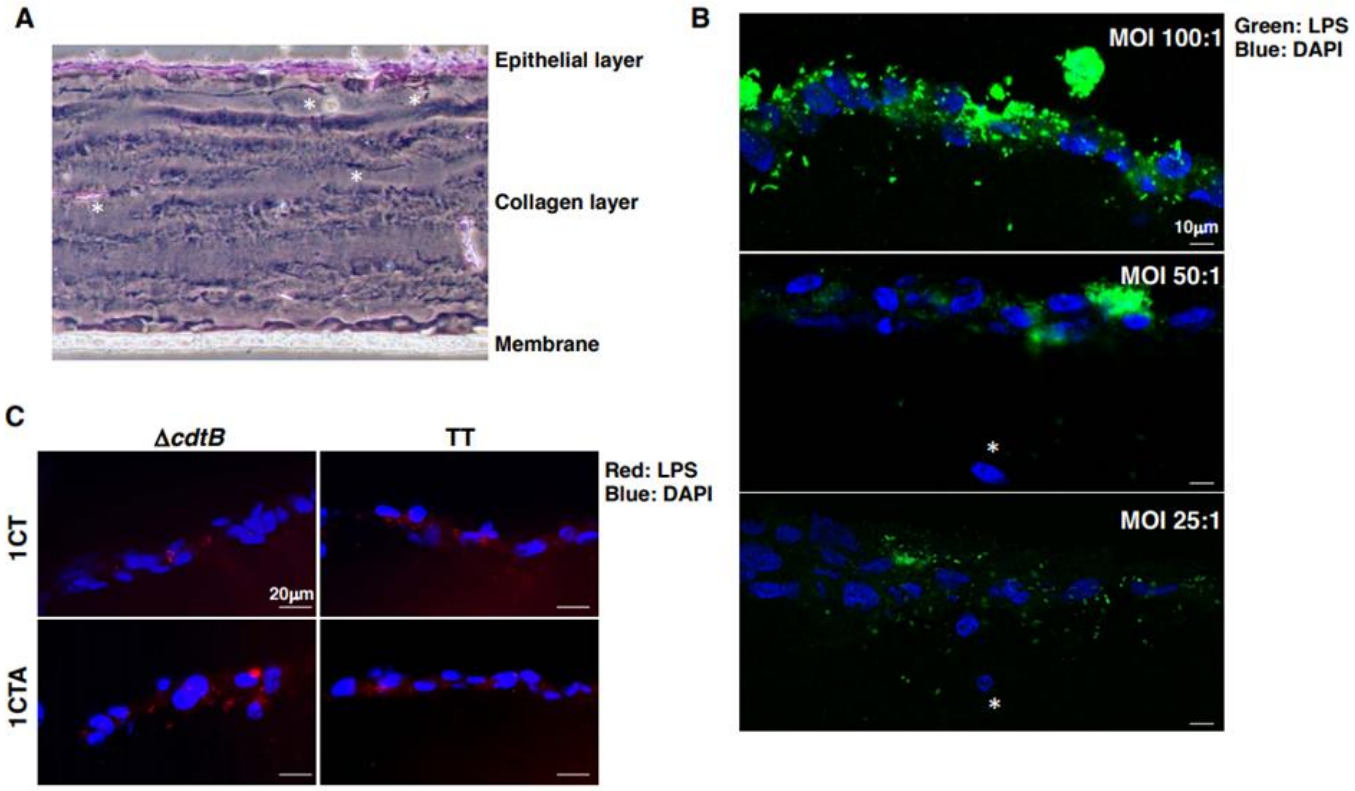

Figure S7. Colonic organotypic 3D model. A. Representative phase contrast micrograph of 1CT cells, grown in 3D culture as described in Material and Methods, stained with hematoxylin and eosin. The white asterisks indicate the presence of colonic fibroblasts embedded in the collagen matrix. **B.** 1CT cells were infected with the MC1 TT strain at the indicated MOI for 24 h. Representative scanning confocal micrographs showing the levels of infection by visualizing the bacteria using a rabbit serum anti-LPS followed by a donkey anti-rabbit secondary antibody conjugated to Alexa-488 (green). Nuclei were counterstained with DAPI (blue). Magnification 40X. **C.** Cells grown in 3D culture were infected with the MC1 ΔcdtB or MC1 TT strains at MOI 25:1. Bacteria were visualized using a rabbit serum anti-LPS followed by a goat anti-rabbit secondary antibody conjugated to Alexa-568 (red). Nuclei were counterstained with DAPI (blue). Representative scanning confocal micrographs at magnification 40X.

2.2 The gut microbiota dynamics during chemotherapy in epithelial ovarian cancer patients are closely related to the therapeutic response

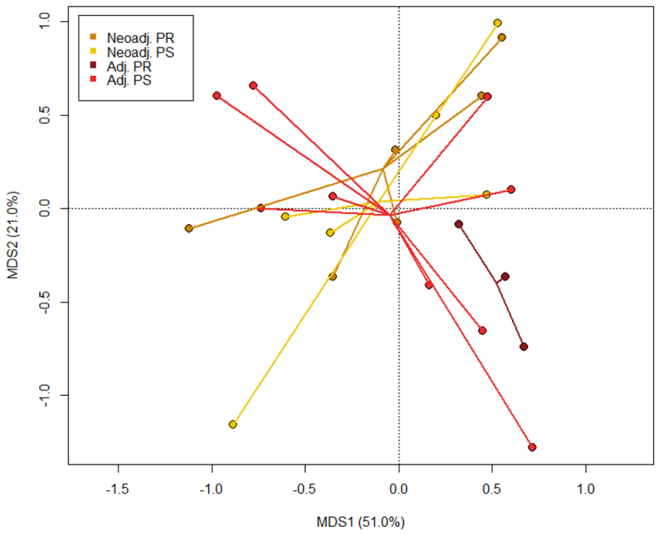

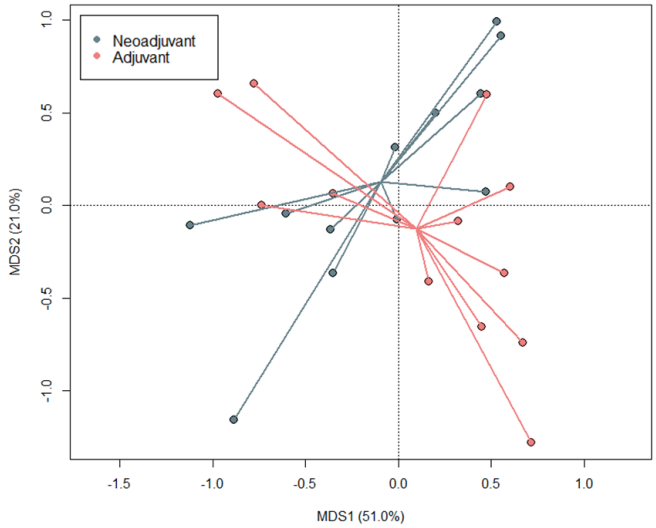

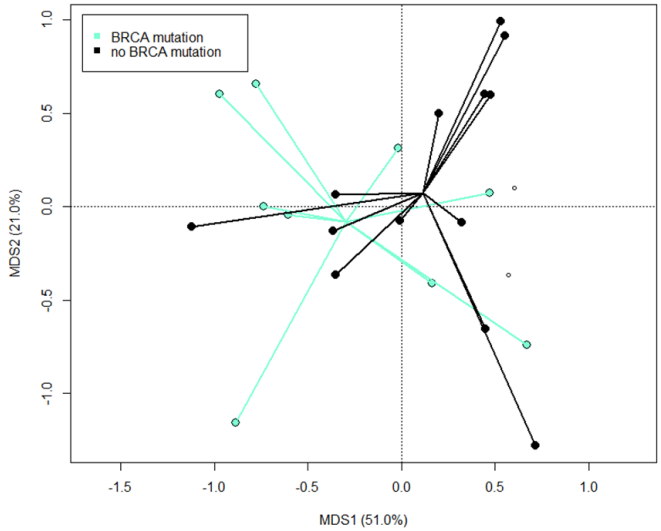

Figure S8. The GM profile of EOC patients at the baseline according to disease severity and BRCA mutation. Principal Coordinates Analysis (PCoA) based on unweighted UniFrac distances between fecal samples of EOC patients at the baseline stratified for therapeutic response (top), type of therapy (middle) and BRCA mutation (bottom). No significant separation was found (p > 0.148, permutation test with pseudo-F ratios). Ellipses include 95% confidence area based on the standard error of the unweighted average of sample coordinates.

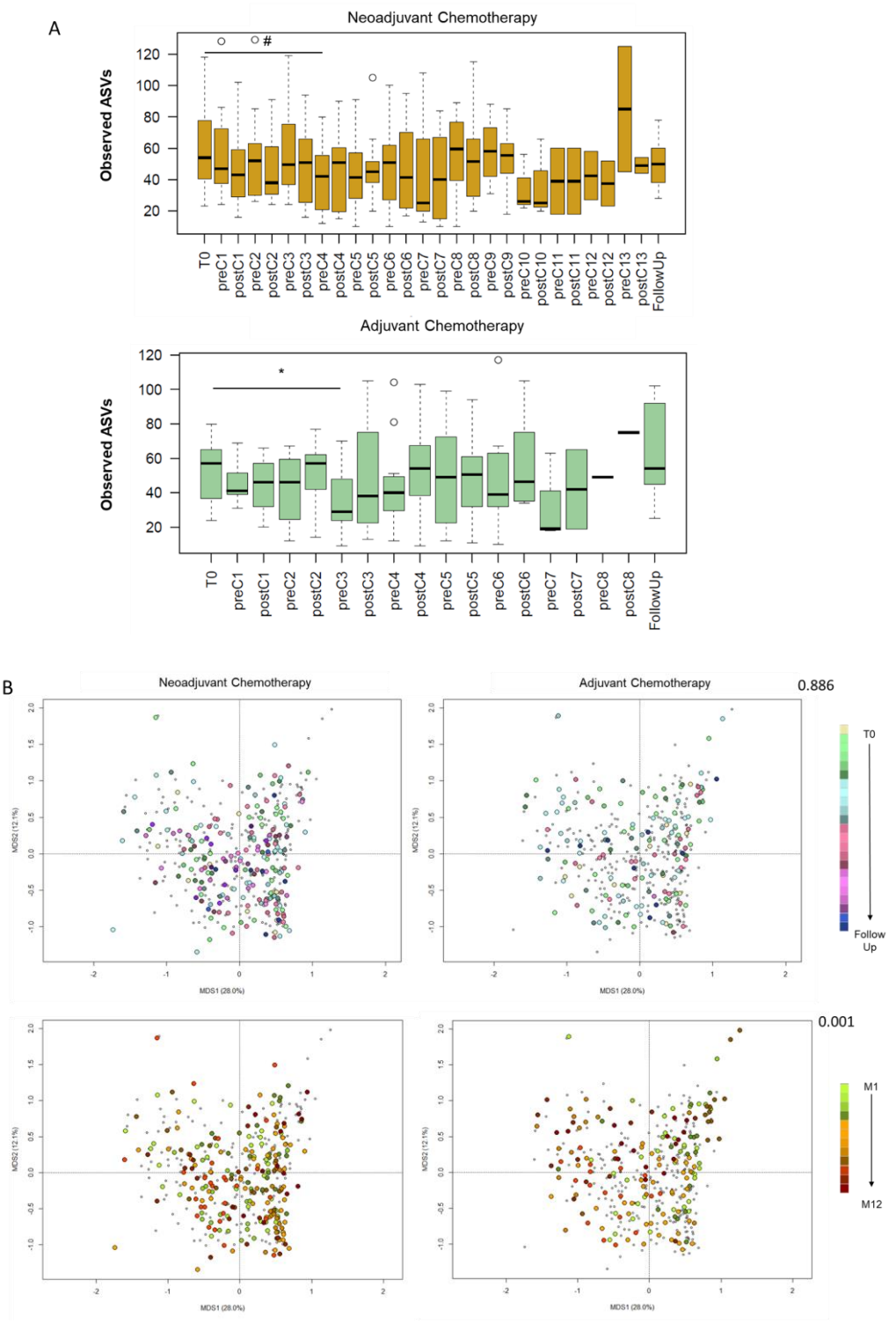
A
Neoadjuvant Chemotherapy
Observed ASVs
#
T0
preC1
postC1
preC2
postC2
preC3
postC3
preC4
postC4
preC5
postC5
preC6
postC6
preC7
postC7
preC8
postC8
preC9
postC9
preC10
postC10
preC11
postC11
preC12
postC12
preC13
postC13
FollowUp
Adjuvant Chemotherapy
Observed ASVs
*
T0
preC1
postC1
preC2
postC2
preC3
postC3
preC4
postC4
preC5
postC5
preC6
postC6
preC7
postC7
preC8
postC8
FollowUp
B
Neoadjuvant Chemotherapy
Adjuvant Chemotherapy
0.886
T0
Follow Up
0.001
M1
M12
MDS1 (28.0%)
MDS2 (12.1%)

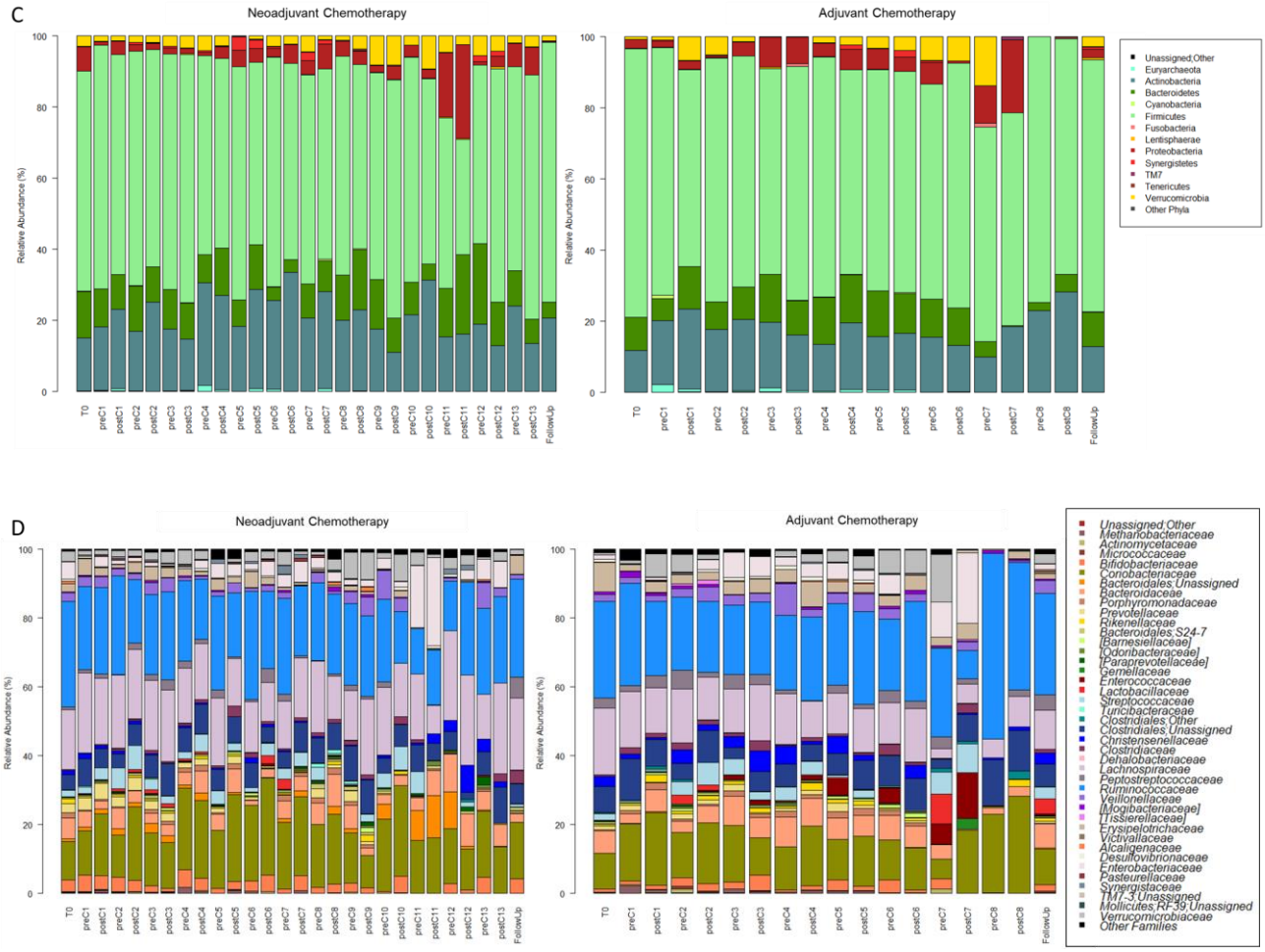

Figure S9. **Gut microbial trajectory of EOC patients following neoadjuvant and adjuvant chemotherapy.** Boxplots showing the distribution of the number of observed ASVs (**A**) and unweighted UniFrac distances (**B, top**) between each time-point of patients during neoadjuvant or adjuvant chemotherapy. In panel **B,bottom**, subject specific diversity is shown by unweighted UniFrac distances. Barplot depicting phyla (**C**) and families (**D**) of patients that followed both neoadjuvant and adjuvant treatments are reported.

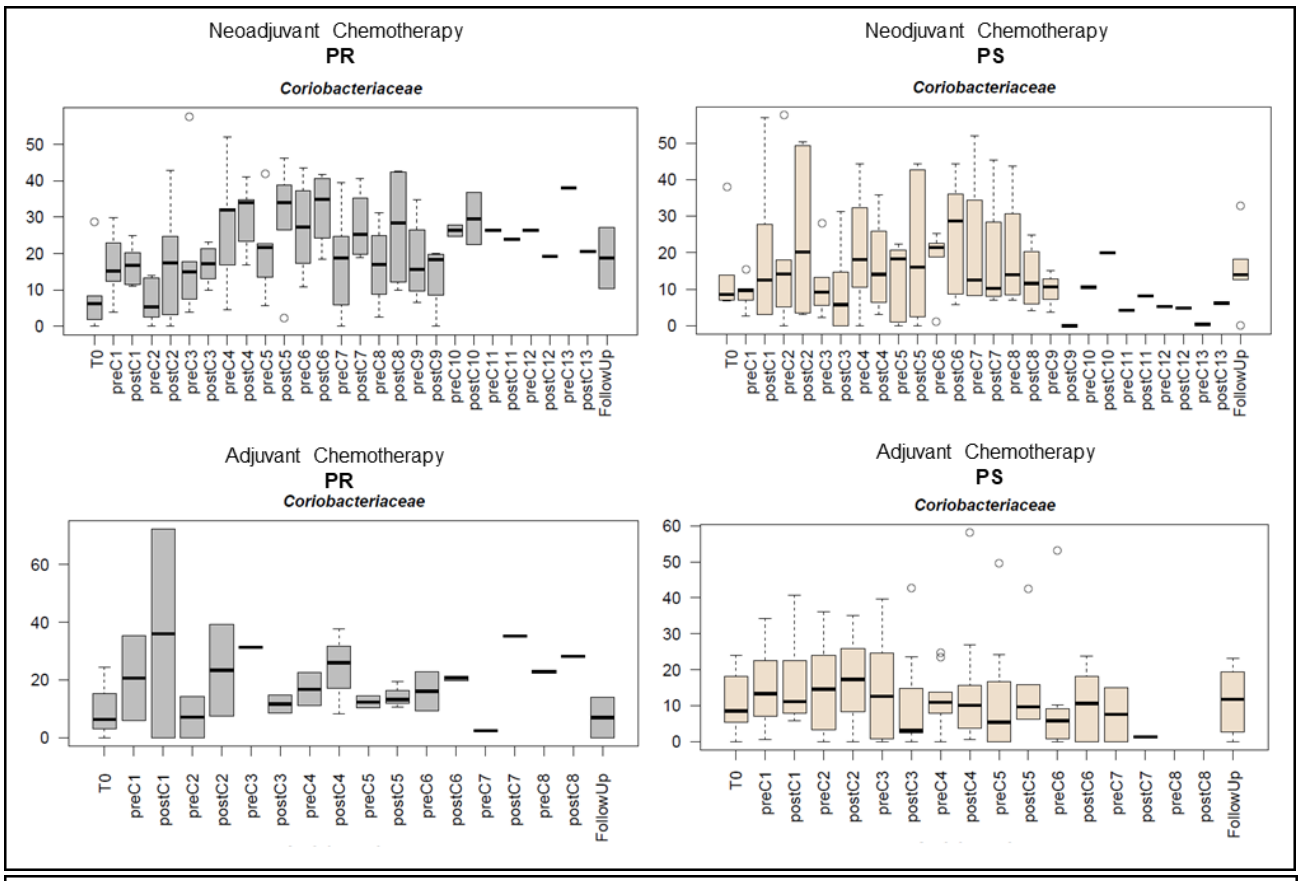
Neoadjuvant Chemotherapy
PR
Coriobacteriaceae
Neodjuvant Chemotherapy
PS
Coriobacteriaceae
Adjuvant Chemotherapy
PR
Coriobacteriaceae
Adjuvant Chemotherapy
PS
Coriobacteriaceae

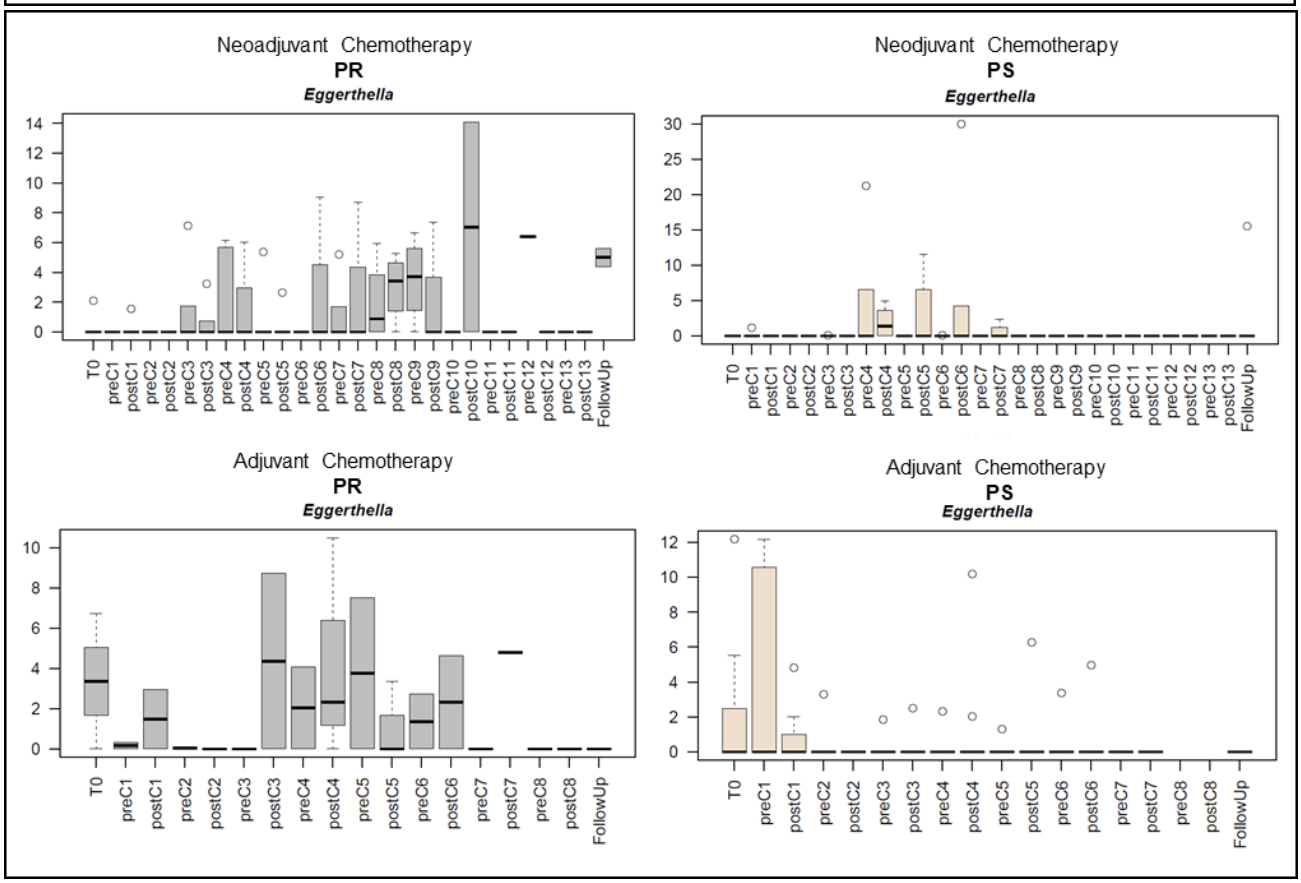
Neoadjuvant Chemotherapy
PR
Eggerthella
Neodjuvant Chemotherapy
PS
Eggerthella
Adjuvant Chemotherapy
PR
Eggerthella
Adjuvant Chemotherapy
PS
Eggerthella

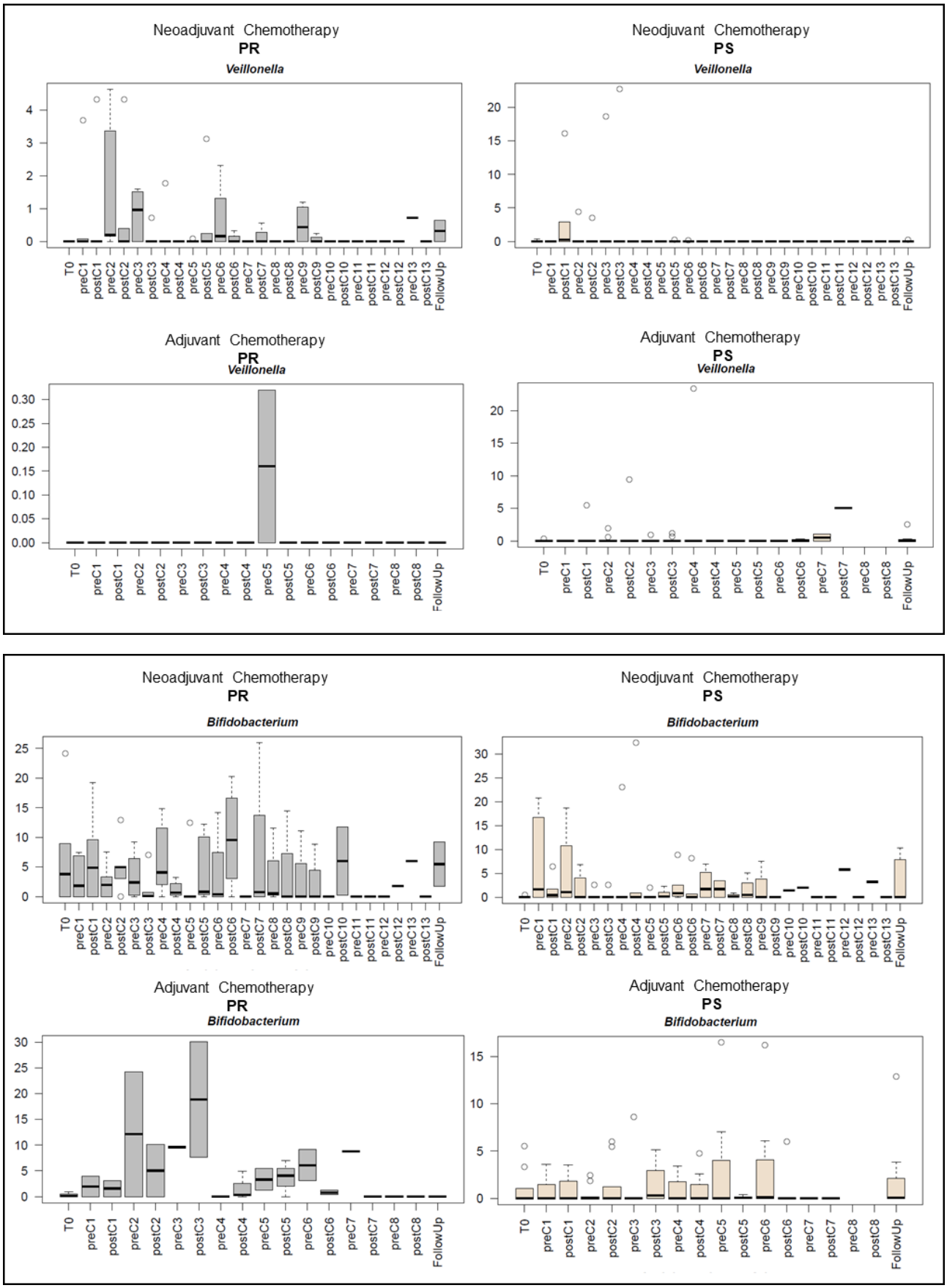

Figure S10. Temporal dynamics of the main taxa identified as discriminating between PR and PS patients for neoadjuvant and adjuvant chemotherapy.

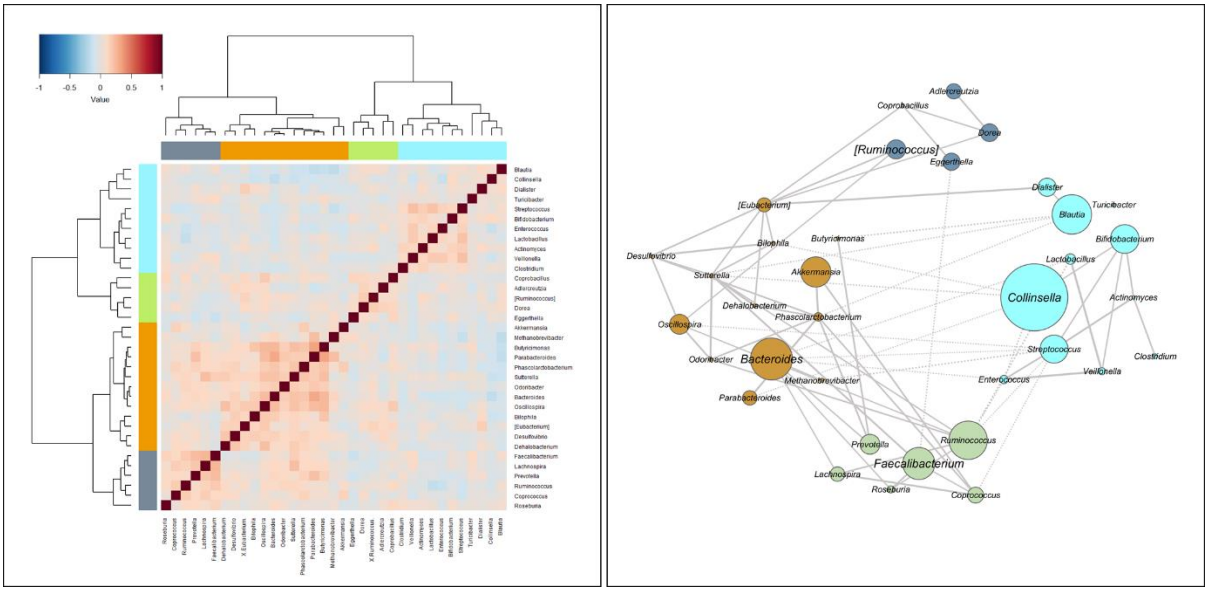

Figure S11. Assignment of co-abundance groups of the most abundant genera (CAGs). CAGs were determined by heat plot showing Kendall correlations between the most abundant genera clustered by Spearman correlation and Ward linkage. All CAGs displayed significantly different inter-relationships from each other ($p < 0.001$, permutational MANOVA). Network plots show correlations between the identified CAGs. Each node represents a taxon and its dimension is proportional to the relative abundance. Connections between nodes indicate positive and significant Kendall correlations between genera ($p < 0.05$). Line thickness is proportional to correlation strength. OTUs were filtered for those with >0.1% of mean relative abundance among the individual steady state profiles.

2.3 Enteral nutrition in pediatric patients undergoing hematopoietic SCT promotes the recovery of gut microbiome homeostasis

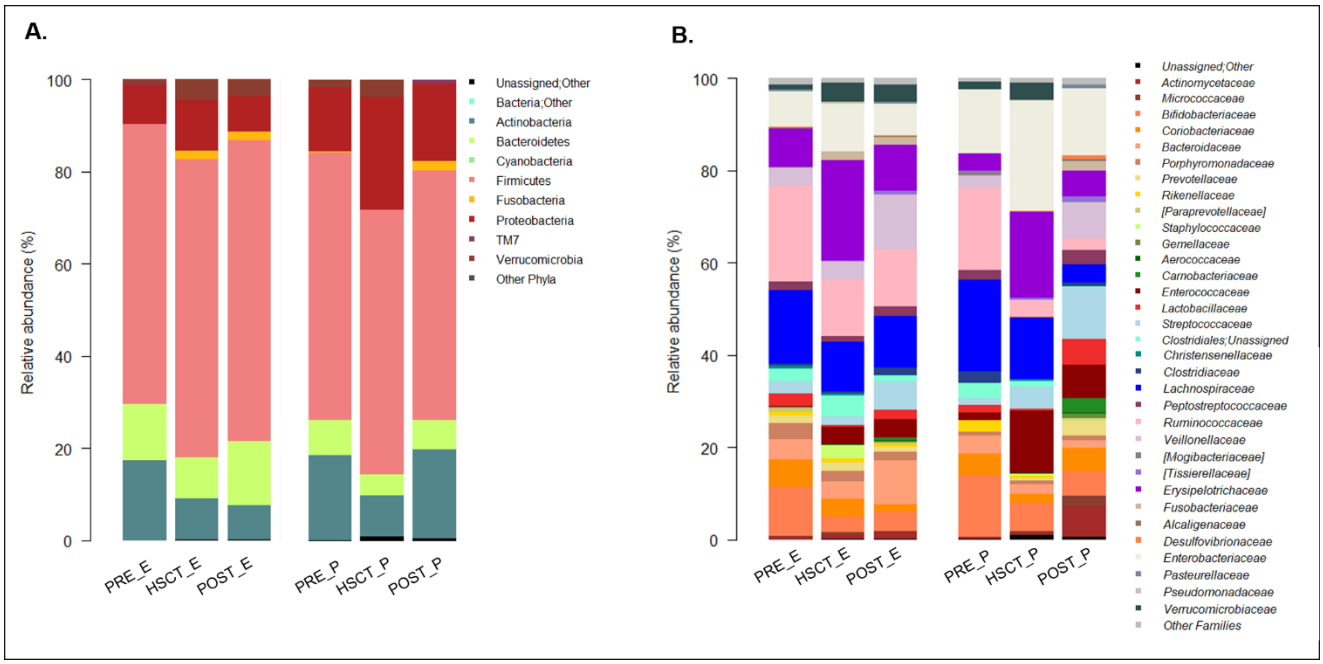

Figure S12. Gut microbiome composition of pre- and post-HSCT samples of patients fed with enteral and parenteral nutrition. Bar plots indicate the relative abundance of the most represented phyla (A.) and families (B.) in both enteral (E) and parenteral (P) nutrition-fed patients pre-HSCT (PRE), during the transplant (HSCT) and up to 120 days post-HSCT (POST). Only taxa with relative abundance >0.1% in at least two samples were included.

Subject	Nutritional Regimen	Sex/Age(yr)	Diagnosis	Donor Type	Stem cell source	Conditioning regimen	Engraftment (day)		aGvHD			Mucositis	BSI	Outcome at +100
							PMN (day)	PLT > 20000 (day)	Site	Day	Corticosteroid resistant	Grade		
E1	EN (+0/+18)	F/8	ALL B	Haploidentical	BM	BU, TT, FLUDARA	+14	+87	Skin ++, Gut ++, LIver +++	+24	n	III		a
E2	EN (+0/+12)	M/18	TM	MMUD	PBSC	TREO,TT,FLUDARA	+14	+20	Skin ++, Gut +	+14	n	/		a
E3	EN (+1/+21)	M/8	ALL B	MMFD	BM	BU, TT, FLUDARA	+16	+33				II		a
E4	EN (+1/+19)	F/8	ALL T	MUD	BM	BU, TT, EDX	+12	+46				III		a
E5	EN (+1/+18)	M/16	AML	Haploidentical	BM	BU, TT, FLUDARA	+23	+41						a
E6	EN (-2/+25)	F/16	AML	Haploidentical	BM	BU, TT, FLUDARA	+22	+35	Skin +, Gut ++	+36	n	II		a
E7	EN (+0/+18)	F/2	HLH	MUD	BM	BU, TT, FLUDARA	+14	+27				II		a
E8	EN (+1/+27)	F/12	RCC	MUD	BM	TREO,TT,FLUDARA	+24	+33				I		a
E9	EN (+0/+22)	F/3	ALL B	MUD	BM	BU, TT, FLUDARA	+19	+19	Skin +, Liver ++	+18	n	I		a
E10	EN (+1/+10); PN (+10/+13)	M/13	ALL B	MUD	BM	BU, TT, FLUDARA	+13	Not Obtained	Skin ++, Gut +	+60	n	II		a

Subject	Nutritional Regimen	Sex/Age(yr)	Diagnosis	Donor Type	Stem cell source	Conditioning regimen	Engraftment (day)		aGvHD			Mucositis	BSI	Outcome at +100
							PMN (day)	PLT > 20000 (day)	Site	Day	Corticosteroid resistant	Grade		
P1	PN (+5/+25)	M/15	CGD	MUD	BM	TREO,TT,FLUDARA	+19	+12				II	*S.epidermidis* (+5)	a
P2	PN (+6/+19)	M/7	AML	Haploidentical	BM	BU, TT, FLUDARA	+15	+28				II	*S.aureus* (+7)	a
P3	PN (+0/+16)	M/18	ALL B	MUD	BM	TREO, TT, EDX	+12	+16	Skin ++, Gut +	+28	n	I		a
P4	PN (+0/+18)	F/10	AML	MFD	BM	TREO,TT,FLUDARA	+11	+7				II	*S.epidermidis* (+6); *E.faecalis* (+6)	a
P5	PN (+1/+36)	M/4	JMML	MUD	BM	BU, EDX, L-PAM	+29	+37	Gut ++++	+29	y	I	*E.faecalis* (+57); *S.mitis* (+57); *S.oralis* (+57)	a
P6	EN (+1/+4); PN (+5/+23)	F/1	ALL B	MMUD	BM	BU, TT, EDX	+15	+25				I	*E.coli* (+2)	d
P7	PN (+5/+31)	M/17	RCC	MUD	BM	EDX, FLUDARA, TBI	+28	+36				II	*K.pneumoniae* (+6); *P.aeruginosa* (+15)	a
P8	PN (+4/+13)	M/16	AML	MFD	BM	BU, EDX, L-PAM	+13	+14	Gut +++, Liver +	+21	y	II	*S.aureus* (+94)	a
P9	EN (+2/+4); PN (+5/+20)	M/17	MDS	MUD	PBSC	BU, EDX, L-PAM	+19	+21	Skin ++	+20	n	II		a
P10	PN (+0/+17)	M/18	ALL B	MUD	BM	BU, TT, EDX	+13	+23	Skin +++	+15	n	III		a

Abbreviations: a= alive; aGvHD= acute Graft-versus-Host disease; ALL= Acute Lymphoblastic Leukemia; AML= Acute Myeloid Leukemia; BM= Bone Marrow; BSI= Blood Stream Infections; BU= Busulphan; CGD= Chronic Granulomatous Disease; d= deceased; EDX= Cyclophosphamide; EN = Enteral Nutrition; F=Female; FLUDARA= Fludarabine; HLH= Hemophagocitic LymphoHistiocytosis; JMML= Juvenile Myelomonocytic Leukemia; L-PAM= Melphalan; M= Male; MDS= Myelodisplastic Syndrome; MFD= Matched Familiar Donor; MMFD= Mismatched Familiar Donor; MMUD= Mismatched Unrelated Donor; MUD= Match Unrelated Donor; n= no; PBSC= Peripheral Blood Stem Cell; PLT=Platelets; PMN=Polymorphonuclear Neutrophil; PN= Parenteral Nutrition; RCC= Refractory Citopenia of Childhood; TBI= Total Body Irradiation; TM= Thalassemia Major; TREO= Treosulphan; TT= Thiotepa; y= yes; The plus near by the aGvHD site indicate the grade of severity (from 1 to 4); The numbers between parenthesis indicate the starting and the ending day for the nutritional treatment post-transplant.

Table S1. Anagraphical and clinical information of the twenty enrolled patients.

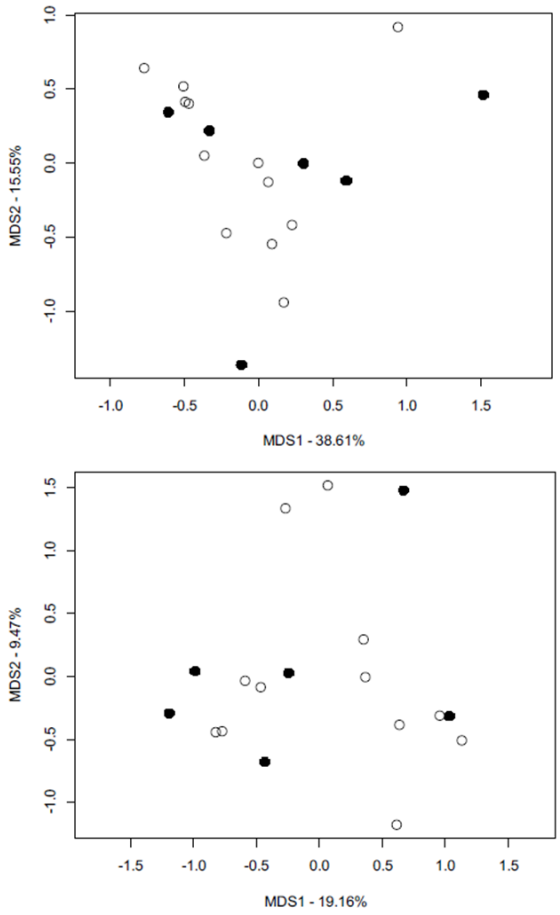

Figure S13. PCoA plots based on weighted (top) and unweighted (bottom) Unifrac distances of microbiota profiles of samples collected before transplant (PRE) from patients who received (black cirles) and did not receive (empty white circles) levofloxacin prophylaxis prior to HSCT). p = 0.46 and p = 0.63, for weighted and unweighted Unifrac distances, respectively (permutation tests with pseudo-F ratios (Adonis)).

3.1 Gut resistome plasticity in pediatric patients undergoing hematopoietic stem cell transplantation

	pre-HSCT	pre-HSCT SD	Healthy subjects	Healthy subjects SD	p value
ARU0	0.000	0.000	0.000	0.000	NA
ARU1	0.000	0.000	0.000	0.000	NA
ARU2	0.000	0.000	0.000	0.000	NA
ARU3	0.000	0.000	0.000	0.000	NA
ARU4	7.714	5.936	72.800	66.530	0.008
ARU5	0.000	0.000	0.000	0.000	NA
ARU6	0.000	0.000	0.000	0.000	NA
ARU7	0.000	0.000	0.000	0.000	NA
ARU8	0.000	0.000	0.000	0.000	NA
ARU9	0.000	0.000	0.000	0.000	NA
ARU10	0.000	0.000	0.000	0.000	NA
ARU11	0.000	0.000	0.000	0.000	NA
ARU12	0.000	0.000	0.000	0.000	NA
ARU13	0.000	0.000	4.600	9.709	0.257
ARU14	0.000	0.000	0.000	0.000	NA
ARU15	0.000	0.000	0.000	0.000	NA
ARU16	0.000	0.000	0.000	0.000	NA
ARU17	0.143	0.378	0.500	1.581	0.931
ARU18	0.714	1.890	0.000	0.000	0.282
ARU19	0.000	0.000	0.000	0.000	NA
ARU20	0.000	0.000	0.000	0.000	NA
ARU21	0.000	0.000	0.000	0.000	NA
ARU22	0.000	0.000	0.000	0.000	NA
ARU23	0.000	0.000	0.000	0.000	NA
ARU24	0.000	0.000	6.500	11.257	0.076
ARU25	0.000	0.000	0.000	0.000	NA
ARU26	18.857	36.334	25.400	26.056	0.654
ARU27	0.143	0.378	0.000	0.000	0.282
ARU28	0.143	0.378	0.000	0.000	0.282
ARU29	0.000	0.000	0.700	1.636	0.257
ARU30	0.000	0.000	3.400	7.230	0.257
ARU31	0.286	0.756	2.600	5.797	0.714
ARU32	0.000	0.000	0.000	0.000	NA
ARU33	0.143	0.378	0.000	0.000	0.282
ARU34	0.000	0.000	0.000	0.000	NA
ARU35	0.000	0.000	0.000	0.000	NA
ARU36	0.000	0.000	0.000	0.000	NA
ARU37	0.000	0.000	0.000	0.000	NA
ARU38	8.000	8.185	2.900	7.578	0.071
ARU39	0.143	0.378	4.600	6.398	0.203
ARU40	0.000	0.000	0.000	0.000	NA
ARU41	0.000	0.000	0.000	0.000	NA
ARU42	0.000	0.000	0.000	0.000	NA
ARU43	0.286	0.756	8.800	21.953	0.394
ARU44	0.000	0.000	15.500	36.189	0.077

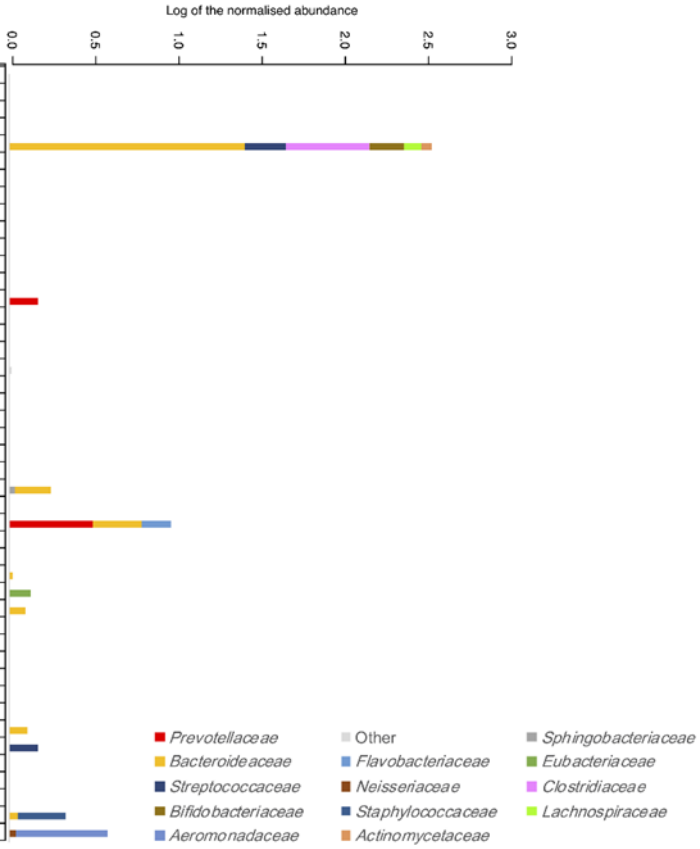

Figure S14. Table showing the mean and standard deviation of the relative abundance of each ARU in the two groups analyzed: pre-HSCT samples and healthy subjects. Wilcoxon signed rank-sum test was used to assess significant difference between the two groups of subjects. Bar plots showing the normalized abundance of the families assigned to each ARU for healthy subjects are shown on the right.

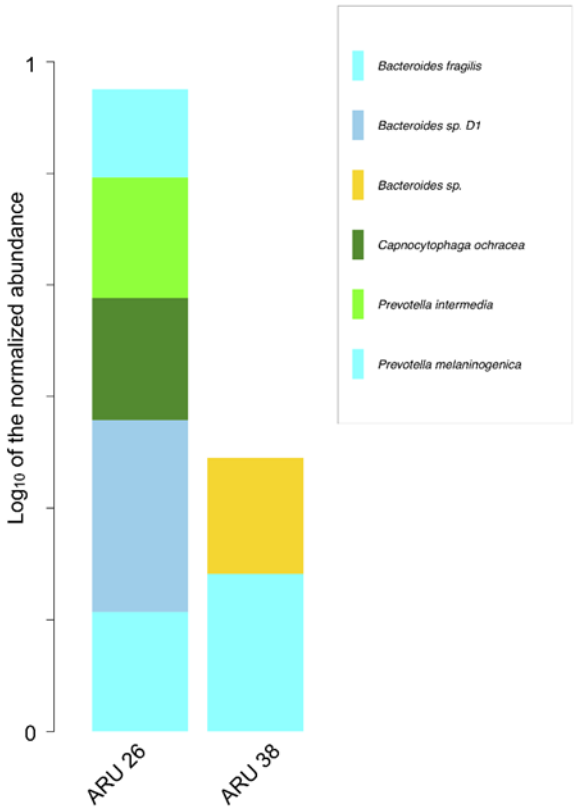

Figure S15. Taxonomic classification to species level of ARU26 and ARU38.

Subject	Sex/Age	Diagnosis	Donor Type	Stem cell source	Conditioning regimen	aGvHD prophylaxis	TNC /Kg	Engraftment (day)			aGvHD			Outcome	Antibiotic prophylaxis	Antibiotic treatment
								PMN	PLT	Grade	Site	Day	Therapy			
4	F/12	AML	MUD	BM	BU+EDX+ L-PAM	ATG-CSA-MTX	4.2x 10^8	+13	+20	I	Skin	+25	Steroid	ANED 2 years	Levofloxacin ± (-9/+21)	Ceftazidime* (+7/+13) Piperacillin/ tazobactam* (+13/+19)
11	M/9	ALL	MUD	BM	BU+TT+EDX	ATG-CSA-MTX	3.4x 10^8	+15	+27	II	Skin	+11	Steroid	Dead from relapse	Levofloxacin ± (-9+21)	Ceftazidime* (+7/+19) Amikacin# (+7/+21)
5	M/10	ALL	MFD	BM	BU+TT+EDX	CSA	2.9x 10^8	+12	+17	III	Skin	+23	Steroid-PHEC	ANED 2 years +1/12	Levofloxacin ± (-9/+21)	Ceftazidime* (-9/+7) Piperacillin/ tazobactam* (+7/+16) Amikacin# (+3/+16)
15	M/8	ALL	MFD	BM	BU+TT+EDX	CSA	5.8x 10^8	+12	+17	IV	Skin, GI	+11	Steroid-PHEC Infliximab	ANED 1 year +6/12	Levofloxacin ± (-9/+21)	Ceftazidime* (+8/+15)
19	F/10	ALL	MUD	BM	BU+TT+EDX	ATG-CSA-MTX	7.1x 10^8	+34	+35					ANED 1 year +3/12	Levofloxacin ± (-9/+21)	Ceftazidime* (+9/+14) Amikacin# (+11/+18) Meropenem* (+14/+23, +34/+43) Linezolid ± (+34/+41)
16	M/16	ALL	MFD	BM	BU+TT+EDX	CSA	4.6x 10^8	+11	+30					ANED 1 year +6/12	Levofloxacin ± (-9/+21)	Ceftazidime* (+7/+16) Piperacillin/ tazobactam* (+16/+23) Amikacin# (+9/+15)
20	M/7	ALL	MUD	BM	BU+TT+EDX	ATG-CSA-MTX	4.8x 10^8	+12	+15					ANED 1 year +4/12	Levofloxacin ± (-9/+21)	Teicoplanin ± (+9/+16)
26	M/8	AML	MUD	BM	BU+EDX+L-PAM	ATG-CSA-MTX	7.2x 10^8	+12	+21					ANED 1 year +9/12	Levofloxacin ± (-9/+21)	Ceftazidime* (+6/+19) Teicoplanin ± (+10/+21)

Abbrevations: aGvHD=acute graft-versus-host disease; ALL=acute lymphoblastic leukemia; AML=acute myeloid leukemia; ANED=alive no evidence of disease; ATG=anti-thymocyte; BM=bone marrow; BU=busulfan; CSA=cyclosporin A; EDX=cyclophosphamide; F=female; GI=gastrointestinal tract; L-PAM=melphalan; M=male; MFD=match family donor; MTX= methotrexate; MUD=match unrelated donor; PHEC=extracorporeal photopheresis; PMN=polymorphonuclear neutrophil; PLT=platelets; TNC= total nucleated cells; TT=thiotepa; globulin.

*Beta-lactam antibiotic; # Aminoglycoside antibiotic; ± Others. The numbers between parenthesis indicate the starting and the ending day for the antibiotic treatment post-transplant.

Table S2. Anagraphical and clinical information of the enrolled patients.

Antibiotic Resistance Unit	Antibiotic Class	Identity Name	Resistance Type	Function
[ARU0]	Multidrug resistance	ZP_02346647	acrb	Multidrug resistance efflux pump
[ARU1]	Tetracycline	XP_002333050	tetc	Tetracycline efflux pump
[ARU2]	Multidrug resistance	YP_001460869	mdto	Multidrug resistance efflux pump
[ARU3]	Polypeptide	AAL23678	arna	Resistance to polymyxin
[ARU4]	Tetracycline	BAD46890	tetq	Inhibition of tetracycline
[ARU5]	Macrolide	BAB64542	macb	Macrolide-specific efflux pump
[ARU6]	Fosfidomycin	YP_001477377	rosb	Efflux pump/potassium antiporter system
[ARU7]	Multidrug resistance	YP_002807373	tolc	Multidrug resistance efflux pump
[ARU8]	Multidrug resistance	ZP_04437889	lsa	ABC efflux family that is resistant to MLS antibiotics
[ARU9]	Aminoglycoside	BAG12278	aac6ie	Aminoglycoside N-acetyltransferase
[ARU10]	Tetracycline	P13924	tetl	Tetracycline efflux pump
[ARU11]	Multidrug resistance	YP_403489	mdtk	Multidrug resistance efflux pump
[ARU12]	Beta-lactam antibiotics	ZP_04534300	bl1_ec	Class C beta-lactamase
[ARU13]	Beta-lactam antibiotics	ZP_03615711	tet37	Inhibition of tetracycline
[ARU14]	Multidrug resistance	ABE06672	mdth	Multidrug resistance efflux pump
[ARU15]	Multidrug resistance	BAG80136	mdtm	Multidrug resistance efflux pump
[ARU16]	Multidrug resistance	BAA35851	mdtg	Multidrug resistance efflux pump
[ARU17]	Tetracycline	ACI02010	tet40	Tetracycline efflux pump
[ARU18]	Macrolide	AAQ62546	mefa	Macrolide efflux pump
[ARU19]	Multidrug resistance	YP_002396538	acra	Multidrug resistance efflux pump
[ARU20]	Multidrug resistance	CAS09877	bcr	Multidrug efflux system
[ARU21]	Multidrug resistance	YP_002393667	emrd	Multidrug resistance efflux pump
[ARU22]	Multidrug resistance	ZP_04439153	emea	Multidrug resistance efflux pump
[ARU23]	Multidrug resistance	ZP_03063399	mdtl	Multidrug resistance efflux pump
[ARU24]	Tetracycline	CAC47932	tetx	Tetracycline modification
[ARU25]	Multidrug resistance	YP_410370	mdtn	Multidrug resistance efflux pump
[ARU26]	Beta-lactam antibiotics	ZP_04543532	bl2e_cfxa	Class A beta-lactamase
[ARU27]	Sulphonamide	YP_001969930	sul2	Sulfonamide-resistant dihydropteroate synthase
[ARU28]	Macrolide	AAG14406	mpha	Macrolide phosphotransferase

[ARU29]	Beta-lactam antibiotics	ZP_02068298	bl2e_cepa	Class A beta-lactamase
[ARU30]	Polypeptide	YP_002937728	baca	Undecaprenyl pyrophosphate phosphatase
[ARU31]	Aminoglycoside	ABP57330	ant6ia	Aminoglycoside O-nucleotidylyltransferase
[ARU32]	Aminoglycoside	ACI02996	aac3iia	Aminoglycoside N-acetyltransferase
[ARU33]	Macrolide	ZP_03973325	ermx	Resistance to erythromycin
[ARU34]	Aminoglycoside	CAZ48657	aph6id	Aminoglycoside O-phosphotransferase
[ARU35]	Beta-lactam antibiotics	ACO55744	bl2d_oxa1	Class D beta-lactamase
[ARU36]	Aminoglycoside	BAE76038	ksga	Kasugamycin resistance
[ARU37]	Lincosamide	AAL05554	lnub	Lincosamide nucleotidyltransferase
[ARU38]	Macrolide	AAA27431	ermf	Resistance to erythromycin
[ARU39]	Aminoglycoside	CAP17165	aph3iiia	Aminoglycoside O-phosphotransferase
[ARU40]	Beta-lactam antibiotics	ACI47262	bl2be_ctxm	Class A beta-lactamase
[ARU41]	Aminoglycoside	CAQ06465	aadd	Aminoglycoside O-nucleotidylyltransferase
[ARU42]	Beta-lactam antibiotics	CAH41960	bl3_ccra	Class B beta-lactamase
[ARU43]	Macrolide	BAH18720	ermb	Resistance to erythromycin
[ARU44]	Cloramphenicol	YP_001144149	cata13	Group A chloramphenicol acetyltransferase

Table S3. Classification of the Antibiotic Resistance Units (ARUs) detected in the gut resistome of pediatric patients undergoing HSCT and healthy patients. For each ARU, antibiotic class, identity name, resistance type and function are indicated.

3.2 Low-dose antibiotic prophylaxis alters the gut microbiota of infants with vesicoureteral reflux

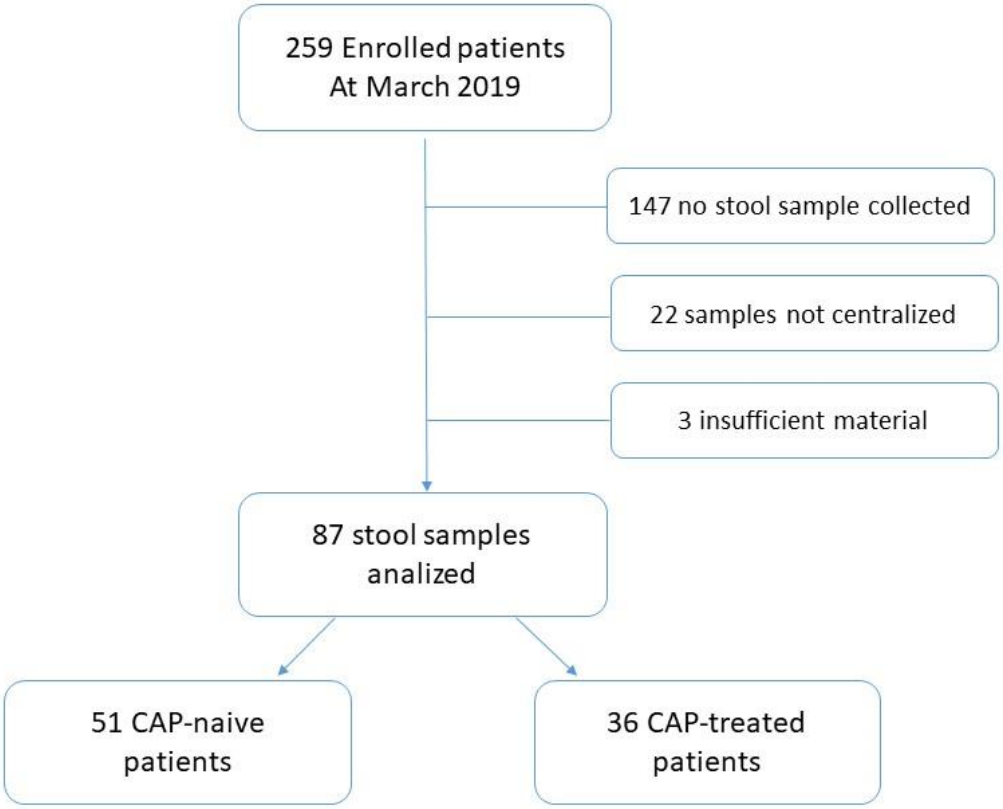

Figure S16. Flow diagram of screened and enrolled population.

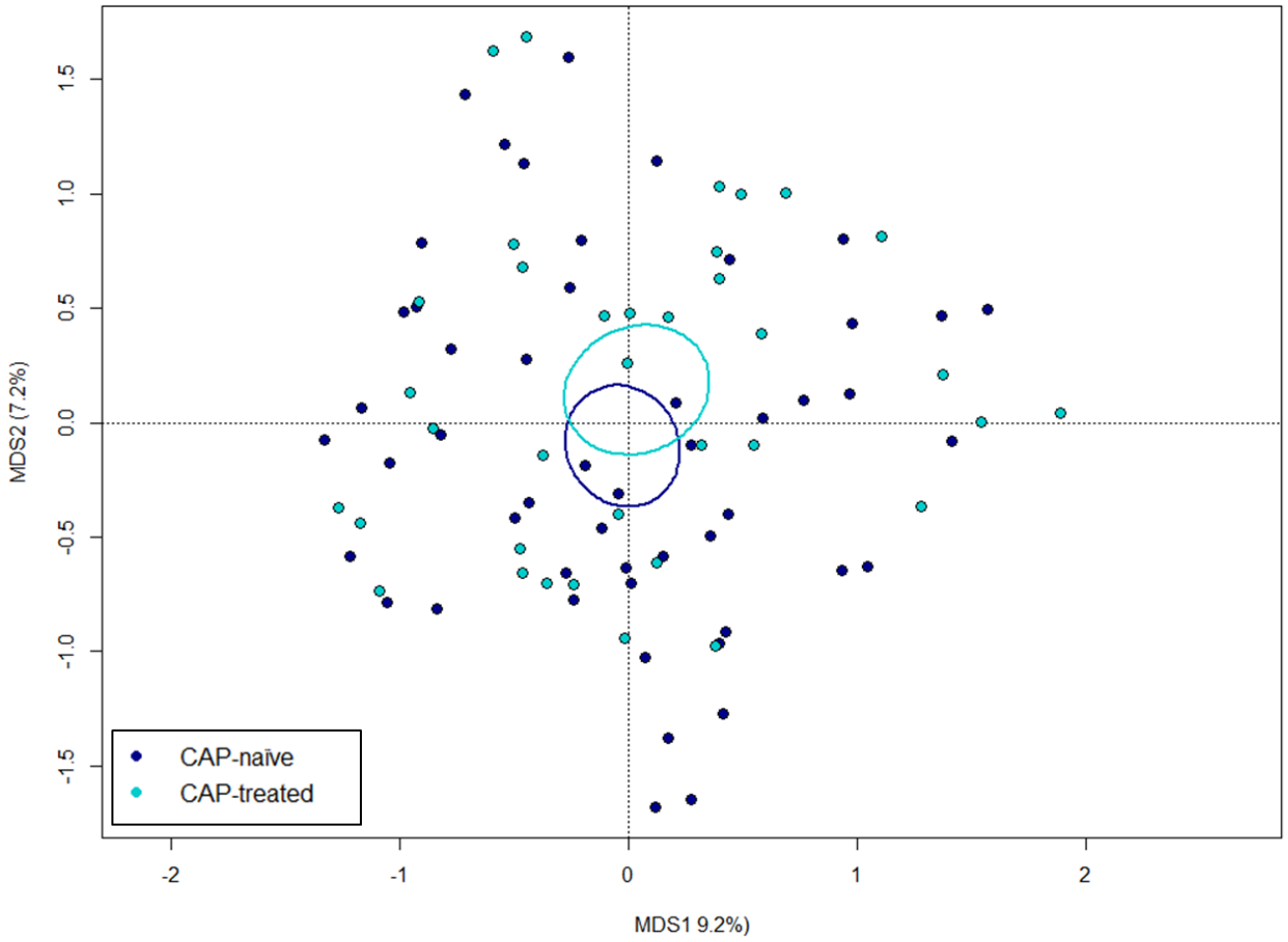

Figure S17. Principal Coordinates Analysis (PCoA) based on unweighted UniFrac distances between fecal samples from CAP-treated vs. CAP-naïve infants. No significant separation between groups was found (p-value = 0.346, permutation test with pseudo-F ratios). Ellipses include 95% confidence area based on the standard error of the weighted average of sample coordinates.

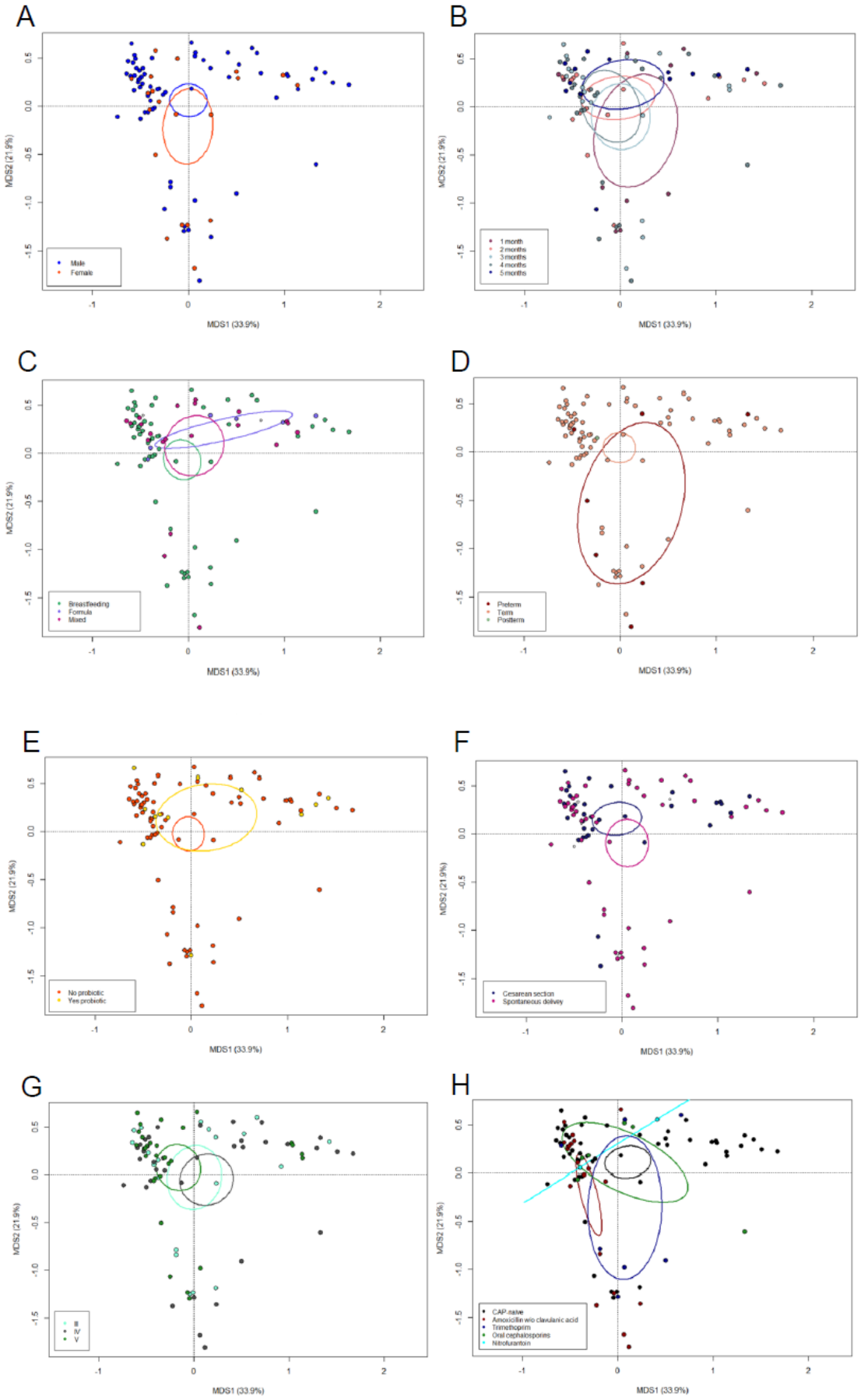
A
MDS2 (21.9%)
MDS1 (33.9%)
Male
Female
B
MDS2 (21.9%)
MDS1 (33.9%)
1 month
2 months
3 months
4 months
5 months
C
MDS2 (21.9%)
MDS1 (33.9%)
Breastfeeding
Formula
Mixed
D
MDS1 (33.9%)
Preterm
Term
Postterm
E
MDS2 (21.9%)
MDS1 (33.9%)
No probiotic
Yes probiotic
F
MDS2 (21.9%)
MDS1 (33.9%)
Cesarean section
Spontaneous delivey
G
MDS2 (21.9%)
MDS1 (33.9%)
III
IV
V
H
MDS2 (21.9%)
MDS1 (33.9%)
CAP naive
Amoxicillin w/o clavulanic acid
Trimethoprim
Oral cephalosporins
Nitrofurantoin

Figure S18. **The GM dysbiosis in CAP-treated infants is independent of potential confounding factors.** Principal Coordinates Analysis (PCoA) based on weighted UniFrac distances between fecal samples from CAP-treated vs. CAP-naïve infants, stratified by gender (male vs female, **A**), age group (1 to 5 months, **B**), feeding modality (breastfeeding vs formula vs mixed, **C**), gestational age (term vs preterm vs post-term, **D**), probiotics consumption (yes vs no, **E**), delivery mode (cesarean section vs spontaneous delivery, **F**) VUR grade (grade III vs IV vs V, **G**), and class of antibiotics (amoxicillin or amoxicillin+clavulanic acid, trimethoprim, oral cephalosporins and nitrofurantoin, H). No significant separation was found ($p > 0.264$, permutation test with pseudo-F ratios). Ellipses include 95% confidence area based on the standard error of the weighted average of sample coordinates.

		CAP-naïve (n=51)	CAP-treated (n=36)	Tot (n=87)	P-value
Gender	Males	37 (72.5%)	30 (83.3%)	67 (77%)	0.24
	Females	14 (27.5%)	6 (16.7%)	20 (23%)	
Age (months)	Median (IQR)	3.6 (2.6-4.3)	2.6 (1.7-3.53)	3.1 (2.2-3.9)	**0.002**
Feeding modality	Breastfeeding	30(58.8%)	28 (77.7%)	58 (66.7%)	0.26
	Mixed	16 (31.4%)	5 (13.9%)	21 (4.1%)	
	Formula	4 (7.8%)	2 (5.6%)	6 (6.3%)	
	Unknown	1 (2%)	1 (2.8%)	2 (2.3%)	
Gestational age	Term	45 (88.2%)	34 (94.4%)	79 (90.8%)	0.53
	Preterm	5 (9.8%)	2 (5.6%)	7 (8%)	
	Postterm	1 (2%)	0	1 (1.1%)	
Probiotics consumption	Yes	8 (15.7%)	4 (11.1%)	12 (13.8%)	0.54
	No	43 (84.3%)	32 (88.9%)	75 (86.2%)	
Mode of delivery	Cesarean section	27 (52.9%)	6 (16.7%)	33 (37.9%)	**0.001**
	Spontaneous delivery	23 (45.1%)	26 (72.2%)	49 (56.3%)	
	Unknown	1 (2%)	4 (11.1%)	5 (5.7%)	
Grade of VUR	Grade III *n* (%)	13 (25.5%)	8 (22.2%)	21 (24.1%)	0.37
	Grade IV *n* (%)	18 (35.3%)	18 (50%)	36 (41.4%)	
	Grade V *n* (%)	20 (39.2%)	10 (27.8%)	30 (34.5%)	

Table S4. Clinical characteristic of enrolled patients. VUR, vesico-ureteral reflux. P-values were obtained by Chi squared test for categorical variables and Wilcoxon signed-rank test for continuous variables (significant values are reported in bold).

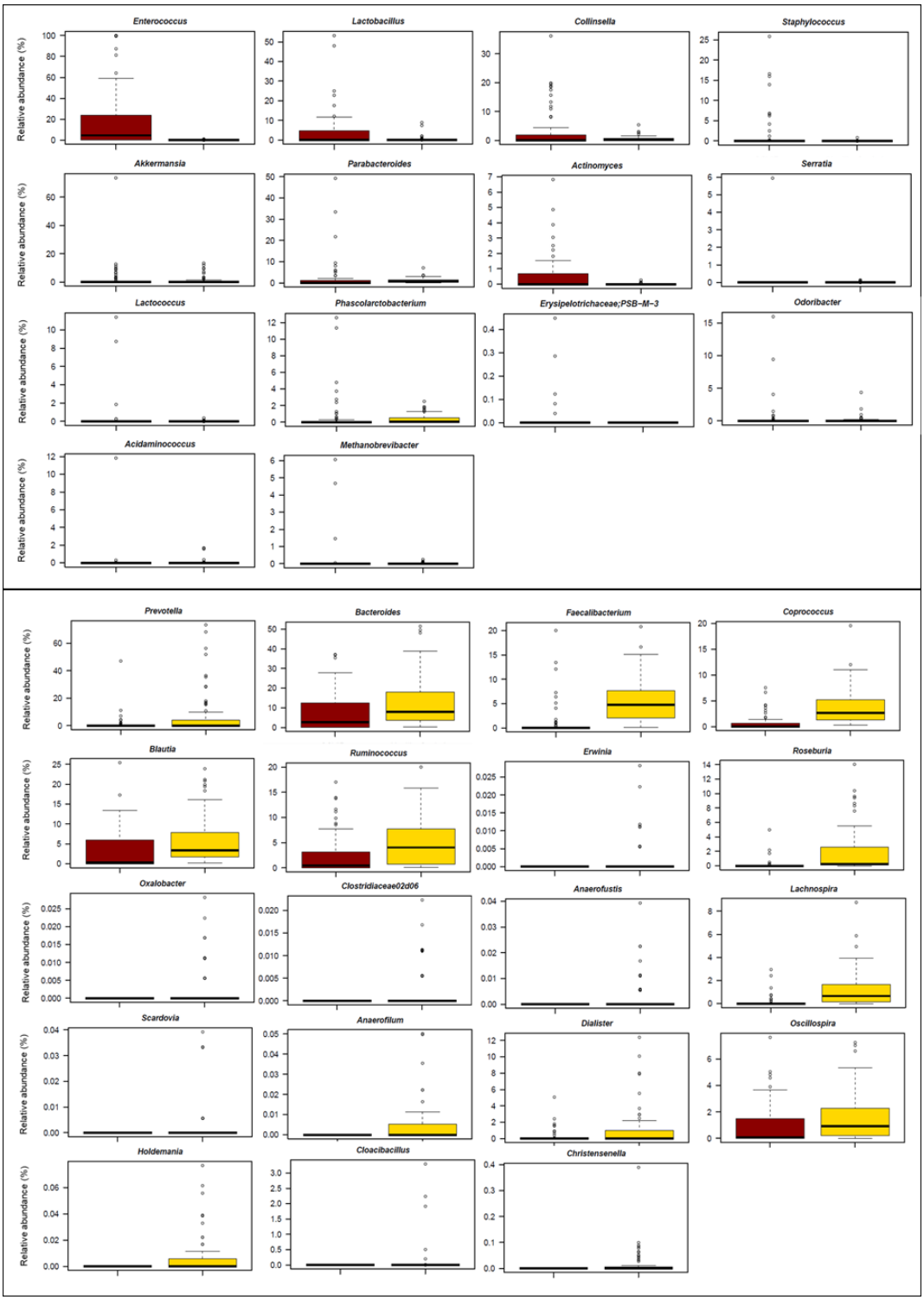

Figure S19. Bacterial genera differentially represented between COVID-19 patients and healthy controls. Boxplots showing the relative abundance distribution of the genera differentially represented between groups according to the LEfSe algorithm with LDA score threshold of 3 (on a log10 scale). Red, COVID-19 patients; yellow, healthy controls.

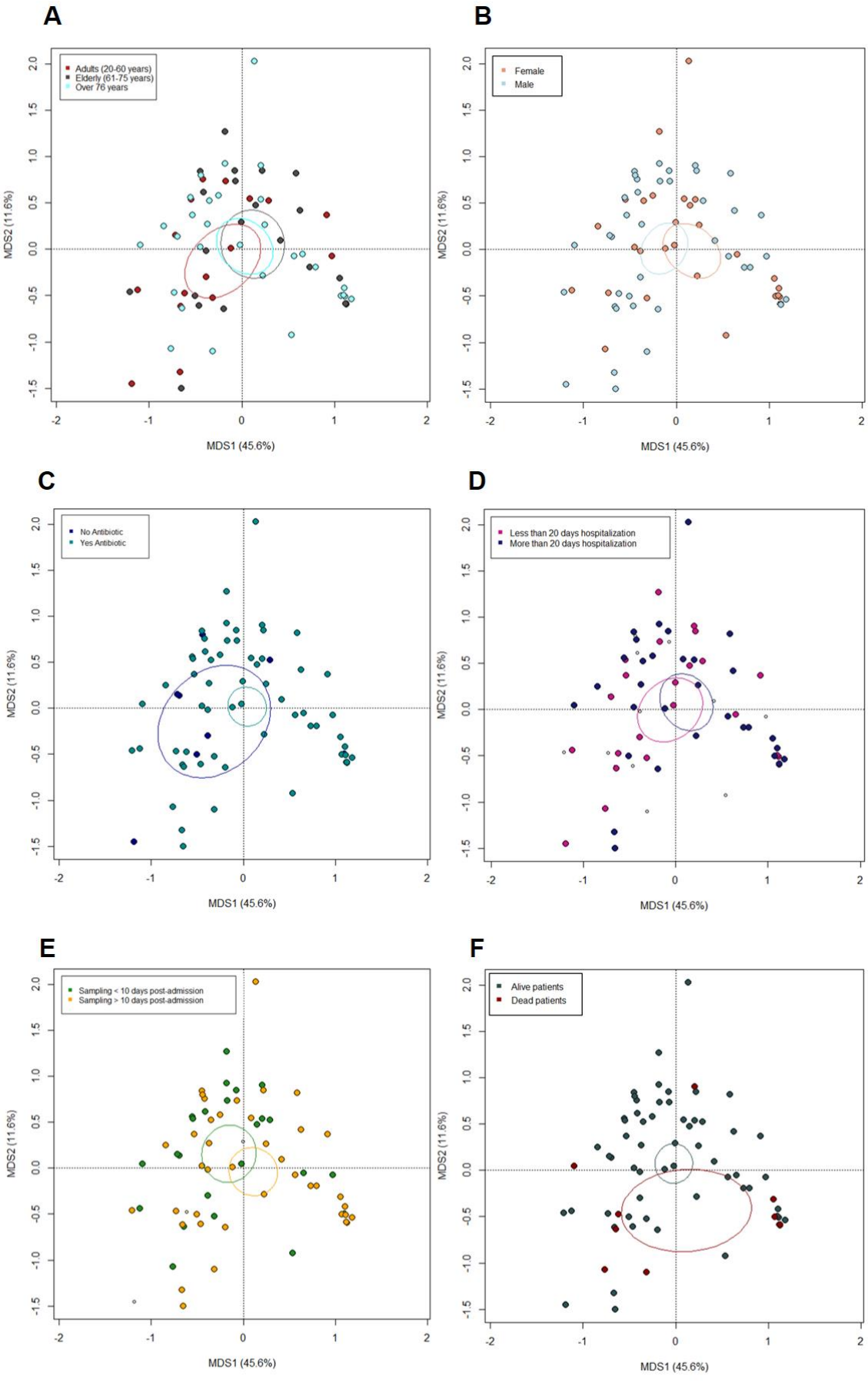
A
Adults (20-60 years)
Elderly (61-75 years)
Over 76 years
B
Female
Male
C
No Antibiotic
Yes Antibiotic
D
Less than 20 days hospitalization
More than 20 days hospitalization
E
Sampling < 10 days post-admission
Sampling > 10 days post-admission
F
Alive patients
Dead patients
MDS1 (45.6%)
MDS2 (11.6%)

Figure S20. Gut microbiota dysbiosis of COVID-19 patients is robust to several confounding factors. Principal Coordinates Analysis (PCoA) based on weighted UniFrac distances between fecal samples from COVID-19 patients stratified by age group (adults, elderly and over 76 years, **A**), gender (males vs females, **B**), antibiotic intake in the 2 weeks prior to fecal sampling (yes vs no, **C**), length of hospital stay (more or less than 20 days, **D**), time interval between fecal sampling and hospital admission (more or less than 10 days, **E**) and final outcome (dead vs alive patients, **F**). Ellipses include 95% confidence area based on the standard error of the weighted average of sample coordinates. No significant separation was found (p value > 0.05, permutation test with pseudo-F ratio).